Atmospheric Pollution & Climate Change (APCC)

Environmental Information System (ENVIS)

Resource Partner

(Sponsored by Ministry of Environment, Forest & Climate Change, Govt. of India)

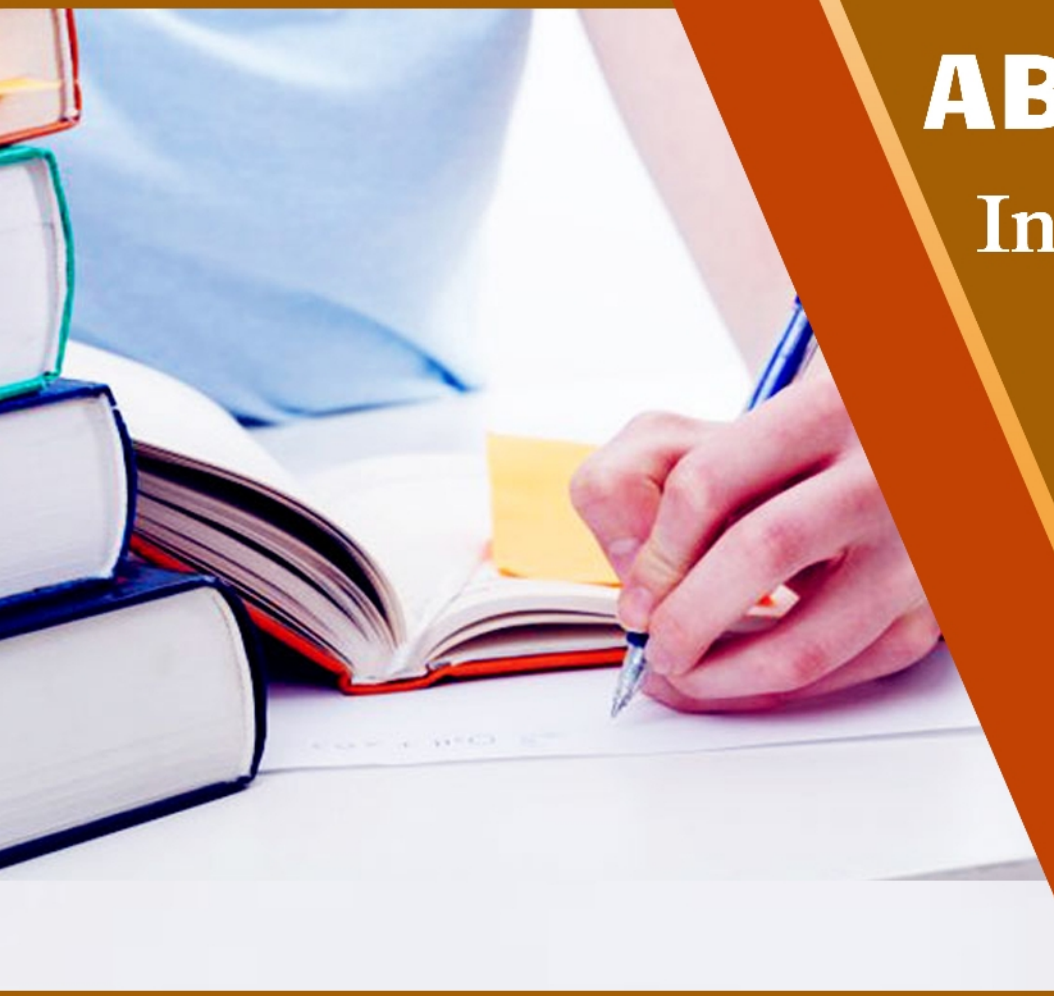

ABSTRACTS

India & Global

2018-19

INDIAN INSTITUTE OF TROPICAL METEOROLOGY
PUNE - 411 008

Contributed by

Dr. Gufran Beig

Dr. Suvarna Tikle

Mr. Samir Dhapare

Mr. Gaurav Shinde

Ms. Darshana Jadhav

Environmental Information System's (ENVIS) centre on Atmospheric Pollution & Climate Change (APCC) at Indian Institute of Tropical Meteorology (IITM, Pune) is compiling the abstracts of new research done in the field air pollution and climate change categories, for the year 2018. This book has those abstracts which would help scientists, environmentalists and conservationists regarding monitoring, & controlling for atmospheric pollution and climate change.

CONTENTS

Influence of Environmental Conditions on Forecasting of an Advection-Radiation Fog: A Case Study from the Casablanca Region, Morocco

Driss Bari 1, Thierry Bergot 2

Source: Aerosol and Air Quality research, Volume: 18 | Issue: 1 | Pages: 62-78 ;DOI: 10.4209/aaqr.2016.11.0520

In this study, a dense advection-radiation fog that occurred over the Grand Casablanca region, Morocco, during the night of 23–24 December 2013, is investigated. The adverse visibility induced by the fog patch led to a series of collisions and loss of life on a highway of the region. This fog event is simulated by the Meso-NH research model. Conventional observations from two synoptic stations, satellite imagery, and the European Center for Medium-Range Weather Forecasts (ECMWF) reanalysis are used to analyze the physical processes during the whole life cycle of the event. Some hypotheses on the influence of environmental conditions (topography, land-sea heterogeneity, urbanization) on the numerical fog prediction are presented. Observational analysis together with numerical results show that the horizontal moisture transport, linked to a northerly wind during the afternoon, drove the onset of this fog event. The formation stage was governed by weak turbulence and nocturnal radiative cooling at both stations (costal station, GMMC, and inland station, GMMN). Horizontal moisture flux convergence was observed at the top of the fog layer, over the coastal station, during the mature phase, in addition to the radiative-turbulent interactions. The latter was the main mechanism leading to fog thickening at the inland station. The dissipation phase was governed by a zone of horizontal moisture flux divergence linked to a dry wind from the south. Sensitivity experiments show that numerical coastal fog prediction is influenced by local topography, urbanization and aerosol types, but less by land cover.

Keywords: Advection-radiation fog; Coastal fog; Urbanization; Topography; Land-sea thermal contrast; Aerosols

---

Preface to the AAQR Special Issue "Fog, Fog Collection and Dew"

Otto Klemm 1, Werner Eugster2, Martha Scholl3, Fábio Luiz T. Gonçalves4, Genki Katata5, Neng-Huei Lin6

Source: Aerosol and Air Quality research, Volume: 18 | Issue: 1 | Pages: I-II;
DOI: 10.4209/aaqr.2018.01.fog.

Fog is a "suspension of very small, usually microscopic water droplets" that "reduce horizontal visibility at the Earth's surface to less than 1 km" (WMO, 2017). Fog may also be considered as a cloud in contact with the Earth's surface. Dew is a "deposit of water drops on objects, produced by the direct condensation of water vapour from the surrounding air" (WMO, 2017). Both fog and dew formation are driven by the condensation of water vapor to liquid water in the very lowest part of the atmospheric boundary layer, i.e., in association with air masses with terrestrial or marine surface contact. Fog as a phenomenon is the object of various science and engineering fields such as meteorology, transportation safety, hydrology, and biology. Fog can scavenge airborne pollutants in urban and industrial areas, creating a health hazard, but can also deliver nutrients to natural environments. As part of the ecohydrology of natural systems around the world, fog creates unique endemic species distributions. Through its unique impact on humans' perception of the environment, fog has also found its way into literature and the art of painting. In some areas of the world, fog is even utilized as a valuable source for freshwater production. To lesser degree, this is also true for dew, which may be collected with the aim to generate potable water.

The triannual International Conference of Fog, Fog Collection and Dew started some 20 years ago in Vancouver (Canada, 1998), went on through St. John's (Canada, 2001), Cape Town (South Africa, 2004), La Serena (Chile, 2007), Münster Germany, 2010), Yokohama (Japan, 2013), Wrocław (Poland, 2016), and will be continued in Taipei (Taiwan) in 2019. This special issue of "Aerosol and Air Quality Research" (AAQR) is a selection of contributions as presented at the most recent 7th International Conference of Fog, Fog Collection and Dew at the University of Wrocław from 24 through 29 July, 2016. Of the 162 contributions to the conference, 33 were submitted to AAQR as manuscripts to be included in this special issue. Twenty one were accepted after a peer-review process and guest editors' decisions.

Keywords: Fog; Fog; Collection; Dew; Special issue.

Chemical Composition and Bacterial Community in Size-Resolved Cloud Water at the Summit of Mt. Tai, China

Chao Zhu1, Jianmin Chen 1,2,3, Xinfeng Wang1, Jiarong Li1, Min Wei1, Caihong Xu1, Xianmang Xu1, Aijun Ding3, Jeffrey L. Collett, Jr.4

Source: Aerosol and Air Quality research, Volume: 18 | Issue: 1 | Pages: 1-14; DOI: 10.4209/aaqr.2016.11.0493

A three-stage collector was used to collect size-resolved cloud samples at the summit of Mt. Tai. Subsequently, analyses of pH values, water-soluble ions, and trace metals were performed and bacterial community were conducted using MiSeq amplicon sequencing. The pH values of the samples decreased as droplet sizes decreased. Sulfate (SO42–), nitrate (NO3–) and ammonium (NH4+) were the main secondary inorganic ions which their concentration distributed significantly different from size-resolved cloud water. The NH4+ concentration was higher in smaller droplets. The SO42– and NO3– concentrations were higher in larger droplets. The Ca2+ concentration increased as droplet size increased. Small droplet samples tended to have lower pH value, mainly because of the more acidic (SO42– and NO3–) and less acid-neutralizing (NH4+ and Ca2+) components. The bacterial community in size-resolved cloud samples were firstly recognized and dominated by the genera of Lactococcus (average abundance 34.9%) and Bacillus (average abundance 34.0%). Linear discriminant analysis effect size (LEfSe) revealed differences of the bacterial community in size-resolved cloud water samples, which was probably caused by the bacterial size. Redundancy analysis suggested several minor correlations that the H2O2, NO2– concentrations, and trace metals exert effects on the bacterial community.

Keywords: Cloud sample; Three-stage collector; Chemical composition; Bacterial community.

Aqueous Secondary Organic Aerosol Formation in Ambient Cloud Water Photo-Oxidations

Misha I. Schurman 1,2, Alexandra Boris1, Yury Desyaterik1, Jeffrey L. Collett, Jr.1

Source: Aerosol and Air Quality research, Volume: 18 | Issue: 1 | Pages: 15-25, DOI: 10.4209/aaqr.2017.01.0029

The current understanding of aqueous secondary organic aerosol (aqSOA) formation is based largely on laboratory investigations of very simple surrogate cloud water solutions that aid mechanistic understanding of aqueous oxidation but may not accurately reflect the influence of the complex ambient matrix present in authentic cloud waters on organic chemistry. In this study, unaltered ambient cloud water and 'biogenically influenced' ambient cloud water (with added pinonic acid) were photo-oxidized, atomized, and dried to simulate the formation of aqSOA in clouds, then analyzed using an Aerodyne Aerosol Mass Spectrometer. Two major chemical regimes were identified: in the first, particle organic mass is gained, then lost; sustained increases in highly

oxidized fragments indicate overall organic acid formation, while increases in nominally volatile fragments suggest that evaporation may contribute to the observed mass decrease. In the second regime, the oxidation level of cloud water organic matter decreases as mass decreases, suggesting that oxidized functional groups are fragmented and lost to evaporation. Overall, the rate of aqSOA production in unaltered cloud water decreases as oxygenation increases, until organic mass loss beginning at consistent values of $f44 > 0.23 \pm 0.05$ and $O:C > 0.61 \pm 0.05$. We hypothesize that there may be a parameterizable 'maximum oxidation level' for cloud water above which functional group fragmentation is dominant. These experiments are among the first to quantify organic mass production in ambient cloud water and employ the most atmospherically relevant oxidant concentrations to date.

Keywords: Secondary organic aerosol; Cloud chemistry; Photooxidation; Aqueous.

Fog Spatial Distributions over the Central Namib Desert - An Isotope Approach

Kudzai Farai Kaseke1, Chao Tian1, Lixin Wang 1, Mary Seely2,3, Roland Vogt4, Theo Wassenaar3, Roland Mushi3

Source: Aerosol and Air Quality research, Volume: 18 | Issue: 1 | Pages: 49-61, DOI: 10.4209/aaqr.2017.01.0062.

Fog is a characteristic feature of the Namib Desert and is essential to life in this fog dependent system. It is often acknowledged that advective fog from the ocean is the dominant fog type over the Namib Desert fog-zone but recent evidence suggests that other fog types occur in this area. Knowledge of the existence and spatial distribution of different fog types will enhance the mechanistic understanding of fog formation and potential changes in this region, but such knowledge is limited in literature. In this study, we investigated fog spatial variations within the Namib Desert fog-zone by applying stable isotope ($\delta 18O$ and $\delta 2H$) techniques to differentiate various fog types and identify their source waters. Isotope based results showed that at least three types of fog (advective, radiation and mixed) occurred in this region and what appears as a single fog event may include all three types. Results suggest that radiation fog was the dominant fog type during our study period. The results also suggest that advective fog (with Atlantic Ocean origins) either dissipated 30–50 km inland and the residual humidity combined with locally derived moisture to form mixed fog or advective fog incorporated local moisture along its trajectory inland resulting in mixed fog. Fog in the Namib Desert was consistently depleted in 18O and 2H compared to rainfall and this was attributed to sub-cloud evaporation of the rainfall as well as different sources of fog and rainfall. Sub-cloud evaporation led to enrichment of 18O and 2H in rainfall beyond that of the first stage condensate, fog. Advective fog is often considered the architect of the fog-zone in the Namib Desert, but our results demonstrated multiple dominant fog types during the

study period, suggesting knowledge of both fog frequency and fog type is needed to better predict climate change impacts on the fog-zone.

Keywords: Advective; Climate change; Ecohydrology; Isotopes; Mixed; Radiation δ18O δ2H.

A Comparative Study on Fog and Dew Water Chemistry at New Delhi, India

Supriya Nath, Sudesh Yadav

Source: Aerosol and Air Quality research, Volume: 18 | Issue: 1 | Pages: 26-36,
DOI: 10.4209/aaqr.2017.01.0033.

Fog and dew, formed via different formation mechanisms, are suitable to study the liquid-gas-solid phase chemical interactions in the ambient atmosphere. A total of 24 fog and 19 dew samples were collected using Caltech Active Strand Cloud water Collector 2 and dew condensers, respectively, over New Delhi during winter months of 2014–15 and were characterised for pH and soluble inorganic ion using ion chromatograph. Dew samples were alkaline (pH = 6.26 ± 0.37) in comparison to natural rainwater pH of 5.6 and fog collected at rooftop (pH = 5.38 ± 1.3) and at ground level (pH = 5.96 ± 0.3). The volume weighted mean equivalents of cations followed the order $NH_4^+ > Ca^{2+} > Mg^{2+} \sim K^+ > Na^+$ and of anions as $SO_4^{2-} > NO_3^- \sim Cl^- > HCO_3^- > F^- > NO_2^-$ in fog whereas the order for dew was $Ca^{2+} > NH_4^+ > Na^+ > K^+ > Mg^{2+}$ and $SO_4^{2-} \sim HCO_3^- > Cl^- > NO_2^- > NO_3^- > F^-$. The Ca^{2+} ions were higher than NH_4^+ in dew while NH_4^+ was higher than Ca^{2+} in fog. Nitrite was higher in comparison to nitrate in dew while this was reverse in fog. Alkaline pH of dew samples might have played a role in the gas phase transfer and the base catalyzed transformation of NOx to HONO and subsequent dissolution of HONO in dew in comparison to fog. Acidity was caused more by sulphate ions (SO_4^{2-}/NO_3^- ratio was 2.2 and 4.18 for fog and dew, respectively) but was effectively neutralised. Neutralisation factors were different in fog ($NH_4^+ > Ca^{2+} > Mg^{2+}$) and dew ($Ca^{2+} > NH_4^+ > Mg^{2+}$). The differences in the fog and dew composition are primarily linked to their formation processes.The agricultural fields and fossil fuel combustion were sources for ammonium, sulphates, nitrate and nitrite whereas locally resuspended crustal materials added calcium and magnesium carbonates. Vehicular and plant emissions, biomass burning and the oxidation of volatile organic compounds seems to be responsible for higher organic acids in dew and fog.

Keywords: Neutralisation factors; Nitrite; Organic acids.

Fog Water Chemical Composition on Ailaoshan Mountain, Yunnan Province, SW China

Felix Nieberding 1, Bettina Breuer1, Elisa Braeckevelt1, Otto Klemm1, Qinghai Song2, Yiping Zhang2

Source: Aerosol and Air Quality research, Volume: 18 | Issue: 1 | Pages: 37-48, DOI: 10.4209/aaqr.2017.01.0060

Between December 2015 and March 2016, fog water was collected at the subtropical mountain cloud forest site Ailaoshan in SW China at 2476 m above mean sea level. An active fog collector was employed to collect 117 samples during more than 140 hours of fog, covering 6 major fog events. The chemical analysis included acidity and inorganic ion concentrations. The median pH values of the fog events varied between 3.7 and 4.2, characterizing the fog water as acidic (pH < 5.0) to very acidic (pH < 4.0). The ion composition was dominated by H+, NH4+, SO42– and NO3–, which made up more than 86% of the total ionic concentration (TIC). The generally rather high ion concentration levels cannot be explained by nearby emission sources but rather by long-range transport of air pollutants from various sources in East Asia. During one event on February 8, 2016, it is evident that it was the emissions from a large coal-fired power plant in Myanmar that led to high concentrations of sulphuric acid. This pilot study of fog chemistry in rural, mountainous SW China should be complemented by studies spanning the moist summer monsoon season and covering more chemical species.

Keywords: Fog chemistry; Acidic fog; Rural China; Ion loadings; Trajectories.

Characterization and Modeling of Fog in the Mexico Basin

Pohema González-Viveros1, Ernesto Caetano2, Fernando García-García 3

Source: Aerosol and Air Quality research, Volume: 18 | Issue: 1 | Pages: 79-90, DOI: 10.4209/aaqr.2016.12.0548.

The character of fog in a region centered at Mexico City International Airport was investigated using 10 years of historical data. Hourly surface observations, synoptic charts, satellite images and twice-a-day radiosondes were used to identify fog events under the influence of various synoptic and mesoscale features. A quantitative assessment on the likelihood of which mechanisms lead to fog formation was obtained. Also, three fog events (radiation, advection and frontal) were simulated with the Weather Research and Forecasting (WRF) model, and the results were compared to observations. The study included a comparison of the skills of different planetary boundary layer (PBL) and microphysical schemes. A sort of generalization cannot easily be applied, but allows one to determine which parameterizations performed better for each case in a high, tropical region. In general, from the model results for liquid water content, the cloud microphysics WSM3 and PBL Yonsei University schemes reproduced advection and frontal fog events quite well,

whereas CAM 5.1 and Quasi-Normal Scale Elimination schemes worked better for radiation fog episodes.

Keywords: Fog types; Fog modeling; Mexico; Basin WRF model.

A Fog Event off the Coast of the Hangzhou Bay during Meiyu Period in June 2013

Qian Wang1,2, Su-Ping Zhang 1,2, Qi Wang3, Zhao-Xi Meng4, Darko Koračin5,6, Shan-Hong Gao1,2

Source: Aerosol and Air Quality research, Volume: 18 | Issue: 1 | Pages: 91-102,
DOI: 10.4209/aaqr.2016.11.0489.

A dense fog with the visibility less than 100 m over 6 hours occurred around the Hangzhou Bay off the coast of the western part of the East China Sea on 24–25 June 2013 during Meiyu period. This study focuses on the physical mechanism involved in the fog process by using in-situ observations and model. The analysis indicates that the land-sea thermal contrast played an essential role in the fog episode, while a weak low-pressure wedge associated with the Meiyu front and the diurnal variation in temperature provided background conditions. Induced by the strong land-sea thermal contrast, a secondary circulation formed in the lower levels of the atmospheric boundary layer (ABL) over the coast. The southeasterly wind and subsiding motion associated with the secondary circulation contributed to the moisture supply and the lowering of the boundary layer, favoring fog formation and maintenance. The fog maintained until the weakening of the temperature gradient between land and sea, when the downward flow was replaced by upward motion controlled by the approaching of a low-pressure center. These results are helpful for improving coastal fog forecast in Meiyu period and for our understanding of mechanisms involved in coastal fog processes.

Keywords: Coastal fog; Land-sea thermal contrast; Meiyu period; Secondary circulation.

Combined Impact of Tropical Cyclones and Surrounding Circulations on Regional Haze-Fog in Northern China

Ziqi Cao1, Lifang Sheng 2,3, Qian Liu1, Yina Diao1,2, Wencai Wang1,2, Wenjun Qu2,3

Source: Aerosol and Air Quality research, Volume: 18 | Issue: 1 | Pages: 114-126,
DOI: 10.4209/aaqr.2016.12.0549.

Some haze-fog events in Asia have been attributed to tropical cyclone activity; however, uncertainty exists regarding the relationship between the influence of tropical cyclones and the occurrence of haze-fog events. In this study, the statistical relationship between tropical cyclones in the Northwest Pacific and the haze-fog events in northern China during summers from 2001 to 2012 were analyzed. It was found that 30.5% of regional haze-fog events were related to tropical

cyclones. The influence of tropical cyclones on haze-fog events was analyzed and compared based on classification of tropical cyclones by position and path. The results showed that tropical cyclones can form advantageous conditions for regional haze-fog events through dynamic and thermal processes, such as strengthening the downdraft, and increasing relative humidity and stability. The dynamic influence was dominant when the distance between a tropical cyclone and northern China was larger than the range of tropical cyclone airflow, and the contribution of thermal influence increased as the distance decreased. Furthermore, the surrounding circulations, such as the Northwest Pacific subtropical high and the westerly trough, also contributed to the regional haze-fog events. Their position, intensity and collocation with tropical cyclones could be the determining factors for haze-fog occurrence. This study illuminates the primary mechanisms of the combined effect of tropical cyclones and the surrounding circulations on regional air quality, which could improve forecasts of summer regional haze-fog events in northern China.

Keywords: Haze-fog; Tropical cyclone; Circulation; Northwest; Pacific subtropical high; Westerly trough.

ENSO Influence on Coastal Fog-Water Yield in the Atacama Desert, Chile

Camilo del Río 1,2, Juan-Luis Garcia1,2, Pablo Osses1,2, Nicolás Zanetta1,2, Fabrice Lambert1, Daniela Rivera1, Alexander Siegmund3,4, Nils Wolf4, Pilar Cereceda1,2, Horacio Larraín2, Felipe Lobos2

Source: Aerosol and Air Quality research, Volume: 18 | Issue: 1 | Pages: 127-144, DOI: 10.4209/aaqr.2017.01.0022.

Fog water represents an alternative, abundant and currently unexploited fresh water resource in the coastal Atacama Desert (~20°S). Here, the stratocumulus clouds meet the Coastal Cordillera, producing highly dynamic advective marine fog, a major feature of the local climate that provides water to a hyper-arid environment. One of the main issues that arises in harvesting fog water is our limited understanding of the spatial and inter-annual variability of fog clouds and their associated water content. Here we assess the role of regional-wide El Niño Southern Oscillation (ENSO) forcing on local inter-annual fog-water yields along the coast of Atacama. We contrast 17 years of continuous fog-water data, with local and regional atmospheric and oceanographic variables to determine the link between them and the inter-annual dynamics of fog in northern Chile. Sea surface temperature (SST) in ENSO zone 1 + 2 shows significant correlations with offshore and coastal Atacama SST, as well as with local low cloud cover and fog water yields, which go beyond the annual cycle beat, exposing a potential causal link and influence of ENSO on fog along the Atacama. On the inter-annual time scale, we found that when ENSO 3 + 4 zone SST, specifically during summer, overcome a > 1°C temperature threshold, they incite significantly higher summer fog water yields and explain 79% of the fog variability. Furthermore, satellite images displaying regional extent Sc cloud and fog presence during ENSO extremes reveal higher cloud abundance during El Niño at this latitude. However, 75% of the yearly fog water is collected during winter, and does not appear to be affected in a significant manner by Pacific oscillations. Thus, our results

suggest that the utilization of fog as a fresh water resource may be sustainable in the future, regardless of ENSO-induced variability in the region.

Keywords: Southeast Pacific (SEP); Stratocumulus cloud; Fog-water; El Niño Southern Oscillation (ENSO) Estación Atacama UC Oasis de Niebla Alto Patache.

Favourable and Unfavourable Scenarii of Radiative Fog Formation Defined by Ground-Based and Satellite Observation Data

Thierry Elias 1, Dominique Jolivet1, Marie Mazoyer2, Jean-Charles Dupont3

Source: Aerosol and Air Quality research, Volume: 18 | Issue: 1 | Pages: 145-164, DOI: 10.4209/aaqr.2017.01.0044.

An innovative set of six observed predictors of fog formation by radiative cooling is proposed, which describes: 1) one of the main processes of fog formation that is the water uptake by aerosols at surface level; 2) the fog development along the vertical up to 30 meters, as well as the cloud cover; and 3) the temporal evolution of the parameters describing the water uptake by aerosols and the cloud cover. The visibility is used as a signal of atmospheric and surface processes affecting the water uptake by aerosols. The vertical fog development is described by the vertical thermal gradient along a 30-m meteorological mast. The cloud cover is described using a ceilometer for low and middle clouds above the instrument, and satellite data for clouds in a pixel and in a larger 9 × 9-pixel region around the site. The set of predictors can be observed in operational conditions, such as on airport fields. Data acquired at the SIRTA platform (Paris, France) during two autumns and two winters were analysed, and the cloud cover classification derived from the SEVIRI instrument on the METEOSAT Second Generation satellite by the EUMETSAT/NWCSAF program was also utilized. The training data set was acquired in November 2011 while the validation data set extended over 12 months.

All situations were discriminated between favourable and unfavourable scenarii of radiative cooling fog formation, with a factor of 10 in probability. 246 moderate visibility events (with visibility between 5 and 10 km) were observed under a clear sky in 12 months at SIRTA. While developed fog formed according to one scenario, thin fog formed according to six scenarii. On the contrary to thin fog, developed fog did not form when cirrus clouds were observed above moderate visibility situations. The fog formation probability varied from 12 to 43%, and even reached 100% for one thin fog. As the training data set was acquired in autumn, the predictor set seems more appropriate to nowcast fog in humid autumn conditions, when the fog formation probability was multiplied by ∼2. The predictive set could be enriched by predictors proposed in literature, and tests suggest that relative humidity would improve the fog formation probability in winter. Five predictors identify 65 of the 217 no-fog events counted in 12 months, with ∼3 h anticipation time. If visibility decreased below 5 km, 88 additional no-fog events were identified. In this case, the formation probability was 35% for developed fog, and 24–60% for thin fog, but with an anticipation

time reduced to ~1.5 h. Only one fog, which represents 3% of the fog events, would be missed with such a predictive scheme.

Keywords: Fog; Ground-based, Satellite; Observation; Visibility; Formation; Probability.

Determination of Fog-Droplet Deposition Velocity from a Simple Weighing Method

Jackie Tav 1, Olivier Masson1, Frédéric Burnet2, Pascal Paulat1, Thierry Bourrianne2, Sébastien Conil3, Laurent Pourcelot1

Source: Aerosol and Air Quality research, Volume: 18 | Issue: 1 | Pages: 103-113,
DOI: 10.4209/aaqr.2016.11.0519

Fog water deposition can represent an important part of the atmospheric water, nutrient and pollutant inputs in specific areas such as mountainous or coastal regions (Shimadera et al., 2011). In order to determine the potential of fog water deposition on plants, a field experiment has been performed in the northeast of France to determine fog droplet deposition velocity on different types of plants. The main objective is to improve deposition models by enabling them to accurately account for water inputs from fog or low clouds at ground level.

The flux of deposited fog water was estimated by exposing plants to fog and weighing them with a precision balance. Contrary to other flux measurement methods, the weighing method is simple to set up. Three plant types (small conifers, grass and cabbages) plus bare soil were used as impaction and deposition surfaces. A Particulate Volume Monitor (PVM-100) provided the liquid water content (LWC) to calculate fog droplet deposition velocities, and a Fog Monitor (FM-120), the characterization of the droplet size distribution.

Two fog events with different features (visibility, LWC and droplet number) were compared with regard to deposition velocity.

When wind speed was below 4 m s–1, mean fog droplet deposition velocities ranged from less than 2.2 cm s–1 on bare soil to 40 cm s–1 on cypress. Thus, the impaction of fog droplets can be an important part of fog water deposition on plants.

Keywords: Atmospheric aerosols; Liquid water content; Fog; Droplets; Aerosol deposition; Measurement techniques; Leaf area index.

Impact of Natural and Anthropogenic Factors on Fog Frequency and Variability in Kraków, Poland in the Years 1966–2015

Anita Bokwa 1, Agnieszka Wypych1, Monika J. Hajto1,2

Source: Aerosol and Air Quality research, Volume: 18 | Issue: 1 | Pages: 165-177,
DOI: 10.4209/aaqr.2016.12.0580.

The aim of the study was to determine the long term variability of fog occurrence in Kraków in the light of the changeability of fog favoring factors. The annual number of days with several fog characteristics was studied for the period 1966–2015, using data from two meteorological stations located in the city center and in the suburbs. For all these data series on fog, a strong decrease was observed in the study period, i.e., the number of days with fog decreased on average by about 60%, with the tendency being more distinct in the city center. Fog favoring conditions were determined by atmospheric circulation, wind speed, relative humidity, urban heat island (UHI) and air pollution and correlated with data on fog. Results statistically significant at $p < 0.01$ show that the relationship is the strongest between fog frequency and air pollution. However, as the air pollution levels decreased, especially after the change of political and economic system in 1989, environmental factors became decisive in controlling fog occurrence. Although the role of atmospheric circulation in fog formation is unquestionable, fog favoring circulation types (Sa, SWa, Ca, Ka) show no meaningful tendency and no significant correlation with long-term fog occurrence frequency. Therefore, decreasing trends in days with low wind speed and in days with relative humidity RH ≥ 80% and RH ≥ 95% are considered as additional factors which contributed to the observed fog frequency decrease. UHI showed no impact on fog frequency as in Kraków relief modified UHI (RMUHI) is observed and no significant changes in the part of UHI defined for the lowest part of the city were observed.

Keywords: Fog; Air pollution; Atmospheric circulation; Relief modified urban heat island.

Role of Fog in Urban Heat Island Modification in Kraków, Poland

Anita Bokwa 1, Agnieszka Wypych1, Monika J. Hajto1,2

Source: Aerosol and Air Quality research, Volume: 18 | Issue: 1 | Pages: 178-187,
DOI: 10.4209/aaqr.2016.12.0581.

The impact of fog on relief modified urban heat island (RMUHI) in Kraków has been presented using fog observations at 06 UTC from two meteorological stations: a rural one (Balice, B) and an urban one (Botanical Garden, BG) from the period 2006–2015. Daily UHI magnitude for the valley floor for the same period was estimated as TminBG–TminB, while for the period 2010–2015, eight daily courses of UHI were available, for the urban areas in the valley floor and 50 m above it, together with air temperature inversion data. UHI data for days with various combinations of fog occurrence and weather conditions were compared using non-parametric statistical tests: Wald-

Wolfowitz test, Kolmogorov-Smirnov test and U Mann-Whitney test. Data of 2010–2015 were also the subject of cluster analysis (k-means method). Fog is an important factor decreasing UHI magnitude by about 1 K but mainly during weather conditions with little or no cloudiness and small wind speed or atmospheric calm, during anticyclonic synoptic situations, and only in the valley floor areas. With an increase in cloudiness and wind speed, the role of fog decreases and is similar in all parts of the city.

Keywords: Fog; Relief modified urban heat island; Atmospheric circulation; Cluster analysis.

PM10 Sampling and AOD Trends during 2016 Winter Fog Season in the Islamabad Region

Gufran Bulbul1, Imran Shahid1, Farrukh Chishtie 3,4, Muhammad Zeeshaan Shahid5, Rabia Ali Hundal1, Fatima Zahra1, Muhammad Imran Shahzad2

Source: Aerosol and Air Quality research, Volume: 18 | Issue: 1 | Pages: 188-199, DOI: 10.4209/aaqr.2017.01.0014

PM10 samples were collected during intensive fog days in Islamabad, Pakistan, to investigate the impact of particulate matter on fog formation. The PM10 concentrations were monitored at the Institute of Space Technology site using a high-volume air sampler and its elemental composition was studied using Scanning Electron Microscopy-Energy Dispersive Spectroscopy (SEM-EDS). Sampling was done for a duration of 24 hours on selected days, including all foggy days in a period from January 2016 to February 2016. The concentration of PM10 varied from 123 μg m−3 to 202 μg m−3 with an overall mean concentration of 177 μg m−3. On most occasions, PM10 levels were considerably high as compared to permissible limits of both Pak-NEQS and WHO guidelines. It has been observed that the air quality during fog days was much worse, with elevated levels of particulate matter observed during foggy days. The SEM- EDS revealed the presence of different elements including some metals Si, K, Ca, Mg, Zn, Fe, Cr, Pb, Al etc. The morphological studies suggest that most of the particles are crystalline in shape, suggesting their main source as soil. Some samples also showed round spherical shape which refers their anthropogenic source. The sun photometer observations of aerosol optical depth (AOD) and satellite observations from Aqua's Moderate-resolution Imaging Spectro-radiometer (MODIS) showed significant correlation. Moreover, elevated level of AOD were found during heavy fog days. The validated high satellite AOD were associated with high PM10 concentration during heavy fog days.

Keywords: Aerosol optical depth, Aerosol sampling and transport, Air pollution, PM10 Fog.

Fogs and Air Quality on the Southern California Coast

Alexandra J. Boris1, Denise C. Napolitano2, Pierre Herckes2, Andrea L. Clements1, Jeffrey L. Collett, Jr. 1

Source: Aerosol and Air Quality research, Volume: 18 | Issue: 1 | Pages: 224-239, DOI: 10.4209/aaqr.2016.11.0522

Fog acts as a reservoir and transport vector for chemicals in the atmosphere, altering the distribution of species between the gas and particle phases, and allowing deposition of nutrients and pollutants onto ecosystems and crops. Fog water and trace gas samples were collected from Casitas Pass along the Santa Barbara Channel in June 2015 to identify emissions sources and aqueous processes impacting Southern California air. Fog water composition was dominated by NH4+ (volume weighted mean, VWM = 232 μM, range = 85–640 μM), with lesser contributions from NO3– (126 μM, 30.4–778 μM) and SO42– (28.3 μM, 12.1–90.0 μM), pushing the VWM pH to 5.92 (5.34–6.67). Organic carbon contributed substantially to fog composition (8.27 mg C L–1, 4.70–16.8 mg C L–1). Carboxylic acids, products of aqueous oxidation, were abundant (20.1% of carbon mass on average), with > 1% contributions by acetate, formate, oxalate, malonate, succinate, and lactate. Sulfur- and nitrogen-containing organic species were detected, often after 3–5 hours of fog, suggesting aqueous formation. Sampled air was advected over the coastline near oil extraction operations, urban and agricultural areas; regional oil and natural gas processing and mobile sources were the most influential organic emissions at Casitas Pass. Fog composition in 2015 was contrasted with that from a study in July-September 1985/6. Concentrations of major fog constituents appear to have decreased in response to successful air quality regulations. While natural species concentrations in fog were similar (e.g., 2015 VWM [Na+] = 101 μM, range = < 30–320 μM; 1985/6 [Na+] = 129 μM, 12–1000 μM), anthropogenic species concentrations were lower in 2015 (e.g., 1985/6: [NO3–] = 236 μM, 141–2800 μM vs. 2015: 126 μM, 30.4–778 μM). These results overall highlight changes in Southern California air quality issues, including improvement of some anthropogenic emissions and the current influence of organic emissions from industrial and mobile sources.

Keywords: Fog chemistry; Aqueous atmospheric chemistry; Aqueous secondary organic aerosol; Organic sulfur; Organic nitrogen.

A Low Cost System for Detecting Fog Events and Triggering an Active Fog Water Collector

Peter Weiss-Penzias 1, Daniel Fernandez2, Robert Moranville1, Chad Saltikov1

Source: Aerosol and Air Quality research, Volume: 18 | Issue: 1 | Pages: 214-233, DOI: 10.4209/aaqr.2016.11.0508.

A simple method of activating the Caltech Active Strand Cloud-water Collector (CASCC) is described. This system detected the onset of wet deposition events associated with the advection of marine stratus clouds using an optical rain sensor (ORS) and a standard passive fog collector (SFC) in combination with a relative humidity threshold. The system was deployed on a rooftop between May 10 and September 20, 2016 (134 days) at the University of California, Santa Cruz, six km from Pacific Ocean, at 240 m elevation. Twenty-nine fog water samples (daily mean volume = 174 ± 71 mL) were collected for the purposes of quantifying the concentration of monomethylmercury (MMHg) and its possible marine origins. For 20 days during the study, a visibility sensor (VS) was collocated with the ORS and both sensors detected 7 fog events. The ORS detected 2 additional marine stratus drizzle events missed by the VS. The start time of the events detected by the ORS was delayed relative to the onset of visibility reduction in 6 of 7 events by 4.5 ± 3.3 hours. Low wind speeds at night at this location limited the wet deposition to the SFC. Average CASCC sampling time during these events was 6.2 ± 2.8 hours and 4 liquid samples were obtained (80 to > 275 mL). As a comparison, fog water collections at UCSC during the fog seasons of 2014 and 2015 yielded 35 and 12 samples, respectively using a trigger based on relative humidity (RH) and sampling times of > 12 h per day. The main benefit of triggering with the ORS in 2016 was to cut in half the sampling time without loss of sample collection volume. Mean MMHg concentrations between the 3 years were not significantly different suggesting that the SFC/ORS triggering system is appropriate for use at multiple fog collection sites simultaneously.

Keywords: Fog water collector; Activation mechanism; Visibility; Moisture detection; Deposition; Mercury.

Simplified Modeling and Analysis of the Fog Water Harvesting System in the Asir Region of the Kingdom of Saudi Arabia

Palanichamy Gandhidasan , Habib I. Abualhamayel, Faheemuddin Patel

Source: Aerosol and Air Quality research, Volume: 18 | Issue: 1 | Pages: 200-213
DOI: 10.4209/aaqr.2016.11.0481

Scarcity of fresh water is one of the greatest obstacles to achieve the sustainable development in the Kingdom of Saudi Arabia. About thirty desalination plants are built to satisfy the Kingdom needs. The Kingdom is in need of new unconventional water resources such as fog water harvesting system which will complement the existing water resources in the Asir region. This region is facing major challenges due to the flourishing tourism, irrigation in agriculture and rising living standards. Passive mesh type fog collector is analyzed in the current study to predict the rate of fog water collection by combining a physically based impaction and aerodynamic models. The results indicate that the greater volumes of water can be harvested from the fog associated with higher wind speeds, bigger sizes of fog droplet and higher liquid water content in the fog-laden winds with the threshold mesh shade coefficient of about 0.56. It is found that the aerodynamic efficiency has a significant impact on the overall fog collection efficiency compared to the impaction efficiency. The

model shows that for the fog droplet size of 30 μm with the wind speed of 4 m s–1, it is possible to collect the fog water at the rate of 0.65 to 9.7 L m–2 per hour when the liquid water content (LWC) in the fog varies from 0.2 to 3 g m–3, respectively.

Keywords: Fog harvesting; Passive artificial mesh type fog collector; Impaction and aerodynamic models; Optimum shade coefficient; Overall fog water collection efficiency.

A Case Study on Fog/Low Stratus Occurrence at Las Lomitas, Atacama Desert (Chile) as a Water Source for Biological Soil Crusts

Lukas W. Lehnert 1, Boris Thies1, Katja Trachte1,2, Sebastian Achilles1, Pablo Osses3, Karen Baumann4, Jakob Schmidt1, Elena Samolov5, Patrick Jung6, Peter Leinweber4, Ulf Karsten5, Burkhard Büdel6, Jörg Bendix1

Source: Aerosol and Air Quality research, Volume: 18 | Issue: 1 | Pages: 254-269
DOI: 10.4209/aaqr.2017.01.0021.

The Atacama Desert is well known for the high occurrence of large-scale fog (spatial extents: hundreds of kilometers) emerging as low stratus (LST) decks over the Pacific Ocean. By contrast, the small-scale and heterogeneous occurrence of small-scale fog (hundreds of meters) particularly during summers is widely unconsidered. However, these events are important for the local vegetation and particularly for the biological soil crusts (BSC) that are widely distributed in this extreme ecosystem. Consequently, a case study in a typical fog oasis in the Pan de Azúcar National Park was conducted to test the feasibility combining field measurements, drone profiling, remote sensing and numerical modeling (i) to investigate fog-type specific differences regarding dynamics, physical properties and formation, (ii) to test the applicability of remote sensing technology for fog monitoring based on existing low-resolution and a proposed new high-resolution product and (iii) to estimate the related fog water input to BSCs. Two types of fog were observed. The well-known fog/LST deck emerging from the Pacific Ocean with high water path and large spatial extent was the first type. Fog of the second type was patchier, small-scale and not necessarily connected to the LST over the ocean. Instead, fog formation of the second type was related to thermal breeze systems, which produced shallow clouds containing less water than those of type 1. In general, such small-scale fog events were not captured well by existing remote sensing products but could be detected with the proposed new high-resolution product which provided promising results. Both fog types were important water resources for the BSCs, with approximately 8% to 24% of the fog water flux available to the BSCs at the surface. The results indicated the feasibility of the proposed methods' pool to estimate the water budget of BSCs with a high spatial resolution in the future.

Keywords: Orographic fog; Landsat WRF-modeling; Biological soil crusts; Vertical fog droplet spectra.

Testing Water Yield, Efficiency of Different Meshes and Water Quality with a Novel Fog Collector for High Wind Speeds

Christian Schunk 1, Peter Trautwein2, Herbert Hruschka2, Ernst Frost2, Leslie Dodson3, Aissa Derhem4, Jamila Bargach4, Annette Menzel1,5

Source: Aerosol and Air Quality research, Volume: 18 | Issue: 1 | Pages: 240-253, DOI: 10.4209/aaqr.2016.12.0528.

Fog harvesting techniques for water collection have been implemented successfully worldwide for several decades. However, at locations with high wind speeds, traditional installations require high maintenance efforts endangering the sustainability of projects. Furthermore, the efficiency of fog collection meshes and the water quality in the field are key questions for the implementation of large-scale facilities. This study presents a novel, durable fog collector design and investigates the yield (fog + rain) and inorganic water quality of different potential collection meshes at a test site in Morocco. The pilot facility proved very reliable with only minimal maintenance required. Rankings of the efficiency of different fog nets were set up, with monofilaments and three-dimensional structures tending to show higher yields than woven fabrics such as the traditional 'Raschel' mesh. However, differences from fog event to fog event could be identified. Water quality was better than that of local wells and met WHO guidelines, except for the 'first flush' just after the start of fog events.

Keywords: Fog collection; Mesh; Collector; Water quality.

Fog Water Collection Effectiveness: Mesh Intercomparisons

Daniel M. Fernandez 1, Alicia Torregrosa2, Peter S. Weiss-Penzias3, Bong June Zhang4, Deckard Sorensen4, Robert E. Cohen5, Gareth H. McKinley5, Justin Kleingartner5, Andrew Oliphant6, Matthew Bowman1

Source: Aerosol and Air Quality research, Volume: 18 | Issue: 1 | Pages: 270-283, DOI: 10.4209/aaqr.2017.01.0040.

To explore fog water harvesting potential in California, we conducted long-term measurements involving three types of mesh using standard fog collectors (SFC). Volumetric fog water measurements from SFCs and wind data were collected and recorded in 15-minute intervals over three summertime fog seasons (2014–2016) at four California sites. SFCs were deployed with: standard 1.00 m2 double-layer 35% shade coefficient Raschel; stainless steel mesh coated with the MIT-14 hydrophobic formulation; and FogHa-Tin, a German manufactured, 3-dimensional spacer fabric deployed in two orientations. Analysis of 3419 volumetric samples from all sites showed strong relationships between mesh efficiency and wind speed. Raschel mesh collected 160% more fog water than FogHa-Tin at wind speeds less than 1 m s–1 and 45% less for wind speeds greater than 5 m s–1. MIT-14 coated stainless-steel mesh collected more fog water than Raschel mesh at all wind speeds. At low wind speeds of < 1 m s–1 the coated stainless steel mesh collected 3% more

and at wind speeds of 4–5 m s–1, it collected 41% more. FogHa-Tin collected 5% more fog water when the warp of the weave was oriented vertically, per manufacturer specification, than when the warp of the weave was oriented horizontally. Time series measurements of three distinct mesh across similar wind regimes revealed inconsistent lags in fog water collection and inconsistent performance. Since such differences occurred under similar wind-speed regimes, we conclude that other factors play important roles in mesh performance, including in-situ fog event and aerosol dynamics that affect droplet-size spectra and droplet-to-mesh surface interactions.

Keywords: Fog mesh Fog water collection efficiency Raschel mesh Hydrophobic coating

---

Design and Performance Evaluation of a PN1 Sensor for Real-Time Measurement of Indoor Aerosol Size Distribution

Junho Hyun[1], Jangseop Han[2], Sang-Gu Lee[1], Jungho Hwang [1,2]

Source: Aerosol and Air Quality research, Volume: 18 | Issue: 2 | Pages: 285-300,
DOI: 10.4209/aaqr.2017.08.0263.

Airborne particulate matter is an important factor in the quality of an indoor environment. In this study, a miniaturized particle sensor was developed to detect submicron-sized aerosols based on number counting. This particle number (PN) sensor was designed and fabricated for real-time measurement of total aerosol number concentration and geometric mean diameter. The sensor (hereafter called as PN1 sensor) comprised a particle-classification unit, a particle-charging unit, and a particle-detection unit. After integrating all the three units, the total number concentration and the geometric mean diameter of test aerosol particles were determined and the results were compared with those obtained using commercial instruments. First, the PN1 sensor was compared with a condensation particle counter (CPC) in lab-test. For this, different groups of monodisperse sodium chloride particles between 20 and 700 nm in diameter were used. Then the PN1 sensor was compared with a scanning mobility particle sizer (SMPS) and an aerodynamic particle sizer (APS). For this, the PN1 sensor data were obtained by varying the combination of two corona voltage and test particles (sodium chloride and polystyrene latex) size distribution. In addition to lab-test, field test was carried out with indoor aerosols in different places. The number concentration and geometric mean diameter of indoor aerosols were measured by PN1 sensor and compared with SMPS data. The number concentration was also compared with the results of CPC and Pegasor AQ Indoor (Pegasor, Finland) measurements.

Keywords: PN1 sensor; Virtual impactor; Corona charger; Aerosol electrometer; Particle size distribution.

Characterization of PM10 and PM2.5 Source Profiles of Fugitive Dust in Zhengzhou, China

Nan Jiang, Zhe Dong, Yuanqian Xu, Fei Yu, Shasha Yin, Ruiqin Zhang , Xiaoyan Tang

Source: Aerosol and Air Quality research, Volume: 18 | Issue: 2 | Pages: 314-329
DOI: 10.4209/aaqr.2017.04.0132

As a result of rapid urbanization, the road lengths and built-up areas in Zhengzhou are steadily expanding along with increasing fugitive dust emissions. Identifying the physical and chemical characteristics and the chemical profiles of fugitive dust is important in achieving effective atmospheric pollution management. In this study, soil dust, road dust (RD), building demolition dust, and cement (CE) were chosen as the research objects. A total of 94 dust samples were collected from 20 sites. PM2.5 (particulate matter with diameter ≤ 2.5 μm) and PM10 (particulate matter with diameter ≤ 10 μm) samples were obtained by using a re-suspension device and their physical and chemical properties were analyzed. The scanning electron microscopy of four types of dust particles showed that most of the dust particles presented an irregular shape. In terms of particle size distribution, the mass concentration of PM2.5 accounted for less than 10% of the total PM10, whereas the number concentration of PM2.5 accounted for more than 96% of the total number. Chemical component analysis revealed that crustal elements such as Al, Mg, Fe, and K were abundant in all samples, and they were the most abundant species in PM2.5 and PM10 in the reconstruction results. The percentage of NO3– in the RD sample was higher than that in the other three fugitive dust samples because of the influence of vehicles. Furthermore, the CE sample had higher SO42– and Ca2+ percentages than the other three types of fugitive dust samples. Enrichment factor analysis showed that the significant enrichment of Cd and Ag was mainly caused by anthropogenic sources. The coefficients of divergence values between the profiles for different sites of dust ranged from 0.21 to 0.68, indicating the fugitive dust profiles from various sites mostly different. The chemical profiles of four dust sources obtained from this study is limited in Zhengzhou.

Keywords: Scanning electron microscope; Size distribution; Chemical profile; Coefficient of divergence; Enrichment factor.

Identification and Chemical Characteristics of Distinctive Chinese Outflow Plumes Associated with Enhanced Submicron Aerosols at the Gosan Climate Observatory

Xiaona Shang1, Meehye Lee 1, Jihyun Han1, Eunha Kang2, Sang Woo Kim3, Örjan Gustafsson4, Limseok Chang5

Source: Aerosol and Air Quality research, Volume: 18 | Issue: 2 | Pages: 330-342
DOI: 10.4209/aaqr.2017.03.0115.

From October till November in 2010 and during March of 2011, when Chinese outflow events were frequently encountered, the chemical composition of submicron particles (PM1.0) was determined hourly using a particle-into-liquid sampler at the Gosan Climate Observatory. Three distinctive pollution plume types were identified: haze aerosols impacted by biomass combustion, nanoparticle bursts associated with outflow from Beijing, and saline soil particles from salt deposits. The highest PM1.0 concentration was observed in a fall haze event, under near-stagnant high-pressure synoptic conditions that were characterized by the lowest visibility (< 5 km) and the highest K+ and OC concentrations, indicating the influence of biomass combustion. When strong high-pressure systems develop in China, they efficiently export fresh urban emissions from Beijing to the study region, as distinguished by nanoparticle bursts of > 104 cm–3 with highly elevated SO2 levels, even during the night. When air masses move rapidly from northeastern China to Gosan under strong wind conditions, the Ca2+ concentration, along with that of Cl– and Na+, is enhanced in PM1.0, which is attributed to the influence of saline transport from dry lakes. The results of this study reveal compositional details and information on both number and mass concentration for different PM1.0 plumes from anthropogenic and natural sources, all of which are associated with different kinds of Chinese outflow events.

Keywords: Submicron particles; Particle-into-liquid sampler; Chinese outflow plume; Haze Gosan.

Characteristics, Sources, and Health Risk Assessment of Trace Elements in PM10 at an Urban Site in Chengdu, Southwest China

Xin Cheng1,2, Yi Huang 1,2, Shi-Peng Zhang2, Shi-Jun Ni1,2, Zhi-Jie Long2

Source: Aerosol and Air Quality research, Volume: 18 | Issue: 2 | Pages: 357-370,
DOI: 10.4209/aaqr.2017.03.0112.

To investigate trace element pollution of PM10 in urban Chengdu, a Southwest megacity of China, as well as to assess the human health risks caused by exposure to PM10, we analyzed ambient PM10 samples collected at an urban site in Chengdu from November, 2014 to October, 2015. The annual mean concentration of PM10 in the sampling period was 173.6 ± 77.9 μg m–3, which is 2.5 times higher than the national recommended standard of 70 μg m–3. The mean metals content in PM10 was in the following order: iron (Fe) > zinc (Zn) > titanium (Ti) > copper (Cu) > manganese (Mn) > lead (Pb) > barium (Ba) > chromium (Cr) > strontium (Si) > nickel (Ni) > arsenic (As) > vanadium (V) > antimony (Sb) > cobalt (Co) > cadmium (Cd) > bismuth (Bi). The concentration of As in PM10 was observed to be 2.9 times higher than the secondary level recommended by the China National Ambient Air Quality Standard (GB3095-2012), whereas the concentrations of other metals were within the limit. Enrichment factor analysis indicated that As, Pb, Zn, Cu, Cd, and Sb mainly originated from anthropogenic sources. Five factors were identified by positive matric factorization (PMF) model. The sources identified were soil dust (48.4%), road dust (19.4%), fossil fuel combustion (14.9%), electroplating industry (13.8%), and metallurgy industry (3.5%). Particle

morphology and chemical composition analysis revealed six major particle types, namely aluminosilicate, sulfur-containing, carbon-containing, chlorine-containing, biomass burning, and metal particles. The results of the health risk assessment indicated that Cr can be carcinogenic to both children and adults, and other trace elements were determined to be below the legislation threshold (Environmental Protection Agency limit values), except for As, which was observed to be above the threshold.

Keywords: PM10; Trace elements; Seasonal variation; Source apportionment; Health risk.

Ground-Level NO2 in Urban Beijing: Trends, Distribution, and Effects of Emission Reduction Measures

Nianliang Cheng1,2,3, Yunting Li 2, Feng Sun2,4, Chen Chen2,4, Buying Wang2,5, Qian Li2,4, Peng Wei3, Bingfen Cheng 1,3

Source: Aerosol and Air Quality research, Volume: 18 | Issue: 2 | Pages: 343-356,
DOI: 10.4209/aaqr.2017.02.0092.

The characteristic of nitrogen dioxide (NO2) concentrations, including the long-term trends, spatial distribution, and effects of emission reduction measures-particularly those related to traffic management-were analyzed in Beijing by multimethods. The annual mean concentration of NO2 in Beijing decreased significantly from 71.0 μg m−3 in 2000 to 49.0 μg m−3 in 2008 while it fluctuated between 49.0 and 58.0 μg m−3 and decreased slightly from 2008 to 2015. Unfavorable diffusion conditions could increase NO2 concentrations while emission reduction measures especially the reduced vehicle NOx emissions could decrease NO2 concentrations significantly. The observed mean concentration of NO2 was 54.47 ± 7.71 μg m−3 from 2013 to 2015, while it changed to 94.62 ± 7.99 μg m−3 for 149 heavily polluted days. The NO2 concentration was lower in the northern and western regions and higher in the urban and southern areas in Beijing. After the implementation of air quality assurance measures (particularly traffic management) during the Asia-Pacific Economic Cooperation Summit (APEC, 1–12 November, 2014) and the Parade on the 70th Victory Memorial Day for the Chinese People's War of Resistance against Japanese Aggression (PARADE, 20 August–3 September, 2015), the mean NO2 concentrations during the APEC summit and PARADE decreased 46.2% and 39.5% respectively compared with those before and after these major activities while diurnal NO2 peaks decreased 24.5%–85.3% and 4.1%–70.8%, respectively during the APEC summit and PARADE period. To decrease NO2 concentrations, a high level of commitment must be given to promote coordinated regional air pollution prevention and control mechanisms in Beijing and its surrounding areas.

Keywords: NO2; Spatiotemporal distribution; Beijing; Mega events; Vehicle population; Odd-and-even license.

Distribution and Source of Chemical Elements in Size-Resolved Particles in Zhengzhou, China: Effects of Regional Transport

Shenbo Wang, Qishe Yan, Fei Yu, Qun Wang, Liuming Yang, Ruiqin Zhang, Shasha Yin

Source: Aerosol and Air Quality research, Volume: 18 | Issue: 2 | Pages: 371-385,
DOI: 10.4209/aaqr.2017.04.0126.

To investigate the characteristics of elements in size-segregated atmospheric particulates, samples were collected using a 14-stage electrical low-pressure impactor (ELPI+) at an urban site in Zhengzhou from October 1 till 25, 2016, and analyzed for 25 elements. Results show that crustal elements were concentrated in coarse particles and toxic elements were concentrated in ultra-fine particles. The size distributions of Na, Mg, Al, Si, Ca, Fe, Ti, S and Cl were uni-modal with dominant peaks in the size range of 1.43–2.14 μm or 0.295–0.487 μm. K, P, Mn and Ba exhibited bimodal distributions, and the remaining elements showed multimodal distributions. Enrichment factor, correlation and principal component analyses indicated that vehicles were the dominant source of particles. Biomass burning, coal combustion and dust also contributed to the accumulation of particles. The elemental concentrations affected by different air masses are discussed to investigate the effects of regional transport. An increase in elemental concentrations related to vehicle and coal sources was observed when air masses came from eastern areas. Furthermore, air masses from the southeast could be a major factor in air pollution for Zhengzhou during special times, such as periods of biomass burning or naked cropland. When air masses came from the northwest, the majority of elements from dust and coal combustion were lower in concentration compared with clean days, while elements originating from vehicle emissions increased.

Keywords: Particle; Element; Size distribution; Principal component analysis; Regional transport.

Characteristics of Pollutants and Boundary Layer Structure during Two Haze Events in Summer and Autumn 2014 in Shenyang, Northeast China

Xiaolan Li, Yangfeng Wang, Hujia Zhao, Ye Hong, Ningwei Liu, Yanjun Ma

Source: Aerosol and Air Quality research, Volume: 18 | Issue: 2 | Pages: 386-396
DOI: 10.4209/aaqr.2017.03.0100.

The characteristics of pollutants and the boundary-layer structure during two haze events in the summer and autumn of 2014 in Shenyang, Northeast China, were comparatively analyzed by using measurements of the mass concentrations of PM10, PM2.5, O3, NO2, SO2, and CO; vertical profiles of meteorological parameters from a 100-m high tower; and radiosonde data. The results showed that PM concentrations increased rapidly during the two haze events, resulting in visibility that decreased to 1400 and 405 m, respectively. The weak haze event on 16 June was characterized by

high O3 but low NO2 mainly due to the photochemical reaction, while all the pollutants increased during the severe haze event on 31 October, which was affected by pollutant emissions and meteorological conditions. The PM2.5 concentration had a good correlation with friction velocity (u*) but did not have an obvious relationship with , which means that the haze events were largely affected by the dynamic effect of turbulence and less so by its thermal effect. According to the radiosonde data, a single inversion layer with an inversion intensity of 1.6°C/100 m existed during the weak haze event, whereas double inversions and even more occurred during the severe haze event, with the inversion intensity larger than 2–4°C/100 m. Such stable atmospheric conditions favored the accumulation of pollutants. Backward trajectory analyses showed that the weak haze event was probably caused by pollutant transport from North China, whereas the severe haze event was generated mostly by local pollutants.

Keywords: Haze event; Boundary layer structure; Pollutant concentration; Northeast; China.

Seasonal Characteristics of Black Carbon Aerosol and its Potential Source Regions in Baoji, China

Bianhong Zhou1,2, Qiyuan Wang 2, Qi Zhou1, Zhangquan Zhang1, Gehui Wang2, Ni Fang1, Meijuan Li1, Junji Cao2,3

Source: Aerosol and Air Quality research, Volume: 18 | Issue: 2 | Pages: 397-406,
DOI: 10.4209/aaqr.2017.02.0070.

Continuous measurements of black carbon (BC) aerosol were made at a midsized urban site in Baoji, China, in 2015. The daily average mass concentrations varied from 0.6 to 11.5 μg m−3, with an annual mean value of 2.9 ± 1.7 μg m−3. The monthly variation indicated that the largest loading of BC occurred in January and the smallest in June. The mass concentrations exhibited strong seasonality, with the highest occurring in winter and the lowest in summer. The large BC loadings in winter were attributed to the increased use of fuel for domestic heating and to stagnant meteorological conditions, whereas the low levels in summer were related to the increase in precipitation. BC values exhibited similar bimodal diurnal patterns during the four seasons, with peaks occurring in the morning and evening rush hours and an afternoon trough, which was associated with local anthropogenic activities and meteorological conditions. A potential source contribution function model indicated that the effects of regional transport mostly occurred in spring and winter. The most likely regional sources of BC in Baoji were southern Shaanxi province, northwestern Hubei province, and northern Chongqing during spring, whereas the northeastern Sichuan Basin was the most important source region during winter.

Keywords: Black carbon aerosol; Seasonal characterization; Diurnal variation; Potential source region.

Gas- and Water-Phase PAHs Emitted from a Single Hydrogen-Oxygen PEM Fuel Cell.

Kuo-Lin Huang 1, Tsung-Hsuan Tsai1, Shui-Jen Chen1, How-Ran Chao1, Yi-Ming Kuo2, Jen-Hsiung Tsai1

Source: Aerosol and Air Quality research, Volume: 18 | Issue: 2 | Pages: 433-443,
DOI: 10.4209/aaqr.2017.10.0410.

This study focuses on the comparison between gas- and water-phase polycyclic aromatic hydrocarbons (PAHs) emitted from a single hydrogen–oxygen proton exchange membrane (PEM) fuel cell (FC) at different flowrates and temperatures. The results show that among 21 PAHs, the most and least dominant species were Nap and BeP, respectively. At 65°C, the concentrations of individual gas- and water-phase PAHs decreased with increasing flowrate, and the PAH concentrations were lower at the anode than those at the cathode. The concentrations of gas-phase Total-PAHs and Total-BaPeq were slightly lower at 65°C than those at 90°C, but an opposite trend was observed for water-phase ones. The temperature influenced water-phase PAH concentration profiles more than gas-phase ones, and the gas- and water-phase PAHs had different concentration profiles. The performance of membrane-electrode assembly (MEA) decreased with increasing flowrate or temperature. The emission factor (EF) sum (anode + cathode) for gas- or water-phase Total-PAHs increased with increasing flowrate. This tendency was also true for gas-phase Total-PAHs EFs but not for water-phase ones when raising the temperature from 65°C to 90°C. At 65°C and 52/35 sccm, the EF sums of water-phase Total-PAHs and Total-BaPeq were 2.18 ± 0.04 and 0.09 ± 0.00 μg g-MEA–1, respectively—smaller than those of gas-phase ones (3.02 ± 0.09 and 0.12 ± 0.00 μg g-MEA–1, respectively). More environmental concern should be directed at emitted gas-phase PAHs than at water-phase ones because the anode and cathode water effluents are usually recycled during PEMFC operations.

Keywords: Polycyclic aromatic hydrocarbon, Proton exchange membrane fuel cell, Emission factor.

Characterization of Polychlorinated Dibenzo-p-dioxins and Dibenzofurans of the Flue Gases, Fly Ash and Bottom Ash in a Municipal Solid Waste Incinerator

Yen-Kung Hsieh1, Wei-Sheng Chen 1, Jinning Zhu 2, Qianli Huang3

Source: Aerosol and Air Quality research, Volume: 18 | Issue: 2 | Pages: 421-432,
DOI: 10.4209/aaqr.2017.12.0564.

The emissions factors of PCDD/Fs from the stack flue gas, bottom ash and fly ash of a municipal solid waste incinerator (MSWI) were analyzed in this study. The congner profiles of PCDD/F mass

were dominant in OCDD and OCDF; however, those of PCDD/Fs-TEQ were mainly 2,3,4,7,8-PeCDF and 1,2,3,7,8-PeCDD in all samples. The PCDD/F emission factors of MSWI per metric ton of waste incinerated from the stack flue gas, bottom ash and fly ash were at an averaged of 0.0919, 7.20 and 12.8 μg PCDD/Fs-WHO2005-TEQ ton–1, respectively. Futhermore, the emission factor of MSWI in the unit of electricity produced averaged 0.185, 14.5 and 26.3 μg PCDD/Fs-WHO2005-TEQ (MWh)–1, respectively. As the results shown in this study, the majority of total PCDD/Fs-WHO2005-TEQ were mainly in both bottom ash and fly ashes. From long-term perspective, the disposal of both bottom and fly ashes should pay more attention to this issue. The results of this study provide useful information for both further studies and environmental control strategies aimed at persistent organic compounds (POPs).

Keywords: PCDD/Fs Municipal solid waste incinerator Fly ash Bottom ash Flue gas.

Sensitivity Analysis of PM2.5-Bound Total PCDD/Fs-TEQ Content: In the Case of Wuhu City, China

Weiwei Wang1, Kangping Cui 1, Rong Zhao1, Jinning Zhu 1, Qianli Huang1, Wen-Jhy Lee1,2

Source: Aerosol and Air Quality research, Volume: 18 | Issue: 2 | Pages: 407-420,
DOI: 10.4209/aaqr.2017.11.0507.

During 2015–2017, the atmospheric PM2.5, PM2.5/PM10, PCDD/Fs, PCDD/F phase distribution and PM2.5-bound total PCDD/Fs-WHO2005-TEQ content in Wuhu and Bengbu were investigated in this study. In addition, the sensitivity analysis for PM2.5-bound total PCDD/Fs-WHO2005-TEQ of Wuhu was also studied. During 2015–2017, the three-year average PM2.5 concentration in Wuhu was 53.0 μg m–3, and in Bengbu was 61.4 μg m–3; the results also showed the annual average PM2.5 concentrations of these two cities had declined, but the levels were still far above the WHO annual PM2.5 standard (10 μg m–3). In addition, in Wuhu, the PM2.5-bound total PCDD/Fs-WHO2005-TEQ contents in summer (0.166 ng-WHO2005-TEQ g–1) were approximately only 68.8% in magnitude lower than the average value of other three seasons (0.532 ng-WHO2005-TEQ g–1), and that of Bengbu in summer (0.187 ng-WHO2005-TEQ g–1) was approximately 66.7% in magnitude lower than the average value of other three seasons (0.561 ng-WHO2005-TEQ g–1). Sensitivity analysis showed that the PCDD/F concentration was the most positively correlated sensitive factor for PM2.5-bound total PCDD/Fs-WHO2005-TEQ, and when ΔP/P was changed from 0% to +50%, ΔS/S responded from 0% to +106%. The second positively correlated sensitive factor was PM10 concentration, and when ΔP/P was changed from 0% to +50%, ΔS/S responded from 0% to +72%. This was followed by atmospheric temperature, and its effect was negatively correlated, when ΔP/P was changed from –50% to +50%, ΔS/S responded from +73% to –112%. The last sensitive parameter was PM2.5 concentration, with the impact divided into two stages: when ΔP/P was changed from 0% to+70%, ΔS/S responded from 0% to +33%, but when ΔP/P was changed from +70% to +100%, ΔS/S responded from +33% to +25%.The results of this study provide useful information that can be used to achieve more insights into both atmospheric PM2.5 and PCDD/Fs.

Keywords: PM2.5; PM10; PCDD/Fs Phase distribution; Sensitivity analysis.

Variation of Bacterial and Fungal Community Structures in PM2.5 Collected during the 2014 APEC Summit Periods

Pengrui Du1, Rui Du 1, Zedong Lu1, Weishan Ren1, Pingqing Fu2

Source: Aerosol and Air Quality research, Volume: 18 | Issue: 2 | Pages: 444-455,
DOI: 10.4209/aaqr.2017.07.0238.

The biological fraction of PM2.5 is considered to be a major cause of various allergies and respiratory diseases. Nonetheless, differences in bacterial and fungal communities in PM2.5 under different air quality conditions are not well known. In the present study, we collected PM2.5 samples from October 15, 2014 to November 12, 2014 when several successive "Asia-Pacific Economic Cooperation (APEC) blue" days were recorded, following the implementation of strict emission control measures to ensure the APEC summit held during November 5–11, 2014 in Beijing. This study analyzed bacteria and fungi in PM2.5 samples through rRNA gene high-throughput sequencing. In total, 690 genera of bacteria and 229 genera of fungi were detected. The variations of species richness and community diversity of bacteria and fungi in PM2.5 were not affected significantly by the emission control measures adopted during the summit and different air quality levels. The bacterial and fungal community structures in PM2.5 collected during the summit exhibited over 83.7% and 79.6% similarities respectively, with PM2.5 collected from air graded as "good" quality (AQI ≤ 100) before the APEC summit. Bacteria and fungi in PM2.5 samples collected at AQI levels between 101–200 and 201–300 before the APEC summit had more than 73.4% and 76.3% community structure similarity, respectively, with PM2.5 samples collected at AQI ≤ 100. The difference between day and night PM2.5 samples was very small for bacterial and fungal community structures. Furthermore, most of the inhalable bacteria and fungi were nonpathogenic and no a clear relationship between air quality levels and pathogens was observed. Our results showed that bacteria and fungi in PM2.5 were less affected by emission control measures and different air quality levels. However, due to the limited number of samples, the relationship between air pollution levels and airborne bacteria and fungi still needs further study.

Keywords: APEC Emission control, Bioaerosols, PM2.5, AQI.

PM2.5 Meets Blood: In vivo Damages and Immune Defense

Xiangyu Zhang1, Jingjing Kang2, Haoxuan Chen1, Maosheng Yao 1, Jinglin Wang 2

Source: Aerosol and Air Quality research, Volume: 18 | Issue: 2 | Pages: 456-470,
DOI: 10.4209/aaqr.2017.05.0167.

Recent evidence shows that inhaled PM2.5 can enter the blood circulatory system and even the brain. However, the damage of blood-borne PM2.5 is not clearly elucidated. This work aims to understand and characterize the toxicity, i.e., the acute health effects, of PM2.5 that is directly injected into the blood circulatory system. Rats were injected with different dosages (568, the equivalent of 1 year of inhalation for a rat; 93; and 9.3 μg) of PM2.5 sampled from Beijing via a sterile catheter injected into the jugular vein. The behaviors of the rats upon external interruptions were recorded. Blood samples were collected before exposure and 1 h, 3 days, 5 days, 7 days, and 9 days after the PM2.5 injection for analyzing serum interleukin-6 (IL-6), C-reactive protein (CRP), tumor necrosis factor-α (TNF-α), endotoxin, and 8-hydroxydeoxyguanosine (8-OHdG) levels. After euthanization, the heart, lung, liver, kidney, and spleen were taken and processed for histopathological analysis. PM2.5 components were also analyzed. Acute inflammation with 102% and 90% increases for IL-6 and CRP, respectively, was observed 1 h after the 568 μg-PM2.5 injection, while oxidative DNA damage occurred only five or more days later, which was accompanied by significantly elevated endotoxin levels. Hemorrhage of lung alveoli and behavioral changes, including fear and non-responsiveness, were also observed. Surprisingly, all exposed rats seemingly survived the PM2.5 injection, behaving similarly to the control groups. The immune defense might have played an important role in combating the PM2.5 injection. The results showed acute health effects from directly injected PM2.5, including rapid inflammation, oxidative damage, and routine-behavioral changes. Further study about the long-term effects of injection and the immune defense is warranted. Nonetheless, the results here suggest that PM2.5 health effects may have to some extent been exaggerated in the literature.

Keywords: Air pollution; Venous injection; Inflammation; Oxidative stress; Catheter-buried rat model.

Impact of Dust Storms on NPAHs and OPAHs in PM2.5 in Jinan, China, in Spring 2016: Concentrations, Health Risks, and Sources

Pan Jiang1, Lingxiao Yang 1,3, Xiangfeng Chen4, Ying Gao2, Yanyan Li1, Junmei Zhang1, Tong Zhao1, Hao Yu2, Wenxing Wang1

Source: Aerosol and Air Quality research, Volume: 18 | Issue: 2 | Pages: 471-484
DOI: 10.4209/aaqr.2017.08.0274.

To better understand the influence of dust storms on nitrogen polycyclic aromatic hydrocarbons (NPAHs) and oxygen polycyclic aromatic hydrocarbons (OPAHs), PM2.5 was collected using prebaked quartz filters at Shandong University, Jinan, China, in spring 2016. The concentrations of 16 NPAHs and 5 OPAHs in PM2.5 were measured using gas chromatography-mass spectrometry. The highest concentration of NPAHs was recorded during dust storm 1 (DS1; 4.62 ng m−3), which was higher than those recorded during haze (2.28 ng m−3) and on clear days (0.17 ng m−3). The concentrations of 2+3N-FLA and 9N-ANT were considerably higher during haze and dust storms. The total concentration of OPAHs was highest during haze (7.72 ng m−3) and was 2–4.2 times higher than those during DS1, dust storm 2 (DS2), dust storm 3 (DS3) (all 2.38–3.07 ng m−3) and on clear days (1.82 ng m−3). The three most abundant OPAHs were 9-fluorenone, 9,10-anthraquinone, and naphthalene-1-aldehyde during all studied periods. The 2+3N-FLA/1N-PYR ratio indicated that NPAHs were dominated by secondary generation throughout the sampling period and that dust storm days were more conducive to the secondary generation of NPAHs than were hazy days. During dust storms, NPAHs and OPAHs were influenced by long-distance transport originating in Mongolia and Inner Mongolia. NPAHs and OPAHs in PM2.5 were mainly derived from vehicle exhausts, solid fuel combustion, secondary generation, and crustal sources throughout the sampling period. The highest ∑BaPeq value (0.0928 ng m−3) was recorded during DS2. The incremental lifetime cancer risk and total risk on hazy days and the three dust storm episodes were higher than those on clear days.

Keywords: Nitrogen polycyclic aromatic hydrocarbons; Oxygen polycyclic aromatic hydrocarbons; Dust storms; Long-distance transport; Secondary generation Cancer risk.

Spatial and Temporal Trends of Short-Term Health Impacts of PM2.5 in Iranian Cities; a Modelling Approach (2013-2016)

Philip K. Hopke1,2, Seyed Saeed Hashemi Nazari3, Mostafa Hadei4, Maryam Yarahmadi5, Majid Kermani6, Elham Yarahmadi7, Abbas Shahsavani 8,9

Source: Aerosol and Air Quality research, Volume: 18 | Issue: 2 | Pages: 497-504; DOI: 10.4209/aaqr.2017.09.0325.

Estimation of the spatial and temporal trends of health impacts attributable to air pollution is an effective measure for evaluating implemented interventions. The aim of this study was to estimate the short-term mortality attributable to exposure to PM2.5 among individuals older than 30 years old in ten Iranian cities from March 2013 to March 2016 using the World Health Organization's (WHO) AirQ+ software. Hourly concentrations of PM2.5 were acquired from the Department of Environment and Tehran Air Quality Control Company. Only stations with 75% and 50% of valid data were qualified for Tehran and other cities, respectively. The annual average PM2.5 concentrations in all ten of the cities were higher than the WHO guideline value of 10 μg m−3. The total number of attributable short-term deaths during the three-year period in these 10 cities was 3284 (95% CI: 1207–5244). The average daily premature deaths were calculated to be 3. The highest number of premature deaths within the three-year period was estimated to be 548 in

Tehran, largely reflecting its population of nearly 9 million. The western and southern cities of Iran experience severe dust storms and showed a high estimated rate of death attributed to air pollution. The health impacts in all cities decreased in the third year compared to the first year except for Ahvaz, Khoram Abad, and Ilam. Governmental interventions need to be enforced more effectively to reduce the high level of adverse health impacts in Iran. Special considerations should be given to the air quality of cities affected by dust storms.

Keywords: Particulate matter, AirQ+ Middle Eastern dust storm, Health impact assessment, Air pollution.

Intra-Urban Levels, Spatial Variability, Possible Sources and Health Risks of PM2.5 Bound Phthalate Esters in Xi'an

Jingzhi Wang1,2, Zhibao Dong1,3, Xiaoping Li1, Meiling Gao4, Steven Sai Hang Ho2,5, Gehui Wang2, Shun Xiao1, Junji Cao 2,6

Source: Aerosol and Air Quality research, Volume: 18 | Issue: 2 | Pages: 485-496
DOI: 10.4209/aaqr.2017.09.0333.

Phthalate esters (PAEs) are abundant semi-volatile organic compounds in fine particulate. PM2.5 bound PAEs can inhale into the body with breath, which can cause negative effects to human health. In this study, total of 266 PM2.5 samples dispersed from nineteen communities in Xi'an, were collected at December, 2013, the heavy pollution periods. Most of them are from residential areas, and four of them are in universities. Much high levels of PAEs were obtained in this study, which were from 271.7 to 2134 ng m–3 (952.6 ng m–3 on average). DEHP was the dominant species, with an average of 402.4 ng m–3, and attributed for 42.2% of the total PAEs, followed by BBZP (146.8 ng m–3 on average) and accounted for 15.4% of the total PAEs. Relative humidity and ventilation coefficient are the two meteorological factors affect the PAEs pollutions during the sampling periods. PAEs showed a declined trend from the urban to suburban. The principal component analysis (PCA) investigated that the release from plasticizer using in vinyl flooring, inks, synthetic leather, adhesives, and food contact wrapping; and emissions from cosmetics and personal care products, varnish, and volatilization from solid waste landfill or sewage sludge from wastewater treatment plant are the main sources for PAEs (86.8% of total PAEs). The daily inhalation and cancer risk assessment displayed that possible risk for all age group persons in this area, and infants are the most susceptible population.

Keywords: Phthalate esters; Nineteen communities; Spatial variability; Possible sources; Health risks.

Sensitivity Analysis of Chemical Mechanisms in the WRF-Chem Model in Reconstructing Aerosol Concentrations and Optical Properties in the Tibetan Plateau

Junhua Yang1, Shichang Kang 1,3, Zhenming Ji2

Source: Aerosol and Air Quality research, Volume: 18 | Issue: 2 | Pages: 505-521
DOI: 10.4209/aaqr.2017.05.0156.

To investigate the effect of gas-phase chemical schemes and aerosol mechanisms on the reconstruction of the concentrations and optical properties of aerosols in the Tibetan Plateau (TP) and adjacent regions, two simulation experiments using the mesoscale Weather Research and Forecasting (WRF) meteorological model with the chemistry module (WRF-Chem) were performed in 2013. The RADM2 gas-phase chemical mechanism and the MADE/SORGAM aerosol scheme were selected in the first configuration, whereas the CBMZ gas and MOSAIC aerosol reaction schemes were included in the second simulation. The comparison demonstrated that chemical mechanisms play a key role in affecting the evolution of gas-phase precursors and aerosol processes. Specifically, compared with RADM2, CBMZ revealed lower O3 and higher NO2 surface concentrations, because of more efficient O3-NO titration, and higher HNO3 concentrations owing to more effective NO2 + OH reaction. SO2 could easily form particulate sulfate through cloud oxidation in RADM2. The MADE/SORGAM module presented higher surface PM2.5 and PM10 concentrations than did the MOSAIC module over the TP and in surrounding regions, because of the difference in aerosol compounds and the distribution of computed aerosol concentrations between modes and bins. The aerosol optical depth at 550 nm indicated a potential correlation with surface secondary inorganic aerosols concentrations. Higher surface sulfate and nitrate concentrations appeared to determine higher AOD values in MADE/SORGAM than in MOSAIC. Finally, the comparison with observations suggested that, the simulation performed using the CBMZ gas-phase chemical mechanism and MOSAIC aerosol module could be suitable for the efficient reconstruction of aerosols and their optical depth over the TP.

Keywords: Chemical schemes; Aerosol concentration; Aerosol optical properties; Tibetan Plateau.

Impact of Diwali Festival on Aerosol Optical Properties over an Urban City, Ahmedabad (India)

Nisha Vaghmaria, Niyati Mevada, James Maliakal

Source: Aerosol and Air Quality research, Volume: 18 | Issue: 2 | Pages: 522-532,
DOI: 10.4209/aaqr.2017.04.0124.

An attempt has been made to investigate changes in the characteristics of aerosol optical properties induced during Diwali/ New Year celebrations of 2012 over an urban city, Ahmedabad (India). Ground based measurements of average Aerosol Optical Depth (AOD) were carried out using a Microtops-II at Physics Department, Gujarat University, Ahmedabad during 10th to 16th Nov, 2012. AOD on the day just after Diwali is found to increase significantly; around 75% compared to pre-Diwali days for visible wavelength, remained at higher level for one more day (next day of New Year). Turbidity factor (β) also changed considerably, to a high value of 0.34 on the next day of Diwali, indicating a significant increase in aerosol loading associated with Diwali/ New Year festivities. Normal anti-correlation between Angstrom exponent (α) and turbidity parameter (β) is not seen on days following Diwali. The AOD and β values in the evening of the next day of Diwali increased to about 164% and 171% respectively compared to pre-Diwali days evenings; such an increase associated with the festivities has not been reported at any part of the country. Spectral variation of AOD also shows a significant change in the pattern during following two days of celebrations compared to pre-Diwali days. It is seen to follow power law more closely. Significant increase in AOD and change in spectral pattern suggest an increase of fine/accumulation mode particles due to Diwali/ New Year festivities.

Keywords: Optical properties of aerosol; Aerosol Optical Depth (AOD); Angstrom parameters; Anthropogenic aerosol; Aerosol physics.

Computer Simulation Studies of Structure Characteristics of Ordered Mesoporous Carbons and its Naphthalene Adsorption Performance

Keliang Wang1, Mingli Fu2, Junliang Wu2, Guangying Zhou3, Daiqi Ye 2

Source: Aerosol and Air Quality research, Volume: 18 | Issue: 2 | Pages: 542-548,
DOI: 10.4209/aaqr.2016.12.0562.

Through naphthalene-adsorption experiments, we were able to draw some valuable conclusions about adsorption capacity, the adsorption isotherm, adsorption kinetics, and adsorption thermodynamics, although the experiments could not directly reveal the exact location and state of adsorption on the surface of ordered mesoporous carbons (OMCs). In fact, due to the restrictions of characterization technology, human factors, and experimental conditions, we still do not understand the microscopic structure of OMCs very well. However, molecular simulation technology could compensate for these disadvantages. In this study, the Grand Canonical Monte Carlo method has been used to simulate the naphthalene adsorption behavior in the OMC-structure model for the first time. The atomic structure model of OMCs was built firstly by using molecular modeling techniques and was characterized by calculating the accessible solvent surface area, total pore volume, and small-angle X-ray diffraction patterns. The calculated results showed that the structural model of OMCs was reasonable and that the structural characteristics were in agreement with experimental data. The adsorption isotherm curve is of the type Langmuir IV, which is a typical characteristic of ordered mesoporous materials. Also, the adsorption isotherm curve revealed that the adsorption capacity of naphthalene on OMCs gradually increased to a balance,

with the maximum capacity reaching 105.4 mg g–1. Additionally, as the number of naphthalene molecules increased, the adsorption state was observed progressing from a monolayer to a multilayer state in the mesopores.

This work deepened the understanding of the adsorption state of naphthalene for OMCs on the mesoscopic level. It also demonstrated that the GCMC method is effective for studying the adsorption process and gives useful guidance on research of the structure-activity relationship and performance prediction of carbon material.

Keywords: Grand Canonical Monte Carlo Ordered mesoporous carbons Adsorption Naphthalene.

Analysis of Reduction Potential of Primary Air Pollutant Emissions from Coking Industry in China

Yan Wang1,2, Ke Cheng 2, He-Zhong Tian3, Peng Yi4, Zhi-Gang Xue4

Source: Aerosol and Air Quality research, Volume: 18 | Issue: 2 | Pages: 533-541,
DOI: 10.4209/aaqr.2017.04.0139.

Air pollutant emissions from the coking industry in China, the world's largest coke producer, are a major societal concern. This study employed a bottom-up emission-factor methodology to estimate the country's coking-industry air-pollutant emissions. Total suspended particulate matter (TSP), particulate matter with an aerodynamic diameter less than or equal to 2.5 μm (PM2.5), sulfur dioxide (SO2), nitrogen oxides (NOx), volatile organic compounds (VOCs), polycyclic aromatic hydrocarbons (PAHs), carbon monoxide (CO), and methane (CH4) were considered. The emissions in 2015 were estimated to be 368.36, 23.28, 402.54, 174.43, 1325.42, 28.24, 2036.43, and 71.68 kt for TSP, PM2.5, SO2, NOx, VOCs, PAHs, CO, and CH4, respectively, with an annual average growth rate of 1.1% during the 12th five-year-plan (2011–2015). A comparative analysis was performed on emission contributions from air pollutants produced by various types of coke ovens and using various coking procedures. The objectives of the 13th five-year-plan (2016–2020) were used to predict China's production of coke and methods of control in 2020 and to analyze the potential reduction in typical air pollutants. The results show that emissions of TSP, SO2, and NOx will be reduced by 82.9%, 94.4%, and 6.9%, respectively. Moreover, this study proposes a series of feasible control measures for air-pollutant emissions from the coking industry in China.

Keywords: Coking industry;Primary air pollutants; Emission characteristics; Reduction potential.

Estimates of Atmospheric Aerosols Adhered to the High Voltage Electric wire in the Yangtze River Delta Region of China

Jingliang Hao1, Leiming Zhang2, Tianliang Zhao 1, Song Gao3, Jie Li3, Yongwei Wang

Source: Aerosol and Air Quality research, Volume: 18 | Issue: 2 | Pages: 555-559,
DOI: 10.4209/aaqr.2017.06.0218.

Atmospheric aerosol particles can collect on and adhere to high voltage electrical wires, causing power loss as well as other detrimental effects on electrical insulation. The mass of fine particles (PM2.5) adhering to wires has been estimated using a modified size-resolved particle dry deposition model and a range of annual average PM2.5 concentrations found in literature for the Yangtze River Delta region of China. Annual mass collected by the surface of a unit length (1 m) of wire with a radius of 0.5 cm is estimated to be in the range 1.56 × 104–1.46 × 105 μg. The actual mass adhering to the wire may be reduced by 85% of these estimated values considering the washing-off effects of rain. For a wire of 1.0 cm in radius, the annual mass on the wire is estimated to be in the range of 4.68 × 103–4.35 × 104 μg after considering the effects of rain. This study provides a first estimation of particle mass collected by electrical wires, although

Keywords: Dry deposition model; Electric wire; Mass of PM2.5.

Evaluation of the NanoAerosol Generator by Kanomax FMT Inc. in Aerosolization of Size Standard Nanoparticle and Protein

Hiromu Sakurai , Yoshiko Murashima

Source: Aerosol and Air Quality research, Volume: 18 | Issue: 2 | Pages: 549-554,
DOI: 10.4209/aaqr.2017.09.0352

A new nebulizer called NanoAerosol Generator (NAG) by Kanomax FMT, Inc. was evaluated experimentally in their performance in aerosolizing sub-100 nm particles and sub-10 nm protein molecules which cannot be aerosolized with conventional compressed-air jet nebulizers due to the interference by a number of residue particles. For the challenge particles, 29 nm-polystyrene latex (PSL) particles and bovine serum albumin (BSA) protein molecules were used as sub-100 nm and sub-10 nm test materials, respectively. For both particles, the aerosolization by the NAG was successful with a clear separation between the peak of the challenge particles and the peak of residual particles in the size distribution spectra. The size distributions of aerosolized 29 nm-PSL particles were compared between the NAG and an electrospray aerosol generator (EAG) with liquid samples of the same particle concentration. The EAG showed clearer separation of the PSL peak from the residual peak; on the other hand, the peak height was taller for the NAG by a factor of 6 than for the EAG, which indicated the generation of airborne particles from a liquid suspension/solution of the same concentration was more efficient for the NAG than for the EAG.

Keywords: Nebulizer; Electrospray; Polystyrene latex; Bovine serum albumin.

Corrigendum to "PM2.5 Emissions from Hand-Held Sparklers: Chemical Characterization and Health Risk Assessment" [Aerosol Air Qual. Res. 14: 1477–1486]

Raghu Betha, Rajasekhar Balasubramanian

Source: Aerosol and Air Quality research, Volume: 18 | Issue: 2 | Pages: 560-563
DOI: 10.4209/aaqr.2018.01.1801.

The authors regret that inadvertent errors occurred in the estimation of excess lifetime cancer risk (ELCR) in the above-referenced paper due to an oversight. Specifically, the slope factor of nickel (Ni) we used in the ELCR calculation should have been 8.4 × 10–1 (mg/kg/day)–1 instead of 8.4 × 101 (mg/kg/day)–1. Further, to be consistent with other publications where we assumed the measured chromium (Cr) to exist entirely as hexavalent chromium (Cr(VI)) in airborne particulate matter, we revised the slope factor of Cr to the USEPA recommended value of 42 and recalculated the ELCR accordingly. These revised slope factors do not affect, or influence our overall qualitative conclusion made earlier in the published paper in that whistling sparklers have higher carcinogenic risk compared to low smoke and colored sparklers. The revised ELCR estimates are given below in Tables 2, 3 and 4.

The authors apologize for any inconvenience caused.

Keywords: N/A

Computational Fluid Dynamic Modelling of Particle Charging and Collection in a Wire-to-Plate Type Single-Stage Electrostatic Precipitator

Ji-Woon Park, Chul Kim, Jaehong Park, Jungho Hwang

Source: Aerosol and Air Quality research, Volume: 18 | Issue: 3 | Pages: 590-601,
DOI: 10.4209/aaqr.2017.05.0176.

Electrostatic precipitators (ESPs) have been widely used to control particulate pollutants, which adversely affect human health. In this study, a computational fluid-dynamic model for turbulent flow, particle trajectory, and particle charging in ESPs is presented using a pre-developed corona discharge model (Kim et al., 2010), wherein electric field and space charge distributions in the plasma region are numerically calculated. The ESP under consideration is a wire-to-plate single-stage ESP, which consists of a series of discharge wires and two collecting plates. Two different kinds of particulates are considered in this study; fly ash and sucrose particles. Fly ash was selected because many ESPs have been utilized in coal-fired power plants to capture fly ash particles generated from combustion. Sucrose was selected to compare our numerical calculation results with experimental data found in literature. The electrical characteristics of the ESP, particle trajectories, particle charge numbers, and collection efficiencies under various operating conditions are demonstrated. For fly ash, the overall collection

efficiencies based on particle mass are 61, 86, 95, and 99% at 45, 50, 55, and 60 kV, respectively, at a flow velocity of 1 m s–1.

Keywords: Electrostatic precipitator; Corona discharge; Plasma region; Particle charge; PM2.5.

Nano- and Submicron Particles Emission during Gas Tungsten Arc Welding (GTAW) of Steel: Differences between Automatic and Manual Process

Elena Baracchini1, Carlotta Bianco1, Matteo Crosera1, Francesca Larese Filon2, Elena Belluso3,4,5, Silvana Capella3,4, Giovanni Maina6, Gianpiero Adami 1

Source: Aerosol and Air Quality research, Volume: 18 | Issue: 3 | Pages: 579-589 , DOI: 10.4209/aaqr.2017.07.0226.

Welding operations originate micro and nanoparticles represented by metal oxides, unoxidized metals and compounds, such as fluorides and chlorides. Welding fumes exposure is associated to lung cancer, chronic bronchitis, asthma and early Parkinson disease. Ultrafine (nanosized) particles in welding fumes are considered a risk factor in terms of occupational exposure: when inhaled, they are efficiently deposited in all regions of the respiratory tract and can translocate to other target organs as brain and systemic circulation. The study of nanoparticles emissions during welding can help to understand effects related also to new-engineered nanoparticles exposure.

In our study two real sources of Gas Tungsten Arc Welding (GTAW) fume particles, collected in an automotive plant, were characterized by means of a transmission electron microscope coupled with an energy-dispersive X-ray analytical system (TEM-EDS) and compared to a zone of the plant far from the two sources used as a reference background. The particles sampled during the automatic GTAW process were mainly constituted by iron/manganese oxide with a mean diameter of 47 nm, followed by smaller iron oxide nanoparticles (21 nm). During the manual welding process mostly aggregates with larger diameters that showed an X-ray spectrum characteristic of different kinds of silicates were found. Iron and cobalt oxides nanoparticles were present only inside bigger aggregates mainly composed of aluminum and titanium oxides.

This study confirms that welders are exposed to nano- and submicron particles and that iron/manganese oxide nanoparticles are the most representative in automatic process, despite the low concentration of manganese in welding wires (1–2%). Our results help to understand hazard related to welding fumes exposure and possible effects of nanoparticles on lung, brain and systemic circulation.

Keywords: Welding fumes GTAW; Nanoparticles; TEM-EDS; Occupational exposure.

Field Test of Several Low-Cost Particulate Matter Sensors in High and Low Concentration Urban Environments

Karoline K. Johnson 1, Michael H. Bergin1, Armistead G. Russell2, Gayle S.W. Hagler3

Source: Aerosol and Air Quality research, Volume: 18 | Issue: 3 | Pages: 565-578
DOI: 10.4209/aaqr.2017.10.0418

Detailed quantification of the spatial and temporal variability of ambient fine particulate matter (PM2.5) has, to date, been limited due to the cost and logistics involved with traditional monitoring approaches. New miniaturized particle sensors are a potential strategy to gather more time- and spatially-resolved data, to address data gaps in regions with limited monitoring and to address important air quality research priorities in a more cost-effective manner. This work presents field evaluations and lab testing of three models of low-cost (< $200) PM sensors (SHINYEI: models PPD42NS, PPD20V, PPD60PV) in three locations: urban background (average PM2.5: 8 μg m−3) and roadside in Atlanta, Georgia, USA (average PM2.5: 21 μg m−3), and a location with higher ambient concentrations in Hyderabad, India (average PM2.5: 72 μg m−3). Sensor measurements were compared against reference monitors in the lab using one-minute averages and in field locations using one-hour averages. At the Atlanta sites the sensors were weakly correlated with a tapered element oscillating microbalance (TEOM) at best ($R2 \leq 0.30$). In Hyderabad, the PPD20V sensors had the highest correlation with the environmental beta attenuation monitor (E-BAM) ($R2 > 0.80$), however the same sensors had poor agreement if the comparison was restricted to lower concentrations ($R2 = \sim 0$, < 40 μg m−3). The results of this work indicate the potential usefulness of these sensors, including the PPD20V, for higher concentration applications (< ~250 μg m−3). These field-testing results provide important insights into the varying performance of low-cost PM sensors under highly contrasting atmospheric conditions. The inconsistent performance results underscore the need for rigorous evaluation of optical particle sensors in the laboratory and in diverse field environments.

Keywords: Field calibration; Fine particulate matter; SHINYEI Low-cost sensor.

Recent Advances in Passive Air Sampling of Volatile Organic Compounds

Cenyan Huang1,2,3, Wenpo Shan1,3, Hang Xiao 1,3

Source: Aerosol and Air Quality research, Volume: 18 | Issue: 3 | Pages: 602-622 ,
DOI: 10.4209/aaqr.2017.12.0556.

Volatile organic compounds (VOCs) are not only harmful to human health, but also important precursors of ozone and PM2.5, which cause severe air pollution. Therefore, it is critical to study these compounds, and monitor them by developing reliable and effective techniques. Passive air samplers (PASs) are small and uncomplicated, with the advantages of simple operation, easy transportation, and do not require external power; therefore, they are more economical and practical to monitor VOCs compared to active sampling techniques. As an alternative method, passive sampling is particularly suitable for long-term monitoring in remote regions and wilderness areas, simultaneous large-scale measurement, and

recording of individual exposure. In recent years, commercial PASs have been improved continuously, while emerging samplers have been developed for new applications. The following main trends can be distinguished: (1) many novel PASs were specifically designed to monitor only one or few VOCs also including numerous redesigned commercial PASs; (2) the improvement of sorbents is still ongoing towards high efficiency, low cost, and multiple choices for more analytes; (3) structural improvement is another important aspect of PAS development mainly focusing on both sampler performances and applications; (4) the development of new technologies provides more sampling conveniences such as using unmanned aerial vehicles and sampling robots to special monitoring sites e.g., a stack or a ventilating duct.

Keywords: Volatile organic compounds; Passive sampling; Air monitoring; Passive sampler; Diffusive sampler.

In Situ FT-IR and DFT Study of the Synergistic Effects of Cerium Presence in the Framework and the Surface in NH3-SCR

Yinming Fan1, Wei Ling1, Lifu Dong1, Shihui Li1, Chenglong Yu1, Bichun Huang 1,2, Hongxia Xi3

Source: Aerosol and Air Quality research, Volume: 18 | Issue: 3 | Pages: 655-670
DOI: 10.4209/aaqr.2017.04.0148

Mn-Ce/CeAPSO-34 was prepared, in which manganese and cerium were supported on the surface through using the Ethanol dispersion method, while cerium was incorporated in the SAPO-34 framework by a one-step hydrothermal method. Based on our previous study, a strong synergistic effect of cerium presented in the framework and the surface was existing in Mn-Ce/CeAPSO-34 catalyst, which showed outstanding SO2 tolerance and H2O resistance in the low-temperature NH3-SCR. In situ FT-IR and DFT calculations were used to investigate the synergistic effects. Based on the characterization results of in situ FT-IR study, it was found that more amount of nitrate species and NH3 species adsorbed on the surface of Mn-Ce/CeAPSO-34, while less the amount of sulfate species deposited during reaction process, which in the presence of SO2. Meanwhile, DFT calculations revealed that Ce site supported on the surface, which neighbored by Ce site in the framework more were capable of reacting with NO and NH3.

Keywords: Mn-Ce/CeAPSO-34, NH3-SCR Synergistic effect SO2 tolerance

---

Black Carbon and Ozone Variability at the Kathmandu Valley and at the Southern Himalayas: A Comparison between a "Hot Spot" and a Downwind High-Altitude Site

Davide Putero 1, Angela Marinoni1, Paolo Bonasoni, Francescopiero Calzolari1, Maheswar Rupakheti2, Paolo Cristofanelli1

Source: Aerosol and Air Quality research, Volume: 18 | Issue: 3 | Pages: 623-635 ,
DOI: 10.4209/aaqr.2017.04.0138.

Several studies have reported the transport of short-lived climate forcers/pollutants (SLCF/P) from the highly polluted areas in southern Asia (e.g., the Indo-Gangetic Plain and the Himalayan foothills) to the Himalayas, with significant implications for the global and regional climate, crop yields, and human health. In this work, we perform a comparison of nearly three years (February 2013–October 2015) of simultaneous black carbon (BC) and surface ozone (O3) measurements at two sites in Nepal, viz., Paknajol (1380 m a.s.l.), in the Kathmandu Valley, and the WMO/GAW global station Nepal Climate Observatory-Pyramid (NCO-P, 5079 m a.s.l.), near the base camp of Mt. Everest. The two sites are only 150 km apart and are characterized by different situations: While the Kathmandu Valley is one of the regional urban "hot spots" for concerns related to air pollution, NCO-P is representative of the background conditions of the high Himalayas and the free troposphere. Therefore, the possible role played by emissions occurring in the planetary boundary layer (PBL) of the Kathmandu Valley in influencing the variability in SLCF/P at NCO-P was investigated. BC and O3 concentrations at NCO-P showed a linear correlation with the modeled PBL height over the Kathmandu urban area, providing evidence that the anthropogenic emissions occurring within the Kathmandu PBL could affect the variability in BC and O3 at NCO-P. Furthermore, when introducing an additional constraint into the analysis (viz., back-trajectories), we show that on days when air mass transport between the two measurement sites was observed (10% of the period), at least 22% and 16% of BC and O3 variability at NCO-P can be explained by concurrent variability in SLCF/P over the Kathmandu Valley.

Keywords: Black carbon; Ozone; Comparison; Planetary boundary layer; Himalayas.

Spectral Properties of Black Carbon Produced during Biomass Burning

Chaithanya D. Jain 1, Harish S. Gadhavi1, Tushar Wankhede1, Kanakaraju Kallelapu1, Suryasree Sudhesh2, Lidiya N. Das2, Rahul U. Pai2, Achuthan Jayaraman1

Source: Aerosol and Air Quality research, Volume: 18 | Issue: 3 | Pages: 671-679 ,
DOI: 10.4209/aaqr.2017.03.0102

Spectral properties of Black Carbon (BC) produced during the burning of different biofuels have been studied using a 7 channel Aethalometer (Magee Scientific, USA). Different biofuels used for household purpose in the rural regions were selected after a survey conducted in Gadanki, A.P. – a typical village in South India. Biofuels were burnt in a custom made burning chamber and BC produced has been allowed to mix with ambient air and measured using Aethalometer kept 4 meters away from the burning

chamber. The observed absorption coefficient spectra have been characterized by fitting to a power-law equation. The power co-efficient (α) values found to be ranging from 1.2–2.1 for different biofuels. It has been observed that the α values are related to the speed of burning; fast burning biofuels shown low values, whereas slow burning biofuels have shown higher values.

Keywords: Black carbon; Aethalometer; Biofuels; Spectral properties; Angstrom exponent.

Chemical Compositions and Liquid Water Content of Size-Resolved Aerosol in Beijing

Jie Su, Pusheng Zhao , Qun Dong

Source: Aerosol and Air Quality research, Volume: 18 | Issue: 3 | Pages: 680-692 ,
DOI: 10.4209/aaqr.2017.03.0122.

For aerosol related studies, the size distribution and hygroscopicity of chemical components are very important information. In order to characterize the distributions of chemical compositions and the water absorption ability for ambient aerosols of Beijing, a MOUDI-120 sampler was used to collected size-resolved samples in three seasons. All the samples were analyzed in the laboratory for water-soluble inorganic ions and carbon fractions. The size-resolved aerosol liquid water content (ALWC) of the sampled particles was modeled by the ISORROPIA II. The distributions of the chemical compositions, the ALWC, and the charge balance conditions were all discussed for three different pollution levels. During the sampling, the aerosols in stages 6–10 (< 1.0 μm) were under relatively dry conditions due to the significant pressure drops. Three modes (condensation mode, droplet mode, and coarse mode) could be identified from the distributions of the main chemical components and the ALWC. For the droplet mode, the ammonium was not enough to balance NO3– and SO42– during the heavily polluted period. The influence of relative humidity on ALWC is greater than that of the chemical compositions.

Keywords: Size-resolved; Size distribution; Chemical compositions; Aerosol liquid water content.

Concentration, Chemical Composition and Origin of PM1: Results from the First Long-term Measurement Campaign in Warsaw (Poland)

Grzegorz Majewski 1, Wioletta Rogula-Kozłowska2,3, Katarzyna Rozbicka1, Patrycja Rogula-Kopiec3, Barbara Mathews3, Andrzej Brandyk1

Source: Aerosol and Air Quality research, Volume: 18 | Issue: 3 | Pages: 636-654 ,
DOI: 10.4209/aaqr.2017.06.0221.

This paper presents a 120-day-long variability of chemical composition of submicron particulate matter (PM1) over Warsaw. The content of the following components was examined in the PM1 mass: primary (POM) and secondary (SOM) organic matter, secondary inorganic matter (SIM), elemental carbon (EC)

as well as Na and Cl ions (primary inorganic matter). The 24-hour concentrations of PM1 were subject to seasonal fluctuations which are typical of urban areas in Poland; their values averaged 11 μg m–3 in summer and 17 μg m–3 in winter. Most of the PM1 components and gaseous pollutants (SO2, NO2 and NOx) revealed higher mean concentrations in winter than in summer. A statistical analysis of meteorological parameters and 24-h concentrations of PM1, PM10, SO2, NO2 and NOx confirmed a significant influence of air temperature and precipitation on the concentration patterns of these pollutants over Warsaw. The highest concentrations of PM1 occurred in winter for the following wind directions: S, SE, N and NE; in summer for NE, E and S. The analysis of back trajectories demonstrated that on days with the highest 24-h concentration of PM1 polluted air masses arrived from S and SE and affected the concentration of PM1 over Warsaw. The submicron particulate matter, in as much as 62%, comprises secondary matter (SOM and SIM). The primary sources of its precursors and – to a smaller extent – of the primary matter as well – are traffic and combustion of various fuels for the purpose of heat and power generation. Their average contribution to the development of PM1 was 15% and 51%, respectively, for the entire period of observations.

Keywords: Secondary aerosol Carbonaceous matter Submicron particles Air mass inflow Fossil fuels combustion.

Evaluation and Application of an Online Coupled Modeling System to Assess the Interaction between Urban Vegetation and Air Quality

Jianbo Yang1,2, Hongnian Liu 1,3, Jianning Sun1,3

Source: Aerosol and Air Quality research, Volume: 18 | Issue: 3 | Pages: 693-710, DOI: 10.4209/aaqr.2017.06.0199.

Vegetation has always been an integral part of the urban scene, affecting ambient air quality through both direct and indirect ways: by enhancing the dry deposition process of air pollutants and by contributing to the formation of ozone due to the emission of biogenic volatile organic compounds (BVOC). In this study, hourly measurements of gaseous dry deposition velocities are used to evaluate the performance of two dry deposition modules. Based on verification against measurements, an online coupled modeling system (RBLM-Chem) is introduced to investigate the dry deposition process of air pollutants (both gas and particles), the diurnal and seasonal variation patterns, and the discrepancy between different vegetation species as well as to assess the role of urban vegetation in affecting local air quality under different greening scenarios. Results indicate that trees are generally more efficient in removing air pollutants than shorter vegetation (e.g., grass). Moreover, conifers exhibit higher dry deposition velocities than broadleaf trees in terms of annual average. The introduction of vegetation (either trees or grass) clearly raises the dry deposition velocity of air pollutants. The air pollutant that is most removed by urban vegetation in Suzhou is PM10, with an annual removal rate of 1484.5 t a–1. The current urban greening scenario within Suzhou contributes to a reduction in daily mean concentration of 8.1% (SO2), 7.1% (NO2), 5.6% (O3), 4.7% (PM10) and 4.4% (PM2.5) in summer, while the reduction

in winter is 4.6%, 5.5%, 4.5%, 3.6% and 3.7%, respectively. The improvement in pollutant concentration can be strengthened by increasing vegetation coverage. Additionally, the peri-urban forest ecosystem plays a role in air quality improvement within an urban area. As for the effect of BVOC emissions, the emission from urban trees under 40% coverage results in the consumption of NOx (–3.2%) and the formation of O3 (2.3%).

Keywords: Urban vegetation; Dry deposition; Air pollutant; Urban air quality; Greening scenarios.

Significant Decrease of PM2.5 in Beijing Based on Long-Term Records and Kolmogorov–Zurbenko Filter Approach

Ziyin Zhang 2, Zhiqiang Ma2, Seong-Joong Kim3

Source: Aerosol and Air Quality research, Volume: 18 | Issue: 3 | Pages: 711-718
DOI: 10.4209/aaqr.2017.01.0011

Severe haze episodes have hit Beijing many times in the past few years, especially the "crazy bad" pollution described by the US Embassy in Beijing. The publication of numerous multimedia reports on the severe haze has increased awareness among the people in China regarding air pollution and PM2.5. It is assumed that the severe haze occurred suddenly for unclear reasons. In this context, long-term evaluation of the air pollution in Beijing is necessary. Through hourly and daily PM2.5 concentration records, meteorological datasets from August 2004 onward, and the Kolmogorov–Zurbenko (KZ) filter approach, the evolutions of the long-term components (or background values) of PM2.5 concentrations at an urban and a rural station in Beijing were statistically analyzed, and the possible causes of variation in the trends of these components were evaluated in this study. The long-term components of PM2.5 concentrations decreased significantly at both the urban (–3.40 μg m–3 y–1) and rural (–1.16 μg m–3 y–1) stations. The most serious pollution predominantly occurred in an earlier period than recent years, when little attention was being paid. The decrease in PM2.5 concentration was mainly attributed to the reduction in pollutant emission, despite the distinct increase in total energy consumption and motor vehicle use. However, the unfavorable climate changes (i.e., a reduction in wind speed and an increase in relative humidity) reduced the efficiency of atmospheric environmental governance. Because of the unfavorable climate or meteorological changes, the trends of PM2.5 reduction derived from the pollutant emission controls have been offset by up to approximately 15% in both urban and rural areas of Beijing during the last decade.

Keywords: PM2.5; KZ filter; Haze; Air quality; Beijing.

Health Risk Assessment and Correlation Analysis on PCDD/Fs in the Fly Ash from a Municipal Solid Waste Incineration Plant

Yen-Kung Hsieh1, Wei-Sheng Chen 1, Jinning Zhu 2, Yi-Jing Wu3, Qianli Huang4

Source: Aerosol and Air Quality research, Volume: 18 | Issue: 3 | Pages: 734-748,
DOI: 10.4209/aaqr.2017.12.0587

Polychlorinated dibenzo-p-dioxins and dibenzofurans (PCDD/Fs) in fly ash may pose health threats to onsite workers due to their inevitable dispersion in the working environments during recycling and disposal of fly ash from Municipal Solid Waste Incinerators (MSWIs). Here, PCDD/Fs in fly ash from an MSWI in Southern Taiwan was analyzed from several perspectives. The results can be summarized as follows: (1) Through multiple comparison analyses, it was revealed that four types of congeners (OCDD, OCDF, 1,2,3,4,6,7,8-HpCDD and 1,2,3,4,6,7,8-HpCDF) have significantly higher concentrations than other species ($p < 0.01$). (2) 2,3,4,7,8-PeCDF represented the main contributor to the total toxic equivalent concentration (TEQ). The top three candidate indicators of total TEQ are OCDF, 1,2,3,4,6,7,8-HpCDF and 2,3,4,7,8-PeCDF, in which OCDF might be most powerful indicator of fly ash from similar sources. (3) It was indicated that all congeners correlated positively with each other (with R2 values in the range between 0.707–0.939); Meanwhile, the results of the cluster analysis unveiled the specific features of several congeners (such as 1,2,3,7,8,9-HxCDF, OCDD and OCDF). (4) Through assessing health risk with a Monte Carlo simulation, both the 95th percentile carcinogenic risk (CR) and non-carcinogenic risk (non-CR) for onsite workers exceeded the threshold limit and should be considered as significant risks for onsite workers. (5) The results of the sensitivity analysis suggested that concentration (CC) and exposure duration (ED) were the two most sensitive parameters in both the CR and non-CR assessment. The above findings could be useful for improving existing health risk mitigation/management strategies for onsite workers in waste incineration plants.

Keywords: PCDD/Fs; Health; Risk Monte; Carlo simulation; Sensitivity analysis; Fly ash.

Sensitivity Analyses for Atmospheric Scavenging Ratio of Total PCDD/Fs-TEQ Wet Deposition: Case of Wuhu City, China

Weiwei Wang1, Kangping Cui 1, Rong Zhao1, Wen-Jhy Lee 1,2, Ping Yan1

Source: Aerosol and Air Quality research, Volume: 18 | Issue: 3 | Pages: 719-733 ,
DOI: 10.4209/aaqr.2018.01.0032.

This study investigated the monthly average dry, wet and total deposition fluxes in total-PCDD/Fs-WHO2005-TEQ in Wuhu and Bengbu, respectively. In addition, sensitivity analyses for both scavenging ratio and wet deposition of total-PCDD/Fs-WHO2005-TEQ in Wuhu were also conducted. In 2015, the annual dry deposition fluxes, wet deposition fluxes, and total deposition fluxes were 6407, 1538, and 7945 pg WHO2005-TEQ m–2 year–1 in Wuhu, and were 7101, 1525, and 8626 pg WHO2005-TEQ m–2 year–1 in Bengbu. The annual scavenging ratios of total-PCDD/Fs-WHO2005-TEQ were 30144 and 31267 in Wuhu and Bengbu, respectively. As to the sensitivity analysis for the scavenging ratio of total-PCDD/Fs-WHO2005-TEQ, the most positive sensitivity parameters were PCDD/Fs concentration and PM10 concentration; the second positively correlated sensitivity parameter was PM2.5 concentration, then, followed by atmospheric temperature, which was negatively correlated; the last negative correlated sensitivity factor was the rainfall. In terms of the sensitivity analysis for wet deposition of total-PCDD/Fs-WHO2005-TEQ, the most positive sensitivity parameter was air temperature; the second positive or negative correlated sensitivity factor was atmospheric PCDD/Fs mass concentration, followed by PM2.5 and PM10 concentration, which were positively correlated; the last positive correlated sensitivity factor was the rainfall. This study led to greater insight into the parameters affecting the atmospheric wet deposition of PCDD/Fs, which will benefit development of appropriate control strategies for PCDD/Fs and provided useful information for the scientific community.

Keywords: Dry deposition; Wet deposition; Scavenging ratio; Sensitivity analyses; PCDD/Fs Wuhu Bengbu.

PAH Profiles of Emitted Ashes from Indoor Biomass Burning across the Beijing-Tianjin-Hebei Region and Implications on Source Identification

Zhiyong Li 1, Lin Fan1, Lei Wang2, Huiqiao Ma1, Yao Hu1, Yunjun Jiang2, Caixiu An2, Aiqin Liu2, Jinbao Han3, Hui Jin4

Source: Aerosol and Air Quality research, Volume: 18 | Issue: 3 | Pages: 749-761
DOI: 10.4209/aaqr.2017.12.0588

Sixty-four bottom ash (BA) samples from indoor burning of eight bio-fuels (BFs) including cotton (COT), corn (COR), millet (MIL), soybean (SOY), sorghum (SOR) and sesame (SES), firewood walnut (WAL), and corn cob (COC) were collected across the Beijing-Tianjin-Hebei (BTH) region. Each BA was divided into five differently sized parts for the analysis of eighteen PAHs using the GC/MS system. The Σ18PAHs values for all the BAs varied from 65.0 ± 10.6 to 1310 ± 129 ng g–1. SOR had the highest PAH level, and COC produced the lowest level. The Σ18PAHs for SOY, WAL, COT, COR, COC, and SES were negatively

correlated with the BA sizes. The NA, PHE, ACL, AN, FA, PY, FL, and AC dominated in all the BAs except for SES. All the BAs were dominated by 2, 3-ring PAHs. The PAH profiles for differently sized BAs within MIL, SOR, COC, COR, and SES were similar based on lower coefficient of divergence values, while the other three BFs did not exhibit this trend. All the BF pairs except for SOR vs. SES and COC vs. COR had the different PAH profiles. No series of coincident diagnostic ratios (DRs) could represent all BFs based on their significantly varied DRs. AN/(AN + PHE) and BA/BgP might be used in identification of combustion sources of different types of BFs. SOR and SES had higher potential toxicity risk based on higher TEQ, BaPE, and CPAHs values. BgF and BgP were the indicatory PAHs for SOY, MIL, COR, SOR, and COC, while they were AC and FL for the remaining three BFs.

Keywords: Polycyclic aromatic hydrocarbon; Bottom ash; Bio-fuel; Diagnostic ratio; Indicatory PAHs.

Atmospheric PM2.5 and Polychlorinated Dibenzo-p-dioxins and Dibenzofurans in Taiwan

Yen-Yi Lee1, Lin-Chi Wang 2, Jinning Zhu 3, Jhong-Lin Wu4, Kuan-Lin Lee1

Source: Aerosol and Air Quality research, Volume: 18 | Issue: 3 | Pages: 762-779
DOI: 10.4209/aaqr.2018.02.0050

In this study, the atmospheric PM2.5, increases/decreases of the PM2.5, the PM2.5/PM10 ratio, total PCDD/Fs-TEQ concentrations, PM2.5-bound total PCDD/Fs-TEQ content, and PCDD/F gas-particle partition in Taiwan were investigated for the period 2013 to 2017. In Taiwan, the annual average PM2.5 concentrations were found to be 28.9, 24.1, 21.4, 20.2, and 19.9 μg m−3 in 2013, 2014, 2015, 2016, and 2017, respectively, which indicated that the annual variations in PM2.5 levels were decreasing during the study period. The average increases (+)/decreases (–) of PM2.5 concentrations were –16.7%, –11.1%, –5.75%, and –1.73% from 2013 to 2014, from 2014 to 2015, from 2015 to 2016, and from 2016 to 2017, respectively. Based to the relationship between PM10 values and total PCDD/F concentrations obtained from previous studies, we estimated that in 2017, the annual average total PCDD/Fs-TEQ concentrations ranged between 0.0148 (Lienchiang County) and 0.0573 pg WHO2005-TEQ m−3 (Keelung City), and averaged 0.0296 pg WHO2005-TEQ m−3, while the PM2.5-bound total PCDD/Fs-TEQ content ranged from 0.302 (Kaohsiung City) to 0.911 ng WHO2005-TEQ g−1 (Keelung City), at an average of 0.572 ng WHO2005-TEQ g−1. These values are suggested to be validated in the future study because the sources and formations of PM10 and PM2.5 in different areas were diverse, and may be not closely related to combustion sources. The seasonal variations in the gas fraction of total PCDD/Fs-WHO2005-TEQ concentrations were 68.6%, 86.6%, 82.3%, and 52.3% in the

spring, summer, autumn, and winter, respectively. Due to the fact that Taiwan is located mostly in the sub-tropical zone, which had annual average temperatures between 23.0 and 24.4°C, averaging 23.8°C during the study period, the majority of PCDD/Fs-TEQ were dominant in the gas phase.

Keywords: PM2.5 PCDD/Fs PM10 Particle-bound PCDD/F content Gas-particle partition

Model-Integration of Anthropogenic Heat for Improving Air Quality Forecasts over the Beijing Megacity

Ting Yang 1,2, Alex Gbaguidi1, Wei Zhang3, Xiquan Wang1,2, Zifa Wang1,2, Pingzhong Yan1

Source: Aerosol and Air Quality research, Volume: 18 | Issue: 3 | Pages: 790-802
DOI: 10.4209/aaqr.2017.04.0155

In air quality forecasting systems, failure to consider the considerably large anthropogenic heat emissions generated daily in the Beijing megacity by intensive human activities is one of the major causes of model failure. In this paper, we employ the nested air quality prediction model system coupled with the weather research and forecasting model and an urban canopy model to integrate anthropogenic heat emissions over Beijing into the modeling system and exhaustively evaluate their potential effects on air quality forecast by analyzing the wind field, boundary layer structure (height and atmospheric circulation), and surface and vertical distribution of pollutants. Consequently, the effects of anthropogenic heat on the boundary layer structure, greatly pronounced in urban areas, exhibited substantial variability at different levels depending on the time. The effects were evident during both daytime and night, but played a more prominent singular role in the night in the absence of solar short-wave radiation. Basically, anthropogenic heat acts not only by directly inducing the ascent of a warm air mass from the low parts of the atmosphere over urban areas to the top of the boundary layer, but also by indirectly driving wind convergence and inducing the descent of a cooled air mass from a high altitude to the boundary layer through a complex atmospheric circulation process. Incorporating anthropogenic heat emissions into the modeling system was effective in improving predictions by reducing the normalized mean bias by 20%–30% (for wind speed) and root mean square error by 361–558 m (for boundary layer height) and by 10–23 μg m–3 (for surface PM10), with a significant reduction in the underestimation of ozone concentration by approximately 20 ppb at urban sites. This paper is expected to provide new insights into the improvement of model accuracy for air quality forecasts over megacities.

Keywords: Anthropogenic heat ; Air quality; Model Forecast; Megacity.

Review on Numerical Simulation of Airflow and Pollutant Dispersion in Urban Street Canyons under Natural Background Wind Condition

Yunwei Zhang, Zhaolin Gu , Chuck Wah Yu

Source: Aerosol and Air Quality research, Volume: 18 | Issue: 3 | Pages: 780-789
DOI: 10.4209/aaqr.2017.09.0303

Observation data show that natural wind has a characteristic of regular time-variation in speed and direction. However, the time-varying inflow conditions are usually simplified as a constant wind profile in simulations on airflow and pollutant dispersion in urban street canyons and/or building cluster. The study on characteristics of urban canopy layer (UCL) flow under time-varying inflow conditions should be further contribute to the understanding of pollutant and energy transport processes in the urban atmospheric environment. In the current work, typical studies on air flow and pollutant dispersion in urban street canyons and building array are reviewed. The time-varying upstream inflows could commonly enhance the transportation of pollutant and energy in actual UCL. Studies have revealed that the variation of natural inflow conditions could be one of the primary factors that influencing the transport efficiency of pollutant in urban street canyons. Perspectives on methods in performing the time-varying inflow conditions are provided as well. Gradual and/or stepped variation of wind data would be expected in numerical simulations.

Keywords: Pollutant dispersion; Natural wind condition; Urban street canyon; Gusty wind; Time-varying inflow.

Intercomparison of Atmospheric Dispersion Models Applied to an Urban Street Canyon of Irregular Geometry

Mariana Dezzutti 1, Guillermo Berri1, Laura Venegas2

Source: Aerosol and Air Quality research, Volume: 18 | Issue: 3 | Pages: 820-828
DOI: 10.4209/aaqr.2017.11.0489

The NOx concentrations measured at the sampling site of Cordoba Avenue, Buenos Aires City, characterised by an irregular geometry on both sides of the street, are used to intercompare results of five urban street canyon dispersion models, STREET, OSPM, AEOLIUSF, STREET-BOX and SEUS. Three different wind directions with respect to the street axis are considered, i.e., leeward, windward and parallel. Additionally, two wind speed classes are considered, above and below 2 m s–1. In order to evaluate the models

performance, observed and calculated concentrations are compared using different statistical measures, i.e., mean values, bias, mean square error and fractional error. In general, all models estimate better leeward conditions and wind speeds above 2 m s–1, with SEUS providing the overall best result.

Keywords: Atmospheric dispersion models; Intercomparison of results; Urban street canyon with irregular geometry.

Measurement of Variation of Radon-Thoron and their Progeny Concentrations in Dwellings using Pin Hole Based Dosimeters

Deep Shikha1, Vimal Mehta 1, Rishi Pal Chauhan2, Gurmel Singh Mudahar3

Source: Aerosol and Air Quality research, Volume: 18 | Issue: 3 | Pages: 811-819
DOI: 10.4209/aaqr.2017.10.0405

In the present investigation, newly designed pin hole based radon-thoron dosimeter with LR-115 track detectors has been used for the integrated determination of radon, thoron and their progeny levels in the indoor air of the dwellings of the Union Territory (U.T.) Chandigarh for checking the indoor air quality. The soil and the building materials are the major source of the indoor radon and the contribution of these towards indoor radon levels depends upon the radium content and exhalation rates and so can be used as a primary index for radon levels in the dwellings. Due to this the radon exhalation rate of some soil samples of the study area has been measured using active technique. The exhalation rate of the sand samples, utilized for the construction purpose, available from the study area has also been measured.

The concentration of indoor radon was varying from 24.2 ± 1.1 Bq m–3 to 62.1 ± 3.1 Bq m–3. The thoron concentration was found to be varying from 3.0 ± 0.1 Bq m–3 to 99.2 ± 4.9 Bq m–3. The annual inhalation dose received by the inhabitants of these dwellings is in the safe limits. A good positive correlation was found between indoor radon concentration and radon mass exhalation rate of the soil samples of the study area.

Keywords: Indoor radon; Indoor thoron; Annual effective dose; Exhalation rate.

The Effect of Cr Addition on Hg0 Oxidation and NO Reduction over V2O5/TiO2 Catalyst

Hao Song, Menglei Zhang, Jinpin Yu, Weihong Wu, Ruiyang Qu, Chenghang Zheng, Xiang Gao

Source: Aerosol and Air Quality research, Volume: 18 | Issue: 3 | Pages: 803-810
DOI: 10.4209/aaqr.2017.10.0411

A series of V2O5-Cr2O3/TiO2 catalysts with various chromium loadings prepared by the impregnation method were studied for Hg0 oxidation and NO reduction. The results indicate that Cr2O3-modified V2O5/TiO2 exhibited improved catalytic activity for both Hg0 oxidation and NO reduction. In fact, with the addition of 5% Cr2O3 to the V/Ti catalyst, the mercury oxidation efficiency increased significantly from 6.5% to 97% in the presence of O2 at 350°C, and its SCR performance also improved in the temperature range of 250°C to 400°C. To explore the effect of individual flue gas components on Hg0 oxidation, a series of activity tests were conducted over 1% Cr-V/Ti at 350°C, and it was found that O2 and HCl promote mercury oxidation, while SO2 and H2O exhibited a somewhat inhibitive influence. H2-TPR and XPS results indicated that the enhanced catalytic performance of V2O5-Cr2O3/TiO2 is attributable to the synergetic interactions between the two active phases.

Keywords: Mercury oxidation; NH3-SCR V2O5/TiO2 Cr2O3.

An Overview: Reaction Mechanisms and Modelling of CO2Utilization via Mineralization

Shu-Yuan Pan 1, Tung-Chai Ling2, Ah-Hyung Alissa Park3,4, Pen-Chi Chiang

Source: Aerosol and Air Quality research, Volume: 18 | Issue: 4 | Pages: 829-848
DOI: 10.4209/aaqr.2018.03.0093

Accelerated carbonation using alkaline solid wastes has been considered an effective approach to mineralizing flue gas CO2 from industries or power plants. Despite its recent progress, mechanistic understanding and modelling at interface levels are still needed to control the reactivity and equilibrium of the reaction system. This review focuses on several phenomenological models for accelerated carbonation that look at the solid-fluid interface. We first illustrate the principles of kinetic and mass transfer driven reactions for CO2-mineral-water systems. Then, we provide an overview into the reaction mechanisms

and modelling for CO2 mineralization including leaching-precipitation model, shrinking core model and surface coverage model. Advanced models considering multiple mechanisms, such as two-layer diffusion model, are also discussed. Finally, the perspectives and prospects are provided to shine a light on future directions, including incorporation of structural and physical properties in phenomenological models, identification of dynamic speciation by in-situ high-resolution equipment, and integration of heat transfer in reaction modelling for system optimization.

Keywords:Mechanism; Diffusion; Kinetics; Shrinking core model; Surface coverage model.

Carbonaceous Nanoparticle Layers Prepared using Candle Soot by Direct- and Spray-based Depositions

Ferry Faizal1, M.P. Khairunnisa1,2, Shunichiro Yokote2, I. Wuled Lenggoro 1,3

Source: Aerosol and Air Quality research, Volume: 18 | Issue: 4 | Pages: 856-865
DOI: 10.4209/aaqr.2017.10.0426

To investigate the properties and structures of soot particles derived from candle combustion, two deposition routes were performed. In "Route-1," the aerosol (soot) particles were collected by direct exposure of a substrate in a chamber with controlled airflows. In "Route-2," deposited soot nanoparticles was transferred into suspension and subsequently, the deposition of particles on to the substrate was achieved by an electrospray. Raman spectral analysis has shown the difference of G-band intensity relative to D-band between hydrophobic and hydrophilic particle layers obtained from different collection regions of the candle flame. It also reveals the effect of airflows during the collection to the ratio of the D to G peak. Meanwhile, the Raman spectra of the particles seem invariant to the preparation methods of suspension and electrospray deposition process. From the curve gradient of spectroscopy (190–2500 nm) results, the electrospray-deposited particle layers (Route-2) show higher absorbance in the near-infrared region compared to direct-deposited particle layers (Route-1). This change in the spectrum may due to the change in morphology of nanoparticle layers formed by each route.

Keywords: Aerosol deposition; Carbonaceous aerosols, Nanostructured materials Optical spectroscopy Soot.

A Comparison of PAH Emission Sampling Methods (Cyclone, Impactor) in Particulate and Gaseous Phase

Jiří Horák1, Lenka Kuboňová 1, Kamil Krpec1, František Hopan1, Petr Kubesa1, Jan Koloničný1, Daniela Plachá2,3

Source: Aerosol and Air Quality research, Volume: 18 | Issue: 4 | Pages: 849-855
DOI: 10.4209/aaqr.2017.10.0408

Four different domestic heating boilers and four types of fuel (lignite, wet wood, wood pellets and mixed fuel) were tested, and the emissions of the particulate matter (PM) and polycyclic aromatic hydrocarbons (PAHs) were correlated. Dekati low-pressure impactor (DLPI, Dekati) sorting of the PM fractions into PM0.1, PM1, PM2.5 and PM10 was used to determine the emission factors of the PAHs in a dilution tunnel via isokinetic sampling and was compared with a cyclone (Tecora). The 4 PAHs were mostly detected on the fine particles of PM1 in the DLPI and on the fine particles of PM2.5 in the cyclone, and in some cases, they were mainly detected in polyurethane foam (PUF) used for the collection of the gas phase placed behind the DLPI and cyclone. The effectiveness of DLPI sampling was generally comparable or lower than the cyclone sampling of the range 0.01–1.33 mg kg–1.

Keywords: Domestic heating; Particulate matter; PAH sampling; Impactor DLPI; Cyclone.

Flow Dynamics and PM2.5 Deposition in Healthy and Asthmatic Airways at Different Inhalation Statuses

Wei-Hsin Chen 1,2, Kuo-Hao Lee1, Justus Kavita Mutuku3, Chii-Jong Hwang1

Source: Aerosol and Air Quality research, Volume: 18 | Issue: 4 | Pages: 866-883
DOI: 10.4209/aaqr.2018.02.0058

Public health reports indicate that high PM2.5 concentration can impair the respiratory health of the residents, especially for those affected by asthma. Therefore, there is a need to determine the deposition mechanism and efficiencies for PM2.5 in asthmatic human airways. In this study, gas flow dynamics and deposition fractions (DFs) of PM2.5 in generations 10–11 of Weibel's lung model were investigated where the two-phase gas-solid flow behaviors in healthy and asthmatic airways were considered. The gas phase was

modeled as a transient laminar and incompressible flow while the discrete phase model (DPM) was applied for the particle phase. Three different air flow rates under rest, light activity, and moderate exercise were considered. For the healthy airways, higher total mass DFs were observed during a moderate exercise as compared to rest and light activity conditions. Deposition fractions were higher in asthmatic airways compared to those of healthy ones, stemming from tapering in the airways as well as complex secondary flow fields, namely, Dean vortices, in the folds. Deposition was mainly due to inertial forces of particles, but a small amount of PM2.5 was deposited near the entrance of asthmatic tube, as a result of the secondary flow. The numerical results revealed that the Dean vortices was an important factor for particle deposition. With increased DF, asthmatic people have a higher total respiratory dose of PM2.5 for a given exposure compared to healthy individuals. Thus contributing to their increased susceptibility to adverse health effects caused by PM2.5.

Keywords: PM2.5 Airway and asthma; Transient flow and inhalation; Two-phase flow; Computational fluid dynamics (CFD).

Radiative Forcing of Carbonaceous Aerosols over Two Urban Environments in Northern India

Abhilash S. Panicker 1, Rathod Aditi1, Gufran Beig1, Kaushar Ali1, Fabien Solmon2

Source: Aerosol and Air Quality research, Volume: 18 | Issue: 4 | Pages: 884-894
DOI: 10.4209/aaqr.2017.01.0056.

The radiative forcing of elemental carbon (EC) and organic carbon (OC) has been estimated over two urban environments in Northern India (Jabalpur [JBL] and Udaipur [UDPR]) from November 2011 till November 2012 (till September 2012 over Jabalpur). The elemental carbon concentrations reached 7.36 ± 1.99 μg m–3 over JBL and were as high as 10.78 ± 4.85 μg m–3 over UDPR, whereas the corresponding OC concentrations were much higher in different months (as high as 19.37 ± 12.6 μg m–3 over JBL and 39.71 ± 13.05 μg m–3 over UDPR). The radiative forcing for OC and EC has been estimated using an optical model along with a radiative transfer model. The surface OC radiative forcing was found to range from –2.19 ± 1.93 W m–2 to –3.083 ± 2.29 W m–2 over JBL and –1.97 ± 1.37 to –5.89 ± 2.17 W m–2 over UDPR, whereas the estimated top of the atmosphere (TOA) forcing ranged from –0.87 ± 0.49 to –1.87 ± 0.90 W m–2 over JBL and from –1.23 ± 0.31 to –3.44 ± 1.51 W m–2 over UDPR. However, the effect of EC forcing (as high as –21.75 W m–2 at the surface of and +6.3 W m–2 at TOA over JBL and –38.21 W m–2 at the surface of and +5.05 W m–2 at TOA over UDPR) was found to be more than tenfold higher than OC forcing due to its strong atmospheric absorption, in spite of much lower concentrations compared to OC.

Keywords: Elemental carbon; Organic carbon; Radiative forcing.

Effects of Chemical Composition of PM2.5 on Visibility in a Semi-Rural City of Sichuan Basin

Yun-Chun Li 1,2, Man Shu1, Steven Sai Hang Ho 3, Jian-Zhen Yu4, Zi-Bing Yuan4, Zi-Fang Liu5, Xian-Xiang Wang1, Xiao-Qing Zhao1

Source: Aerosol and Air Quality research, Volume: 18 | Issue: 4 | Pages: 957-968
DOI: 10.4209/aaqr.2017.08.0264.

The rate of visibility deterioration in Ya'an city in the Sichuan Basin has been accelerating since the 2000s. Issues related to the air quality as well as meteorological conditions are reported in this study. Fine particulate matters (PM2.5) were collected in Ya'an from June 2013 till June 2014. The chemical compositions of the samples were determined. The annual average visual range (VR), PM2.5 concentrations, and ambient light extinction coefficient (bext) were 11.9 ± 9.2 km, 64.1 ± 41.6 μg m−3, and 452 ± 314 Mm−1, respectively. The highest concentration of PM2.5, the highest bext, and the lowest VR were all seen in winter, followed by spring, autumn, and summer. Organic matter (OM), ammonium sulfate [(NH4)2SO4], and ammonium nitrate [NH4NO3] were the major constituents, accounting for 32.8%, 28.3%, and 12.1%, respectively, of the total PM2.5 mass. The revised Interagency Monitoring of Protected Visual Environments (IMPROVE) equation was applied to estimate ambient bext. On an annual basis, (NH4)2SO4 was the most significant contributor (43.1%), followed by OM (27.1%) and NH4NO3 (22.4%), which, in total, accounted for 92.6% of the ambient bext. Rayleigh, elemental carbon, fine soil, nitrogen dioxide, and chloride salt accounted for a minor fraction (7.4%). Up to ~40.8% of the ambient bext was ascribed to relative humidity (RH), of which 26.4% and 14.0% were attributed to the hygroscopic growth of (NH4)2SO4 and NH4NO3, respectively. More efforts are needed to reduce the average daily PM2.5 concentration of < 59 μg m−3 to avoid the occurrence of haze under a high average RH of 78.3 ± 10%, which significantly impacts visibility through various physico-chemical processes. Emissions of precursor gases, such as sulfur dioxide, nitrogen oxides, ammonia, and volatile organic compounds, should be reduced to improve the air quality and visibility in Ya'an.

Keywords: Fine particulate matter, Visibility, Light extinction coefficient, Chemical composition.

Chemical Characteristics and Source Apportionment of PM2.5 and Long-Range Transport from Northeast Asia Continent to Niigata in Eastern Japan

Ping Li 1,2, Keiichi Sato3, Hideo Hasegawa4, Minqun Huo3, Hiroaki Minoura3, Yayoi Inomata3, Naoko Take3, Akie Yuba3, Mari Futami3, Tsukasa Takahashi3, Yuka Kotake3

Source: Aerosol and Air Quality research, Volume: 18 | Issue: 4 | Pages: 938-956
DOI: 10.4209/aaqr.2017.05.0181

Seasonal intensive sampling was undertaken for two weeks during each of four seasons from May 2015 to February 2017 at Niigata-Maki station in Niigata, eastern Japan. Daily mean concentrations of PM2.5 ranged from 4.2 μg m–3 to 33.4 μg m–3 during the observation period, which were lower than Japanese Environmental Quality Standard for PM2.5 (35 μg m–3). The higher concentrations of SO42–, NH4+ and OC were observed in spring and summer, which may result from photochemical activity and secondary OC production. The major chemical components of PM2.5 at Niigata-Maki site were SO42–, NO3–, NH4+, OCM, EC and crustal elements. Compared with data at other urban sites, a lower concentration of EC and NO3– and higher OC/EC ratio were observed at Niigata-Maki site, which may result from no significant stationary source and low vehicular traffic in the rural site. PM2.5 source apportionment was characterized by positive matrix factorization (PMF) analysis, and the results inferred four major sources: sea salt (10.2%), biomass combustion (18.9%), soil dust (13.2%) and secondary aerosol (44.4%). The potential source contribution function (PSCF) analysis suggested that the major sources of secondary aerosol and sea salts were domestic in southwest Japan and the Sea of Japan, whereas the sources of biomass combustion and soil dust in specific seasons were long range transportation from the Northeast Asian continent (NEA). Comparing with previous studies in western Japan, this study showed a large domestic contribution of southwest Japan for secondary aerosol, while a larger contribution of the NEA was observed in the previous studies. Significant contribution of biomass combustion from northeast China in autumn, and local area in Niigata and southwest Japan in the other seasons was uniquely observed in this study.

Keywords: Secondary aerosol, Biomass combustion, Northeast, Asian continent , PMF PSCF

Aerosol Vertical Distribution and Typical Air Pollution Episodes over Northeastern China during 2016 Analyzed by Ground-based Lidar

Hujia Zhao1,2, Huizheng Che 1, Yaqiang Wang1, Yunsheng Dong3, Yanjun Ma2, Xiaoxiao Li4, Ye Hong2, Hongbin Yang2, Yuche Liu2, Yangfeng Wang2, Ke Gui1, Tianze Sun1, Yu Zheng1, Xiaoye Zhang1

Source: Aerosol and Air Quality research, Volume: 18 | Issue: 4 | Pages: 918-937
DOI: 10.4209/aaqr.2017.09.0327.

The industrial city of Shenyang in northeastern China has undergone a period of rapid development; long-term aerosol vertical properties could be relevant to more clearly understanding local emissions and their regional transportation. Aerosol optical depth (AOD), planetary boundary layer (PBL) height, and the vertical profiles of extinction coefficient, were measured and analyzed with ground-based Lidar during 2016 in Shenyang. Ground-level particulate matter mass concentrations, meteorological parameters, backward trajectories, and Moderate Resolution Imaging Spectroradiometer products were used to study the pollutant sources in four cases using the potential source contribution function and concentration-weighted trajectory methods. The results indicate that the AOD was 0.10 ± 0.10 to 0.23 ± 0.34 from January to May, and approximately 0.49 ± 0.39 in July. The PBL height was highest in March (1318.7 ± 696.5 m) and lowest in winter (877.1 ± 508.1 m to 950.7 ± 762.3 m). The mass concentrations of PM10, PM2.5, and PM1.0 were highest in January at 148.2 ± 77.8 μg m−3, 106.0 ± 58.8 μg m−3, and 33.8 ± 20.5 μg m−3; and lowest in June at 56.2 ± 27.8 μg m−3, 33.7 ± 18.3 μg m−3, and 9.3 ± 6.0 μg m−3, respectively. The concentrations of SO2 and CO were higher in winter and lower in summer, whereas O3 concentrations were higher in summer and lower in winter. The monthly extinction coefficient was affected by dust events in spring and new particle generation in summer, as well as by biomass-burning and coal-burning emissions in autumn and winter. Four pollution sources—from northwestern, eastern, northern, and northeastern China—were selected to analyze the different paths and sources of pollutants affecting Shenyang. The results of this paper will be helpful in the study of continuous year-round aerosol vertical properties and the regional pollution features of northeast China.

Keywords: Aerosol vertical distribution; Extinction coefficient; Ground-based lidar; Northeastern; China.

Weather Condition Dominates Regional PM2.5 Pollutions in the Eastern Coastal Provinces of China during Winter

Zhe Cai1,4, Fei Jiang 1,3, Jingming Chen1,2, Ziqiang Jiang1, Xiaoyuan Wang5

Source: Aerosol and Air Quality research, Volume: 18 | Issue: 4 | Pages: 969-980
DOI: 10.4209/aaqr.2017.04.0140.

China has suffered from severe particulate matter (PM) pollution in recent years. Both pollution areas and levels are increasing gradually. The PM pollution episodes not only occur in the traditional developed areas like the Yangtze River Delta (YRD) and the Beijing-Tianjin-Hebei (BTH) region, but also frequently happen in the eastern coastal provinces (ECPs) of China. Based on hourly fine-PM (PM2.5) concentrations during December 2013 to February 2014 of 55 cities located in the ECPs, we investigated the spatial and temporal variabilities of PM2.5 concentration and the corresponding meteorological conditions during winter. The results generally showed that the winter mean concentrations over all ECPs exceeded China's national standard of 75 μg m–3, and the most polluted areas with mean concentrations exceeding 150 μg m–3 were in the southwest of Hebei and the west of Shandong Province. The PM2.5 concentrations in February were lower than December in most areas, especially in the YRD, but they were higher over the north of Hebei Province. The spatial distributions and monthly variations were strongly related to weather conditions. Overall, severe PM pollution corresponded with stable weather conditions: small Sea Level Pressure gradient, lower Planetary Boundary Layer (PBL) height and weaker winds. Statistics showed that the changes of the mean PM2.5concentration over the ECP region lagged behind the variations in the PBL height and wind speeds by about 12–18 h, and the variations in weather conditions could explain about 71% (R2) of the overall changes in PM2.5 concentrations, indicating that regional PM2.5 pollution was dominated by weather conditions in the ECPs. This study gives insight into the PM2.5 pollution in the ECPs of China during winter, which would be helpful to predict and control the PM2.5 pollution for this area in the future.

Keywords: Weather condition; Regional PM2.5 pollution; China eastern coastal provinces.

Concentration of Ultrafine Particles near Roadways in an Urban Area in Chicago, Illinois

Sheng Xiang, Zhice Hu, Wenjuan Zhai, Dongqi Wen, Kenneth E. Noll

Source: Aerosol and Air Quality research, Volume: 18 | Issue: 4 | Pages: 895-903
DOI: 10.4209/aaqr.2017.09.0347

Monitoring ambient concentrations of ultrafine particles (UFPs) is important due to their negative impact on human health. This paper provides measurements of UFP concentrations near roadways because emissions from light duty vehicles (LDVs) and heavy duty vehicles (HDVs) have been shown to be a major source of UFPs. The concentration of UFPs was measured near two different roadways in Chicago IL for 2 to 4 hours on 52 days between 2014 and 2016. One of the sites was restricted to LDVs (Lake Shore Drive, LSD) and had a near roadway concentration from vehicles (background subtracted) that averaged nearly 8,000 particles cm–3. The other site had a mix of LDVs and HDVs (Dan Ryan Expressway, DRE) and the near roadway concentration from the vehicle fleet (background subtracted) averaged nearly 11,000 particles cm–3. The contribution of UFPs from HDVs was almost 80% of the total emissions on the DRE demonstrating that HDVs emit many more UFPs than LDVs. Background concentrations of UFP were measured upwind of the near roadway sampling sites and were subtracted from the near roadway measurements in order to determine the vehicle contribution to the total UFP concentration. The background concentrations varied with wind direction and therefore were divided into ambient background categories based on wind direction. The four different background categories are defined as remote, lake, industrial and urban. Each category has a distinct different average ambient background concentration (particles cm–3) as follows: remote, 2,700; lake, 6,000; industrial 12,000 and urban 11,000. The large background concentrations in urban areas indicate that total near roadway measurements are generally near 20,000 particles cm–3 with 50 to 60% from vehicles and reach to 60,000 particles cm–3 depending on the background and traffic emission. The results indicate high UFP readings near roadway and one possible solution is mitigation of traffic congestion.

Keywords: Ultrafine particles; Urban region; Ambient category; Vehicle emission; Human exposure Illinois.

Size-fractionated Particulate Matter in Indoor and Outdoor Environments during the 2015 Haze in Singapore: Potential Human Health Risk Assessment.

Ruchi Sharma, Rajasekhar Balasubramanian

Source: Aerosol and Air Quality research, Volume: 18 | Issue: 4 | Pages: 904-917
DOI: 10.4209/aaqr.2017.11.0515

Landscape fires in Indonesia during the 2015 resulted in large-scale emissions of airborne particulate matter (PM) that degraded ambient air quality of several countries in Southeast Asia (SEA) including Singapore. During this transboundary haze episode, the general public was advised to remain indoors as much as possible in order to mitigate their exposure to high concentrations of PM in the outdoor environment. To understand the quantitative relationship between outdoor and indoor air quality, we measured PM2.5 as well as the size-fractionated PM (coarse, accumulation and quasi-ultrafine (q-UF) particles) simultaneously inside and outside a naturally ventilated apartment and studied the potential health risk associated with exposure to PM of different sizes under the three levels of smoke haze (light, moderate and severe). PM mass concentrations increased with a decrease in particle size, and the q-UF particles (diameter ≤ 250 nm) were observed to be as high as 80 to 85 μg m–3 both indoors and outdoors. Estimation of PM deposition patterns along the human respiratory tract revealed that q-UF particles were mainly deposited in the deeper alveolar region, thereby posing severe health threats. Potential human health risk assessment results based on bioavailable concentrations of toxic elements in PM raised further concerns about health impacts of q-UF particles deposited in the alveolar region. Moreover, uncertainty analysis of exposure parameters used in potential carcinogenic health risk assessment model indicated much higher exceedance of potential health risk than the threshold limit for 95th percentile values of the health risk (11.5 times higher for PM2.5) during severe-haze episodes. The potential health risk estimated in this study indicates the need to conduct further studies focused upon mitigation of human exposure to achieve health benefits during haze episodes.

Keywords: Smoke haze, Size-fractionated particles, Bioavailable toxic elements, Potential human health risk, Uncertainty analysis.

Behavior of PCDD/Fs, PCBs, CBzs and PAHs during Thermal Treatment of Various Fly Ash from Steel Industry

Shuaixi Xu, Tong Chen, Xiaodong Li , Jianhua Yan, Kefa Cen

Source: Aerosol and Air Quality research, Volume: 18 | Issue: 4 | Pages: 1008-1018
DOI: 10.4209/aaqr.2017.11.0514

The integrated iron and steel industry is the main source of polychlorinated dibenzo-p-dioxins (PCDDs) and dibenzofurans (PCDFs), or, more briefly, of dioxins. These mainly arise from the sintering process but also from other operations, such as blast furnace, basic oxygen furnace and electric arc furnace. In this study, we investigated the contribution of fly ash from the above-mentioned operations to PCDD/Fs as well as other organic pollutants (polychlorinated biphenyls [PCBs], chlorobenzenes [CBzs] and polyaromatic hydrocarbons [PAHs]). The experiments were conducted using a lab-scale vertical tube reactor, and target pollutants in off-gas and residue were collected for analysis. The experimental results show that sintering fly ash generates far greater amounts of these pollutants than other fly ash, especially in terms of PCDD/Fs and dioxin-like PCBs, which are 2–3 orders of magnitude higher. The homologue group profiles of the target pollutants also show significant differences. Both the PCBs and CBzs are dominated by low-chlorinated compounds in all samples; however, the STA sample generated a much more high-chlorinated compounds. In addition, the correlations between various target pollutants based on all samples show that PCDDs are clearly related to the low-chlorinated PCBs and CBzs, and PCDFs are strongly related with high-chlorinated PCBs and CBzs. Within each homologue group of PCDD/Fs, the isomer signature was also further scrutinized, with special emphasis on the seventeen 2,3,7,8-substituted PCDD/Fs, as well as the seven PCDD-congeners and two TCDF usually associated with chlorophenol precursor routes, with the goal of shedding more light on the mechanism of PCDD/Fs-formation.

Keywords: PCDD/Fs; PCBs; CBzs; PAHs; Fly ash; Steel industry; Homologue profiles.

Atmospheric Deposition Impact of Polychlorinated Dibenzo-p-dioxin and Dibenzofuran on an Aquatic System in Central Taiwan

Shih-Tsung Tang1, Yi Chang 1, Jinning Zhu 2, Sheng-Lun Lin3

Source: Aerosol and Air Quality research, Volume: 18 | Issue: 4 | Pages: 981-993
DOI: 10.4209/aaqr.2018.03.0100

The content and congener profiles of 17 PCDD/Fs were measured in an aquatic system in central Taiwan that included both aquatic animals and sediment. The total averaged mass content of PCDD/Fs was 0.432, 0.671, 0.244 and 0.727 pg g–1, and the corresponding total

PCDD/Fs-WHO2005-TEQ were 0.070, 0.015, 0.024 and 0.018 pg WHO2005-TEQ g–1 in O. mossambica, M. meretrix, L. calcarifer and O. gigas, respectively. The total PCDD/Fs in the sediment in the coastal area (72.63 ng kg–1) was much higher than that in the fishponds (29.53 ng kg–1), but the corresponding WHO2005-TEQ values in the coastal area (0.545 ng WHO2005-TEQ kg–1) were lower than those in the fishponds (0.655 ng WHO2005-TEQ kg–1). The mass PCDD/F congener profiles of the aquatic animals and sediment samples in the fishponds and coastal area were dominated by more highly chlorinated PCDD/F congeners such as OCDD and OCDF, while the WHO2005-TEQ PCDD/F congener profiles were dominated by the less-chlorinated PCDD/F congeners such as 1,2,3,7,8-PeCDD and 2,3,4,7,8-PeCDF. Over a time periods ranging from 30 and 60 years, the modeled PCDD/F contents in the sediment ranged between 9.27 and 18.53 ng WHO2005-TEQ kg–1 in scenario A, and the PCDD/F contents ranged from 6.18–12.36 ng WHO2005-TEQ kg–1 in scenario B. Compared with the observed average values of sediment in this study, the ratios of the modeled and observed values ranged from 9.4–34.0.

Keywords: PCDD/Fs;Aquatic animal; Sediment POPs, Atmospheric deposition, Fishpond, Biota.

Atmospheric PM2.5 and total PCDD/Fs-WHO2005-TEQ Level: A Case of Handan and Kaifeng Cities, China.

Rong Zhao, Kangping Cui , Weiwei Wang, Lin-Chi Wang , Ping Yan

Source: Aerosol and Air Quality research, Volume: 18 | Issue: 4 | Pages: 994-1007
DOI: 10.4209/aaqr.2018.02.0040

From 2015 to 2017, the atmospheric PM2.5, the total PCDD/Fs-WHO2005-TEQ concentrations, PM2.5-bound total PCDD/Fs-WHO2005-TEQ contents, and the gas-particle partitioning of PCDD/Fs in Handan and Kaifeng were investigated. In addition, a regression analysis of the air quality index (AQI) and total PCDD/Fs-WHO2005-TEQ concentration was also studied. From 2015-2017, in Handan, the three-year average PM2.5 concentrations in spring, summer, autumn and winter were 66.9, 61.3, 74.8, and 138 μg m–3, respectively and averaged 85.3 μg m–3, which was 1.2 orders of magnitude higher than that in Kaifeng (71.1 μg m–3). The three-year average PM2.5-bound total PCDD/Fs-WHO2005-TEQ content in spring, summer, autumn, and winter in Handan were 0.88, 0.28, 0.67, and 0.72 ng WHO2005-TEQ g–1, respectively, and averaged 0.64 ng WHO2005-TEQ g–1, which was 1.1 order of magnitude higher than that in Kaifeng (0.57 ng WHO2005-TEQ g–1). The three-year average fraction of gas phase total PCDD/Fs-WHO2005-TEQ concentrations in spring, summer, autumn, and winter in Handan were 26.4%, 62.8%, 28.9%, and 3.34%, respectively, and averaged 30.4%. The three-year average fraction of

gas phase total PCDD/Fs-WHO2005-TEQ concentrations in Kaifeng (34.3%) was 1.1 order of magnitude higher than that in Handan (30.4%). Positive correlations between the AQI and the total PCDD/Fs-WHO2005-TEQ concentration were found and their R2 values in 2015, 2016, and 2017 were 0.929, 0.921, and 0.876, respectively. Therefore, the AQI can be used to roughly predict the level of total PCDD/Fs-WHO2005-TEQ in ambient air through the use of a regression equation in these two cities.

Keywords: AQI; PM2.5; PM10; PCDD/Fs; Phase distribution; Regression analysis TEQ.

Suppression of PCDD/Fs by Raw Meal in Cement Kilns

Xiaoqing Lin1, Longjie Ji2, Mingxiu Zhan 1,3, Lingshu Wang1, Tong Chen1, Shengyong Lu1, Xiaodong Li1, Jianhua Yan1

Source: Aerosol and Air Quality research, Volume: 18 | Issue: 4 | Pages: 1032-1043
DOI: 10.4209/aaqr.2018.01.0023

Raw meal of the cement production process could probably suppress the formation of polychlorinated dibenzo-p-dioxins and dibenzofurans (PCDD/Fs). In this study, these suppression effects were studied and compared during the co-processing of municipal solid waste (MSW) with conventional feed materials such as pure CaCO3, and pure CaO. A top suppression efficiency of 96% was achieved for a ratio of MSW to raw meal of 1:15. Moreover, NaCl and CuCl2 were added to the mix of feed material and MSW, to reveal the impact of additional chlorine and cations on PCDD/F formation. Similarly, the raw meal was mixed with the kiln dust to investigate possible suppression effects of those PCDD/Fs formed through the precursor or the de novo synthesis at a temperature of 350°C. The raw meal suppressed the formation of PCDD/Fs from kiln dust. Furthermore, the raw meal could not suppress the formation of PCDD/Fs on mixtures of kiln dust and NaCl or CuCl2, which could be associated with a potential increase in the formation effects of PCDD/Fs on the raw meal. The results can help in potential decision-making on the applicability of certain cement kilns on the co-processing of MSW containing high levels of Cl and Cu.

Keywords: PCDD/Fs; Cement kiln; Raw meal; Suppression; MSW co-processing.

Variation of Atmospheric PAHs in Northern Taiwan during Winter and Summer Seasons

Nguyen-Duy Dat, Jia-Ming Lyu, Moo-Been Chang

Source: Aerosol and Air Quality research, Volume: 18 | Issue: 4 | Pages: 1019-1031
DOI: 10.4209/aaqr.2018.01.0038

Ambient air samples were collected simultaneously at three sites in winter and summer to investigate the characteristic variations of PAHs in northern Taiwan. In winter, the highest concentration was observed at urban site (225 ± 25.0 ng m−3), followed by industrial and rural sites (173 ± 28.7 and 148 ± 12.9 ng m−3, respectively). However, in summer, the highest PAHs concentration was measured at rural site (230 ± 8.0 ng m−3), followed by urban and industrial sites (205 ± 29.2 and 200 ± 44.1 ng m−3, respectively). Based on the air mass back trajectory, the air mass passing through more PAH sources before reaching the sampling site is the reason for higher PAH level being measured at rural site in summer. The highest BaP-TEQ concentration measured at rural site in summer suggests that human exposure to PAHs in summer should receive more attention. Based on the diagnostic ratios, samples collected at industrial site in two seasons are closely related to combustions of solid fuel and petroleum. At rural and urban sites, PAHs measured in winter are influenced by mixed sources of solid fuel/petroleum combustions and petroleum evaporation, while the sources of PAHs are more related to petroleum evaporation in summer. The gas/particle partitioning coefficients (Kp) correlated well with the sub-cooled liquid vapor pressures (PoL) of PAHs with the slopes higher than −1 (the r2 ranging from 0.835 to 0.909). The slope values indicate that both adsorption and absorption might govern gas/particle partitioning of PAHs. Comparison between different models reveals that adsorption of soot carbon is the major mechanism governing gas/particle partitioning.

Keywords: Junge-Pankow model; Absorption KOA model; Soot-air model; PAHs concentration; Distribution.

Impact of Aerosol Direct Effect on Wintertime PM2.5 Simulated by an Online Coupled Meteorology-Air Quality Model over East Asia

Ami Sekiguchi , Hikari Shimadera, Akira Kondo

Source: Aerosol and Air Quality research, Volume: 18 | Issue: 4 | Pages: 1068-1079
DOI: 10.4209/aaqr.2016.06.0282

This study aims to evaluate the impacts of the aerosol direct effect on simulated concentrations of fine particulate matter (PM2.5) over East Asia, which is controlled by heavy local air pollution and long-range transport. The online coupled Weather Research and Forecasting-Community Multiscale Air Quality (WRF-CMAQ) modeling system was applied to one-way and two-way simulations (without and with the aerosol direct effect) of a period from January till March of 2014. The differences between the two simulations showed that there were particularly large impacts of the aerosol direct effect on the eastern Asian continent with high aerosol loading. The temporal mean contributions of the direct effect averaged over the regions from Northeast to Central China were a 15%

decrease in the surface shortwave radiation, a 9.0% decrease in the planetary boundary layer (PBL) height, and an 8.6% increase in the ground-level PM2.5 concentration. In addition, there were negative contributions of the direct effect to the PM2.5 concentration over the ocean from the Sea of Japan to the East China Sea (a 1.0% decrease on average throughout the period). The PM2.5 decrease over the ocean was likely attributable to a reduction in the secondary PM2.5 outflow from the continent to the downwind region, which was caused by the increased dry deposition of PM2.5 precursors from the increased ground-level concentrations within a more stable PBL over the continent. Overall, the substantial decrease in the surface shortwave radiation due to the aerosol direct effect led to enhanced atmospheric stability and therefore increased the ground-level PM2.5 in the heavily polluted region.

Keywords: Online coupled WRF-CMAQ model; Shortwave radiative feedback; Atmospheric stability; Fine particulate matter.

Impacts of Air-sea Interactions on Regional Air Quality Predictions Using a Coupled Atmosphere-ocean Model in Southeastern U.S.

Jian He, Ruoying He, Yang Zhang

Source: Aerosol and Air Quality research, Volume: 18 | Issue: 4 | Pages: 1044-1067
DOI: 10.4209/aaqr.2016.12.0570

Air-sea interactions have significant impacts on coastal convection and surface fluxes exchange. They are important for the spatial and vertical distributions of air pollutants that affect public health, particularly in densely populated coastal areas. To understand the impacts of air-sea interactions on coastal air quality predictions, sensitivity simulations with different atmosphere-ocean coupling are conducted in this work over southeastern U.S. in July 2010 using the Weather Research and Forecasting Model with Chemistry (WRF/Chem). The results show that comparing to WRF/Chem without air-sea interactions, WRF/Chem with a 1-D ocean mixed layer model (WRF/Chem-OML) and WRF/Chem coupled with a 3-D Regional Ocean Modeling System (WRF/Chem-ROMS) predict the domain averaged changes in the sea surface temperature of 0.06°C and 0.94°C, respectively for July average. The simulated differences in the surface concentrations of O3 and PM2.5 between WRF/Chem-ROMS and WRF/Chem can be as large as 17.3 ppb and 7.9 μg m–3, respectively, with the largest changes occurring not only along coast and remote ocean, but also over some inland areas. Extensive validations against observations show that WRF/Chem-ROMS improves the predictions of most cloud and radiative variables, and surface concentrations of some chemical species such as SO2, NO2, maximum 1-h and 8-h O3, SO42–, NH4+, NO3–, and PM10. This illustrates the benefits and needs of using coupled

atmosphere-ocean model with advanced model representations of air-sea interactions for regional air quality modeling.

Keywords: O3 PM2.5, Air-sea interaction, WRF/Chem, ROMS COAWST, Coupled atmosphere-ocean model.

NO Adsorption and Oxidation on Mn Doped CeO2 (111) Surfaces: A DFT+U Study

Lu Liu1, Chenghang Zheng2, Junfeng Wang1, Yongxin Zhang2, Xiang Gao [2], Kefa Cen[2]

Source: Aerosol and Air Quality research, Volume: 18 | Issue: 4 | Pages: 1080-1088
DOI: 10.4209/aaqr.2017.12.0597

The adsorption of NO molecules on Mn-doped CeO2 (111) surfaces for NO oxidation has been studied by employing the periodic density functional theory plus U (DFT+U) method. Through our calculations, it is demonstrated how Mn-doped CeO2 with superior NO oxidation activity benefits from the high mobility of the oxygen near the Mn cations. On unreduced Mn-doped CeO2 (111) surfaces, the NO molecule preferentially interacted with the first neighboring O of the Mn cation, with the N also bonding to an Mn cation (Eads = –3.30 eV) or Ce cation (Eads = –2.90 eV). When NO adsorbs on the surface of defective Mn-doped CeO2 with O2 adsorbed in advance, an ONOO* four atoms species is formed on the surface (Eads = –2.51 eV and –2.02 eV), which is an intermediate and can decompose into NO2, NO2* and O*. The adsorption structure with higher adsorption energy has a closer geometry to NO2, indicating a deeper oxidation of NO. The calculation results indicate that the presence of Mn only has a strong effect on the nearby oxygen atoms and that the Mn-doped CeO2 surface has similar properties to a noble metal in NO oxidation catalysis. In DOS plots, the spin of the electron state of the adsorption structures involving the oxidation of NO is symmetric, indicating that electron transfer occurs from the slab to NO and strong covalent bonds are formed between N and O on the slab, which can also be confirmed by the charge density difference plots.

Keywords: Adsorption; Ceria Manganese NO ; Density functional theory.

Immiscible Multiphase Flow Behaviours of Water-Oil-CO2 Ternary System Flooding Using X-ray CT

Shu Wang 1, Duoxing Yang 2, Rongshu Zeng3

Source: Aerosol and Air Quality research, Volume: 18 | Issue: 4 | Pages: 1089-1101
DOI: 10.4209/aaqr.2017.12.0598

Carbon dioxide (CO2) injection into oil reservoirs has been widely accepted as an effective technique for enhanced oil recovery (EOR) after waterflooding. More recently, the development of carbon capture and storage (CCS) to reduce CO2 emissions has made CO2-based EOR increasingly attractive. Waterflooding is widely employed in China and, even after several years of water injection, considerable oil deposits remain in the thick, positive rhythm reservoirs in eastern China. The majority of these reservoirs may not be suitable for miscible CO2 flooding. The present work investigated immiscible CO2 flooding after waterflooding in such sites by laboratory trials. Series of large artificially-consolidated sandstone models with different levels of heterogeneity were used to simulate thick, positive rhythm oil reservoirs. Gaseous CO2 was continuously injected into these models at a constant injection pressure and an X-ray CT scanner (with a resolution of 0.7 × 0.7 mm) was used to monitor and record changes in the fluid saturation and migration. Based on the experimental results, it indicates that immiscible CO2 flooding following waterflooding is an efficient means of enhancing oil recovery. It is evident that both the reservoir heterogeneity and injection pressure differential affect oil recovery and CO2 distribution. The heterogeneity has a remarkable impact on oil recovery when the permeability differential between layers is lower than 2 millidarcy (md) or the permeability variation coefficient is less than 0.2. Fitting of the experimental results also demonstrates that there is an optimum pressure differential between inlet and outlet that maximizes oil recovery under specific inhomogeneous conditions.

Keywords: CO2 capture and storage (CCS); Flooding X-ray CT Heterogeneity.

Electrostatic Precipitation of Submicron Particles with an Enhanced Unipolar Pre-Charger

Zelong Liao1, Yuheng Li1, Xiangsheng Xiao1, Chen Wang1, Shang Cao1, Yong Yang 1,2

Source: Aerosol and Air Quality research, Volume: 18 | Issue: 5 | Pages: 1141-1147
DOI: 10.4209/aaqr.2017.08.0261

A two-stage electrostatic precipitator (ESP) has been developed using an enhanced unipolar pre-charger with dielectric coated ground electrodes. The electrical and particle collection performance was evaluated for particles in the submicron range. By varying the voltage applied to the pre-charger, the particle charging characteristics was compared with that calculated by the theoretical model. The experimental results show that with the adoption of the pre-charger, the charging of the particles at submicron range was enhanced. Further results indicate that the collection efficiency can be improved by about 12.1%–15.9%, compared with the results obtained without the pre-charger. Higher particle

collection efficiency can be achieved by increasing the voltage applied to the pre-charger. The unipolar pre-charger studied in this paper proves to be a simple and useful device to improve the submicron particle collection efficiency of conventional ESPs.

Keywords: Unipolar pre-charger; Electrostatic precipitator; Particulate matter; Corona discharge, Submicron particle.

Langley Calibration of Sunphotometer using Perez's Clearness Index at Tropical Climate

Jackson H.W. Chang 1, Nurul H.N. Maizan2, Fuei Pien Chee2, Jedol Dayou2

Source: Aerosol and Air Quality research, Volume: 18 | Issue: 5 | Pages: 1103-1117
DOI: 10.4209/aaqr.2016.10.0455

In the tropics, Langley calibration is often complicated by abundant cloud cover. The lack of an objective and robust cloud screening algorithm in Langley calibration is often problematic, especially for tropical climate sites where short, thin cirrus clouds are regular and abundant. Errors in this case could be misleading and undetectable unless one scrutinizes the performance of the best fitted line on the Langley regression individually. In this work, we introduce a new method to improve the sun photometer calibration past the Langley uncertainty over a tropical climate. A total of 20 Langley plots were collected using a portable spectrometer over a mid-altitude (1,574 m a.s.l.) tropical site at Kinabalu Park, Sabah. Data collected were daily added to Langley plots, and the characteristics of each Langley plot were carefully examined. Our results show that a gradual evolution pattern of the calculated Perez index in a time-series was observable for a good Langley plot, but days with poor Langley data basically demonstrated the opposite behavior. Taking advantage of this fact, the possibly contaminated data points were filtered by calculating the Perez derivative of each distinct air mass until a negative value was obtained. Any points that exhibited a negative derivative were considered bad data and discarded from the Langley regression. The implementation was completely automated and objective, rendering qualitative observation no longer necessary. The improved Langley plot exhibits significant improvement in addressing higher values for correlation, R, and lower values for aerosol optical depth, τa. The proposed method is sensitive enough to identify the occurrence of very short and thin cirrus clouds and is particularly useful for sun-photometer calibration over a tropical climate.

Keywords: Langley calibration; Perez model; Sunphotometer; Tropical climate; Aerosol optical depth.

Design and Performance Evaluation of a Laboratory-made 200 nm Precut Electrical Cascade Impactor

Jangseop Han1, Joohee Seo1, Dongho Park2, Junho Hyun3, Jungho Hwang 1,3

Source: Aerosol and Air Quality research, Volume: 18 | Issue: 5 | Pages: 1118-1130
DOI: 10.4209/aaqr.2017.11.0471

Increasing public concern regarding air quality has led to the development of efficient aerosol-monitoring techniques. Among the various aerosol measurement instruments based on electrical methods, in this study, an electrical cascade impactor (ECI) was designed and fabricated in our laboratory and was used to measure the real-time size distribution of submicron-sized aerosols. In the study by Park et al. (2007), it was assumed that the size distribution of incoming particles follows a unimodal lognormal distribution. However, in this study, the distribution of particles captured at each stage (including the Faraday cage) was assumed to be a unimodal lognormal distribution; hence, the incoming particles may follow any size distribution. After the particle charging characteristics were obtained for different particle sizes, experiments were performed with monodisperse test particles to determine the collection efficiency of each stage. The current measured in each stage was converted into a number based size distribution of aerosols by using the data inversion algorithm, which utilized the experimentally obtained collection efficiency. Then, a performance evaluation was performed, both in the laboratory and in the field. The results obtained by our ECI were in agreement with the scanning mobility particle sizer (SMPS) data.

Keywords: Electrical cascade impactor, Submicron-sized aerosols, Corona charger, Data inversion algorithm, Particle size distribution.

Effects of Three-partitioned Horizontal Inlet and Clean Air on Collection Efficiency and Wall Loss of Slit Virtual Impactors

Muhammad Zeeshan Zahir, Ji-Eun Heo, Se-Jin Yook

Source: Aerosol and Air Quality research, Volume: 18 | Issue: 5 | Pages: 1131-1140
DOI: 10.4209/aaqr.2017.12.0563

A numerical and experimental investigation comparing two configurations for a slit nozzle virtual impactor, one using a three-partitioned horizontal inlet and the other using a typical vertical inlet, was conducted to improve collection efficiency and reduce wall loss. All parameters, such as the length and width of the acceleration nozzle, the width of the

collection nozzle, the distance between the two nozzles, and the inlet flow rate, were kept constant, and only the inlet configuration was changed. The ratio of the minor to the total flow rate was fixed at 0.1. Parametric analysis was performed to study the flow-rate influence of incoming clean air and aerosol on the performance of the three-partitioned horizontal inlet virtual impactor. The square root of the Stokes number, (Stk)1/2, was used to characterize the collection efficiency and wall loss of both configurations. It was observed that by using the three-partitioned horizontal inlet, the cut-off diameter was reduced from (Stk)1/2 = 0.80 to (Stk)1/2 = 0.41, and the wall loss near the cut-off diameter decreased from 25%–45% to below 4.5%. Moreover, using the three-partitioned horizontal inlet reduced the contamination by particles smaller than the cut-off size in the minor outflow section of the virtual impactor to almost 0%.

Keywords: Virtual impactor; Slit nozzle; Collection efficiency; Wall loss; Stokes number.

Seasonal Variations of Atmospheric Particulate Matter and its Content of Heavy Metals in Klang Valley, Malaysia

Rasheida E. Elhadi1, Ahmad Makmom Abdullah 1, Abdul Halim Abdullah2, Zulfa Hanan Ash'aari1, Md Firoz Khan3

Source: Aerosol and Air Quality research, Volume: 18 | Issue: 5 | Pages: 1148-1161
DOI: 10.4209/aaqr.2017.03.0113

The composition of atmospheric particulate matter (PM10) can help to identify its potential sources and possible impact on human health. This study investigates the seasonal variations and sources of heavy metals in PM10 in the Cheras area. PM10 samples were collected on a 24-h basis using a high-volume air sampler in June during the southwest monsoon and in December during the northeast monsoon of 2014. Selected hazardous trace metals, viz., As, Pb, Cu, Ni, Cd, Co, Mn, Zn, Fe, Cr, V and Ba, were measured by inductively coupled plasma mass spectrometry (ICP-MS). The result showed that the mean concentrations of PM10 were 207.63 ± 7.82 and 138.32 ± 4.67 during the southwest and northeast monsoons, respectively. The heavy metal concentrations during the southwest monsoon followed the order Ba > Fe > Cu > V > Zn > Pb > Mn > Cr > As > Ni > Cd > Co, while those during the northeast monsoon followed the order Zn > Fe > Ba > Cu > Pb > V > Cr > As > Mn > Ni > Cd > Co. The results of the enrichment factors (EFs) showed that the major trace metals mainly originated from anthropogenic sources. A correlation analysis indicated that pairs of trace metals from similar sources were suspended in PM10 in the ambient air. The source apportionment by principal component analysis (PCA) and cluster analysis (CA) suggested that vehicle exhaust and brake and tire wear, industrial emissions

and the re-suspension of dust, as well as oil combustion, were the most dominant sources of PM10 in this study.

Keywords: Particulate matter PM10 Heavy metals Seasonal change Enrichment factors Meteorological factors Multivariate modeling.

Fragrances and Aerosol during Office Cleaning

Aikaterini Maria Zarogianni, Glykeria Loupa , Spyridon Rapsomanikis

Source: Aerosol and Air Quality research, Volume: 18 | Issue: 5 | Pages: 1162-1167
DOI: 10.4209/aaqr.2017.08.0270

Fragrance compounds emitted during and after the use of cleaning products in an office were monitored. Mopping the floor with a general purpose cleaner and a domestic bleach and cleaning the windows with an aerosol glass cleaner, as well as a combination of these cleaning activities, were carried out. The following compounds were found in detectable amounts: d-limonene, α-pinene, α-terpineol, 2-butoxyethanol, 1,3,5-trimethylbenzene, eucalyptol, tetrahydrolinalool and diphenyl ether.

Along with the fragrances, the number concentrations of airborne particles with an aerodynamic diameter range between 0.2 μm and 10 μm were monitored continuously. Cleaning affected the number concentrations of all particle sizes, but particles with an aerodynamic diameter above 0.4 μm were the most affected. The largest increase above background concentrations was observed during mopping the floor with a solution of general purpose cleaner in combination with cleaning the windows with a glass-cleaning spray. In this case, for particles larger than 0.4 μm, indoor number concentrations were 19 times larger than the background concentrations. Conversely, for particles below 0.4 μm, number concentrations increased only 4 times above the background concentrations during the same event. Auxiliary measurements included carbon dioxide (CO2) concentrations and the indoor micro-climatic conditions (air velocity, light intensity, temperature and relative humidity).

Keywords: Household cleaning products, Mopping, Window cleaning, Terpenes, Particles.

Vertical Ozone Concentration Profiles in the Arabian Gulf Region during Summer and Winter: Sensitivity of WRF-Chem to Planetary Boundary Layer Schemes

Christos Fountoukis 1, Mohammed A. Ayoub1, Luis Ackermann1, Daniel Perez-Astudillo1, Dunia Bachour1, Ivan Gladich1, Ross D. Hoehn1,2

Source: Aerosol and Air Quality research, Volume: 18 | Issue: 5 | Pages: 1183-1197
DOI: 10.4209/aaqr.2017.06.0194

Air quality in the Middle East is changing due to extensive land conversion, intense industrialization and rapid urbanization. In this study, we analyze data from an ozonesonde station operated in Doha, Qatar, by the Qatar Environment and Energy Research Institute (QEERI). Ozonesondes were launched weekly at 13:00 LT (10:00 UTC) during a summer month (August 2015) representative of extremely hot and humid atmospheric conditions and during a winter period (January–February 2016) representative of cool conditions in the area. Unlike similar studies in the region, this work focuses on the lower troposphere and combines high frequency vertical measurement data with the use of the Weather Research Forecasting model coupled with Chemistry (WRF-Chem). A sensitivity study was conducted to identify the most representative planetary boundary layer (PBL) parameterization. Although all three parameterizations that were examined produced similar results, the Yonsei University (YSU) PBL scheme was found to be statistically superior. Comparisons of model predictions against observations show high correlation coefficients and encouragingly low biases in all meteorological variables. During wintertime, ozone is well predicted overall (fractional bias = –0.1). Results from the summertime comparison are more challenging and point towards possible biases in the anthropogenic emission inventory of the Middle East, especially for rapidly-changing urban environments.

Keywords: PBL; Mixing height; Lower troposphere; WRF-Chem; Middle East.

Meteorological Influences on Tropospheric Ozone over Suburban Washington, DC

Mayra I. Oyola 1, Anna Schneider2, James Campbell3, Everette Joseph4

Source: Aerosol and Air Quality research, Volume: 18 | Issue: 5 | Pages: 1168-1182
DOI: 10.4209/aaqr.2017.12.0574

During the NASA DISCOVER-AQ (Deriving Information on Surface conditions from Column and Vertically Resolved Observations Relevant to Air Quality) campaign conducted in July 2011 across metropolitan Washington, DC, 25 daytime ozonesondes were launched from the Howard University Beltsville Campus (HUBC), representing the highest temporal density of measurements ever taken over the region. Time-height depiction of ozone concentration reveals considerable variability near the surface and in the mid/upper troposphere. Meteorological influences are assessed using the synoptic and mesoscale information, which revealed that periodic stratospheric intrusion of ozone-rich air was the main mechanism for elevated levels in the upper troposphere. It is also shown that high concentrations of ozone prevalent in the free troposphere were due to a combination of advection and aged air masses, which accounted for over 40% of the total budget. Poor air quality episodes with high surface concentration were due local emissions of precursors and associated synoptic-scale conditions. Breaks in the elevated ozone concentrations in the boundary layer and free troposphere occurred from frontal passages and accompanying storms. In the most unusual case (26 July, 2011), the combined effect of storms followed by two frontal passages and high pressure positioned west of the region led to decrease column ozone as much as 70%. The unusually deep extent of the reduction appears to be related to the temporary cutoff of air advected from fire locations and polluted regions, which dominated the upper troposphere throughout the period.

Keywords: Tropospheric ozone, Stratospheric injections , Laminar analysis, Meteorological influence on ozone, NASA DISCOVER-AQ Beltsville MD.

Spatio-temporal Variations in NO2 and PM2.5 over the Central Plains Economic Region of China during 2005-2015 Based on Satellite Observations.

Kun Cai1,2, Shenshen Li 3, Fengbin Zheng 2, Chao Yu3, Xueying Zhang4, Yang Liu2, Yujing Li2

Source: Aerosol and Air Quality research, Volume: 18 | Issue: 5 | Pages: 1221-1235
DOI: 10.4209/aaqr.2017.10.0394

The Central Plains Economic Region (CPER) is located in central eastern China and has experienced tremendous economic growth in the last decade. Like many areas in China, the rapid economic development of the CPER has led to serious air pollution problems, including extremely high concentrations of nitrogen dioxide (NO2) and particulate matter with an aerodynamic diameter less than 2.5 μm (PM2.5). However, the current air pollution monitoring system lacks good spatial and temporal coverage. Therefore, we used high-resolution satellite remote sensing techniques to analyze the variation in NO2 and PM2.5 in

the CPER from 2005 through 2015. The Ozone Monitoring Instrument (OMI) and the Moderate Resolution Imaging Spectroradiometer (MODIS) were used to retrieve the tropospheric NO2 columns and ground-level PM2.5 concentrations, respectively. High NO2 and PM2.5 concentrations were mainly located in the central and northern areas of the CPER. The highest 11-year average concentrations were found in the city of Jiaozuo for NO2 (19.54 × 1015 molecules cm–2) and in the city of Hebi for PM2.5 (107.8 μg m–3). The western and southern mountainous areas had lower NO2 and PM2.5 concentrations. The average seasonal NO2 and PM2.5 concentrations were both highest in winter and lowest in summer. The average monthly concentrations of NO2 and PM2.5 were as high as 24.60 × 1015 molecules cm–2 and 152.2 μg m–3, respectively, in January 2013 and as low as 43.86 × 1015 molecules cm–2 and 40.2 μg m–3, respectively, in July 2006. During the 11-year study period (2005–2015), the CPER concentrations of both NO2 and PM2.5 decreased from 2011 to 2015 by 31.5% and 36.8%, respectively. This study successfully applies satellite remote sensing data to quantitatively analyze the spatial-temporal distributions of tropospheric NO2 and ground-level PM2.5. This approach can support air pollution monitoring in the CPER, and the estimated concentrations can provide references for environmental policymaking.

Keywords: PM2.5, NO2, CPER, OMI, MODIS.

Characterization of the Air Quality Index for Wuhu and Bengbu Cities, China.

Weiwei Wang1, Kangping Cui 1, Rong Zhao1, Lien-Te Hsieh 2, Wen-Jhy Lee3

Source: Aerosol and Air Quality research, Volume: 18 | Issue: 5 | Pages: 1198-1220
DOI: 10.4209/aaqr.2018.04.0135

From 2015–2017, the atmospheric PM10, SO2, NO2, CO, and O3 in Wuhu and Bengbu were investigated in this study. In addition, the AQI values and seasonal variations in six AQI classes and corresponding primary pollutants were also studied. In Wuhu, the daily AQI ranged from 23 to 298 in 2015, from 33 to 290 in 2016, and from 34 to 278 in 2017, and the corresponding mean values were 81, 80 and 90, respectively. In Bengbu, the daily AQI ranged from 23 to 288 in 2015, from 32 to 286 in 2016, and from 27 to 500 in 2017, and the corresponding mean values were 88, 89 and 97, respectively. During the three-year study, in Wuhu, the mean proportion of levels with Grade I, II, III, IV, V and VI were 9.33%, 69.3%, 18.3%, 3.00%, 0% and 0% in spring; were 35.0%, 55.0%, 7.00%, 3.00%, 0% and 0% in summer; were 13.6%, 65.0%, 18.0%, 3.33%, 0% and 0% in fall, and were 5.33%, 48.7%, 30.7%, 9.67%, 5.67% and 0% in winter. In Bengbu, the mean proportion of levels with Grade I, II, III, IV, V and VI were 3.00%, 64.0%, 30.3%, 2.67%, 0.333% and 0.333% in

spring; were 19.3%, 68.7%, 11.3%, 0.667%, 0% and 0% in summer; were 20.7%, 56.3%, 17.3%, 4.67%, 1.00% and 0% in fall, and were 9.67%, 36.7%, 31.0%, 32.0%, 5.67% and 0% in winter. Generally, the air quality in the two cities were in the following order: summer > fall > spring > winter. AQI ranged between 101–150, where in Wuhu, the primary air pollutants were PM2.5 and NO2 in 2015; were PM2.5, NO2 and O3 in 2016, and were PM2.5, PM10, NO2 and O3 in 2017. In Bengbu, PM2.5, PM10 and O3 were the primary air pollutants during the three years. When AQIs ranged between 151 and 200, in Wuhu, the primary air pollutant was PM2.5 in 2015; were PM2.5 and PM10 in 2016, and were PM2.5, PM10, and O3 in 2017. In Bengbu, the primary air pollutant was PM2.5 in 2015 and 2016 and comprised PM2.5 and O3 in 2017. When AQIs were between 201 and 300, in Wuhu, PM2.5 was the primary air pollutant in 2015–2017. In Bengbu, the primary air pollutant was PM2.5 in 2015 and 2016 and comprised PM2.5 and PM10 in 2017. When the AQI ranged between 301–500, which did not occur in Wuhu from 2015–2017 or in Bengbu during 2015–2016, PM2.5 was as the primary air pollutant in Bengbu in 2017. When the AQI can be analyzed in more detail, the control strategies for air pollution will be more precise.

Keywords: AQI; PM10; PM2.5; SO2; NOx; CO; O3.

Evaluation of Uncertainty Associated with Determination of Particle-bound PAHs in Ambient Area by TD-GC/MS and Soxhlet-GC/MS

Iñaki Elorduy, Nieves Durana, José Antonio García, María Carmen Gómez, Lucio Alonso

Source: Aerosol and Air Quality research, Volume: 18 | Issue: 5 | Pages: 1236-1245
DOI: 10.4209/aaqr.2017.12.0578

Knowing the uncertainty associated with an analytical method is necessary to evaluating the quality of the results. In this work, the uncertainty associated with the analytical measurement of polycyclic aromatic compounds (PAHs) in ambient air using thermal desorption coupled with gas chromatography-mass spectrometry (TD-GC/MS) was evaluated. The study focused on analyses of the particulate phase (PM10), and the results were compared to those obtained with a conventional solvent extraction (Soxhlet-GC/MS). The main sources of the combined uncertainty were the calibration curve, recovery of the extraction stage, area or volume of the sample and volume of air. TD-GC/MS reported a lower combined uncertainty (< 10%) than Soxhlet-GC/MS (values between 11% and 18%) for the measurement of particle-bound PAHs in the air, which was primarily contributed by the recovery of the analyzed PAHs and the calibration curves.

Keywords: Uncertainty PAHs Thermal desorption Soxhlet extraction GC-MS PM10 samples.

Emission Characteristics of Particulate Matter and Particle-bound Metals from a Diesel Engine Generator Fueled with Waste Cooking Oil-based Biodiesel Blended with n-Butanol and Acetone

Jen-Hsiung Tsai1, Sheng-Lun Lin2,3, Shui-Jen Chen 1, Ciao-Jhen Guo1, Kuo-Lin Huang1, Jia-Twu Lee1, Kuei-Jyum C. Yeh1, Juei-Yu Chiu1, Chih-Chung Lin1

Source: Aerosol and Air Quality research, Volume: 18 | Issue: 5 | Pages: 1246-1254
DOI: 10.4209/aaqr.2018.03.0090

This study examines the emission properties of particulate matter and particle-bound metals from a diesel engine generator fueled by traditional fossil diesel (D100) with the addition of n-butanol (B), hydrous n-butanol (B′), acetone (A), hydrous acetone (A′), isopropyl alcohol (I) or waste cooking oil-based biodiesel (W). The fuel blends were B30W20D50 (abbr. B30), B′30W20D50 (abbr. B′30), A3I1W20D76 (abbr. A3), A′3I1W20D76 (abbr.A′3), B30A3I1W20D46 (abbr. B30A3) and B′30A′3I1W20D46 (abbr. B′30A′3) tested at loads of 1.5 kW and 3.0 kW for the diesel engine generator. Experimental results indicate that adding B30, A3 or B30A3 reduces the PM mass concentration in the exhaust at both engine loads compared to using only W20. Additionally, the PM emission concentrations are lower when using B′30, A′3 and B′30A′3 than when using B30, A3 and B30A3, respectively; in other words, replacing pure n-butanol/acetone with hydrated n-butanol/acetone in the blends further reduces the PM emission concentrations. However, B30 or B30A3 is more effective than A3 in reducing the PM emissions, irrespective of the water content in the fuel blends. Conversely, using B30, B′30, A3, A′3, B30A3 or B′30A′3 instead of W20 reduces the metal content in the PM emissions at both engine loads. The major metal components in PM are Na, Mg, Al, K, Ca, Fe and Zn, accounting for about 97 wt.% of 21 overall metals. The remaining analyzed metals were dominated by Mn, Ni, Cu, Mo and Ba. Accordingly, adding biodiesel from waste cooking oil and hydrous acetone/n-butanol to diesel fuel for diesel engine generators reduces the levels of PM and particle-bound metals. The waste hydrous acetone/n-butanol can be used for recycling purposes during this process.

Keywords: Diesel engine generator; Waste cooking oil-based biodiesel; Acetone n-Butanol Particle-bound metal.

Sensitivity Analyses for the Atmospheric Dry Deposition of Total PCDD/Fs-TEQ for Handan and Kaifeng Cities, China

Rong Zhao1, Kangping Cui 1, Weiwei Wang1, Lin-Chi Wang 2, Ya-Fen Wang3

Source: Aerosol and Air Quality research,Volume: 18 | Issue: 5 | Pages: 1255-1269
DOI: 10.4209/aaqr.2018.03.0109

During the period 2016–2017, the atmospheric wet, dry, and total deposition fluxes and scavenging ratios of the total PCDD/Fs-WHO2005-TEQ in Handan and Kaifeng were investigated. In addition, a sensitivity analysis for the dry deposition fluxes of the total PCDD/Fs-WHO2005-TEQ was conducted. The annual wet deposition fluxes of total PCDD/Fs-WHO2005-TEQ in Handan ranged between 51.1 and 83.5 and averaged 72.3 pg WHO2005-TEQ m–2 year–1, which was approximately 1.04 times of magnitude higher than that in Kaifeng (69.3 pg WHO2005-TEQ m–2 year–1). From 2016–2017, the contribution fraction of dry deposition to the total PCDD/Fs-WHO2005-TEQ deposition flux ranged between 60.8% and 100% and averaged 80.4%. Dry deposition fluxes were more dominant than wet deposition fluxes. In terms of the seasonal variations in total PCDD/Fs-WHO2005-TEQ dry deposition fluxes (the mean values for 2016 and 2017) in Handan, those in spring, summer, fall, and winter were 1084, 563, 964, and 1325 pg WHO2005-TEQ m–2 month–1, respectively, while in Kaifeng, they were 963, 428, 715, and 1016 pg WHO2005-TEQ m–2 month–1, respectively. The total PCDD/Fs-WHO2005-TEQ deposition fluxes in winter was approximately 2.0 times of magnitude higher than that in summer. The sensitivity analysis of total PCDD/FsWHO2005-TEQ dry deposition fluxes in Handan and Kaifeng showed that the PM10 concentration was the most positively correlated sensitive factor. When ΔP/P was changed from 0% to +50%, ΔS/S responded from 0% to +46.1% and +46.3%, respectively. The second positively correlated sensitive factor was the PM2.5 concentration, where when ΔP/P was changed from 0% to +50%, ΔS/S responded from 0% to +47.8% and +40.8%, respectively. For PCDD/Fs mass concentration, when ΔP/P was changed from 0% to +50%, ΔS/S responded from 0% to +32.2% and +28.1%, respectively. This was followed by the atmospheric temperature, and its effect was negatively correlated. When ΔP/P was changed from –50% to +50%, ΔS/S responded from +46.4% to –26.9% and +57.0% to –30.5%, respectively. The results of this study provide useful information that can be used to achieve more insights into both atmospheric deposition of total PCDD/Fs-WHO2005-TEQ and the sensitive factors for dry deposition fluxes.

Keywords: Dry deposition; Wet deposition; Scavenging ratio; Sensitivity analysis.

Size-selective Assessment of Respirator Protection against Airborne Fungi and (1→3)-β-D-glucan in Farms

Shu-An Lee 1, Chien-Hua Liao1, Tsai-Yu Lin2

Source: Aerosol and Air Quality research, Volume: 18 | Issue: 5 | Pages: 1270-1281
DOI: 10.4209/aaqr.2017.08.0285.

(1→3)-β-D-glucan is a major component of the fungal cell wall. It is commonly used to evaluate human exposure to fungi. A personal sampling system was developed to size-selectively evaluate the workplace protection factors (WPFs) of N95 filtering facepiece respirators (FFRs) and surgical masks (SMs) against fungi. This field study was performed with human subjects wearing an N95 FFR or a SM during farming activities. The geometric means of the WPFs of N95 FFRs and SMs were 156.2 and 12.2 for the total culturable fungi, 55.4 and 9.0 for the total fungi, and 10.5 and 11.1 for (1→3)-β-D-glucan. The WPFs for N95 FFRs against fungal contaminants were mostly greater than those for SMs; however, about 4.8%–35.0% of WPFs in the spore size range > 1.8 μm were still below 10 (the assigned protection factor designated for N95 FFRs by the US Occupational Safety and Health Administration). The WPFs of N95 FFRs and SMs against culturable fungi and (1→3)-β-D-glucan increased with the particle size. The total (1→3)-β-D-glucan significantly correlated with the total fungi ($r = 0.588$, $p < 0.001$) and total culturable fungi ($r = 0.463$, $p = 0.002$), which suggests that (1→3)-β-D-glucan can be used as an indicator to assess respiratory protection against airborne fungi on agricultural farms.

Keywords: Culturable fungi, Total fungi, (1→3)-β-D-glucan Protection, Respirator.

Airborne Particulate Matter: An Investigation of Buildings with Passive House Technology in Hungary

Krisztina Szirtesi 1, Anikó Angyal2, Zoltán Szoboszlai2, Enikő Furu1,2, Zsófia Török1,2, Titusz Igaz1, Zsófia Kertész1,2

Source: Aerosol and Air Quality research, Volume: 18 | Issue: 5 | Pages: 1282-1293
DOI: 10.4209/aaqr.2017.05.0158

In this case study, we investigate the building infiltration rate and indoor aerosol concentration levels in two buildings equipped with passive house technology and one “conventional” house in Ócsa, Hungary. We have aimed to determine the indoor aerosol pollution level and its elemental composition, establish the relationship between the indoor and outdoor concentration levels, and study how the different ventilation rates and modes affect the indoor particulate matter (PM) contamination. Our results indicate that the measured PM concentration levels were well below the recommended limits overall. In

particular, the mean PMfine (aerodynamic diameter < 2.5 μm) concentration was around 5 μg m–3 while the outdoor PMfine level was 20 μg m–3. The mean indoor concentration of the coarse fraction aerosols (aerodynamic diameter > 2.5 μm) varied between 2.5 and 7 μg m–3, with higher values corresponding to better airtightness of the house. As assessed by the indoor/outdoor elemental ratios and mass size distribution data, the filtration of the coarse mode particles was adequate in the passive houses. However, the PMfine fraction could get through the filters unhindered, as indicated by PMfine levels independent of the ventilation modes. The coarse mode particles inside the passive houses mainly originated from indoor sources.

Keywords: Passive; House; Mechanical ventilation; with heat recovery; Indoor air quality; Airborne particulate matter; Elemental composition of PM.

Source Apportionment and Risk Assessment of Atmospheric Polycyclic Aromatic Hydrocarbons in Lhasa, Tibet, China

Pengfei Chen1, Shichang Kang 1,2, Chaoliu Li2,3, Quanlian Li1, Fangping Yan4, Junming Guo1, Zhenming Ji3, Qianggong Zhang2,3, Zhaofu Hu1, Lekhendra Tripathee1, Mika Sillanpää4,5

Source: Aerosol and Air Quality research, Volume: 18 | Issue: 5 | Pages: 1294-1304
DOI: 10.4209/aaqr.2017.12.0603

Much attention has been given to the distributions, sources, and health risks of atmospheric polycyclic aromatic hydrocarbons (PAHs) in cities. In this study, a total of 62 suspended particle samples were collected from April 2013 till March 2014 in the city of Lhasa. Positive matrix factorization (PMF) was applied to investigate the source apportionment of 15 priority PAHs, the lifetime carcinogenic risk (LCR) levels of which were assessed. The average annual particle phase PAH concentration was 43.9 ± 60.4 ng m–3. Evident seasonal variations of PAHs were observed, with the highest concentration observed in winter, followed by autumn, spring, and summer. Four- and five-ring PAHs accounted for the predominant proportion (63.3%–84.4%) throughout the year. Correspondingly, gas phase PAHs showed the opposite variations, with the highest and lowest concentrations observed in summer and winter, respectively; also, three-ring PAHs, especially Ace, Acel, and Flu, were the largest contributors. Compositions of particle phase PAHs varied seasonally, with four-ring PAHs contributing more in winter than in summer and five-ring PAHs exhibiting the opposite trend, thereby reflecting the variety of emission sources. PMF analysis showed that biomass combustion (48.4%) and vehicle emissions (27.9%) were the two main sources, followed by coal combustion and the air–surface exchange. These results were consistent with the diagnostic molecular ratios. The benzo(a)pyrene equivalent (BaPeq) concentration of particle phase PAHs ranged from 1.48

to 24.5 ng m–3, which exceeds were higher than the new limit in China (1 ng m–3). The average BaPeq of gas phase PAHs was 6.43 ± 4.15 ng m–3, which was similar to that of particle phase PAHs. The LCR of the total PAHs (9.08 × 10–6) was one time higher than that of the particle phase; however, it was slightly lower than the acceptable level, thereby indicating that atmospheric PAHs in Lhasa pose little or no carcinogenic risk to the local population.

Keywords: Polycyclic aromatic hydrocarbons, Source apportionment, Health risk, Tibetan Plateau.

Improvement of the Real-time PM2.5 Forecast over the Beijing-Tianjin-Hebei Region using an Optimal Interpolation Data Assimilation Method

Haitao Zheng1,2,3, Jianguo Liu 1, Xiao Tang3, Zifa Wang 3, Huangjian Wu3, Pingzhong Yan3, Wei Wang4

Source: Aerosol and Air Quality research, Volume: 18 | Issue: 5 | Pages: 1305-1316
DOI: 10.4209/aaqr.2017.11.0522

A routine air quality data assimilation (DA) system was established at the China National Environmental Monitoring Center (CNEMC) based on the optimal interpolation (OI) method. The surface observations from more than 1,400 stations across China were assimilated into a real-time air quality forecast system with three nested domains. The initial conditions of NO2, SO2 and PM2.5 in the three domains were optimized by the data assimilation system. The impact of the data assimilation on the real-time PM2.5 forecast over the Beijing-Tianjin-Hebei (BTH) Region during the heavy haze season of 2015 was evaluated. The results show that the DA can significantly improve real-time PM2.5 forecasts, reducing the root mean square error (RMSE) by 23%, 8.2% and 4.8% in the forecasts of the first, second and third day, respectively. The mean fractional bias and the mean fractional error of the forecast were reduced from 50.9% and 70.67% to 40% and 62.3%, respectively, and the performance changed from “criteria” to approaching “goal” (as defined by Boylan and Russell, 2006). Additionally, increasing the assimilation frequency can improve the DA system performance for real-time forecasts. As can be seen from the various cases studied here, the improvement in data assimilation is more significant when the bias of the model is higher and there is still much room for correction. The results also show a rapid decay of the DA effects on the PM2.5 forecast, which highlights the limitations of the current routine data assimilation system in which only initial conditions are optimized. Further improvements in the data assimilation system with meteorological data assimilation and chemical parameter optimization are needed.

Keywords: Real-time; PM2.5 forecast; Data assimilation; Optimal interpolation; Beijing-Tianjin-Hebei region.

Analysis of Aerosol Optical Properties due to a Haze Episode in the Himalayan Foothills: Implications for Climate Forcing

Khan Alam 1,4, Rehana Khan1, Armin Sorooshian2,3, Thomas Blaschke4, Samina Bibi1, Humera Bibi1

Source: Aerosol and Air Quality research, Volume: 18 | Issue: 5 | Pages: 1331-1350
DOI: 10.4209/aaqr.2017.06.0222

A super haze episode occurred over the Himalayan region in October 2010. This haze reduced the air quality in the region and spread across India and Pakistan. The purpose of this study is to investigate the optical and radiative properties of aerosols during this episode using data from the MODerate resolution Imaging Spectroradiometer (MODIS) and the AErosol RObotic NETwork (AERONET). Maximum Aerosol Optical Depth (AOD) values on 19 October exceeded two at various locations in Pakistan (Sialkot = 2.56, Faisalabad = 2.67) and India (Ambala = 2.03, Amritsar = 3.4, Ludhiana = 4.29). Maximum AOD values recorded on 20 October were slightly lower in parts of Pakistan (Lahore = 2.5) and India (Gurdaspur = 1.89, New Delhi = 1.90, Batala = 2.89, Bathinda = 1.89, Kanpur = 1.6). Data for aerosol properties such as Volume Size Distributions (VSD), Single Scattering Albedo (SSA), Refractive Index (RI), and ASYmmetry parameter (ASY) suggest that fine mode aerosols were predominant relative to coarse mode aerosols during the haze episode. The dominant aerosol types were classified by analyzing AOD vs. Ångström Exponent (AE) and Extinction Ångström Exponent (EAE) vs. Absorption Ångström Exponent (AAE). The results revealed that during the haze episode, the prevailing aerosol types were biomass burning and urban/industrial aerosol. The Aerosol Radiative Forcing (ARF) values were computed during the hazy and non-hazy days using the Santa Barbara DISORT Atmospheric Radiative Transfer (SBDART) model. The shortwave ARF values at the Top Of the Atmosphere (TOA), SuRFace (SRF), and within the atmosphere were found to be in the range of –17.6 to –81.6, –64 to –193, and +47 to +119 W m–2, respectively, over Lahore. Likewise, over Kanpur, the ARF values were found to be in the range of +15.32 to –91.6, –38 to –134 and +33 to +75.91 W m–2, respectively.

Keywords: AOD Haze; SSA; ARF; AERONET; Lahore; Kanpur.

Statistical Comparison of Regional-Scale Tropospheric Aerosol Extinction Coefficient across China Based on CALIPSO Data

Yujun Qiu 1, Leiming Zhang2, Yongsheng Chen3

Source: Aerosol and Air Quality research, Volume: 18 | Issue: 5 | Pages: 1351-1359
DOI: 10.4209/aaqr.2017.10.0385

Two years of CALIPSO level 2 version 2 data were analyzed to obtain regional distributions of vertical profiles of the aerosol extinction coefficient (AEC) across China. 10 typical geographical regions were selected for comparison, which cover various aerosol pollution levels, climate zones, and underlying surfaces. The whole troposphere was split into two-layers: the Lower- and the Upper-layer—separated by the maximum boundary layer height—which represent the boundary layer and the upper tropospheric layer, respectively. The annual average of the column-average AEC in the 10 regions ranged from 0.066 to 0.243 km−1 in the Lower-layer and from 0.022 to 0.059 km−1 in the Upper-layer. The regional AEC in the Lower-layer was the highest in central and eastern China, followed by that in the Sichuan Basin, the Yunnan-Guizhou Plateau, the capital economic circle, the Pearl River Delta, the desert region, the Tibetan Plateau, northeast China, the northwest semi-arid plateau, and, finally, the East China Sea. The seasonal AEC in the Lower-layer was the highest during spring in the desert and marine regions, during the summer on the Tibetan Plateau, and during autumn or winter in the other regions. The regional and seasonal patterns of AEC in the Lower-layer agreed to a large extent with known regional distributions of surface-layer PM2.5 distributions and dominant seasonal emission sources in their respective regions. Regional and seasonal patterns in the Upper-layer were slightly different from those in the Lower-layer due to different transport pathways of aerosol pollution in different regions. The proportion of occurrence under different pollution conditions and the number of polluted days were also estimated separately for the Lower- and the Upper-layer, based on AEC vertical profiles for each region.

Keywords: Tropospheric aerosol; Aerosol pollution; Aerosol column average; Occurrence frequency.

Impacts of Aerosols on the Retreat of the Sierra Nevada Glaciers in California

Hesham El-Askary 1,2,3, Jingjing Li4, Wenzhao Li1, Thomas Piechota1, Tommy Ta5, Ariane Jong6, Xinyi Zhang7, Tiantian Yang8

Source: Aerosol and Air Quality research, Volume: 18 | Issue: 5 | Pages: 1317-1330
DOI: 10.4209/aaqr.2018.03.0089

The snowpack in the Sierra Nevada mountain range is the primary source of water for California. Many studies have shown that the increase in aerosols could lead to a reduction of the snowpack in this region. This study focuses on evaluating changes in the snowpack during the winter and summer seasons from 2000 till 2016 and determining the relationship between aerosols and the retreat of glaciers in the Sierra Nevada.The change detection analysis has shown reductions of 76.4% and 91.4% in the snowpack during winter and summer, respectively. Utilizing the aerosol optical depth (AOD), Angstrom exponent, snow depth anomalies, snowfall, radiation fluxes, and albedo, the effect of aerosols on snowfall over the Sierra Nevada glaciers has been examined for this 17-year period. Overall, based on correlation analysis, a negative relationship exists between the AOD and the snowfall.

Keywords: Aerosols; Snowpack; Sierrea; Nevada; Glacier; Retreat.

Selective Collection of Airborne Particulate Matter

Meng-Dawn Cheng

Source: Aerosol and Air Quality research, Volume: 18 | Issue: 6 | Pages: 1361-1365
DOI: 10.4209/aaqr.2018.02.0076

Airborne particulate matter (PM) or aerosol particles or simply aerosol are ubiquitous in the environment. They originate from natural processes such as wind erosion, road dust, forest fire, ocean spray and volcanic eruption, and man-made sources consuming fossil fuels resulting from utility power generation and transportation, and numerous industrial processes. Aerosols affect our daily life in many ways; PM reduces visibility in many polluted metropolitan areas, adversely impact human health and local air quality around the world (Tang et al., 1981; Mage et al., 1996; Molina and Molina, 2004; Davidson et al., 2005; Baklanov et al., 2016). Aerosol alters cloud cycles and change atmospheric radiation balance (Seinfeld and Pandis, 2000; Lohmann and Feichter, 2005; Flossmann and Wobrock,

2010; Rosenfeld et al., 2014; Seinfeld et al., 2016). Changes in daily mortality associated with particulate air pollution were typically estimated at approximately 0.5–1.5% per 10 μg m–3 increase in PM10 concentrations (Pope, 2000). Laden et al. (2006) found "an increase in overall mortality associated with each 10 μg m–3 increase in PM2.5 concentration either as the overall mean (rate ratio [RR], 1.16; 95% confidence interval [CI], 1.07–1.26) or as exposure in the year of death (RR, 1.14; 95% CI, 1.06–1.22). PM2.5 exposure was associated with lung cancer (RR, 1.27; 95% CI, 0.96–1.69) and cardiovascular deaths (RR, 1.28; 95% CI, 1.13–1.44). Improved overall mortality was associated with decreased mean PM2.5 (10 μg m–3) between periods (RR, 0.73; 95% CI, 0.57–0.95)". Aerosol particles also play an important role in source identification and apportionment (e.g., Hopke, 2016; Varga et al., 2017). Since the PM problem is associated with many facets of societal issues such as energy production and economic development, making progress on reducing the effects of PM will require integrated strategies that bring together scientists, engineers and decision makers from different disciplines to consider tradeoffs.

Keywords: Effect of Aerosol Loading on Separation Performance of PM2.5Cyclone Separators.

Chih-Wei Lin1, Ting-Ju Chen1, Sheng-Hsiu Huang1, Yu-Mei Kuo 2, Hua-Qiao Gui3, Chih-Chieh Chen1

Source: Aerosol and Air Quality research, Volume: 18 | Issue: 6 | Pages: 1366-1374
DOI: 10.4209/aaqr.2017.11.0458

The adverse health effects of particulate matter less than 2.5 μm in diameter (PM2.5) have drawn increasing attention over the past several decades. To obtain reliable measurements, it is critical to efficiently separate PM2.5 in the airstream from the beginning till the end of sampling. However, commonly used separators for PM2.5 monitoring, such as the BGI Very Sharp Cut Cyclone (VSCC), are usually subject to aerosol-loading effects. This study investigates the loading effect on cyclone separation performance as a function of particle size, cyclone size, particle material, and air humidity. Based on the ratios of dimensions to the body diameter of the BGI VSCC, four cyclones with different body diameters (13–35.6 mm) were fabricated. An ultrasonic atomizer was employed to generate micrometer-sized potassium sodium tartrate (PST) particles and sodium chloride (NaCl) particles as solid challenge particles and di-ethyl-hexyl-sebacate (DEHS) particles as liquid ones. Aerosol particles were neutralized to the Boltzmann charge equilibrium. An aerodynamic particle sizer measured the aerosol distributions and number

concentrations upstream and downstream of the cyclones. The experimental results show that solid particles such as PST with sizes close to the cyclone cut-point exhibit a significant loading effect. However, no significant difference is found due to the aerosol loading effect on four different-sized cyclones. The cyclone separation curve appears to shift toward smaller sizes due to aerosol loading. During the loading test, the aerosol penetration of 2.5-μm particles abruptly decreased during the first 20 minutes from 50% to a relatively stable level at 30%—an average decrease of 20%. Thus, the performance of cyclone PM2.5samplers with progressive aerosol loading might result in an underestimation of PM2.5, particularly for continuous monitoring.

Keywords: Aerosol loading Size-selective separator Cyclone Continuous aerosol monitoring.

Chemical Characteristics and Source Apportionment by Two Receptor Models of Size-segregated Aerosols in an Emerging Megacity in China

Nan Jiang, Ke Wang, Xue Yu, Fangcheng Su, Shasha Yin, Qiang Li, Ruiqin Zhang

Source: Aerosol and Air Quality research, Volume: 18 | Issue: 6 | Pages: 1375-1390
DOI: 10.4209/aaqr.2017.10.0413.

PM2.5, PM2.5-10, and PM10 samples were collected in Zhengzhou in 2014 to examine the chemical characteristics and sources of aerosols in this area. The PM concentrations, nine water soluble inorganic ions, organic carbon, elemental carbon, and twenty-two elements were determined, and positive matrix factorization (PMF) and chemical mass balance (CMB) were used for source apportionments. The meteorological impact was also evaluated by back-trajectory cluster analysis. Severe PM pollution was present in the study area, and the aerosol concentrations of PM2.5 samples (92%) and PM10 samples (85%) significantly exceeded the recommended levels of the Chinese National Ambient Air Quality Standard (NAAQS), with the average annual mass concentrations of PM2.5 and PM10 reaching 187 and 281 μg m−3, respectively. Secondary inorganic aerosols were the major ions in PM and accounted for 36%, 10%, and 27% of PM2.5, PM2.5-10, and PM10, respectively. The annual concentration of As (0.029 μg m−3) and Cd (0.010 μg m−3) in PM10 also exceeded the Chinese NAAQS levels, indicating a high health risk. Results from source apportionment by PMF modelling indicated that dust, vehicular traffic, coal combustion, secondary aerosols, and industry were the main pollution sources, accounting for 13.1%, 14.1%, 16.1%, 35.8%, and 14.6% of PM2.5; 25.1%, 20.8%, 21.8%, 10.5%, and 11.6% of PM2.5-10; and 19.8%, 15.8%, 18.5%, 22.5%, and 13.5% of PM10, respectively. Dust sources played an important role in PM pollution, especially coarse particles;

however, secondary aerosol sources contributed the most to PM2.5. Both of these observations were consistent with the results of mass reconstruction of the size-segregated aerosols. The CMB results coincided with the PMF results for PM2.5. Cluster analysis showed that air quality in the study area across the four seasons was mainly affected by air masses from the northeast and the east.

Keywords: Size-segregated Positive matrix factorization Chemical mass balance Back-trajectory clustering analysis

Oxidative Capacity and Radical Chemistry in a Semi-arid and Petrochemical-industrialized City, Northwest China

Chenhui Jia1, Yanan Wang2, Yaojie Li1, Tao Huang1, Xiaoxuan Mao1, Jingyue Mo3, Jixiang Li3, Wanyanhan Jiang1, Xiaoxue Liang1, Hong Gao1, Jianmin Ma 1,4

Source: Aerosol and Air Quality research, Volume: 18 | Issue: 6 | Pages: 1391-1404
DOI: 10.4209/aaqr.2017.11.0506.

Heavy ozone (O3) pollution is often observed in chemically industrialized Lanzhou and other capital cities located in the semi-arid and mountainous provinces of northwestern China. There are large knowledge gaps regarding the relationship between radical budgets and photochemistry in these cities. To gain insights into this relationship, a photochemical box model based on the Master Chemical Mechanism (MCM v3.3) was applied to investigate oxidative capacity and radical chemistry in the city of Lanzhou. The budgets of ROx (OH + HO2 + RO2) radicals were quantified, and the initiation, propagation, and termination process of the diurnal variation in the ozone chemistry were examined. The MCM model was constrained by in situ measurements at two sampling sites in the city, one located in the City downtown area (S1) and the other in the heavy petrochemical industrial area (S2) in the western suburb of the City, characterized by significant differences in volatile organic compounds (VOCs) and NOx concentrations between the two sites. Results showed that during the high O3 episodes in summer, OH initiation was dominated by the reaction of excited oxygen atoms O(1D) with water and the photolysis of nitrous acid (HONO) at the S1 site. At the S2 site, the most important production of OH was the reaction of O(1D) + H2O, followed by the reaction of O3 with VOCs. HONO photolysis was mostly identified at 7:00–13:00 local time at the S2 site, which is less important than that at the S1 site during the daytime. The photolysis of HCHO and OVOCs (except for HCHO) were the primary sources contributing to the initiation of HO2 and RO2 radicals at both sites. Results also revealed that the ROx termination could be attributed to the reactions of ROx with NO and NO2. The self-reactions between radicals also played an essential role at the S2 site. Overall OH was found to be the predominant oxidant, and NO3 was a major oxidant in the nighttime chemistry in the city.

Keywords: ROx radical; Source; Oxidative capacity; Lanzhou MCM model.

On the Morphology and Composition of Particulate Matter in an Urban Environment

Bahadar Bahadar Zeb1, Khan Khan Alam 2, Armin Armin Sorooshian3,4, Thomas Blaschke5, Ifthikhar Ahmad1, Imran Shahid6

Source: Aerosol and Air Quality research, Volume: 18 | Issue: 6 | Pages: 1431-1447
DOI: 10.4209/aaqr.2017.09.0340

Particulate matter (PM) plays a vital role in altering air quality, human health, and climate change. There are sparse data relevant to PM characteristics in urban environments of the Middle East, including Peshawar city in Pakistan. This work reports on the morphology and composition of PM in two size fractions (PM2.5 and PM10) during November 2016 in Peshawar. The 24 hous mass concentration of PM2.5 varied from 72 μg m−3 to 500 μg m−3 with an average value of 286 μg m−3. The 24 hours PM10 concentration varied from 300 μg m−3 to 1440 μg m−3 with an average of 638 μg m−3. The morphology, size, and elemental composition of PM were measured using Fourier Transform Infra Red (FT-IR) Spectroscopy and Scanning Electron Microscopy (SEM) with Energy Dispersive X-ray (EDX) Spectroscopy. The size of the analyzed particles by EDX ranged from 916 nm to 22 μm. Particles were classified into the following groups based on their elemental composition and morphology: silica (12%), aluminosilicates (23%), calcium rich (3%), chloride (2%), Fe/Ti oxides (3%), carbonaceous (49%), sulfate (5%), biogenic (3%). The major identified sources of PM are vehicular emissions, biomass burning, soil and re-suspended road dust, biological emissions, and construction activities in and around the vicinity of the sampling site.

Keywords: Particulate matter; Morphology and elemental composition; Scanning; Electron; Microscopy; Energy Dispersive; X-ray; Fourier; Transform; Infra; Red Spectroscopy.

The Real-world Emissions from Urban Freight Trucks in Beijing

Haohao Wang1,2, Yunshan Ge1,2, Jianwei Tan 1,2, Legang Wu3, Pengcheng Wu4, Lijun Hao1,2, Zihang Peng1,2, Chuanzhen Zhang1,2, Xin Wang1,2, Yaxin Han1,2, Mengzhu Zhang1,2

Source: Aerosol and Air Quality research, Volume: 18 | Issue: 6 | Pages: 1448-1456
DOI: 10.4209/aaqr.2017.11.0535

The emissions from 7 urban freights were tested using a portable emission measurement system (PEMS) and analyzed based on the vehicle-specific power (VSP) method. The results show that both gaseous pollutants and PM emissions increase with VSP. With regard to CO and HC, emissions decrease with elevated speed and acceleration. The PM and NOx emitted from China IV vehicles are significantly less than those from China III vehicles, but emissions of CO and HC exhibit a different tendency, thus necessitating further research. In addition, speed and acceleration show a slight influence on NOx emissions. The VSP plays an important role in the emissions from urban freight trucks. Therefore, a comprehensive evaluation of the emission characteristics of these vehicles in megacities is needed in order to take effective measures.

Keywords: PEMS; VSP; Urban freight vehicles; Emission.

Variations of Particle Size Distribution, Black Carbon, and Brown Carbon during a Severe Winter Pollution Event over Xi'an, China

Qian Zhang1,2,3, Zhenxing Shen 1,2, Yali Lei1, Yueshe Wang4, Yaling Zeng1, Qiyuan Wang2, Zhi Ning3, Junji Cao1, Linqing Wang1, Hongmei Xu1

Source: Aerosol and Air Quality research,Volume: 18 | Issue: 6 | Pages: 1419-1430
DOI: 10.4209/aaqr.2018.01.0007

Real-time particulate matter (PM) size distributions, 4-hour time resolution, PM2.5, carbonaceous materials, and their optical properties were measured during a severe pollution event in Xi'an, China. High PM2.5/PM10 ratios were observed on both pollution (0.83) and non-pollution (0.73) days, emphasizing the abundance of fine particles during sampling days. The particle number (PN) first peaked with a wide size range (30–100 nm) before morning rush hours (approximately 01:00–05:00) on pollution and non-pollution days, demonstrating that PN was governed by the accumulation of freshly emitted diesel particles and characterized by distinct aerosol condensation growth. By contrast, the second peak time and size range differed between pollution and non-pollution days because of different formation mechanisms. The light-absorbing coefficients of both black carbon (BC, babs-880nm, BC) and brown carbon (BrC, babs-370nm, BrC) were high on

pollution days and decreased to approximately half of those values on non-pollution days, indicating that the degree of light absorption is reduced by rain. The diurnal variation in babs-880nm, BC pollution peaked with traffic on January 1 and 2. By contrast, it remained in relatively stable and high ranges (120–160 Mm–1) in the second period (January 3–5) without traffic peaks, illustrating that the dominant sources changed even during the same pollution period. High values of both babs-370nm, BrC and babs-880nm, BC coincided in the afternoon and evening due to emissions from primary sources, and abundant aqueous secondary organic carbon, respectively. A highly variable mass absorption coefficient of BrC also indicated the variety of fuel combustion sources of primary BrC in Xi'an.

Keywords: Severe pollution periods; Particle size distribution; Black carbon; Brown carbon.

The Role of Sources and Atmospheric Conditions in the Seasonal Variability of Particulate Phase PAHs at the Urban Site in Central Poland

Patrycja Siudek 1, Marcin Frankowski2

Source: Aerosol and Air Quality research, Volume: 18 | Issue: 6 | Pages: 1405-1418
DOI: 10.4209/aaqr.2018.01.0037

The 24-h records of polycyclic aromatic hydrocarbons (PAHs) concentrations in the particulate phase were obtained for the urban site (52.42°N, 16.88°E) in Poznań, one of the largest cities in central Poland, between January and December 2014. The main goal of this study was to identify major emission sources of PAHs congeners and factors controlling their seasonal variability. The most abundant in the particulate matter PAH compound was pyrene (mean concentration of 2.29 ± 4.68 ng m–3, maximum of 22.51 ng m–3), followed by benzo(a)pyrene, dibenz(ah)anthracene, benzo(k)fluoranthene, benzo(b)fluoranthene, phenanthrene, benzo(ghi)perylene, chrysene, benz(a)anthracene and fluoranthene. The results showed a sharp decrease in PAHs concentrations during summer measurements (photodecomposition, high precipitation frequency), and high levels of the quantified PAHs during cold study period (increase anthropogenic emission, low air temperature). During the cold season in 2014, predominant PAHs congeners were: pyrene (26.0%) and 5-ring PAH compounds such as benzo(a)pyrene (19.4%) > dibenz(ah)anthracene (13.7%) ≥ benzo(k)fluoranthene (13.3%) > benzo(b)fluoranthene (9.8%), mostly associated with mixed sources (i.e., combustion, wood burning, industrial emission, traffic emission), whereas during warm study period we observed a large contribution (> 20%) of pyrene, dibenz(ah)anthracene and benzo(a)pyrene in particulate matter. The summertime measurements showed that local emission from the traffic (i.e., diesel and gasoline exhausts) was the second important source of PAHs in aerosol. The coal combustion for

residential heating and industrial usage were most pronounced PAHs sources during the entire study period. The multivariate statistical technique (Principal Component Analysis) combined with some diagnostic ratios were applied to provide detailed characteristics of sources and processes related to the polycyclic aromatic hydrocarbons in different seasons. The results from this study are in good agreement with most of the studies focused on seasonal variability of PAHs in the atmosphere.

Keywords: Polycyclic aromatic hydrocarbons; Low-molecular weight congener; High-molecular weight congener; Particulate matter; Principal; Component; Analysis; Diagnostic atio.

Experimental Investigation of the Filtration Characteristics of Charged Porous Fibers

Chih-Te Wang1, Tsung-Ming Tu1, Jin-Yuan Syu3, Chi-Ching Kuo2, Pei-Chen Kuo1, Yu-Rou Jhong1, Wen-Yinn Lin 1

Volume: 18 | Issue: 6 | Pages: 1470-1482
DOI: 10.4209/aaqr.2017.12.0582

Nanofibers fabricated through electrospinning technology have been successfully applied in various industries. The filtration advantages of nanosized electrospun fibers, particularly their high filtration efficiency and low pressure drop, make them highly suitable for addressing the problems of particulate pollution. Previous research has shown that the higher surface-to-volume ratios of nanoscale porous fibers contribute to their physical properties. However, little research on the filtration characteristics of charged porous fibers has been reported. Accordingly, this study used electrospinning to fabricate micro- and nanoscale PMMA fibers in order to investigate the surface voltage, pressure drop, and filtration efficiency of charged porous fiber filters. The outcomes showed that porous PMMA fibers were successfully fabricated as the mass ratios of DMF:CHCl3 gradually reached 1:15. After corona discharge, the surface voltage of the fine porous fiber (~500 nm) was –0.650 kV higher than the –0.562 kV voltage of fine smooth fiber. Filtration efficiency was evaluated using particles with an average concentration of 1.16 × 106 and with sizes ranging from 21.58–660.62 nm. After negative corona discharge, the most penetrating particulate size of filters made from fine porous fiber decreased from 168.5 to 121.9 nm, and the penetration rate dropped from 34.09% to 5.84%. For smooth fiber, the most penetrating particulate size remained unchanged at 135.8 nm, but the penetration rate dropped from 32.64% to 18.19%. This study also showed that porous fiber performed better than smooth fiber in terms of surface voltage decay and single fiber efficiency.

Keywords: Electrospinning; Filtration characteristics; Porous fibers; Smooth fibers.

Deposition Loss of Particles in the Sampling Lines of Continuous Emission Monitoring System (CEMS) in Coal-fired Power Plants

Runru Zhu1, Yiyang Zhang 2, Ye Yuan3, Shuiqing Li4

Source: Aerosol and Air Quality research,Volume: 18 | Issue: 6 | Pages: 1483-1492
DOI: 10.4209/aaqr.2017.11.0523

Due to the severe air pollution situation, more stringent regulations on pollutant emissions are being promulgated in China, necessitating more accurate and reliable monitoring of particulate matter (PM) emission in coal-fired power plants. In this work, we study the sampling loss of continuous emission monitoring system (CEMS) under different conditions by numerically solving the particle transport equation in the sampling line. With a high Reynolds number, the particle deposition loss is higher than in conventional laminar sampling and increases with the Reynolds number when the plant load changes. The temperature difference between the hot sampling gas and the pipe wall has a great effect on the sampling loss of PM10. A small temperature difference of 2 K, which is very likely to exist even with thick thermal insulation, will increase the deposition velocity of PM1-2.5 by ten times. The surface roughness, from either the pipe itself or deposited particles, also enhances the deposition loss by partly shifting the capture boundary to a higher diffusivity region. Combining all the possible factors, the loss ratio of 10-μm particles can reach 69% after 0.2 s and 95% after 0.5 s. The loss ratios of 2.5- and 1-μm particles are much lower but also reach 4.1% and 7.9%, respectively, after 1 s, which cannot be neglected when high accuracy monitoring is needed.

Keywords: Deposition; CEMS; Sampling; Coal-fired power plant.

Biogas Emission from an Anaerobic Reactor

Yu-Bo Zhang1,2, Yu-Long Wang1, Wei-Hua Li2, Li-Ning Bao2, Li-Han Wang2, Xian-Huai Huang 2, Bo Huang 1

Source: Aerosol and Air Quality research,Volume: 18 | Issue: 6 | Pages: 1493-1502
DOI: 10.4209/aaqr.2018.05.0169

Anaerobic denitrification is accompanied by biogas emissions, which may orient greenhouse gases or air pollutants. Ferrous iron play an important role in wastewater treatment. However, the effect of ferrous ion on biogas emission and the relationship between microbial community and nitrogen removal performance are not fully understood, especially in up-flow anaerobic sludge blanket (UASB) reactors. Here, the

results revealed that nitrogen gas increased rapidly with Fe(II) addition. And ferrous ions enhanced denitrification and COD removal efficiency with more than 60% and 10%, respectively. Moreover, Ferrous ions addition evidently increased Hydrogenophaga, Methylotenera, Zoogloea and Fluviicola during the whole UASB reactor operation progress. The correlation coefficient analysis further confirmed that Fe(II) was positively correlated with the abundances of Hydrogenophaga, Methylotenera and Fluviicola. Based on these results of chemicals transformation kinetics, microbial community and the correlations coefficient analysis, a hypothetical mechanism is proposed: In the UASB system with Fe(II) and NH4+, firstly Paludibacter made a contribution to NH4+ oxidation and generated NO3–, and then Hydrogenophaga, played an important role in NO3– reduction, Zoogloea coupled NO3– reduction to Fe(II) oxidation, Fluviicola combined with Methylotenera conducted NO2– reduction together with Fe(II) oxidation. This study will improve our understanding of ferrous ion's influence on biogas emission, denitrification process and corresponding microbial community.

Keywords: Biogas emission; Nitrogen gas; Ferrous iron; Denitrification; Anaerobic reactors.

Analytic Expression for the Aerosol Mass Efficiencies for Polydispersed Accumulation Mode

Chang H. Jung 1, Junshik Um2, Soo Ya Bae3, Young Jun Yoon4, Seoung Soo Lee5, Ji Yi Lee6, Yong Pyo Kim7

Source: Aerosol and Air Quality research, Volume: 18 | Issue: 6 | Pages: 1503-1514
DOI: 10.4209/aaqr.2018.02.0067

Aerosol mass efficiencies for extinction, scattering, and absorption are important parameters to understand aerosol optical properties. Although the mass efficiency is functions of the refractive index and particle size distribution, due to the complexity of the efficiency, mass efficiency parameters are usually regarded as a size independent and assumed to depend mainly on the chemical composition of aerosols. In this study, we calculated the mass efficiencies of polydispersed aerosols based on different aerosol types. An analytical approach to the approximated formula of the mass efficiency of each chemical species was developed and evaluated by fitting the results to those of the Mie theory that calculated the optical properties of chemical species based on the refractive index and size. We used the lognormal size distributions and external mixture approximations that represent the polydispersity of aerosol particles. Size ranges of 0.5–2.5 μm in the geometric mean diameter were considered for five different chemical species. The parameters of fitting curves were generalized for polydispersed aerosols as functions of the geometric mean diameter and the geometric standard deviation. The results of the newly developed

analytic approach showed a good agreement with those of the Mie theory. The proposed approach provides an effective means to estimate the mass extinction efficiency of polydispersed multi-component aerosols.

Keywords: Analytical approach; Polydisperse aerosol particles; Mass scattering efficiency; Mass absorption efficiency; Mie theory.

Overview of the Special Issue "Aerosol Source, Transport, Chemistry, and Emission Control" for the 10th Asian Aerosol Conference 2017

Neng-Huei Lin 1, Moo-Been Chang2, Jungho Hwang3, Naoki Kaneyasu4, Renjian Zhang5

Source: Aerosol and Air Quality research, Volume: 18 | Issue: 7 | Pages: 1515-1518
DOI: 10.4209/aaqr.2018.07.2017aac

The Asian Aerosol Research Assembly (AARA) advances the promotion of aerosol science mainly within the Asian countries, Australia, and New Zealand. The AARA biennially organizes the most prestigious conference for aerosol researchers in Asian region i.e., The Asian Aerosol Conference (AAC), focusing broadly on the fundamental research as well as the application part of aerosol science. The 10th AAC (AAC-2017) was successfully hosted by Korea Association for Particle and Aerosol Research (KAPAR), on behalf of Asian Aerosol Research Assembly (AARA) at Jeju Island, South Korea during July 2–6, 2017. A total of 600 researchers from 20 countries participated in the conference. There were 6 plenary-lectures, 6 keynote-speeches, 179 oral-presentations, and 227 poster-presentations during the conference. All the aerosol researchers from different countries came together and displayed their latest/recent researches in the domain of aerosol science, strengthening the appreciation and cooperation in this particular field.

Keywords: Aerosol; Asian; Asian Aerosol Conference 2017; Special issue.

Temporal Variation of Atmospheric Static Electric Field and Air Ions and their Relationships to Pollution in Shanghai

Yifan Wang1, Yanyu Wang1, Junyan Duan1, Tiantao Cheng 1,2,3, Hailin Zhu1, Xin Xie1, Yuehui Liu1, Yan Ling1, Xiang Li1, Hongli Wang2, Mei Li3, Renjian Zhang4

Source: Aerosol and Air Quality research, Volume: 18 | Issue: 7 | Pages: 1631-1641
DOI: 10.4209/aaqr.2017.07.0248

Atmospheric electric field (EF) and air ions were measured in Shanghai from December 2014 to December 2015 to examine the influence of particulate pollutants. Fair-weather EF exhibits a diurnal variation of multi-modal oscillations in spring, summer, and autumn. Linear correlation analyses show that the local meteorological conditions of relative humidity, temperature, pressure and wind affect atmospheric electric field, with wind direction exhibiting the highest correlation coefficient. Atmospheric EF is significantly higher in the west compared with that in the east, as the air mass from inland areas carries more polluted aerosols. Air ion concentrations are generally higher in the daytime than at night and correlate with meteorological factors. Atmospheric EF undergoes a substantial fluctuation in polluted periods, but remains flat under clean conditions. Overall, in areas with pollution, the atmospheric EF gradually increases with increased pollution or increased particle loading (e.g., PM2.5), a useful indicator of air pollution. The concentration of PM2.5 is positively correlated with the atmospheric electric field under polluted conditions, because as the concentration of aerosol particles declines, the concentrations of small ions and the atmospheric conductivity decrease accordingly, thus causing an increase in the electric field. Overall, aerosol particles, air ions, and their interactions in the presence of various meteorological parameters can have local effects on the atmospheric electric field.

Keywords: Atmospheric electric field; Air ions; Urban pollution

Understanding the Regional Transport Contributions of Primary and Secondary PM2.5 Components over Beijing during a Severe Pollution Episodes

Wei Wen1,2, Xiaodong He 1, Xin Ma 3, Peng Wei4, Shuiyuan Cheng5, Xiaoqi Wang5, Lei Liu2

Source: Aerosol and Air Quality research, Volume: 18 | Issue: 7 | Pages: 1720-1733
DOI: 10.4209/aaqr.2017.10.0406

This study applied the CAMx model to study the regional transport of various PM2.5 components in Beijing during a severe pollution episodes. The results revealed that during the episodes, Beijing had the average PM2.5 pollution value of 119 μg m−3. It was 1.58 times of the PM2.5 national air quality standard (75 μg m−3 Level II). The wind speed was low (< 2 m s−1) and relative humidity reached 98%. The anticyclone in Eastern China showed weak local flow fields and southerly winds at the surface and strong temperature inversion under 1000 m, which promote pollution accumulation. The contribution of monthly regional transport to primary PM2.5 components and SO42−, NO3−, and secondary organic aerosol concentrations in Beijing were 29.6%, 41.5%, 58.7%, and 60.6%, respectively. The emissions from Baoding had the greatest effect on the primary components of PM2.5 (6.1%) in Beijing. The emissions from Tianjin had the greatest influence on the secondary components of PM2.5 concentrations. These values indicated that the secondary components of Beijing's PM2.5 are more easily affected by transboundary transport than are the primary components. The present findings suggest that control strategies for PM2.5 pollution should include coordinated efforts aimed at reducing secondary aerosol precursors (SO2, NOx, and VOCs) from long-range transport and local generation in addition to primary particulate emissions.

Keywords: PM2.5 pollution; Regional transport; Secondary component; Air quality modeling.

Field Measurements for Quantifying Semi-Volatile Aerosol Influence on Physical and Optical Properties of Ambient Aerosols in the Kathmandu Valley, Nepal

Sujan Shrestha 1,2, Siva Praveen Puppala 1, Bhupesh Adhikary1, Kundan Lal Shrestha2, Arnico K. Panday1

Source: Aerosol and Air Quality research, Volume: 18 | Issue: 7 | Pages: 1617-1630
DOI: 10.4209/aaqr.2017.11.0492

An intensive field campaign was conducted during the pre-monsoon season of 2015 in the urban atmosphere of the Kathmandu Valley to study the influence of the semi-volatile aerosol fraction on physical and optical properties of aerosols. Ambient air was siphoned through a specific ambient air inlet and then split into two parts. The first part connected directly with an ambient air sample while the second received the air sample through a thermodenuder (TDD). The aerosol properties, such as the aerosol number, size distribution, absorption, and scattering, were studied using Condensation Particle Counters (CPCs), Scanning Mobility Particle Sizers (SMPSs), Aethalometers (AE33) and Nephelometers, respectively. The differences in the properties of the aerosol fraction at room temperature and other TDD set temperatures (50°C, 100°C, 150°C, 200°C, 250°C, and 300°C) were calculated to study the influence of the semi-volatile aerosol fraction on ambient aerosols. The evaporated fraction of the semi-volatile aerosols increased with the TDD set temperature. The semi-volatile fraction of the aerosol number increased from 16% to 49% of ambient aerosol, while the peak mobility diameter of particles shifted from around 60 nm to 40 nm as the temperature increased from 50°C to 300°C. However, increasing the TDD set temperature had no influence on the effective diameter of the aerosol size distribution. Larger aerosol size bins of the SMPS experienced a significantly stronger influence (~70%) from temperature increments compared to smaller size bins (~20%). The semi-volatile aerosol fraction amplified BC absorption by up to 28%, while scattering by the semi-volatile aerosol fraction contributed up to 71% of the total.

Keywords: Aerosol number concentration; Absorption; Scattering; Black carbon.

A Modeling Study of the Impact of Crop Residue Burning on PM2.5Concentration in Beijing and Tianjin during a Severe Autumn Haze Event

Yike Zhou1,2, Zhiwei Han 2,3, Ruiting Liu2,3, Bin Zhu1,4, Jiawei Li2, Renjian Zhang2

Source: Aerosol and Air Quality research, Volume: 18 | Issue: 7 | Pages: 1558-1572
DOI: 10.4209/aaqr.2017.09.0334

Crop residue burning is one of the important types of biomass burning in China and has potentially important effect on air quality and climate. A coupled meteorology and aerosol/chemistry model (WRF-Chem) with ground and satellite observations and biomass burning emission inventory were applied to investigate the spatial/temporal distribution and transport pathways of air pollutants and to quantify the contribution of crop residue burning to aerosol concentration in the North China Plain, with focus on Beijing and Tianjin during a severe haze episode on 7–11 October 2014, when the daily mean surface PM2.5 concentration in Beijing reached 317 μg m−3. During this period, intensive crop fires were detected over wide areas of eastern Henan, southern Hebei and western Shandong, and the crop residue burning emission was much larger than anthropogenic emission in major fire areas. Model comparison with ground observations demonstrated the WRF-Chem was able to generally reproduce surface meteorological variables and PM2.5 concentration, although it tended to overpredict wind speed and aerosol concentration in some locations. Taking crop residue burning into account can apparently improve PM2.5 prediction during the haze episode. The stagnant weather condition favored haze formation and maintenance in this region, and crop residue burning intensified haze pollution in both fire source and downwind regions. The crop residue burning emission on average contributed 19% to surface PM2.5 concentration in Beijing during the haze episode, in which it contributed 40% and 29% to organic carbon aerosol and primary PM2.5, respectively, and less to black carbon aerosol (4.9%). The impact of crop residue burning in Tianjin was smaller than that in Beijing, with an average contribution of 7.4% due to different fire sources and transport pathways.

Keywords: Crop residue burning; Beijing and Tianjin Surface; PM2.5 concentration Long range transport; FINN emission inventory; WRF-Chem simulation.

Evolution of Key Chemical Components in PM2.5 and Potential Formation Mechanisms of Serious Haze Events in Handan, China

Chengyu Zhang1, Litao Litao Wang 1, Mengyao Qi1, Xiao Ma1, Le Zhao1, Shangping Ji1, Yu Wang1, Xiaohan Lu1, Qing Wang1, Ruiguang Xu1, Yongliang Ma2

Source: Aerosol and Air Quality research, Volume: 18 | Issue: 7 | Pages: 1545-1557
DOI: 10.4209/aaqr.2017.10.0386

Handan has been one of the most polluted cities in China since 2013 and became the top city for PM2.5 in 2017. In this research, we observed coarse particulate matter (PM10), fine particulate matter (PM2.5), submicron particulate matter (PM1), and the chemical composition of PM2.5 from November 16, 2015, till March 14, 2016, in Handan. During the observation period, hourly concentrations of PM10, PM2.5, and PM1 peaked at 1070.1, 864.4, and 519.5 μg m−3, respectively. Severe pollution occurred on a large fraction of days in the heating season, which was characterized by frequent and long-lasting pollution episodes. A large fraction of the transport trajectories during nine typical episodes during that period in Handan were from the northwest. Water-soluble ions (sulfate, nitrate, and ammonium) in PM2.5 accounted for the largest proportion at all pollution levels. The highest proportion of SIA occurred in a heavily polluted episode, during which it was as high as 50.0% (sulfate: 18.8%, nitrate: 18.7%, and ammonium: 12.5%). The sulfate and ammonium in PM2.5 increased gradually while the nitrate decreased as the level of pollution rose from clean to heavily polluted. The fraction of SOA and OM to PM2.5 decreased as the pollution level increased, indicating a weakening of photochemical reactions. The POA in PM2.5 increased with the aggravation of haze, and the heterogeneous chemistry was enhanced by the aggravation of pollution. Liquid reactions were important in the formation of sulfate during pollution and non-pollution stages. Liquid reactions of NO2 are enhanced in the pollution stage during the heating season in Handan.

Keywords: Particulate matter; Haze; Heterogeneous chemistry; Aerosol water content.

Long-range Transport of Aerosols from Biomass Burning over Southeastern South America and their Implications on Air Quality

Leila Droprinchinski Martins 1,4, Ricardo Hallak1, Rafaela Cruz Alves1, Daniela S. de Almeida1, Rafaela Squizzato1, Camila A.B. Moreira1, Alexandra Beal3, Iara da Silva1, Anderson Rudke1, Jorge A. Martins1,4

Source: Aerosol and Air Quality research, Volume: 18 | Issue: 7 | Pages: 1734-1745
DOI: 10.4209/aaqr.2017.11.0545

The long-range transport of aerosols is a global issue since it may significantly affect the air quality of regions without high concentrations of fine particulate matter (PM2.5). Two significant occurrences of long-range transport of aerosols over the state of Parana in Brazil, which occurred during the periods Aug. 16–18 and Sep. 10–14 of 2016, were studied in order to characterize the atmospheric synoptic conditions of these events and to estimate their contribution to the air quality conditions in the northern region of the state. The South American Low Level Jet (SALLJ) was the key meteorological component used to define the origin of the air mass trajectories over the region. In the first event, the SALLJ lost its configuration, bringing air masses from the western part of São Paulo (state), while in the second event, the SALLJ formed over southern Brazil and brought air masses from the northern and central parts of the nation. The significant number of fires from biomass burning in central Brazil associated with synoptic conditions contributed to the increase in PM2.5 concentrations by approximately 70–87% in the region. The transport of aerosols was a determining factor in PM2.5 exceeding the air quality standard in the region. Therefore, to minimize this problem, it is imperative to control biomass burning in Brazil.

Keywords: Air pollution; Atmospheric conditions; Aerosol sampling and transport Particulate matter.

Pollution Characteristics of Water-soluble Ions in Aerosols in the Urban Area in Beibei of Chongqing

Yanpei Li1, Qingju Hao1, Tianxue Wen2, Dongsheng Ji2, Zirui Liu2, Yuesi Wang2, Xiaoxi Li1, Xinhua He1, Changsheng Jiang 1

Source: Aerosol and Air Quality research, Volume: 18 | Issue: 7 | Pages: 1531-1544
DOI: 10.4209/aaqr.2017.11.0500

To investigate the pollution characteristics of water-soluble ions in aerosols in the urban area of Beibei District, Chongqing, graded aerosol samples were continuously collected by a cascade impactor (Andersen) from March 2014 till February 2015. Water-soluble ions, namely, Na+, NH4+, K+, Mg2+, Ca2+, F–, Cl–, NO3– and SO42– in different particle-size ranges (< 0.43, 0.43–0.65, 0.65–1.10, 1.10–2.10, 2.10–3.30, 3.30–4.70, 4.70–5.80, 5.80–9.00 and 9.00–100 μm), were measured by ion chromatography. The results showed that Mg2+, Ca2+ and F– mainly appeared in coarse particles, and other ions were mainly distributed in fine particles. SO42– was mainly distributed in the droplet mode in spring and autumn from in-cloud processes, while SO42– had both condensation and droplet modes in summer from the oxidation of SO2. NH4+ and SO42– were mainly present in the form of NH4HSO4 in aerosols. Except during summer, NO3– mostly existed in the forms of NH4NO3 in fine particles and Ca(NO3)2 in coarse particles. Na+ was single-peaked in spring and summer and double-peaked in autumn and winter. Fine-mode K+ showed a single-peak

distribution in every season. The existent forms of Cl– were KCl in the fine mode and CaCl2 in the coarse mode. Mg2+ was mainly distributed in coarse particles, which showed a bimodal pattern distribution in spring and summer. Ca2+ mainly existed in coarse modes, whose concentrations increased with particle size. The emissions from motor vehicle exhaust, combustion processes, soil and construction dust were the major sources of water-soluble ions in this area. SOR (the sulfur oxidation ratio) was the highest in summer and the lowest in winter, but NOR (the nitrogen oxidation ratio) was highest in winter. The SOR values for condensation-mode (0.43–0.65 μm) exceeded 0.10 only in summer. SOR was considerably higher than NOR for the same particle sizes during the whole year.

Keywords: Water-soluble ions Fine mode Coarse mode Size distribution

Forming Highly Polluted PMs Caused by the Invasion of Transboundary Air Pollutants: Model Simulation and Discussion

Chung-Hsuang Hung1, Kuo-Cheng Lo 2, Chung-Shin Yuan3

Source: Aerosol and Air Quality research, Volume: 18 | Issue: 7 | Pages: 1698-1719
DOI: 10.4209/aaqr.2017.11.0488

Transboundary air pollutants that deteriorate ambient air quality have become an emerging international concern recently. This study analyzed and simulated an air pollution case of highly concentrated particulate matter (PM) formed by a severe dust storm case from January 17 till 19 in 2014. For this case, concentrations of PM10 and PM2.5 reached up to 680 and 165 μg m−3, respectively. Those concentrations were 5–10 folds higher than the proposed ambient air quality standards of Taiwan. The mechanisms for forming high-concentrated PM in the ambient air of Taiwan and its surrounding area were investigated. Based on the monitored pollutant concentrations and the simulation results with the Weather Research and Forecasting-Chemistry (WRF-Chem) model, both the meteorological conditions and the mechanisms for forming high-concentrated PMs were analyzed. The long-range transported-in air pollutants, travelling with the movement of a strong continental cold high-pressure system originating in northern China, contributed to the poor ambient air quality. Two important mechanisms for forming this highly concentrated PM were proposed, including the transported-in transboundary air pollutants (or their precursors) from China and the leeward side effects on the western side of the Taiwan Island. Low inversion layers in the atmosphere and terrain downwash near the ground surface were observed in this case study while continental cold air approached. The WRF-Chem model simulation results confirmed that the ambient air of western Taiwan was dry and moved downward during the investigated period. Hence, the contribution of transboundary air pollutants to deteriorating ambient air quality cannot be ignored.

Keywords: Transboundary air pollutants; WRF-Chem; PM2.5; PM10; Haze case.

Chemical Characterization of PM1-2.5 and its Associations with PM1, PM2.5-10 and Meteorology in Urban and Suburban Environments

Jana Kozákovác 1,2, Cecilia Leoni2, Miroslav Klán2, Jan Hovorka2, Martin Racek3, Martin Koštejn4, Jakub Ondráček1, Pavel Moravec1, Jaroslav Schwarz1

Source: Aerosol and Air Quality research, Volume: 18 | Issue: 7 | Pages: 1684-1697
DOI: 10.4209/aaqr.2017.11.0479

This study investigated the PM1-2.5 (the intermodal fraction of particulate matter) representing the transition area between the fine and coarse size ranges. Due to this characteristic, PM1-2.5 may contain particles from both modes. The aim of this work was to examine the associations between PM1-2.5 and the coarse (PM2.5-10)/fine (PM1) fraction under different meteorological conditions at various sites in the Czech Republic during winter and summer.

Size-resolved PM mass concentrations were determined and meteorological parameters recorded at an urban industrial and a suburban site in Ostrava during winter 2014 and at an urban traffic site and a suburban site in Prague during summer 2014 and winter 2015. The influence of sources producing the coarse/fine fraction on PM1-2.5 was investigated with an elemental composition analysis and an ion analysis (Ca2+-representing PM2.5-10 and SO42−-representing PM1).

During all campaigns, PM1-2.5 accounted for 1–26% of PM10. In winter, crustal elements (Si, Fe, and Ca) significantly influenced the coarse fraction and even PM1-2.5 at all sites, while sulfur was significant in PM1-2.5 and the fine fraction at suburban sites. The median SO42− concentration was higher than the Ca2+ concentration in PM1-2.5 at all sites, except the industrial site, due to a specific source. The increased SO42− amount in PM1-2.5 was also observed in summer during rainy days (Prague urban site). In summer, crustal elements were important in both, PM1-2.5 and the coarse fraction, while S still dominated in PM1. Median SO42− concentrations in PM1-2.5 and the coarse fraction were significantly lower than in winter. The enrichment factors and wind speed-direction analysis helped to reveal potential air pollution sources.

To conclude, according to the performed analyses, PM1-2.5 was influenced by the sources of the coarse fraction during all campaigns. The additional significant influence of sources producing the fine fraction was evident under increased relative humidity conditions.

Keywords: Aerosol intermodal fraction; Personal cascade impactor sampler; Enrichment factor; Elemental composition; Scanning electron microscope; Multisite measurement.

Source Profiles for PM10-2.5 Resuspended Dust and Vehicle Exhaust Emissions in Central India

Shamsh Pervez 1, Shahina Bano1, John G. Watson2,7, Judith C. Chow 2,7, Jeevan Lal Matawle1,3, Anjali Shrivastava5, Suresh Tiwari5, Yasmeen Fatima Pervez6

Source: Aerosol and Air Quality research, Volume: 18 | Issue: 7 | Pages: 1660-1672
DOI: 10.4209/aaqr.2017.08.0259

Eight composite PM10-2.5 source profiles were developed for resuspended dust and vehicle exhaust emissions with 32 chemical species, including 21 elements (Al, As, Ca, Cd, Co, Cr, Cu, Fe, Hg, K, Mg, Mn, Mo, Na, Ni, Pb, S, Sb, Se, V, and Zn), 9 water-soluble ions (Na+, K+, Mg2+, Ca2+, NH4+, Cl–, F–, NO3–, and SO42–), and carbonaceous fractions (OC and EC). Dust samples were dominated by crustal elements (Al, Ca, Fe, and Mg) while exhaust emissions showed high abundances of carbonaceous aerosol (OC and EC). Crustal species (Al, Fe, Mg, and Na) were more enriched over native soils in PM10-2.5 as compared to PM2.5. The higher coefficients of divergence (COD) indicate that profiles differ from each other. Ca accounted for nearly 30% of PM10-2.5 mass in construction dust while Fe accounted for nearly 20% of PM10-2.5 mass in paved road dust. Three- and four-wheeler diesel exhaust profiles consisted of 5–7% EC, with 6–10 times higher Pb, Se, and S abundances than those in two-wheeler gasoline exhaust profile. The heavy-duty diesel exhaust profile consist of nearly 20% EC with abundant (> 0.5%) trace elements (e.g., Pb, Se, and Zn).

Keywords: PM10-2.5 Source profile Enrichment factor Source markers Resuspended dust Vehicle exhaust

---

Impacts and Effects Indicators of Atmospheric Deposition of Major Pollutants to Various Ecosystems - A Review

L. Paige Wright1, Leiming Zhang 2, Irene Cheng2, Julian Aherne3, Gregory R. Wentworth4

Source: Aerosol and Air Quality research, Volume: 18 | Issue: 8 | Pages: 1953-1992
DOI: 10.4209/aaqr.2018.03.0107.

In this paper, we review the current understanding on ecosystem and human health impacts from the atmospheric deposition of acidifying pollutants, eutrophying nitrogen (N), polycyclic aromatic hydrocarbons (PAHs), mercury (Hg), trace metals, and ozone (O3), as well as the biological indicators that have been used to assess the health of ecosystems following exposure to these pollutants. We provide overviews of the impacts of deposition for these pollutants and discuss the currently known biomonitors for each pollutant. The deposition of acidifying pollutants impacts terrestrial ecosystems by altering plant physiology and growth and by increasing plant susceptibility to stresses that can be indirectly damaging to the health of fish and birds. Indicators of the deposition of acidifying pollutants include soil base cation content and acid neutralizing capacity, among others. Eutrophying N deposition has been studied extensively; N enrichment directly impacts vegetative plant species cover, richness, growth rates, and susceptibility to other stressors. It indirectly impacts wildlife through changes in their habitats and food sources. Indicators for N deposition include changes in plant species and in tissue and litter N content. The deposition of PAHs has been found to cause significant damage to plant organisms and to be carcinogenic and mutagenic to humans and animals. Useful biomonitors of PAH deposition include lichens, mosses, and pine needles. Deposited Hg can undergo methylation (in the presence of sulphur reducing bacteria); bioaccumulation of methylmercury is highly toxic to animals. Effective biomonitors of Hg contamination of aquatic ecosystems are fish and marine birds. The impacts of O3 are well understood, with well-established "flux" models being vast improvements on the previous AOT40 approaches. This review highlights the impacts that the above-mentioned pollutants have on terrestrial and aquatic organisms and the biomonitors that are currently being used to assess the deposition levels and effects of these pollutants.

Keywords: Air pollution; Atmospheric deposition; Ecosystem health; Ecological monitoring.

Gaseous and Carbonaceous Composition of PM2.5 Emitted from Rural Vehicles in China

Xianbao Shen, Hui Wu, Xinyue Cao, Wei Zhang, Zhiliang Yao , Xuewei Hao

Source: Aerosol and Air Quality research, Volume: 18 | Issue: 8 | Pages: 1993-2004
DOI: 10.4209/aaqr.2017.10.0401

Rural vehicles (RVs) could contribute significantly to on-road vehicle emissions, especially PM2.5 and NOx; This study tested 10 three-wheeled (3-W) RVs and 8 four-wheeled (4-W) RVs on real roads in Hebei Province using a portable emissions measurement system to investigate gaseous concentrations (CO, NOx, and HC) and the carbonaceous composition

(EC and OC) of the PM2.5 emitted. The results showed that the tightening emission standards resulted in the CO, HC, and PM2.5 emissions for China II RVs decreasing, but may increasing NOx emission for China II 3-W RVs. The emission level of PM2.5 for China II RVs is between Euro II LDDTs and Euro III LDDTs. The emission factors (EFs) of OC and EC for 3-W RVs were 0.035 ± 0.019 and 0.058 ± 0.055 g km-1, respectively, and for 4-W RVs, they were 0.046 ± 0.018 and 0.031 ± 0.024 g km-1, respectively. The carbonaceous component represents the main fraction of PM2.5 emitted from RVs (84.6% and 87.2% for 3-W and 4-W RVs, respectively), similar to other diesel vehicles. The average distance-based EFs of OC increased with increasing vehicle size (3-W RVs < 4-W RVs). The CO2-based EFs of OC and EC decreased with increasing vehicle mass, consistent with the emission laws of light-, medium-, and heavy-duty diesel trucks. Driving cycles that included more cruise mode and less creep mode resulted in a higher average EC/OC ratio (1.57) for 3-W RVs than for 4-W RVs (0.63), and resulted in the average EC/OC ratios for both types of RV were lower than for highway LDDTs.

Keywords: Carbonaceous composition; Gaseous emission; Particulate matter; Rural vehicle PEMS.

Performance of Small Plate and Tube Unipolar Particle Chargers at Low Corona Current

Xiaotong Chen1,2, Qiaoling Liu2, Jingkun Jiang1, Da-Ren Chen 2

Source: Aerosol and Air Quality research, Volume: 18 | Issue: 8 | Pages: 2005-2013
DOI: 10.4209/aaqr.2018.02.0060

Two small chargers, a plate and a tube particle charger, were compared in terms of their performance at low DC-corona current. Both chargers are designed for compact/miniature electrical-mobility-based particle sizers and were operated at a corona current of 0.3 μA for simultaneous low energy consumption and high charging efficiency. A thin wire was utilized in the plate charger for the ion generation via the DC-corona discharge, while a sharp-tipped needle was used in the tube charger. The intrinsic and extrinsic charging efficiencies of particles in various electrical mobility sizes were measured for both chargers at aerosol flow rates of 0.3 and 0.6 L min–1. In general, the plate charger exhibited a lower intrinsic charging efficiency than the tube charger. Also, its extrinsic charging efficiency was slightly higher at 0.3 L min–1 than 0.6 L min–1 and reached approximately 80% for particles larger than 40 nm. On the other hand, the extrinsic charging efficiency of the tube charger was higher at 0.6 L min–1 than 0.3 L min–1 for particles larger than 60 nm, with the reverse being true for smaller particles. The extrinsic charge distributions of particles with mobility sizes smaller than 300 nm were also characterized. It was found that a multiple-charge status occurred on particles larger than 20 nm for both chargers. At the

same particle size, more charges attached to particles in the tube charger than the plate charger. The birth-and-death charging model was proposed for calculating the extrinsic charge distributions of particles measured in this study. In addition, the Gaussian distribution function was also suggested for best fitting the measured extrinsic charge distributions of particles.

Keywords: Compact/Miniature aerosol charger; DC-corona unipolar charger; Small tube charger; Small plate charger; Ultrafine and fine particles.

Tire Abrasion as a Major Source of Microplastics in the Environment

Frank Sommer1, Volker Dietze2, Anja Baum3, Jan Sauer3, Stefan Gilge2, Christoph Maschowski1, Reto Gieré 4

Source: Aerosol and Air Quality research, Volume: 18 | Issue: 8 | Pages: 2014-2028
DOI: 10.4209/aaqr.2018.03.0099

Traffic-related non-exhaust particulate matter mainly consists of tire wear, brake wear, and road wear. For this study, passive-samplers were placed near highly frequented roads in industrial, agricultural, and urban environments with the aim of collecting and characterizing super-coarse (> 10 μm) airborne particles. Single-particle analysis using SEM-EDX was conducted on more than 500 particles with nearly 1500 spectra to determine their size, shape, volume, and chemical composition. The ambient aerosol near all studied roads is dominated by traffic-related abrasion particles, amounting to approximately 90 vol%. The majority of the particles were composites of tire-, road-, and brake-abrasion material. The particle assemblages differed in size distribution, composition, and structure depending on driving speed, traffic flow, and traffic fleet. Our study documents that tire wear significantly contributes to the flux of microplastics into the environment. A decrease in the release of this abrasion material, however, is unlikely in the near future.

Keywords: Microplastics; Tire wear; Road wear; Brake wear; SEM-EDX analysis; Chemical composition.

Evaluation and Field Calibration of a Low-cost Ozone Monitor at a Regulatory Urban Monitoring Station

Mauro Masiol1, Stefania Squizzato1, David Chalupa2, David Q. Rich1,2, Philip K. Hopke 1,3

Source: Aerosol and Air Quality research, Volume: 18 | Issue: 8 | Pages: 2029-2037
DOI: 10.4209/aaqr.2018.02.0056

The performance of a low-cost ozone monitor (the Aeroqual Series 500 portable gas monitor coupled with a metal oxide sensor for ozone; model OZL) was assessed under field conditions. Ten ozone monitors were initially calibrated in clean-air laboratory conditions and tested at controlled ozone concentrations of 5 to 100 ppb. Results showed good linearity and a fast response with respect to a conventional research-grade ozone monitor. One monitor was then co-located at a regulatory air quality monitoring station that uses a U.S. federal equivalent method (FEM) ozone analyzer. Raw data from the Aeroqual monitor collected over 4 months (June–October) at a 10-minute time-resolution showed good agreement ($r2 = 0.83$) with the FEM values but with an overestimation of ~12%. Data were averaged to different time resolutions; 1-h time averaged concentrations showed the best fit with the FEM results ($r2 = 0.87$). An analysis of the ratio of FEM/monitor concentrations against chemical and meteorological variables suggested potential interference due to temperature, relative humidity, nitrogen oxides, and volatile organic compounds. Three correction models using temperature, humidity, and nitrogen dioxide (NO_2) were then tested to better relate the monitor concentrations to the FEM values. Temperature and humidity are two variables commonly available (or easily measurable) at sampling sites. The model (#3) that added NO_2 did not substantially improve the fit. Thus, the proposed models with only temperature and humidity can be easily adopted and adapted by any user. The corrected data explained up to 91% of the variance and showed a statistically significant improvement in the fit as well as a decreased influence from the interfering variables on the diurnal and weekly patterns. The correction models were also able to lower the effect of seasonal temperature changes, allowing the use of the monitors over long-term sampling campaigns. This study demonstrated that the Aeroqual ozone monitors can return "FEM-like" concentrations after appropriate corrections. Therefore, data provided by a network of monitors could determine the intra-urban spatial variations in ozone concentrations. These results suggest that these monitors could provide more accurate human exposure assessments and thereby reduce exposure misclassification and its resulting bias in epidemiological studies.

Keywords: Semiconductor gas sensor; Tropospheric ozone; Urban air pollution; Air pollution exposure.

The Effect of Emission Control on the Submicron Particulate Matter Size Distribution in Hangzhou during the 2016 G20 Summit

Huan Yu 1, Wei Dai1, Lili Ren1, Dan Liu1, Xintian Yan1, Hang Xiao2, Jun He3, Honghui Xu4

Source: Aerosol and Air Quality research, Volume: 18 | Issue: 8 | Pages: 2038-2046
DOI: 10.4209/aaqr.2018.01.0014

A number of observational and modeling studies have been conducted in China to study the effectiveness of radical short-term emission control measures with regard to air quality improvement. However, none of them have focused on the effect on submicron aerosols. Measurements on the size distribution of particles as small as 3 nm were conducted before, during and after the source emission control period for the 2016 G20 Summit held in Hangzhou, a megacity in eastern China. The measurement provided a unique opportunity to gain insight into the sources of submicron aerosols in Hangzhou and the effectiveness of radical emission control strategies. A WRF-Chem simulation suggested that the sources inside the emission control region contributed more than 70% to PM1 in Hangzhou from September 2 to 7, 2016, even under the strictest control scheme. Source restrictions on emissions from coal-fired power plants, on-road vehicles and industrial VOCs resulted in concentration decreases for PM1, PM0.01 and PM0.1, respectively. New particle formation (NPF) events, which were not suppressed completely by the emission control, enhanced the maximum PM0.01 concentration, at around 11:00 AM, by a factor of 4 compared to non-NPF days. Even during the strictest emission control period, two PM1 episodes still occurred due to the dominance of subsidence airflows, a low wind speed, and a weak vertical temperature gradient.

Keywords: Urban aerosols; Submicron aerosols; Particle size distribution; Emission control strategy.

Levels of Non-PBDE Halogenated Fire Retardants and Brominated Dioxins and their Toxicological Effects in Indoor Environments - A Review

Yi-Chyun Hsu1, Rachelle Anne D. Arcega2, Yan-You Gou3, Lemmuel L. Tayo2, Yi-Hsien Lin4, Sheng-Lun Lin5,6,7, How-Ran Chao 3,[8]

Source: Aerosol and Air Quality research, Volume: 18 | Issue: 8 | Pages: 2047-2063
DOI: 10.4209/aaqr.2018.03.0095.

Non-polybrominated diphenyl ether (non-PBDE) halogenated fire retardants (HFRs) such as new or novel brominated fire retardants (NBFRs) and dechlorane plus (DP) have been widely spread in the environment and recognized as emerging persistent organic pollutants (POPs) in the recent years, mainly due to the continuous increase in their global demand, especially after the worldwide restrictions on PBDE use. Polybrominated dibenzo-p-dioxins/furans (PBDD/Fs) are the unintentional byproducts of PBDE commercial formulations in the indoor environment. Although HFRs, including NBFRs, DP, and PBDD/Fs, are ubiquitous in the indoor environment due to the large-volume release from the surfaces of consumer products, only a few in vitro and in vivo studies have addressed their toxic effects. In this review article, global data on NBFRs, including decabromodiphenyl ethane (DBDPE), 1,2-bis(2,4,6-tribromophenoxy) ethane (BTBPE), bis(2-ethylhexyl)-3,4,5,6-tetrabromophthalate (BEH-TEBP), and 2-ethylhexyl-2,3,4,5-tetrabromobenzoate (EH-TBB), DP, including syn-DP and anti-DP, and PBDD/Fs in indoor aerosol and dust are summarized from recent literature. Based on the gathered data, indoor dust is a major sink for indoor contamination and is of great concern due to the fact that dust ingestion is one of the primary routes for human exposure to these chemicals. Lastly, the toxic effects of NBFRs, DP, and PBDD/Fs identified in in vitro and in vivo studies are summarized and discussed based on the current published reports. However, there is still a lack of sufficient toxicity data for assessing their risks. Future works are encouraged to focus on indoor PM2.5-bound HFR levels to further evaluate their toxic effects on human health.

Keywords: Fire retardants; Polybrominated dibenzo-p-dioxins/furans (PBDD/Fs); Indoor dust; Dechlorane plus (DP); Novel brominated fire retardants (NBFRs); Toxicity.

Outpatient Visits for Allergic Diseases are Associated with Exposure to Ambient Fungal Spores in the Greater Taipei Area

Kraiwuth Kallawicha1,2, Ying-Chih Chuang1, Shih-Chun Candice Lung3, Chang-Fu Wu4,5,6, Bor-Cheng Han1, Yi-Fang Ting1, Hsing Jasmine Chao 1

Source: Aerosol and Air Quality research, Volume: 18 | Issue: 8 | Pages: 2077-2085
DOI: 10.4209/aaqr.2018.01.0028

Allergic diseases are prevalent worldwide and may result from exposure to various substances. Exposure to ambient bioaerosols is a potential risk factor for allergic diseases; however, accurate exposure assessment is challenging due to the limited number of outdoor monitoring stations. In this study, the relationships between ambient bioaerosol exposure and allergic diseases (viz., acute conjunctivitis, allergic rhinitis, and asthma) were evaluated using validated land-use regression (LUR) models to estimate the exposure

levels. Data on the daily outpatient visits were retrieved from the Taiwan National Health Insurance Research Database. The total fungal spore count was associated with acute conjunctivitis in males at the second and third quartiles with relative risks (RRs) of 1.75 (95% confidence interval [CI] = 1.24, 2.48) and 1.32 (95% CI = 1.03, 1.70), respectively. It was also associated with asthma in both sexes when the concentration ≥ 95th percentile with RRs = 3.06 (95% CI = 1.89, 4.95) in males and 1.73 (95% CI = 1.08, 2.76) in females. Cladosporium was correlated with acute conjunctivitis in females at a concentration ≥ 95th percentile with RR = 2.90 (95% CI = 1.40, 6.04). Basidiospores were associated with allergic rhinitis in males at the third and fourth quartiles with RRs = 1.88 (95% CI = 1.44, 2.45) and 1.49 (95% CI = 1.20, 1.84), respectively. Meteorological parameters, including relative humidity and rainfall, were also crucial factors associated with the number of outpatient visits. Our results revealed that ambient fungal spores are critical determinants of allergic diseases. In addition, using LUR models to assess exposure to ambient bioaerosols is feasible.

Keywords: Bioaerosols; Acute conjunctivitis; Allergic rhinitis; Asthma; Land use regression (LUR).

Design and Development of a Novel Nanofiber Nasal Filter (NNF) to Improve Respiratory Health

Taewon T. Han 1, Letao Yang2, Ki-Bum Lee2,3, Gediminas Mainelis1

Source: Aerosol and Air Quality research,Volume: 18 | Issue: 8 | Pages: 2064-2076
DOI: 10.4209/aaqr.2018.03.0086

Currently available nasal filters are not well-suited for protecting humans against the fine and ultrafine airborne particles. In this research, we designed and evaluated a novel nanofiber nasal filter (NNF) capable of reducing personal exposure not only to large allergenic particles but also to ultrafine particles, thus reducing respiratory health risks. A new hybrid filter (HF) medium for the NNF was fabricated by overlaying a carbon filter substrate with nylon nanofibers produced by electrospinning. After optimizing the filter's production parameters, the HF was produced using the Nylon-6 polymer solution with a concentration of 15 wt%, a substrate based on a MERV 5 carbon filter with a density of 61 kg m–3, and a nanofiber surface coating density of 0.72 g m–2 (or 0.54 g m–2 as a second choice). The new HF was tested with fluorescent polystyrene latex beads sized 0.026–3.1 μm and at operating flow rates of 7.5–30 L min–1. The newly developed NNF showed more than a 90% collection efficiency for particles > 1 μm, representing bacteria and molds, and more than a 50% efficiency for particles < 0.5 μm, including ultrafine particles—about a

2.3-fold improvement compared to commercially available nasal filters. Thus, this NNF may serve as a useful tool to minimize our exposure to airborne pollutants.

Keywords: Personal exposure; Electrospinning; Hybrid filter; Carbon filter; Ultrafine; particles.

Characterization of Air Quality Index for both Handan and Kaifeng Cities, China

Rong Zhao1, Kangping Cui 1, Weiwei Wang1, How-Ran Chao 2

Source: Aerosol and Air Quality research,Volume: 18 | Issue: 8 | Pages: 2086-2107
DOI: 10.4209/aaqr.2018.06.0240

In this study, the atmospheric PM10, SO2, NO2, CO, and O3 concentration from 2015-2017, in Handan and Kaifeng were investigated. Besides, the seasonal variations of AQI values and their corresponding primary pollutants of six AQI grades were also discussed. In Handan, the daily AQI values ranged from 22 to 500 in 2015, from 19 to 500 in 2016, and from 27 to 500 in 2017, for which the corresponding average values were 143, 132 and 151, respectively. In Kaifeng, the daily AQI ranged from 25 to 496 in 2015, from 20 to 420 in 2016, and from 21 to 434 in 2017, for which the corresponding average values were 129, 124 and 131, respectively. During the three-year study, in Handan, the average proportion of grades I, II, III, IV, V and VI were 4.0%, 35.0%, 25.6%, 31.7%, 2.5% and 1.2% in spring; were 4.0%, 35.1%, 22.6%, 35.8%, 2.5% and 0% in summer; were 14.2%, 31.0%, 15.3%, 35.8%, 3.7% and 0% in fall, and were 3.3%, 26.1%, 20.0%, 37.8%, 8.1% and 4.7% in winter. In Kaifeng, the average proportion of grades I, II, III, IV, V and VI were 2.6%, 34.0%, 24.4%, 36.1%, 2.6% and 0.3% in spring; were 18.2%, 41.9%, 21.8%, 17.0%, 1.1% and and 0% in summer; were 8.6%, 34.3%, 17.4%, 34.8%, 4.9% and 0% in fall, and were 2.1%, 15.1%, 7.8%, 44.5%, 26.2% and 4.3% in winter. Overall, the air quality in the two cities were the worst in winter. The AQI values were between 101 and 150, where in Handan, PM2.5, PM10, and O3 were the primary air pollutants over the three years. In Kaifeng, the primary air pollutants were PM2.5, PM10, NO2, and O3 in 2015; were PM2.5, PM10, and O3 in 2016, and were PM2.5, PM10, and O3 in 2017. When AQIs ranged between 151 and 200, in Handan, the primary air pollutants were PM2.5, PM10, and O3 in both 2015 and 2016, and were PM2.5, PM10, NO2, and O3 in 2017. In Kaifeng, PM2.5, PM10, and O3 were the primary air pollutants from 2015-2017. When AQIs were between 201 and 300, in Handan, the primary air pollutants were PM2.5 and PM10 in 2015 and were PM2.5 and O3 in 2017. In Kaifeng, the primary air pollutants comprised PM10 in 2015, PM2.5 and PM10 in 2016, and PM2.5 and O3 at the same time. When the AQI values were between 301 and 500, which did not occur in Handan in 2015, the primary air pollutants comprised PM10 in

2016, PM2.5 and PM10 in 2017, and in Kaifeng from 2015-2017, PM2.5, and PM10 were the primary air pollutants. This study investigated the AQI values and corresponding primary pollutants in each season in more detail, the control strategies for these air pollutants will be more precisely.

Keywords: AQI; PM10; PM2.5; SO2; NOx; CO; O3.

Evaluation of Particle Resuspension and Single-layer Rates with Exposure Time and Friction Velocity for Multilayer Deposits in a Turbulent Boundary Layer

Sofia Eirini Chatoutsidou, Mihalis Lazaridis

Source: Aerosol and Air Quality research, Volume: 18 | Issue: 8 | Pages: 2108-2120
DOI: 10.4209/aaqr.2018.01.0022.

The present work deals with the resuspension of small nondeformable particles from multilayer deposits in a turbulent boundary layer. A kinetic force-balance approach was adopted to model particle motion at the point of detachment, whereby intermolecular interactions were modeled by the Lennard-Jones potential. The rate of change of the number of particles was estimated for each discrete layer based on existing kinetic models. In particular, the kinetic equations of Lazaridis and Drossinos (1998), LD, and Friess and Yadigaroglu (2001), FY, were implemented and compared using lattice arranged deposits. The influence of exposure time and friction velocity was investigated through the obtained resuspension rates. It was found that the single-layer resuspension rates were substantially affected by the layer position within the deposit as well as considerably influenced by both the exposure time and the friction velocity. Moreover, the numerical results demonstrate that the LD kinetic estimates higher resuspension rates compared to the FY kinetic only for short exposures to the flow, predominantly due to a different expression for the fraction of exposed particles. In addition, the present study recognized the time dependence (i.e., a short-term vs. long-term regime) of the resuspension rate observed both experimentally (Wu et al., 1992; Wang et al., 2012) and by model predictions (Lazaridis and Drossinos, 1998; Friess and Yadigaroglu, 2001; Reeks and Hall, 2001) and confirmed the inverse dependence of the resuspension rate with time in long-term regime. Two regimes were also identified while evaluating the resuspension rate for a range of friction velocities, viz., a low-friction regime in which the resuspension rate increases with friction and a high-friction regime in which the opposite behaviour was observed.

Keywords: Multilayer deposit; Resuspension; Kinetics; Adhesion.

Enhanced Activity of Nb-modified CeO2/TiO2 Catalyst for the Selective Catalytic Reduction of NO with NH3

Ye Jiang 1, Changzhong Bao1, Shaojun Liu2, Guitao Liang1, Mingyuan Lu1, Chengzhen Lai1, Weiyun Shi1, Shiyuan Ma1

Source: Aerosol and Air Quality research, Volume: 18 | Issue: 8 | Pages: 2121-2130
DOI: 10.4209/aaqr.2018.02.0059

A series of CeO2-Nb2O5/TiO2 catalysts were prepared by an impregnation method and investigated for the selective catalytic reaction (SCR) of NO with NH3. The 15 wt.% CeO2–10 wt.% Nb2O5/TiO2 catalyst (CeNbTi) exhibited the highest activity and resistance to a high gas hourly space velocity and K2O. In the presence of H2O and SO2, it also showed better activity than the CeTi catalyst. The addition of Nb could improve the dispersion of CeO2 and increase the amount of Ce3+ and chemisorbed oxygen species on the catalyst surface, which enhances the catalytic activity of CeTi. The superior SCR activity of CeNbTi might also be attributed to its high redox ability, the enhanced adsorption capacity of NH3 species and the synergistic action between Ce, Nb and Ti species.

Keywords: Selective catalytic reduction; NO NH3 CeO2-Nb2O5/TiO2; Impregnation method.

Recognition of the Source and Nature of Atmospheric Aerosols in Tehran, Iran

Balal Oroji1, Eisa Solgi 1, Asghar Sadighzadeh2

Source: Aerosol and Air Quality research, Volume: 18 | Issue: 8 | Pages: 2131-2140
DOI: 10.4209/aaqr.2018.03.0098.

The size, morphology and chemical characterization of individual atmospheric particles have received significant attention due to their effects on radiative and chemical properties. Tehran is one of the most polluted cities not only in Iran but in the world, which is continuously affected by air pollution. In this study, 25 sites were sampled in urban and non-urban areas. The sampling was performed with a high-volume sampler for a period of 14–24 hours. Scanning Electron Microscopy (SEM) and Energy Dispersive X-ray Spectroscopy (EDS) were used to characterize the aerosols in the urban and non-urban areas during each season. The SEM results indicate that during summer, flaky, irregularly shaped aggregate particles dominated the urban areas, whereas non-urban areas were relatively clean. During winter, the non-urban sites were observed to be dominated by spherical and irregularly shaped particles, suggesting combustion sources, whereas

particles were observed in a more concentrated form at the urban sites. EDS analysis shows varying percentages of C, O, Zn, Si, Ca and Fe at both the urban and non-urban sites for all seasons. Furthermore, this study reveals the variability of the morphological and elemental composition of PM in different seasons at urban and non-urban locations and highlights the various probable sources associated with them.

Keywords: Aerosols; Air pollution; Urban transport; Morphology; Tehran.

Preface to a Special Issue "Megacity Air Pollution Studies (MAPS)"

Yong Pyo Kim 1, Gangwoong Lee2, Louisa Emmons3, Rokjin Park4, Neng-Huei Lin5

Source: Aerosol and Air Quality research, Volume: 18 | Issue: 9 | Pages: I-IV
DOI: 10.4209/aaqr.2018.09.maps

Large urban areas, commonly referred to as megacities, generally consume a huge amount of energy due to the high population density along with concentrated economic activities, and the resulting environmental burden—including air pollution—is an ongoing scientific and public issue. As several common factors and drivers cause air pollution problems in urban areas, it is widely thought that the air quality trends in different cities exhibit similarities in certain aspects correlated with urban development activity and air pollution mitigation practices. However, unique characteristics in the emission, chemistry, and dispersion of air pollutants that are specific to each urban area also exist, which often reflect differing approaches to air pollution control policy. Based on this reasoning, several comprehensive studies in big megacities, mostly in North America and Europe, have been implemented extensively over the last two decades. However, the air quality is often much poorer in the megacities of developing countries, and extensive research is still needed to tackle the urgent goals of understanding the increasing complexity of air quality and identifying appropriate mitigation measures. This MAPS (Megacity Air Pollution Studies) special issue highlights recent scientific findings from megacity air-quality research in many parts of the world. It focuses primarily on the mechanisms and drivers that result in high ozone and aerosol events in megacities but also addresses the latest advances in precursor emissions inventories, chemical transformation assessments, and forecasting models with sets of field observations, including remote sensing applications.

Keywords: Megacity Air Pollution Studies (MAPS); Special issue.

Trend of Air Quality in Seoul: Policy and Science

Yong Pyo Kim 1, Gangwoong Lee 2

Source: Aerosol and Air Quality research, Volume: 18 | Issue: 9 | Pages: 2141-2156
DOI: 10.4209/aaqr.2018.03.0081

The trend of air pollutant concentrations in the Seoul Metropolitan Area (SMA)—particularly the city of Seoul—in the Republic of Korea, is shown and analyzed along with applied policy; furthermore, the remaining challenges are identified, and the direction of future research is discussed. The policies adopted from developed countries, notably, direct emission control measures, such as limiting the sulfur content in fuel and tightening emission standards, have been successful in reducing primary air pollutants, e.g., carbon monoxide, sulfur dioxide, and lead; however, these policies have not been effective in controlling the increased number of emission sources and secondary air pollutants, such as particulate matter with an aerodynamic diameter less than or equal to a nominal 2.5 μm (PM2.5), and ozone. To develop effective control policies on air pollution, the following actions are recommended: (1) creating a reliable emission inventory; (2) reducing uncertainties about the regional contribution to the air quality in Seoul; and (3) understanding the major chemical pathways of ozone and secondary aerosols. Suggestions for accomplishing these goals in future research are also provided.

Keywords: Seoul; Air quality management policy; Trend of air pollutants; Secondary air pollutants; International cooperation

---

Overview of Meteorological Surface Variables and Boundary-layer Structures in the Seoul Metropolitan Area during the MAPS-Seoul Campaign

Moon-Soo Park 1,2

Source: Aerosol and Air Quality research, Volume: 18 | Issue: 9 | Pages: 2157-2172
DOI: 10.4209/aaqr.2017.10.0428

The meteorological surface variables and boundary-layer structures in the Seoul Metropolitan Area (SMA) were examined during the MAPS-Seoul (Megacity Air Pollution Studies in Seoul) intensive field experiment (18 May–13 June 2015). Data were obtained from a surface energy balance system and a ceilometer installed at a UMS-Seoul (urban meteorological observation system in the SMA) station located in the eastern part of the city of Seoul. A series of migratory anticyclone passages under a strong El Niño event meant that the experimental period was much warmer and drier than the climatological

ones. The mean air temperature during this period was 2.6°C higher than the recent 30-year (1981–2010) climatological value, while only one-eighth of the climatological precipitation was recorded. Twelve mist event days were recorded, as were four of haze and six of rainfall events. The SMA was found to be affected by the sea-land breeze: Westerly winds (sea-breezes) were dominant from the afternoon till the early evening, while easterlies (land-breezes) were dominant before the morning. Finally, the vertical profile of the attenuated backscatter obtained by the ceilometer indicated that the maximum daily mixing-layer heights (MLHs) on days with mist/haze and much cloud cover were lower than on days with no-mist/haze and less cloud cover, respectively, mainly due to a decrease in the downward solar radiation. However, the effect of mist/haze on the daytime MLH evolution was larger than that of cloud cover. The MLH also exhibited an altitude similar to that of the steepest vertical gradient of sulfate and organic aerosol concentration, obtained from the airborne measurement on 13 June 2015.

Keywords: Atmospheric boundary-layer structure MAPS-Seoul Mist/haze event Mixing-layer height UMS-Seoul.

Meteorological Overview and Signatures of Long-range Transport Processes during the MAPS-Seoul 2015 Campaign

Cheol-Hee Kim 1, Hyo-Jung Lee1, Jeong-Eon Kang1, Hyun-Young Jo1, Shin-Young Park1, Yu-Jin Jo1, Jong-Jae Lee1, Geum-Hee Yang1, Taehyun Park2, Taehyoung Lee2

Source: Aerosol and Air Quality research, Volume: 18 | Issue: 9 | Pages: 2173-2184
DOI: 10.4209/aaqr.2017.10.0398

During the Megacity Air Pollution Studies-Seoul (MAPS-Seoul) 2015 campaign, which was conducted from May 27 to June 13, 2015, as a pilot for the Korea-US Air Quality (KORUS-AQ) 2016 campaign, seven flights were conducted around the west coast of the Korean Peninsula, the Yellow Sea, the Seoul metropolitan area, and several urban/suburban areas in South Korea. Signatures of the long-range transport processes over Northeast Asia were then summarized from the following: 1) the presentation of a brief description of the synoptic situation for each of the seven flight missions, from RF1 to RF7; 2) interpretations of both streamline and trajectory analyses that described the meteorological history of an air mass; and 3) the calculation of 17 meteorological parameters, including the geostrophic wind speed, the vorticity at a geopotential height of 850 hPa, and several vertical stability indices.

The synoptic conditions during the campaign period were characterized by migratory cyclones and anticyclones with appropriate streamlines and backward trajectories over Northeast Asia. The “stagnant” case was characterized by weak geostrophic wind speed,

smaller vorticity, and lower humidity atmospheric conditions, whereas the "long-range transport" case had higher geostrophic wind speed, positive vorticity, and higher humidity atmospheric conditions. Among the seven flights, RF1 and RF2 were identified as dominant stagnant synoptic cases from several diagnostic variables, while long-range transport processes were observed in RF3, RF6, and RF7. RF4 found two mixed characteristics, an upper atmosphere with long-range transport processes and a lower atmosphere characterized by stagnant conditions, and RF5 showed a transport pattern from the southern marine atmosphere without long-range transport from the high emission area. Other meteorological features were also discussed in association with the signatures of the long-range transport processes occurring over Northeast Asia during the MAPS-Seoul 2015 campaign.

Keywords: MAPS-Seoul 2015; Campaign; Synoptic meteorological conditions; Long range transport process.

Slow Decreasing Tendency of Fine Particles Compared to Coarse Particles Associated with Recent Hot Summers in Seoul, Korea

Greem Lee1, Hye-Ryun Oh1, Chang-Hoi Ho 1, Doo-Sun R. Park2, Jinwon Kim3, Lim-Seok Chang4, Jae-Bum Lee4, Jinsoo Choi5, Minyoung Sung5

Source: Aerosol and Air Quality research, Volume: 18 | Issue: 9 | Pages: 2185-2194
DOI: 10.4209/aaqr.2017.10.0403

In Seoul, South Korea, particulate matters (PMs) significantly decreased for the period 2005–2015 in concert with the implementation of air pollution reduction policies. This study reveals that PM with a diameter smaller than 2.5 μm (PM2.5) has a slower decreasing tendency than PM in the 2.5–10-μm range (PM2.5-10) during summer and that this discrepancy is attributable to the large increase in the summer surface air temperature for the analysis period (0.13°C year−1). During the daytime, especially in the afternoon when the hourly surface air temperature and its increasing rate are high, the difference between the decreasing rates of PM2.5 and PM2.5-10 is pronounced. The slower decrease in PM2.5 compared to PM2.5-10 likely results from the secondary PM2.5 formation being accelerated by the increase in the surface air temperature. Other atmospheric variables that can affect concentrations of PMs, such as insolation, relative humidity, precipitation, wind speed, and sea-level pressure, do not show a meaningful relationship with the discrepancy in the decreasing tendency between the two PMs. Our finding emphasizes the necessity of continuous monitoring and analysis of long-term variability in concentrations of PMs and related meteorological conditions, and the independent establishment of

reduction policies for PM2.5 and PM2.5-10 to prepare for anthropogenic climate change and the subsequent air quality change.

Keywords: PM2.5; PM2.5-10 Surface air temperature; Secondary formation; Urban area.

Characteristics of Classified Aerosol Types in South Korea during the MAPS-Seoul Campaign

Seoyoung Lee1, Jaemin Hong1, Yeseul Cho1, Myungje Choi1, Jhoon Kim1,2, Sang Seo Park3, Joon-Young Ahn4, Sang-Kyun Kim4, Kyung-Jung Moon4, Thomas F. Eck5, Brent N. Holben5, Ja-Ho Koo 1

Source: Aerosol and Air Quality research, Volume: 18 | Issue: 9 | Pages: 2195-2206
DOI: 10.4209/aaqr.2017.11.0474

During the Megacity Air Pollution Studies-Seoul (MAPS-Seoul) campaign from May to June 2015, aerosol optical properties in Korea were obtained based on the AERONET sunphotometer measurement at five sites (Anmyon, Gangneung_WNU, Gosan_SNU, Hankuk_UFS, and Yonsei_University). Using this dataset, we examine regional aerosol types by applying a number of known aerosol classification methods. We thoroughly utilize five different methods to categorize the regional aerosol types and evaluate the results from each method by inter-comparison. The differences and similarities among the results are also discussed, contingent upon the usage of AERONET inversion products, such as the single scattering albedo. Despite several small differences, all five methods suggest the same general features in terms of the regionally dominant aerosol type: Fine-mode aerosols with highly absorbing radiative properties dominate at Hankuk_UFS and Yonsei_University; non-absorbing fine-mode particles form a large portion of the aerosol at Gosan_SNU; and coarse-mode particles cause some effects at Anmyon. The analysis of 3-day back-trajectories is also performed to determine the relationship between classified types at each site and the regional transport pattern. In particular, the spatiotemporally short-scale transport appears to have a large influence on the local aerosol properties. As a result, we find that the domestic emission in Korea significantly contributes to the high dominance of radiation-absorbing aerosols in the Seoul metropolitan area and the air-mass transport from China largely affects the western coastal sites, such as Anmyon and Gosan_SNU.

Keywords: Aerosol type classification optical; property; AERONET MAPS.

Regional Characteristics of NO2 Column Densities from Pandora Observations during the MAPS-Seoul Campaign

Heesung Chong1, Hana Lee1, Ja-Ho Koo1, Jhoon Kim1,2, Ukkyo Jeong3,4, Woogyung Kim3,4, Sang-Woo Kim5, Jay R. Herman3, Nader K. Abuhassan3, Joon-Young Ahn6, Jeong-Hoo Park6, Sang-Kyun Kim6, Kyung-Jung Moon6, Won-Jun Choi6, Sang Seo Park 5

Source: Aerosol and Air Quality research, Volume: 18 | Issue: 9 | Pages: 2207-2219
DOI: 10.4209/aaqr.2017.09.0341

Vertical column density (VCD) of nitrogen dioxide (NO2) was measured using Pandora spectrometers at six sites on the Korean Peninsula during the Megacity Air Pollution Studies-Seoul (MAPS-Seoul) campaign from May to June 2015. To estimate the tropospheric NO2 VCD, the stratospheric NO2 VCD from the Ozone Monitoring Instrument (OMI) was subtracted from the total NO2 VCD from Pandora. European Centre for Medium-Range Weather Forecasts (ECMWF) reanalysis wind data was used to analyze variations in tropospheric NO2 VCD caused by wind patterns at each site. The Yonsei/SEO site was found to have the largest tropospheric NO2 VCD (1.49 DU on average) from a statistical analysis of hourly tropospheric NO2 VCD measurements. At rural sites, remarkably low NO2 VCDs were observed. However, a wind field analysis showed that trans-boundary transport and emissions from domestic sources lead to an increase in tropospheric NO2 VCD at NIER/BYI and KMA/AMY, respectively. At urban sites, high NO2 VCD values were observed under conditions of low wind speed, which were influenced by local urban emissions. Tropospheric NO2 VCD at HUFS/Yongin increases under conditions of significant transport from urban area of Seoul according to a correlation analysis that considers the transport time lag. Significant diurnal variations were found at urban sites during the MAPS-Seoul campaign, but not at rural sites, indicating that it is associated with diurnal patterns of NO2 emissions from dense traffic.

Keywords: Pandora NO2 MAPS-Seoul.

Variation of PM2.5 Chemical Compositions and their Contributions to Light Extinction in Seoul

Seung-Myung Park1,2, In-Ho Song1, Jong Sung Park1, Jun Oh1,2, Kwang Joo Moon1, Hye Jung Shin1, Jun Young Ahn1, Min-Do Lee1, Jeonghwan Kim2, Gangwoong Lee 2

Source: Aerosol and Air Quality research, Volume: 18 | Issue: 9 | Pages: 2220-2229
DOI: 10.4209/aaqr.2017.10.0369

The objective of this study was to determine comprehensive chemical components in PM2.5 from March 2011 till February 2012 in Seoul, South Korea, and their contributions to light extinction. Major chemical components in the aerosol were: ammonium sulfate, 30.3%; ammonium nitrate, 25.2%; organic matter, 21.3%; crustal mass, 16.9%; element carbon, 6.1%; and trace metals, 0.2%. PM2.5 mass concentrations and light extinction were mostly correlated in their diurnal and monthly variations, which indicates that the aerosol mass is the key variable in light extinction in Seoul. However, the aerosol size and composition (of PM2.5) also played significant roles in light extinction. We applied the IMPROVE algorithm to quantify the contributions of observed chemical components to light extinction. It was found that the IMPROVE formula tended to underestimate light extinction by up to 30% in urban conditions where large sources of organic matter (OM) and element carbon (EC) existed unless some revision was made before the light extinction calculations. The IMPROVE algorithm was further optimized for the observed light extinction for OM and EC. The revised light extinction efficiencies of OM and EC in Seoul increased by about 1.5–3 times of those in the original IMPROVE algorithm. The optimized IMPROVE scheme in this study reproduced the observed light extinction more accurately in Seoul. Overall, 41% of the contribution from OM and EC to light extinction in Seoul was close to 50% of the contribution from nitrate and sulfate, although the mass of the former contribution was only half of the latter.

Keywords: PM2.5; Visibility; Light extinction; OM EC.

Investigation of Diurnal Pattern of Generation and Resuspension of Particles Induced by Moving Subway Trains in an Underground Tunnel

Sang-Hee Woo1,2,3, Jong Bum Kim2, Gwi-Nam Bae 2,3, Moon Se Hwang4, Gil Hun Tahk4, Hwa Hyun Yoon4, Se-Jin Yook 1

Source: Aerosol and Air Quality research,Volume: 18 | Issue: 9 | Pages: 2240-2252
DOI: 10.4209/aaqr.2017.11.0444

To protect the health of subway users, it is essential to investigate the generation, resuspension, and decay of particles in underground tunnels. In this paper, we analyzed the diurnal pattern of variation in particle concentration in a subway tunnel. The mass concentration of particles was measured in a shelter located midway in the underground tunnel connecting Janghanpyeong station and Gunja station on Seoul Subway Line 5 by using an aerodynamic particle sizer, a dust monitor, and a fast mobility particle sizer. The particle mass concentration increased uniformly as a train passed through the tunnel, which was followed by an exponential decay. The particle concentration in the tunnel decreased when the decrease in the number of particles between train operations

exceeded the number of particles generated and resuspended by a passing train, and increased in the opposite case. The diurnal variation in particle concentration in the tunnel according to train operations can be predicted by applying such a pattern of variation to the mass concentration of particles.

Keywords: Aerosol; Particle concentration; Subway; Underground tunnel; Train operation.

Generation Characteristics of Nanoparticles Emitted from Subways in Operation

Yongil Lee1,2, Kyomin Choi1,2, Wonseog Jung1,2, Michael E. Versoza2,3, Mona Loraine M. Barabad2,3, Taesung Kim1, Duckshin Park 2

Source: Aerosol and Air Quality research,Volume: 18 | Issue: 9 | Pages: 2230-2239
DOI: 10.4209/aaqr.2017.11.0439

In this study, measurements were carried out to identify the generation characteristics of wear particles emitted under a subway cabin during operation. Along with a fast mobility particle sizer, probes were installed under a subway cabin and in a subway tunnel to measure the size distributions of nanoparticles at 1-s intervals. Based on the particle density measured under the cabin minus that measured in the tunnel, the size distribution of wear particles generated under the cabin during deceleration was estimated to be bimodal at 165.5 nm and 6.98 nm. These particles were most likely generated from wheel-rail contact, as the train utilized electric braking (no mechanical force applied). In addition, a change in the wear mechanism appears to have arisen due to the increased temperature of the wheel-rail contact while nanoparticles were being emitted, leading to an initial generation of 165.5-nm particles followed by 6.98-nm particles 1 s later.

Keywords: Nanoparticle size distribution Urban railway Wear particle Wheel-rail contact.

The Controlling Factors of Photochemical Ozone Production in Seoul, South Korea

Saewung Kim 1, Daun Jeong1, Dianne Sanchez1, Mark Wang1, Roger Seco1, Donald Blake2, Simone Meinardi2, Barbara Barletta2, Stacey Hughes2, Jinsang Jung3, Deugsoo Kim4, Gangwoong Lee5, Meehye Lee6, Joonyoung Ahn7, Sang-Deok Lee8, Gangnam Cho7, Min-Young Sung7, Yong-Hwan Lee7, Rokjin Park9

Source: Aerosol and Air Quality research,Volume: 18 | Issue: 9 | Pages: 2253-2261
DOI: 10.4209/aaqr.2017.11.0452

We present the ambient ozone and relevant observed trace gas dataset in Seoul, South Korea, during the Megacity Air Pollution Studies (MAPS)-Seoul field campaign from May to June of 2015 (MAPS-Seoul 2015). We observed two distinctive periods, one with higher and the other with lower daytime ozone levels despite mostly clear conditions for both periods. The importance of peroxy radical contributions to excess ozone production is illustrated by the substantial differences in the Leighton constant (Φ) for the two periods. Moreover, higher levels of hydroxyl radical (OH) reactivity (s−1) were observed during the high ozone episode compared to the low ozone episode by as much as ∼5 s−1. The contributions of nitrogen oxides (NOx) to OH reactivity become less important than those of volatile organic compounds (VOCs) during the high ozone episode, which suggests the NOx saturated ozone production regime. It was also notable that the biogenic VOC isoprene consistently contributed the most to OH reactivity from among the observed VOCs during the afternoon throughout the whole field campaign. Finally, we ran multiple box model scenarios to evaluate the ozone production rates of three different air mixtures: a high ozone mixture, a low ozone mixture, and a simulation of the regional air quality. The results indicate that the total OH reactivity levels and the relative contributions of VOCs to NOx play critical roles in ozone production rates. The simulated air quality mixture results in lower OH reactivity, causing lower ozone production rates than those calculated for the high ozone mixture, which clearly indicates the need for further improvements in the regional model to accurately simulate ozone precursors in the region. The results of this study suggest that a comprehensive trace gas dataset combined with observations of the OH reactivity enables us to properly diagnose the photochemistry behind ozone pollution, leading to effective ozone abatement policies.

Keywords: Ozone Leighton Constant OH reactivity Ozone production regime

---

High Efficiency Axial Wet Cyclone Air Sampler

Giwoon Sung1, Hyeong-U Kim2, Dongjoo Shin1, Weon Gyu Shin3, Taesung Kim 1,2

Source: Aerosol and Air Quality research,Volume: 18 | Issue: 10 | Pages: 2529-2537
DOI: 10.4209/aaqr.2017.12.0596

Early detection of highly contagious viral diseases is particularly important for controlling and minimizing the spread of these viruses. Moreover, the sampling of airborne viruses is a

crucial step towards an effective epidemic diagnosis. However, most air samplers require long sampling times, and real-time virus detection is consequently not possible. Therefore, in this study, an axial-type wet cyclone capable of obtaining highly concentrated samples in an outdoor environment in real time was developed. In the newly designed axial wet cyclone, the airborne particles are firstly collected by centrifugal force in cyclone vanes rotating several times and then captured by inertial force before the air enters the outlet. The collection efficiency at 500 L min–1 was tested with polystyrene latex (PSL), and it was observed that the air sampler efficiency for 1.1 μm and 2 μm PSL was approximately 50% and 90%, respectively. For the large-sized PSL (> 3 μm), the observed collection efficiency was almost 100%. The Stokes number was used to design geometrically similar cyclones with air sampling rates of 100 L min–1 and 300 L min–1. The results of the scaled sampler show a somewhat lower collection efficiency than for the 500 L min–1 device but with lower liquid consumption and a lower pressure drop. For 100 L min–1 and 300 L min–1 samplers, the cutoff point for collection efficiency was approximately 1.5 μm and 3 μm PSL, respectively.

Keywords: Cyclone; Airborne virus; Axial type; Collection efficiency.

Measurements of the Size and Composition of Volatile Particles Generated from a Heated Tobacco Product with Aerosol Fixation Agents

Nobuyuki Ishikawa1, Kazuhiko Sekiguchi 2

Source: Aerosol and Air Quality research, Volume: 18 | Issue: 10 | Pages: 2538-2549
DOI: 10.4209/aaqr.2018.02.0049

Accurate measurements of the particle size distribution and chemical composition of particles are important to understanding their influence on human health and the indoor environment. In this research, volatile particles generated from a pod-type Heated Tobacco Product (HTP) were measured with an Aerodyne Aerosol Mass Spectrometer (AMS) and Scanning Mobility Particle Sizer (SMPS) using various aerosol fixation agents to reduce the volatility of the particles. A simple method of aerosol fixation was applied, and the effective fixation agents and the primary factor of fixation were elucidated. The effectiveness of a fixation agent was determined based on the solubility between the aerosol substrates and the agent. Although nonadecanoic acid did not work for aerosol substrates with a low polarity, we found that it achieved greater success in fixing propylene glycol and glycerin.

For particles that remained unfixed, the organic mass concentration (derived by AMS) was significantly reduced due to volatilization in the measurement apparatus. By contrast, the fixed volatile particles showed a higher organic mass concentration due to the suppression of volatilization. The peak number diameter of the unfixed volatile particles derived by SMPS was observed to be below 100 nm, whereas that of the fixed volatile particles was about 200 nm. The particle concentration of SMPS with fixation was in agreement with that of a light scattering method (welas®). The elemental and surface compositions of the fixed volatile particles were analyzed by Scanning Electron Microscope-Energy Dispersive X-ray spectrometry (SEM-EDX) and Time-of-Flight Secondary Ion Mass Spectrometry (TOF-SIMS) under vacuum conditions. The results revealed that the fixation agent was localized on the surface of the particles, reducing the volatility of the particles.

Keywords: Aerosol fixation; Aerosol mass spectrometer; Tobacco smoke; Volatile particles; Heated tobacco product.

Small Cyclones with Conical Contraction Bodies

Di Liu1, Peng Wang1, Ta-Chih Hsiao2, Da-Ren Chen 1

Source: Aerosol and Air Quality research, Volume: 18 | Issue: 10 | Pages: 2519-2528
DOI: 10.4209/aaqr.2018.05.0166.

The performance (i.e., cyclone pressure drop and particle penetration curve) of small cyclones with conical contraction bodies was investigated, with the cyclone used either as the size-selective inlet of a miniature/compact particle sensor/monitor or as a personal particle sampler. Prototype cyclones having inner bodies with conical contraction angles of 0°, 15° and 30° were constructed, and their performance was evaluated at various operational flow rates (viz., 1.0–7.0 L min–1); the results indicate that a cyclone with a high body contraction angle is capable of collecting smaller particles than one with a low contraction angle at the same cyclone pressure drop. The effect of the vortex finder insertion length on the cyclone's performance was also studied and was found to be negligible. A linear relationship between the dimensionless particle cut-off size and the annular flow Reynolds number, Reann (in the log-log plot), could be found for the studied cyclones with characteristic cyclone velocity, calculated with the assumption of conservation of angular momentum for the swirling flow in a cyclone. Compared with

previous studies, cyclones with conical contraction bodies have an advantage during lower pressure drops (up to 50%) for the same dimensionless particle cut-off size.

Keywords: Cyclone; Conical contraction body; Cyclone pressure drop; Cyclone particle cut-off size.

Organic Aerosol Characterization and Source Identification in Karachi, Pakistan

Zehra Y. Khan1, Joshua Kettler1, Haider A. Khwaja2,3, Iftikhar I. Naqvi4, Abdul Malik5, Elizabeth A. Stone 1

Source: Aerosol and Air Quality research, Volume: 18 | Issue: 10 | Pages: 2550-2564
DOI: 10.4209/aaqr.2017.12.0579.

With its rapidly growing population and large industrial base, the megacity of Karachi, Pakistan, has been subjected to an increasing amount of ambient particulate matter (PM). Fine particulate matter (PM2.5) in Karachi was collected every 24 hours from January 8 to January 29, 2006. The samples were extracted and analyzed by gas chromatography-mass spectrometry (GC-MS) and ultra-performance liquid chromatography (UPLC) coupled with a triple quadrupole mass spectrometric detector (TQD) and time-of-flight (TOF) mass spectrometer. The daily PM2.5 levels ranged from 99.5 to 251.1 μg m–3 with a mean of 177.4 μg m–3, averaging 4–10-fold higher than the WHO guideline for 24-hour averaged PM2.5 (25 μg m–3). We found that the day-of-the-week variations of PM2.5 demonstrate Sundays have significantly lower concentrations (with a t-based confidence level of 95%), indicating that weekly behavioral patterns affect local PM2.5 concentrations. A significant negative correlation was found between the daily concentrations of levoglucosan, a biomass burning tracer, and the average daily temperatures ($r = -0.589$, $p = 0.004$), implicating heating as a major source of biomass burning emissions. Results indicate that polyaromatic hydrocarbons, hopanes, steranes, and alkanes are mainly emitted from fossil fuels and the combustion of carbonaceous materials. Organosulfates (OSs) and sulfonates were also quantified; significant correlations between OSs and sulfonates indicate a common source and/or similar formation mechanisms, while correlations with hopanes, steranes, and levoglucosan suggest their emission from primary sources such as fossil fuels and biomass burning. Qualitative analysis suggests the presence of a C6–C9 alkyl sulfate series. Through this study, the chemical composition and origin of the organic fraction of

PM2.5 in Karachi has been evaluated for the first time, and the results indicate a strong anthropogenic influence on combustion emissions, particularly those from biomass and fossil fuel burning.

Keywords: Aerosol chemistry; Air quality; Gas chromatography/mass spectrometry; Liquid chromatography/mass spectrometry PM2.5.

Characteristics and Compositions of Airborne Fine Particulate Matter in Southwest Ohio, USA

Chunjuan Xie1,2, Mingming Lu 2, Kaiqi Li2, Jian Li2,3, Anna L. Kelley4

Source: Aerosol and Air Quality research, Volume: 18 | Issue: 10 | Pages: 2565-2574
DOI: 10.4209/aaqr.2017.08.0256

Southwest Ohio has been known for PM2.5 issues due to emissions from multiple local sources, such as industry and multimodal traffic, as well as regional impacts from sulfates, nitrates, and ammonia. To better understand the speciation characteristics of PM2.5 in this area, data from five monitoring sites, Taft, Hook Field, St. Bernard, Lower Price Hill, and Chase, were studied for the time period of 2003 to 2013. The total concentration of PM2.5 has decreased significantly since the last decade, from 13.41 μg m−3 in 2003 to 10.55 μg m−3 in 2013. The overall PM2.5 concentration also exhibited seasonal variations, with four out of five of the highest concentrations occurring in summer and the fifth one occurring in winter. Due to various air pollution control measures (such as the Cross-State Air Pollution Rule, and Mercury and Air Toxics Standards), both the total concentrations and the speciation of PM2.5 have changed over time. The most dominant components of PM2.5 include sulfates, organic matter (OM), and nitrates, which contributed 33.4%, 31.7%, and 17.7%, respectively (Taft data from 2009 to 2013). Elemental carbon (EC) and crustal materials, on the other hand, accounted for much smaller portions—2.84% and 3.61%, respectively. The highest concentrations of sulfate occurred in summer, while those for nitrates occurred in winter. EC and OM followed the same seasonal trends, peaking in fall and summer and dropping to their lowest levels in winter. Crustal materials exhibited the lowest concentrations in winter. A comparison of Cincinnati (the Taft site) with other major cities nearby reveals that the highest concentration of PM2.5 and the largest fraction of sulfates is found in Cincinnati. Efforts to control these emissions are still necessary.

Keywords: PM2.5; Chemical speciation; Southwest Ohio; Sulfate.

Deposition of Toxic Dust with External Fields

Olga Kudryashova , Natalia Korovina, Igor Akhmadeev, Eugeny Muravlev, Sergey Titov, Anatoliy Pavlenko

Source: Aerosol and Air Quality research, Volume: 18 | Issue: 10 | Pages: 2575-2582
DOI: 10.4209/aaqr.2018.04.0138.

The harmful effects of fine dust on health in industrial facilities are a significant problem. The development of new deposition methods for dust particles with a diameter less than 10 microns is particularly difficult. The purpose of this study is to describe and compare new deposition methods for such aerosols by means of external fields: an acoustic wind, an electrostatic field, and specially atomized powder.

It has been shown that the method of spraying a powder affects its adsorption ability. An experimental study of the dispersity and specific surface of nanopowder particles atomized by different methods was carried out. As a result of atomization, the specific surface area of the particles decreases, and this decrease is smaller in the case of atomization by the shock-wave method.

The proposed mathematical model of aerosol coagulation is based on the integral version of the Smoluchowski equation with the type of kernel depending on the types of external influence. In the model, the effect of acoustic wind is considered, as the acoustic wind plays an important role in the deposition of finely divided particles. A calculation of the drift velocity of particles in an electric field and gravitational field is performed. The results of the pilot and theoretical study of the acoustic and electrostatic deposition of fine aerosols are presented in this article. Depending on the deposition method and particle size, calculations confirmed experimentally enable the reference time of the deposition of a dust cloud to be established. Recommendations are provided about the use of ultrasound sources, electrostatic precipitators, water aerosol sprays, and electrostatic spray guns for the optimum removal of dust from air in the workplace, taking into account dust particle sizes. The results of this study can be applied to air purification systems to filter harmful dust emissions.

Keywords: Fine aerosol; Electrostatic charge; Ultrasound; Coagulation; Deposition.

Evaluation of the Relative Health Risk Impact of Atmospheric PCDD/Fs in PM2.5 in Taiwan

Ngo Tuan Hung1,2, Hsu Wei Ting1,3, Kai Hsien Chi 1

Source: Aerosol and Air Quality research, Volume: 18 | Issue: 10 | Pages: 2591-2599
DOI: 10.4209/aaqr.2018.03.0094

Many studies have indicated that the largest amounts of particle-bound polychlorinated dibenzo-p-dioxins and dibenzofurans (PCDD/Fs) are found on small particles, which result in them having the highest PCDD/F TEQ concentrations. Epidemiological studies have found associations between PCDD/F exposure and development of many chronic diseases such as cardiovascular disease or cancers even in low exposure populations. Recently, in many countries, the concentrations of PM2.5 and PCDD/Fs have been one of the main foci of air monitoring systems. Several researches have suggested an association between air pollutants and health outcomes. However, publications about how PM2.5 and PCDD/Fs influence the health outcome in Taiwan are still limited. In this research, the spatial concentrations of PCDD/Fs in the vapor phase and the solid phase (TSP and PM2.5) were investigated during the winter seasons from 2012 to 2014 at different sites in Taiwan. The mean PCDD/F concentrations ranged from 10.8 ± 11.0 to 135 ± 64.3 fg I-TEQ m–3, with the highest concentrations found in the samples collected at industrial parks. Over 45.5% to 73.8% of the total PCDD/F concentrations were partitioned in the solid phase, while about 35.2% to 86.3% were distributed in PM2.5. The total quantities of the PCDD/F TEQs adsorbed onto PM2.5 measured at one northern urban sampling site (1,180 ± 294 pg I-TEQ g-PM2.5–1) and one northern suburban sampling site (1,110 ± 574 pg I-TEQ g-PM2.5–1) were higher than at other sites due to the influence of local municipal solid waste incinerators and long-range transport. Moreover, a significantly higher mortality risk was found for people living in areas with higher exposure rates of PM2.5 and PCDD/Fs.

Keywords: PM2.5 Dioxin, Relative risk, Long-range transport.

Wet Deposition of PCDD/Fs in Taiwan

Yen-Yi Lee1, Wen-Che Hou 1, Jinning Zhu 2, Weiwei Wang2

Source: Aerosol and Air Quality research,Volume: 18 | Issue: 10 | Pages: 2600-2611
DOI: 10.4209/aaqr.2018.07.0270

In 2017, the seasonal variations in the wet deposition fluxes of total-PCDD/Fs-WHO2005-TEQ in ambient air were evaluated in Taiwan. The results showed the annual wet deposition fluxes of total-PCDD/Fs-WHO2005-TEQ to be 42.5 pg WHO2005-TEQ m–2 month–1, and the seasonal distributions were 53.3, 62.9, 26.7 and 27.1 pg WHO2005-TEQ m–2 month–1 in spring, summer, autumn and winter, respectively. The average Stot of total-PCDD/Fs-WHO2005-TEQ was 12300. There were obvious seasonal variations in Stot, for which the values were 13840, 6540, 8280 and 20540 in spring, summer, autumn, and winter, respectively. The average concentration of total-PCDD/Fs-WHO2005-TEQ in the rain were 0.453, 0.176, 0.218 and 0.649 pg WHO2005-TEQ L–1 in spring, summer, autumn and winter, respectively. Atmospheric deposition is the major removal pathway for PCDD/Fs. The results of this study provide an evaluation of the adverse effects of PCDD/Fs exposure on human health, and provide a reason for the government to be concerned and to enact better control on air pollution.

Keywords: PM2.5 PCDD/Fs; Wet deposition; Scavenging ratio.

Characteristics of PM2.5-bound PCDD/Fs, PCBs, PBDD/Fs and PBDEs from a Diesel Generator Using Waste Cooking Oil-based Biodiesel Blends

Jen-Hsiung Tsai1, Shui-Jen Chen 1, Po-Min Li2, Guo-Ping Chang-Chien3,4, Kuo-Lin Huang1, Cheng-Hung Tsai1, Chi-Ying Hsieh1, Chih-Chung Lin1

Source: Aerosol and Air Quality research, Volume: 18 | Issue: 10 | Pages: 2583-2590
DOI: 10.4209/aaqr.2018.08.0310

This study investigates fine particulate matter (PM2.5) bound persistent organic pollutants (POPs) emitted from a diesel generator fueled with three waste cooking oil-based biodiesel (WCO-biodiesel) blends (W0 (pure diesel), W20 (WCO-biodiesel/diesel = 20%/80% (v/v)), and W40). These POPs are polychlorinated dibenzo-p-dioxins and dibenzofurans (PCDD/Fs), polychlorinated biphenyl (PCBs), polybrominated dibenzo-p-dioxins and

dibenzofurans (PBDD/Fs) and polybrominated diphenyl ethers (PBDEs). Experimental results indicate that the mass concentrations of PM2.5-bound PCDD/Fs, PCBs, PBDD/Fs and PBDEs in the engine exhaust are 2.15–3.65, 16.7–35.4, 25.8–46.5 and 303–440 pg Nm–3, respectively, at 1.5–3.0 kW loads for using W0, while the corresponding toxic equivalent (TEQ) concentrations of the above PM2.5-bound pollutants are 0.282–0.527, 0.038–0.051 and 0.064–0.093 pg WHO2005-TEQ Nm–3, respectively (excluding PBDEs, which still have no toxic equivalency factors (TEFs) for TEQ calculation). Using W20 and W40 reduced the mass and TEQ emission concentrations of PM2.5-bound PCDD/Fs, PCBs, PBDD/Fs and PBDEs in comparison with W0. The reductions of mass concentrations in exhausted PM2.5 were in the order PBDEs >> PBDD/Fs > PCBs > PCDD/Fs, while the decrease in toxic concentration followed the order PCDD/Fs > PBDD/Fs > PCBs. Thus, adding WCO-biodiesel to the fuel mixture in generator engines lowers the adverse effects of PM2.5 emissions on the environment and human health.

Keywords: PM2.5; Biodiesel; PCDD/Fs PCBs; PBDD/Fs PBDEs.

Direct Monitoring of Gram-negative Agents of Nosocomial Infections in Hospital Air by a PCR-based Approach

Mahnaz Nikaeen 1, Zahra Shamsizadeh2, Seyed Hamed Mirhoseini3

Source: Aerosol and Air Quality research, Volume: 18 | Issue: 10 | Pages: 2612-2617
DOI: 10.4209/aaqr.2017.11.0441

Gram-negative bacteria (GNB), including Acinetobacter baumannii, Pseudomonas aeruginosa and Legionella, have emerged as causative agents of many problematic infections in healthcare settings worldwide. Using a rapid detection method, this study was designed to investigate the presence of GNB in hospital air as a potential source for spreading and transmitting these bacteria. A total of 51 air samples were taken from different wards in four hospitals over a period of eight months. Air samples were collected using an all-glass impinger and analyzed for the presence of GNB. Detection of P. aeruginosa and Legionella spp. was performed with a nested PCR assay using specific primer sets of the 16S rRNA gene region of the bacteria. For detection of A. baumannii, PCR assay with the specific primers of the inherent blaOXA-51 gene was performed. A. baumannii was the most frequently (29/51) detected gram-negative microorganism in hospital air, followed by P. aeruginosa (15/51). The lowest detection frequency was related

to Legionella (9/51), which was not found in air samples from surgical wards. Intensive care units and operating theatres were high-risk areas due to the greater presence of GNB. The results of this study revealed the presence of GNB in various hospital wards and highlight the usefulness of PCR monitoring of hospital air as a rapid and reliable tool for identifying GNB in order to prevent and control nosocomial infections, especially for the protection of vulnerable patients.

Keywords: Gram-negative bacteria; Nosocomial infection; Hospital Air PCR.

Inflammatory Response and PM2.5 Exposure of Urban Traffic Conductors

How-Ran Chao1,2, Jhih-Wei Hsu3,4, Hsiu-Ying Ku5, Shu-Li Wang3, Han-Bin Huang3,6, Saou-Hsing Liou3, Tsui-Chun Tsou 3

Source: Aerosol and Air Quality research, Volume: 18 | Issue: 10 | Pages: 2633-2642
DOI: 10.4209/aaqr.2018.04.0132

Human exposure to airborne PM2.5 has been linked to an increased risk of respiratory and cardiovascular diseases, possibly via the activation of systemic inflammation. However, the associations between airborne PM2.5 and systemic inflammation in humans remain inconclusive. Traffic-related air pollutants (TRAPs) are the major source of PM2.5 in urban areas; the adverse health effect of PM2.5 from TRAPs is currently a critical issue of public concern. The present cross-sectional study examines the relationship between PM2.5 exposure and systemic inflammation in order to consider the health impacts of TRAP PM2.5 on urban traffic conductors. All study participants, viz., office-based police officers (the reference) and traffic conductors (the exposure), were requested to carry a personal sampler to determine individual PM2.5 exposure. An adenovirus-based NF-κB luciferase reporter assay was used to determine the proinflammatory activity in serum samples collected from the study participants. The blood proinflammatory activity was presented as tumor necrosis factor-α (TNFα) equivalence (TNFα-EQ), which was extrapolated from the sigmoidal semi-logarithmic dose-response curve of the NF-κB reporter assay by TNFα. The levels of both personal PM2.5 exposure and blood proinflammatory activity (TNFα-EQ) in the exposure group (traffic conductors) were significantly higher than in the reference group (office-based police officers) ($p < 0.05$). The present study reveals a positive and significant association between personal PM2.5 exposure levels and blood TNFα-EQ levels

in a linear regression model of y = 0.511x – 3.062 (y = log TNFα-EQ and x = log PM2.5; R = 0.231 and p = 0.047); the results suggest that exposure to TRAP PM2.5 significantly contributes to increased systemic inflammation in humans. This research provides clear evidence that long-term occupational exposure to TRAPs causes adverse health impacts, i.e., inflammation, on traffic conductors.

Keywords: Air pollution; Health effects/risks; Human exposure; Personal exposure; Toxicology.

Electrochemical Detection of Airborne Influenza Virus using Air Sampling System

Hyeong-U Kim1, Junhong Min2, Geunsang Park3, Dongjoo Shin3, Giwoon Sung3, Taesung Kim 1,3, Min-Ho Lee 2

Source: Aerosol and Air Quality research, Volume: 18 | Issue: 11 | Pages: 2721-2727
DOI: 10.4209/aaqr.2018.06.0221

Sampling and pre-detecting infectious diseases are effective ways of preventing them from widely spreading. Among the conventionally used sampling methods, cyclone-based air sampling is considered the simplest and most effective. In this study, we developed a new cyclone-type air sampler device by modifying the size and shape of a commercially available product, Coriolis μ (Bertin Technology). The newly built air sampler's collection efficiency was measured using polystyrene particles by comparing the amounts before and after sampling. Additionally, to test the feasibility of sampling airborne viruses, recombinant influenza virus antigen (H1N1) was injected into the custom-built air chamber where the air sampler's inlet was connected so that the antigen was collected through the sampling process. The solution was measured using a custom-made electrochemical platform that consisted of antibody conjugated Au electrodes on printed circuit board (PCB) and a small size reading system. Our findings showed that the influenza antigen was collected with good efficiency as well as detected with high sensitivity.

Keywords: Airborne; Virus; Sampler; Cyclone; Influenza.

Implication of Light Absorption Enhancement and Mixing State of Black Carbon (BC) by Coatings in Hong Kong

Guo-Liang Li1, Li Sun1, Kin-Fai Ho2, Ka-Chun Wong1, Zhi Ning 3

Source: Aerosol and Air Quality research, Volume: 18 | Issue: 11 | Pages: 2753-2763
DOI: 10.4209/aaqr.2017.11.0473

Simultaneous measurements of black carbon (BC) and non-refractory PM1 aerosol chemical compositions were performed in autumn 2016 at a suburban site in Hong Kong. A thermodenuder (TD) was employed at different heating temperatures to remove semi-volatile aerosol fractions to varying degrees. The light absorption enhancement (Eabs) of BC due to semi-volatile coatings at seven wavelengths was evaluated, and the coating fractions were further analyzed. Results showed that the overall Eabs ranged from 1.58 ± 0.13 (470 nm) to 1.64 ± 0.16 (660 nm) at 280°C and increased very little from 50°C (1.02–1.04) to 200°C (1.13–1.20). The lensing-effect-related Eabs was probably attributable to the presence of ammonium and sulfate. Furthermore, the ratio of the coating thickness to the BC core radius was around 1.0–2.0 based on Mie calculations. This work evaluated the Eabs from coatings in Hong Kong and implied the BC mixing state, thus providing a critical reference for climate models on the role of aerosol in global warming.

Keywords: Thermodenuder; BC coating; Mie calculation.

Seasonal Source Apportionment of PM2.5 in Ningbo, a Coastal City in Southeast China

Mengren Li1, Min Hu 1,4, Qingfeng Guo1, Tianyi Tan1, Bohan Du2, Xiaofeng Huang2, Lingyan He2, Song Guo1, Weifeng Wang3, Yingguo Fan3, Dandan Xu3

Source: Aerosol and Air Quality research, Volume: 18 | Issue: 11 | Pages: 2741-2752
DOI: 10.4209/aaqr.2018.01.0011

With the rapid economic development and urbanization of China, haze and photochemical smog events have been frequently observed during the last decade. To explore the temporal and spatial pollution characteristics in Ningbo, a medium-sized coastal city located in the Yangtze River Delta (YRD) in southeast China, 24-h PM2.5 (particulate matter with aerodynamic diameter ≤ 2.5 μm) samples were simultaneously collected at five sites (two urban residential sites, two urban coastal sites, and one suburban site) from winter 2012 to autumn 2013. The average PM2.5 concentration was 53.2 ± 30.4 μg m−3. Furthermore, the concentration exhibited a seasonal variation: It was highest in winter and

lowest in summer. The urban residential sites had the highest PM2.5 concentrations, followed by the urban coastal sites, and the suburban site had the lowest concentration. OM (Organic Matters) and secondary inorganic ions (sulfate, nitrate, and ammonium) were the dominant components of the PM2.5. As a coastal city with industrial zones, sources are more complex in Ningbo than in inland cities due to ship emissions and the interactions between land and sea, and the marine and atmospheric environments. Positive matrix factorization (PMF) was used to apportion the particle sources. Nine factors were resolved in this study: secondary nitrate, vehicle exhaust, secondary sulfate, coal combustion, industrial emission, ship emission, dust, biomass burning, and aged sea salt, with average contributions of 26%, 21%, 13%, 12%, 9%, 7%, 5%, 4%, and 3%, respectively. Secondary nitrate and vehicle exhaust were the major sources of PM2.5 pollution in Ningbo. Coal combustion contributed significantly in winter and autumn, whereas sea salt formed a considerable contribution in summer. This study suggests that decreasing the PM2.5 pollution in Ningbo requires not only strategies for reducing local primary sources but also joint inter-regional prevention and the control of air pollution in the YRD.

Keywords: PM2.5, Source apportionment, Positive matrix factorization (PMF), Temporal and spatial distribution.

Spatiotemporal Variation, Source Analysis, and Health Risk Assessment of Particle-bound PAHs in Urumqi, China

Maimaiti Simayi1,2, Palida Yahefu 1, Mengxin Han1

Source: Aerosol and Air Quality research, Volume: 18 | Issue: 11 | Pages: 2728-2740
DOI: 10.4209/aaqr.2018.04.0151

The purpose of the present study was to evaluate the polycyclic aromatic hydrocarbons (PAHs) in fine (PM2.5) and coarse (PM10) particles in five functional areas, namely, the traffic, industrial, residential, commercial, and educational areas, in Urumqi, a megacity in northwest China. Airborne PM10 and PM2.5 samples were collected from the five areas during heating (November 2015–March 2016) and non-heating (July–September 2016) periods, and 16 priority PAHs (Σ16PAHs) in the samples were quantified and analyzed. Over the study period, the average Σ16PAHs in the PM10 and PM2.5 were 116.97 ± 41.44 ng m–3 and 88.57 ± 31.22 ng m–3, respectively. During the heating period, Σ16PAHs in both of the fractions were more than 2.5 times those during the non-heating period, with the highest values found in the industrial area during the heating period and in the traffic area during the non-heating period. The northern part of the city had more PAH pollution than the southern part. The compositions of the particle-bound PAHs varied temporally

and spatially, with 4-ring PAHs contributing more during the heating period than during the non-heating period and with 5- and 6-ring PAHs exhibiting the opposite trend. In addition, 4-ring PAHs contributed more in the industrial area, whereas 5- and 6-ring PAHs contributed more in the traffic area, reflecting the variety of emission sources. Principal component analysis and diagnostic molecular ratios showed that vehicular exhaust was the major source of PAHs during both periods at the traffic and central urban sites, while heavy-duty vehicular emissions and natural gas/biomass/coal combustion emissions dominated in the industrial area. The average Benzo[a]pyrene equivalent toxicity (BaPeq) ranged from 4.4 to 37.9 ng m−3, showing a generally similar spatiotemporal distribution with the Σ16PAHs. The results showed that the lifetime excess cancer risk (LCR) during the heating period was higher than during the non-heating period and that people who lived around the industrial and traffic areas had a higher likelihood of getting lung cancer than residents in other parts of the city.

Keywords: Polycyclic aromatic hydrocarbons; Particulate matter; Spatiotemporal variations; Sources apportionment; Health risk.

Characteristics of Organic Carbon and Elemental Carbon in Atmospheric Aerosols in the Urban Area in Beibei, a Suburb of Chongqing

Xiaole Peng1, Qingju Hao1, Tianxue Wen2, Dongsheng Ji2, Zirui Liu2, Yuesi Wang2, Xinhua He1, Xiaoxi Li1, Changsheng Jiang

Source: Aerosol and Air Quality research, Volume: 18 | Issue: 11 | Pages: 2764-2774
DOI: 10.4209/aaqr.2017.11.0450

To investigate the pollutive characteristics of atmospheric carbonaceous aerosols in Beibei District, a suburb of Chongqing Municipal City, graded aerosol samples were continuously collected by cascade impactors over one year, from March 2014 to February 2015. Carbonaceous aerosols, including organic carbon (OC) and elemental carbon (EC), were detected by a DRI 2001A carbon analyzer. The results showed that the average annual concentrations of OC and EC in the PM2.1 were 16.3 ± 7.6 and 1.8 ± 0.7 μg m−3, and in the PM9.0 were 25.0 ± 9.6 and 3.2 ± 1.2 μg m−3, respectively. On the one hand, a more seasonal distribution of OC concentrations appeared in the PM2.1 (winter > spring > summer > autumn) than in the PM9.0 (winter ≈ spring ≈ summer > autumn); furthermore, whereas the OC significantly positively correlated with wind speed for both the PM2.1 ($P < 0.05$) and the PM9.0 ($P < 0.01$), it was negatively correlated with relative humidity ($P < 0.05$) for the latter. On the other hand, both the PM2.1 and the PM9.0 exhibited a more seasonal distribution of EC concentrations (winter > spring > summer > autumn), and the EC in the

PM2.1 significantly negatively correlated with temperature ($P < 0.05$). Additionally, both the OC and the EC were concentrated mainly in the fine particles (< 2.10 μm), and the size distributions of the OC in all four seasons displayed a bi-modal pattern that peaked in the size ranges of 0.43–0.65 μm (for fine particles) and 4.7–5.8 μm (for coarse particles), whereas the EC displayed a uni-modal pattern that peaked in the size range of 4.7–5.8 μm (for coarse particles). Furthermore, the correlations between the OC and the EC were analyzed, and the SOC (secondary organic carbon) in the PM2.1 was estimated using the primary OC/EC ratio. It was found that the OC highly significantly correlated with the EC ($P < 0.01$), with the average annual concentration of the SOC being 6.3 ± 5.9 μg m–3, which accounted for 33.5 ± 22.6% of the OC. Analyzing the sources of the pollutive atmospheric aerosol in Beibei further demonstrated that it mainly originated in biomass burning, gasoline-vehicle exhaust, and coal combustion.

Keywords: Organic carbon; Elemental carbo;n Size distribution; Seasonal patterns; Atmospheric aerosol.

Vertical-distribution Characteristics of Atmospheric Aerosols under Different Thermodynamic Conditions in Beijing

Hua Wang1,2, Zhaobin Sun 1, Hongyu Li 3, Yang Gao3, Jin Wu2, Tiantao Cheng4

Source: Aerosol and Air Quality research, Volume: 18 | Issue: 11 | Pages: 2775-2787
DOI: 10.4209/aaqr.2018.03.0078

Understanding the vertical distribution of atmospheric aerosols is crucial to elucidating their spatial distribution and the formation of extreme air pollution events. Based on multisource data from specialized aircraft, lidar, and conventional surface observations with meteorological reanalysis, the vertical distribution of atmospheric aerosols and related changes during two air pollution cases in Beijing in the spring of 2012 were analyzed and compared. The results indicated that temperature inversion occurred in the atmospheric boundary layer in both cases. Aerosols accumulated considerably within the inversion layer, and the vertical distribution of the aerosol concentration was consistent with the relative humidity. However, the vertical distributions of the pollution layer thickness, aerosol concentration, and particle size differed significantly under different temperature-inversion conditions, primarily because of differences in the air pollution-diffusing abilities, which depended on vertical changes in the atmospheric thermodynamic structure. When radiation inversion occurred, the diurnal variation in the vertical distributions of aerosol and relative humidity was notable: The air pollution layer was thin in the morning, but the aerosol and particle size became more vertically uniform during the

day, and the aerosol concentration and relative humidity near the surface decreased sharply because of enhanced pollutant vertical diffusion, which was influenced by newly developed unstable thermodynamic stratification. During the temperature inversion resulting from coupled subsidence and advection, the inversion layer was higher and more stable, allowing it to inhibit the vertical diffusion of pollutants, which subsequently caused long-lasting and thick pollution with a higher aerosol concentration and relative humidity at lower levels alongside a relatively unchanging vertical distribution of particle sizes. Moreover, in the daytime, as the southerly airflow strengthened below the inversion layer and the mixed-layer height increased, the pollution and wet layers thickened, and the aerosol concentration increased rapidly because of pollutant transport to the Beijing region.

Keywords: Aerosol; Aircraft detection; Temperature inversion; Vertical distribution.

Volatile Organic Compounds Emission from Chinese Wood Furniture Coating Industry: Activity-based Emission Factor, Speciation Profiles, and Provincial Emission Inventory

Ke Cheng 1, Wei-Wei Hao1, Peng Yi 2, Yang Zhang1, Jia-Yu Zhang1

Source: Aerosol and Air Quality research, Volume: 18 | Issue: 11 | Pages: 2813-2825
DOI: 10.4209/aaqr.2018.02.0044

Volatile organic compounds (VOCs) have been identified as the most crucial precursors of tropospheric photochemical O3 formation and secondary organic aerosols. In this study, field measurement was conducted to develop VOCs emission factors and source profiles of the wood furniture coating industry in China. An activity-based database was established, involving coat consumption-based, coating area-based, furniture production-based, and output value-based VOCs emission factors. Combining the results of field tests and literature surveys, emission factors were calculated by enterprise scale, coating type, spraying technology, and emission control device. The uncertainties were quantified by using Monte Carlo simulations. VOCs emission factors were estimated: 0.22 (0.10–0.34, 95% CI) kg kg–1 for coat consumption-based; 21.97 (10.10–29.38) g m–2 for coating area–based; 0.69 (0.34–1.00) kg piece–1 for furniture production-based; and 6.95 (3.42–10.21) kg 10–4 yuan for output value–based calculation, respectively. Aromatics and oxygenated VOCs (OVOCs) were predominant species of solvent borne paint emission, with the proportion of 71.1% and 22.9% of totals, respectively. VOCs emissions from the wood furniture coating industry were estimated at 179.76 × 103 (88.58 × 103–260.52 × 103, 95% CI) t in 2016. Due to the huge production output and intensive distribution of

enterprises, VOCs emissions mainly concentrated in Guangdong, Zhejiang, Shandong, Fujian, Jiangxi, and Sichuan province, with the combined contribution of 43.8% of the national totals.

Keywords: Wood furniture; coating industry; VOCs Activity-based emission factor; Source profile; Emission inventory.

Mercury Speciation and Mass Distribution in Cement Production Process of Taiwan

Chien-Ping Chou1,2, Tien-Chin Chang1, Chun-Hsiang Chiu 3, Hsing-Cheng Hsi 4

Source: Aerosol and Air Quality research, Volume: 18 | Issue: 11 | Pages: 2801-2812
DOI: 10.4209/aaqr.2018.05.0205

In this study, the mercury (Hg) speciation and mass distribution at two cement plants located in northern and eastern Taiwan were investigated. Gaseous Hg in the kiln flue gas was sampled by the Ontario Hydro method, and the solid samples were collected to analyze the Hg mass balance. The total Hg concentrations in the raw mill electrostatic precipitator (ESP) input of the two plants were 155.70 and 64.62 μg Nm–3, respectively, which were higher than those at any other sampling point. Approximately 97.5 and 86.5% of the Hg in the raw mill ESP input at Plants 1 and 2, respectively, was particle-bound. Elemental Hg was the major gaseous Hg species emitted into the atmosphere from these two cement plants, accounting for 56.4 to 98.2% of the total Hg in the flue gas. The total Hg mass output was calculated to be 61.374 and 204.596 mg-Hg per metric ton-clinker (mg ton–1) for cement Plants 1 and 2, respectively. The Hg emission factors for Plants 1 and 2 were thus 0.059 and 0.196 g-Hg per metric ton-cement (g ton–1), respectively. These results improve our understanding of Hg emissions from cement plants in Taiwan and provide useful information for selecting Hg control technology.

Keywords: Cement plant; Precalciner production; Mercury speciation; Mercury distribution; Atmospheric mercury.

Atmospheric (Dry + Wet) Deposition of PCDD/Fs in Taiwan

Yen-Yi Lee1, Wen-Che Hou 1, Jinning Zhu 2, Weiwei Wang2

Source: Aerosol and Air Quality research, Volume: 18 | Issue: 11 | Pages: 2788-2800
DOI: 10.4209/aaqr.2018.10.0363

Air pollution was getting worse and worse with the development of economic, and atmospheric deposition was an important mechanic for the removal of air pollutants. During 2017, the average dry deposition fluxes of total-PCDD/Fs-WHO2005-TEQ in various areas in Taiwan range between 57 (Lienchiang County in autumn) and 589 pg WHO2005-TEQ m–2 month–1 (Keelung City in winter), with an average of 221 pg WHO2005-TEQ m–2 month–1. The average total deposition fluxes of total-PCDD/Fs-WHO2005-TEQ in various areas in Taiwan range between 65 (Lienchiang County in autumn) and 681 pg WHO2005-TEQ m–2 month–1 (Keelung City in winter), with an average of 263 pg WHO2005-TEQ m–2 month–1. The fractions of dry deposition fluxes contribute to the total deposition fluxes range between 37.8% (Yilan County in winter) and 99.9% (Kaohsiung City in winter), with an average of 82.1%.

Keywords: PM2.5; PCDD/Fs; Dry deposition; Total deposition.

Seasonal Variation in Culturable Bioaerosols in a Wastewater Treatment Plant

Mansooreh Dehghani1, Armin Sorooshian2,3, Mohammad Ghorbani4, Mehdi Fazlzadeh5,6, Mohammad Miri7, Parisa Badiee8, Ali Parvizi9, Marziye Ansari9, Abbas Norouzian Baghani 5,9, Mahdieh Delikhoon10,11

Source: Aerosol and Air Quality research, Volume: 18 | Issue: 11 | Pages: 2826-2839
DOI: 10.4209/aaqr.2017.11.0466

Bioaerosols produced from Wastewater Treatment Plants (WWTPs) can pose health risks to plant workers and nearby inhabitants. There is a gap in air quality data for WWTPs in developing countries. The present study aimed to measure airborne bacterial and fungal concentrations in a WWTP in southwestern Iran between September 2015 and May 2016. Active sampling was conducted around operational units, and a total of 600 bacterial and fungal samples were collected. Spatial and seasonal comparisons were made. The highest average concentrations of culturable bacterial aerosol at seasonally dependent locations were, in decreasing order, 2581 ± 401 and 1952 ± 390 CFU m–3 for the selector and aeration tanks, respectively, in autumn; 1363 ± 299 CFU m–3 for the aeration tank in winter; and 1738 ± 350 CFU m–3 for the screw pump in spring. Furthermore, the predominant genera of airborne fungi isolated from the air of the WWTP in all three seasons were Cephalotrichum spp., Alternaria spp., Penicillium spp., Monilia spp., and Aspergillus spp. The results of this work emphasize the necessity of controlling WWTP workers' exposure to bioaerosols when bacteria and fungi become aerosolized during aeration.

Keywords: Air contamination; Bioaerosols; Wastewater treatment plant; Health risk Iran.

Characteristics and Source Apportionment of Volatile Organic Compounds for Different Functional Zones in a Coastal City of Southeast China

Baoye Hu1,2,3, Hui Xu4, Junjun Deng1,2, Zhigang Yi5, Jinsheng Chen 1,2, Lingling Xu1,2, Zhenyu Hong1,2,3, Xiaoqiu Chen6, Youwei Hong 1,2

Source: Aerosol and Air Quality research, Volume: 18 | Issue: 11 | Pages: 2840-2852
DOI: 10.4209/aaqr.2018.04.0122

Volatile organic compounds (VOCs) are the key precursors of tropospheric ozone and contributors to the formation of secondary organic aerosols (SOAs). VOCs from six functional zones in a coastal city in China were collected via SUMMA canister and determined via gas chromatography-mass spectrometry (GC-MS). The average annual concentrations of the total VOCs (TVOCs) were as follows: background site (36.00 μg m−3) < residential site (48.71 μg m−3) < port site (61.09 μg m−3) ≈ development site (62.25 μg m−3) < traffic site (73.82 μg m−3) < industrial site (98.33 μg m−3). The concentrations of TVOCs in spring and summer were higher than in autumn and winter. The ozone formation potentials (OFPs) were calculated, and the results indicated that 1-butene exhibited the highest OFP in the residential zone, while toluene exhibited the highest value in the other functional zones. The ratio of xylene to ethylbenzene was used to analyze the aging of atmospheric VOCs at the background site, which was affected by air pollution transported from urban areas. The sources of VOCs, namely, vehicle exhaust, fuel evaporation, biomass burning, industrial processes, and coal combustion, were identified with the Positive Matrix Factorization (PMF) model. Vehicle exhaust represented the largest source of atmospheric VOCs for every season, ranging 22.41–38.95%; additionally, the percentage of fuel evaporation increased in summer, reaching as high as 25.94%. The contributions of biomass burning were larger in autumn (21.11%) and winter (18.01%) than in spring (11.23%) and summer (16.94%), probably reflecting crop straw burning in the later seasons. Vehicle exhaust was the dominant source of VOCs (30.04–44.39%) in all functional zones, except for the residential site, which received its largest contribution (36.20%) from fuel evaporation.

Keywords: Volatile organic compounds; Source apportionment; Ozone formation potential; Positive matrix factorization; Coastal city.

A New Gas Chromatography Method for Continuous Monitoring of Non-Methane Hydrocarbons as an Analogy of Volatile Organic Compounds in Flue Gas

Chieh-Heng Wang1, Hsi-Che Hua2, Wei-Chuan Lin2, Hsin-Cheng Hsieh2, Jia-Lin Wang 2

Source: Aerosol and Air Quality research, Volume: 18 | Issue: 12 | Pages: 2913-2921
DOI: 10.4209/aaqr.2018.05.0193

A new on-line method of monitoring the total non-hydrocarbons (TNMHC) from the flue or waste gas of stationary sources, which significantly improves upon the current method commonly used in both Taiwan and China, is described. The major problem with the current method is that higher-boiling-point compounds in the waste gas saturate porous materials within the molecular-sieve column used to immobilize TNMHC and elute methane, which sabotages the fixability of TNMHC and leads to false methane and TNMHC readings during continuous monitoring. Our new method effectively circumvents this issue by incorporating a dual-column and back-flush design, rendering it a true gas chromatography (GC) method. Applying this GC method, light hydrocarbons, such as methane, ethane, and propane, can be fully separated by the dual column set. After methane enters the analytical column, a reverse carrier flow immediately back-flushes the pre-column while keeping the analytical column flowing forward by a second flow of the carrier gas for eluting methane. The field application, particularly upon repeated analyses of flue gas laden with complex and elevated levels of volatile organic compounds (VOCs), has shown that self-cleaning by back-flush is necessary when operating at a constant oven temperature.

Keywords: Volatile organic compounds (VOCs) Flue gas Continuous emission monitoring system (CEMS)

A Study on Electrical Charge Distribution of Aerosol Using Gerdien Ion Counter

Yun-Haeng Joe1, Joonmok Shim1, Il-Kyoung Shin1,2, Se-Jin Yook2, Hyun-Seol Park 1

Source: Aerosol and Air Quality research, Volume: 18 | Issue: 12 | Pages: 2922-2928
DOI: 10.4209/aaqr.2018.08.0309

The motion of charged particles strongly depends on its charge characteristics; as a result, information on charge distributions of target particles is an important variable in aerosol research. In this study, the charge distribution of atomized NaCl particles was measured using a Gerdien-type ion counter. Two particle charging conditions were used in this study. First, atomized NaCl particles were passed through an aerosol, resulting in a Boltzmann charge distribution. The charge distribution was experimentally determined, and the percentage of uncharged particles was compared to the percentage obtained from the theoretical Boltzmann charge distribution equation to verify the experimental method. The same experiment was conducted without the aerosol neutralizer to measure the charge distribution of the atomized and un-neutralized NaCl particles. The percentage of uncharged, negatively charged, and positively charged particles was 19%, 62%, and 20%, respectively, for the neutralized particles. For the atomized particles, which were generated without the aerosol neutralizer, a nearly zero charge state was observed, but the standard deviation in the charge distribution was larger than that of the neutralized particles. The experimental method proposed in this study is expected to be applicable to various aerosol research fields because it can be used to obtain simple information regarding the particle charge characteristics more easily and quickly than conventional methods.

Keywords: Aerosol particle; Charge distribution; Current measurement; Gerdien ion counter.

Experimental and Modeling Studies of SO3 Homogeneous Formation in the Post-Flame Region

Haiping Xiao1, Cong Qi 1, Qiyong Cheng1, Chaozong Dou1, Xiang Ning1,2, Yu Ru1

Source: Aerosol and Air Quality research, Volume: 18 | Issue: 12 | Pages: 2939-2947
DOI: 10.4209/aaqr.2018.01.0026

SO3 exists in the atmosphere in the form of sulfuric acid aerosol, heavily polluting the environment and decreasing the safety of boiler equipment. This study focuses on the homogeneous formation mechanism of SO3 in the post-flame region. We conducted experiments and simulations to investigate the influence of various combustion parameters on SO3 generation. The formation of SO3 was affected by factors such as temperature and the concentrations of O2, SO2, NO, and H2O. With a rise in temperature, the SO3 concentration initially increased but then decreased, reaching its maximum at about 1000°C, which indicates that SO2 can promote the formation of SO3 over a certain temperature range. An increase in the O2 concentration promoted the formation of O and OH radicals, which enhanced the generation of SO3 from SO2. The presence of NO resulted

in direct and indirect interactions between NOx and SOx species for different reaction sets, potentially enhancing SO3 generation. With an increase in the H2O concentration, SO3 formation initially increased rapidly before plateauing. ROP (rate of production) and sensitivity analyses suggest that adding H2O will produce O and OH, which strongly influence SO3 formation. Furthermore, the sensitivity analysis indicated that radicals and the direct reaction between SO2 and NO2 play significant roles in SO3 formation.

Keywords: Sulfuric acid aerosol; Chemical kinetics; Mechanism analysis ROP analysis; Sensitivity analysis.

High Resistance to Na Poisoning of the V2O5-Ce(SO4)2/TiO2 Catalyst for the NO SCR Reaction

Yanrong Chen1,2, Mingxuan Wang1,2, Xuesen Du 1,2, Jingyu Ran1,2, Li Zhang1,2, Dingling Tang3

Source: Aerosol and Air Quality research, Volume: 18 | Issue: 12 | Pages: 2948-2955
DOI: 10.4209/aaqr.2017.11.0521

Poisoning by Na is one of the major issues for the commercial SCR catalyst. In this study, Ce(SO4)2 was added to the catalyst system of V2O5/TiO2 to enhance its resistance to Na poisoning. The results show that the addition of Ce(SO4)2 increases the NOx conversion of the V2O5/TiO2 catalyst at medium temperatures of 330°C–450°C. After being doped with sodium with a molar ratio of Na/V = 1/1, the V2O5-Ce(SO4)2/TiO2 catalyst still shows excellent DeNOx efficiency, about 40% higher than the commercial V2O5-WO3/TiO2 catalyst. The fresh and Na-poisoned catalysts were characterized using XRD, SEM, NH3-TPD and H2-TPR. The results show that the Ce(SO4)2 addition remarkably strengthens the surface acidity and redox ability of the V2O5/TiO2 catalyst. Furthermore, the TPD results show that the V2O5-Ce(SO4)2/TiO2 catalyst can maintain its surface acidity after being doped with Na, while the acidity of the V2O5-WO3/TiO2 catalyst dramatically decreases. The redox ability of the catalyst can also be retained more effectively when Ce(SO4)2 is added to the catalyst system.

Keywords: Selective catalytic reduction Ce(SO4)2; Redox properties; Acidity; Alkali poisoning resistance.

Concentration and Influence Factors of Organochlorine Pesticides in Atmospheric Particles in a Coastal Island in Fujian, Southeast China

Liping Jiao 1,2, Qibin Lao2,3,4, Liqi Chen 2, Fajin Chen4, Xia Sun2, Meixun Zhao1

Source: Aerosol and Air Quality research, Volume: 18 | Issue: 12 | Pages: 2982-2996
DOI: 10.4209/aaqr.2018.04.0126

Atmospheric particulate samples collected from Pingtan Island in Fujian province were analyzed for 20 organochlorine pesticides (OCPs) with the aims of elucidating the contamination levels and their influence factors, and providing more comprehensive and fundamental data for the risk assessment of OCPs in this coastal area. The concentration of total OCPs ranged from ND (not detected) to 27.25 pg m−3 (an average of 4.30 ± 4.07 pg m−3) and ND to 13.16 pg m−3 (an average of 3.11 ± 2.54 pg m−3) in 2006 and 2007 respectively, and the level are obviously lower than urban, industrial, suburban, and the similar research areas in the coastal areas of Europe. HCH (Hexachlorocyclohexane) and DDT (Dichlorodiphenyltrichloroethane) were the predominant contaminants, followed by Methoxychlor and Endrin, while the levels of Chlordane, Endosulfan, Aldrin and Dieldrin was relatively lower. Obvious seasonal variations in OCP levels correlate significantly with total particulate levels; higher concentrations of most OCP compounds appeared in winter, whereas lower concentrations appeared in summer. The distribution pattern of the level of most OCP compounds might be directly or indirectly influenced by meteorological conditions, and TOC (total organic carbon) is an important factor influencing the persistence of these OCPs in atmospheric particulates. The source of atmospheric particulates was traced by stable carbon isotopes, which indicate that the increased levels of OCPs in winter and spring influenced by the source of polluted air mass during the "heating season" of Northern China. The cancer risk probability was evaluated based on the residual levels of OCPs, and the results show that dermal contact was the primary pathway affecting human health, and the effect of OCP residuals in atmospheric particulates of the coastal area could not be neglected.

Keywords: Organochlorine pesticides; Fujian coastal area; Carbon stable isotope; Atmospheric particulates; Meteorological conditions.

Size Distributions of Water-soluble Inorganic Ions in Atmospheric Aerosols during the Meiyu Period on the North Shore of Taihu Lake, China

Duanyang Liu 1,2, Yan Su3, Huaqing Peng3, Wenlian Yan1,2, Yi Li4, Xuejun Liu5, Bin Zhu6, Honglei Wang6, Xiliang Zhang7

Source: Aerosol and Air Quality research, Volume: 18 | Issue: 12 | Pages: 2997-3008
DOI: 10.4209/aaqr.2018.04.0123

In order to research the impact on air pollution from Meiyu (a special period of seasonal heavy rainfall between late May and June in the middle-lower Yangtze area in China (Qian et al., 2009)), the pollutant gas concentrations, size distributions, and water-soluble inorganic ions of aerosols were measured on the north shore of Taihu Lake from June 10 to June 26, 2014. Results show that the PM1.1 (aerodynamic diameter ≤ 1.1 μm) grew in particle size, becoming PM1.1-2.1 (1.1 μm ≤ aerodynamic diameter ≤ 2.1 μm) and then CPM (coarse particle matter; aerodynamic diameter > 2.1 μg) due to coagulation growth and chemical reactions, prior to Meiyu. The ions, anions, and cations all exhibited bimodal distributions before Meiyu, with peak positions of 0.43–1.1 and 9–10 μm, and trimodal distributions during Meiyu, with unfixed peak positions. The spectral size distributions of the SO42–, NO3–, and NH4+ were all bimodal or trimodal before Meiyu, and SNA (SO42–, NO3–, and NH4+) was the main component of the PM1.1 and PM1.1-2.1. Vehicle emissions were more important and the secondary formation of SO42– from SO2 occurred more readily during Meiyu than before Meiyu. The nitrogen oxidation ratio (NOR) was lower than the sulfur oxidation ratio (SOR), and the secondary formation of NO3– from NOx infrequently occurred in Wuxi compared to that of SO42– from SO2. The samples collected during the pre-Meiyu season and Meiyu all fell below the line 1:1 (CE:AE) (cation equivalence:anion equivalence), suggesting that the volatilization of ammonium and nitrate as well as unmeasured hydrogen ions may have caused the loss of cations, which resulted in insufficient cations for neutralizing the anions and subsequently, acidic properties for the aerosol. [NH4+ + Ca2+] are evidently sufficient for neutralizing [SO42– + NO3– + NO2– + Cl–].

Keywords: Fine particles; Size distribution; Water-soluble inorganic ions; Meiyu; Taihu; Lake.

Characterization of PM1-Bound Metallic Elements in the Ambient Air at a High Mountain Site in Northern China

Jun-Jie Yue1, Roberta Palmiero1,2, Yang-Yang Han3, Yan Wang4, Qian-Qian Li5, Tuo-Yu Zhang3, Meiqing Sun6, Hong Wang6, Guangping Yu6, Xian-Liang Yi7, Peng-Hui Li 1, Ya-Qin Ji 8, Li-Qiong Guo9

Source: Aerosol and Air Quality research, Volume: 18 | Issue: 12 | Pages: 2967-2981
DOI: 10.4209/aaqr.2018.04.0129

The PM-bound metallic elements in 43 daily PM1 samples collected at Mount Tai during a summer campaign were analyzed by ICP-MS. The PM1 concentrations ranged between 11.02 and 83.71 μg m–3, with an average of 38.98 μg m–3, and were influenced by meteorological events, exhibiting an increasing trend in the early stage of rain, followed by a significant decrease denoting efficient scavenging. Higher elemental concentrations were detected at Mount Tai than at other overseas background sites. According to the enrichment factor (EF) and geo-accumulation index (Igeo) calculations, among the 16 considered elements, Mn, Al, Co, Sr, Mo, Fe, Ca, V, Ti and Ni in the PM1 were mainly of crustal origin, while Cu, Cr, As, Zn, Pb and Cd were primarily due to anthropogenic causes. Source identification via Pearson correlation analysis and principle component analysis showed that coal mining and coal burning activities, metal processing industries and vehicle emissions were common sources of heavy metals on Mount Tai; these results were consistent with the air mass analysis. The estimated hazard indexes for all population groups (the elderly, males, females and children) were smaller than 1, suggesting that non-carcinogenic effects due to heavy metal inhalation were unlikely to occur. However, in the present study, the incremental lifetime cancer risk values were about 10 times higher than the reference value of 1 × 10–6, indicating a potential health risk to the general population.

Keywords: Submicron particles; Metal elements; Air transport; Source analysis Risk assessment.

PMF-GAS Methods to Estimate Contributions of Sources and Oxygen for PM2.5, Based on Highly Time-Resolved PM2.5 Species and Gas Data

Yingze Tian 1, Qianqian Xue1, Zhimei Xiao2, Kui Chen2, Yinchang Feng 1

Source: Aerosol and Air Quality research, Volume: 18 | Issue: 12 | Pages: 2956-2966
DOI: 10.4209/aaqr.2018.07.0244

To gain detailed insight into the gaseous sources of PM2.5, three kinds of positive matrix factorization were developed and applied to hourly elemental and gaseous data (PMF-

GAS). According to the results of PMF-GAS1, which relied on gaseous markers to enhance source discrimination, crustal dust, vehicular exhaust, coal combustion, sulfate and nitrate (CD1, VE1, CC1, SUL1 and NIT1) directly contributed 20%, 17%, 15%, 34% and 14% to the PM2.5, respectively. Using PMF-GAS2, which summed species found in PM2.5, and their corresponding precursors to estimate the overall influence of primary sources, the total contribution from CD2, VE2 and CC2 to PM2.5 was quantified as 30%, 29% and 41%, respectively. Finally, PMF-GAS3 quantified the contribution of oxidation (OXI3; 27%) based on the relationships between the species and their precursors. NH4+ was found mostly in CD2 and CD3 but also in SUL1 and NIT1, implying that crustal dust can provide alkaline conditions for the formation of ammonium salts. High correlations were found between corresponding source contributions, but CD1 showed relatively weak links with CD2 and CD3 due to NH4+ being present in different factors. A fully populated map of classical bootstrap (BS) runs implies the high stability of these PMF-GAS results.

Keywords: PM2.5 Chemical compositions; Gaseous pollutants; Source apportionment; PMF-GAS.

Accumulation and Coarse Modes Particle Concentrations during Dew Formation and Precipitation

Tareq Hussein 1,2, Larisa Sogacheva3, Tuukka Petäjä2

Source: Aerosol and Air Quality research, Volume: 18 | Issue: 12 | Pages: 2929-2938
DOI: 10.4209/aaqr.2017.10.0362

This study investigates the number concentrations of accumulation mode (0.3–1 μm) and coarse mode (1–10 μm) particles in the eastern Mediterranean urban environment with and without precipitation and dew formation. The results show that the number concentrations of both the accumulation mode and coarse mode particles decreased (with ratios of ∼0.7 and ∼0.36, respectively) during precipitation. In our analysis, we assumed that dew formation occurred in Amman during nighttime when the relative humidity (RH) was higher than 80% and the difference between the temperature and dew point temperature (i.e., T–DP) was less than 2.5°C. In general, the accumulation mode particle number concentration increased with relative humidity and doubled, on average, during dew formation. On the other hand, the coarse mode particle number concentration was 30% lower during conditions with dew formation than without. The increased number concentration of the accumulation mode particles during dew formation conditions is most likely due to enhanced water vapor condensation on existing ultrafine aerosols (diameter < 0.1 μm), enabling particles to grow to detectable sizes, including the accumulation mode.

The decreased number concentration of the coarse mode particles during dew formation conditions may be due to enhanced wet deposition.

Keywords: Wet deposition; Rain; Dew; Scavenging; Semi-arid.

Contribution of Regional Transport to Surface Ozone at an Island Site of Eastern China

Lei Tong1,2, Jingjing Zhang1,2,3, Honghui Xu4, Hang Xiao 1,2, Mengmeng He1,2, Huiling Zhang5

Source: Aerosol and Air Quality research, Volume: 18 | Issue: 12 | Pages: 3009-3024
DOI: 10.4209/aaqr.2017.11.0508

The surface ozone (O3) in non-urban areas can be strongly influenced by transported regional air pollutants from distant urban agglomerations. Comprehensively using the polar plot graphical technique, and backward trajectory and potential source contribution analyses, the variations of surface O3 and its potential source regions at an island site of Zhejiang, China, were analyzed based on data from June 2013 to October 2016. Relatively high hourly O3 levels (max.: 154.0 ppb) were often observed, with the total number of hourly O3 exceeding the national standard (75 ppb) being 583, indicating high health risks from O3 exposure. An obvious time-lag for the diurnal O3 peak was observed, with the daily maxima often occurring at 16:00. A decreased O3 level was observed in summer, which was probably due to the comprehensive influence of intense rainfall, high relative humidity and clean marine airmasses during this season. The transport of external air pollutants played a dominant role in affecting local O3, with relatively high O3 concentrations (> 50 ppb) being observed under high wind speeds (> 5 m s–1). Based on all the source identification analyses, the major regions contributing to the surface O3 lay to the north and northwest of the study area. Long-range transported air pollutants from the coastal provinces of the North China Plain may have significantly enhanced surface O3 at the study site, while contributions from local areas and areas to the south of the study site were rather small. A high incidence (64.3%) of O3 pollution was accounted for by the inflowing airmasses from outside of Zhejiang, which quantitatively confirmed the significant background transport of O3 to this province. Coordinated inter-regional control on pollutant emissions should be carried out to reduce O3 in Zhejiang Province.

Keywords: Backward trajectories; Potential source contribution function (PSCF); Polarplot O3 inflow.

Surface Aerosol Optical Properties during High and Low Pollution Periods at an Urban Site in Central China

Boming Liu1, Wei Gong1,2, Yingying Ma 1,2, Ming Zhang1, Jian Yang3, Miao Zhang4,5

Source: Aerosol and Air Quality research, Volume: 18 | Issue: 12 | Pages: 3035-3046
DOI: 10.4209/aaqr.2017.12.0565

The aerosol scattering (σsp) and absorption (σap) coefficients and single scattering albedo (SSA) were continuously measured and analyzed at an urban site in Wuhan of central China from November 2014 to July 2017. The average σsp (532 nm), σap (532 nm), and SSA in Wuhan during the study period were 244 ± 212 Mm–1, 27 ± 17 Mm–1, and 0.86 ± 0.09, respectively. The aerosol optical properties had pronounced and distinctive diurnal cycles in the Wuhan area. The σsp and σap exhibited the highest values between 06:00 and 08:00 local time (LT) and the lowest values between 14:00 and 16:00 LT, which was mainly due to being coupled with increasing traffic emissions. PM2.5 was a major contributor to the large optical parameters. During pollution periods, the mean σsp (624 Mm–1) was roughly 3 times that during clean periods (214 Mm–1), and the σap (58 Mm–1) was about 2.5 times that during clean periods (24 Mm–1). The wind speed and direction also strongly affected the aerosol optical properties during the different periods. The high σsp and σap values for the pollution periods were accompanied by calm winds (0–2 m s–1), from 0° to 45°, whereas the low σsp and σap values of the clean periods were observed with high wind speeds (above 4 m s–1), from 0° to 90°. Moreover, the σap showed a clear positive correlation (R2 = 0.412) with the PM2.5 concentrations for the clean periods, whereas the σsp had a good positive correlation (R2 = 0.406) with the PM2.5 concentrations during the pollution periods.

Keywords: Aerosol scattering coefficients; Aerosol absorption coefficients; Single scattering albedo; Haze pollution PM2.5

Verification of an Approximate Thermodynamic Equation with Application to Study on Arctic Stratospheric Temperature Changes

Renqiang Liu, Yanyan Fu

Source: Journal of the Atmospheric Sciences, https://doi.org/10.1175/JAS-D-18-0109.1;
Published Online: 17 Dec, 2018.

Temperature changes in the Arctic lower stratosphere on both short- and long-term time scales are critical for changing the magnitude of ozone losses in the Arctic vortex. In this paper, an approximate month-to-month temperature change equation is constructed and extended to a new form for decade-to-decade changes. Then we provide a verification of these equations and show an example of an application for partitioning between the dynamical and radiative contributions to the Arctic lower-stratospheric temperature decadal changes, as well as the trends, using the European Centre for Medium-Range Weather Forecasts (ECMWF) interim reanalysis (ERA-Interim) data during the period of 1980–99. At 100 hPa, the month-to-month Arctic temperature increment is a small term compared to the dynamical heating and diabatic heating, which are largely canceling terms with maximum magnitudes in November–April and October–March, respectively. However, it is not the case for their decadal changes and the decadal change of the Arctic current-month temperature compared to those of the regressed dynamical heating and radiative heating, where the current-month decadal changes and the corresponding trends are approached except in March and a rough agreement exists between these trends and those reported in other studies. The dynamical plus diabatic heating term and the temperature increment, as well as their decadal changes, are roughly balanced during the annual oscillation. However, some departures exist in both cases because of the large deviations or uncertainties of relevant terms and also probably due to the quasigeostrophic approximation and the eddy heat flux approximation of the dynamical heating, and a restricted condition of the eddy heat flux approximation is given at the end.

Keywords: Dynamics; Planetary waves; Stratospheric circulation; Regression analysis; Interdecadal variability; Trends

---

On the Time Evolution of Limited-Area Ensemble Variance: Case Studies with the Convection-Permitting Ensemble COSMO-E

Christina Klasa, Marco Arpagaus and André Walser, **Heini Wernli**

Source: Journal of the Atmospheric Sciences, https://doi.org/10.1175/JAS-D-18-0013.1
Published Online: 17 December 2018

Dynamical processes determining the time evolution of difference kinetic energy (DKE) in a limited-area domain are investigated with the convection-permitting ensemble model COSMO-E for a forecasting period of 4 days. DKE is quantified by means of ensemble variance of the irrotational and nondivergent horizontal wind. For three case studies characterized by contrasting predictability levels of precipitation, it is shown that DKE of

the irrotational wind strongly increases during periods of solar-forced moist convective activity and decreases when the latter ceases. The response of DKE of the nondivergent wind is also clearly related to the convective activity, but delayed by a few hours, pointing to interactions between both wind components. Apart from the impact of moist convection, DKE of the nondivergent wind is primarily governed by large-scale advection, imposed at the lateral domain boundaries of the limited-area ensemble. This forcing may also sustain or increase DKE of the irrotational wind when moist convection is absent. Consequently, the large-scale flow and diurnal solar forcing, associated with higher spatiotemporal predictability, determines the overall evolution of the limited-area ensemble variance of the horizontal wind, which increases in the presence of moist convective activity or strong synoptic-scale forcing, and stagnates or decreases otherwise, rendering forecasts of convection-permitting ensembles valuable beyond the very short forecast range.

Keywords : Ensembles; Mesoscale forecasting; Short-range prediction; Nonhydrostatic models; Numerical weather prediction/forecasting; Regional models

---

Why Does Deep Convection Have Different Sensitivities to Temperature Perturbations in the Lower versus Upper Troposphere?

Yang Tian, Zhiming Kuang,

Source: Journal of the Atmospheric Sciences, https://doi.org/10.1175/JAS-D-18-0023.1, Published Online: 17 December 2018.

Previous studies have documented that deep convection responds more strongly to above-the-cloud-base temperature perturbations in the lower troposphere than to those in the upper troposphere, a behavior that is important to the dynamics of large-scale moist flows, such as convectively coupled waves. A number of factors may contribute to this differing sensitivity, including differences in buoyancy, vertical velocity, and/or liquid water content in cloud updrafts in the lower versus upper troposphere. Quantifying the contributions from these factors can help to guide the development of convective parameterization schemes. We tackle this issue by tracking Lagrangian particles embedded in cloud-resolving simulations within a linear response framework. The results show that both the differences in updraft buoyancy and vertical velocity play a significant role, with the vertical velocity being the more important, and the effect of liquid water content is only secondary compared to the other two factors. These results indicate that cloud updraft vertical velocities need to be correctly modeled in convective parameterization schemes in order to properly account for the differing convective sensitivities to temperature perturbations at different heights of the free troposphere.

Keywords: Clouds; Convection; Entrainment; Mass fluxes/transport; Vertical motion; Waves; atmospheric.

The Potential Role of Atmospheric Bores and Gravity Waves in the Initiation and Maintenance of Nocturnal Convection over the Southern Great Plains

David B. Parsons, Kevin R. Haghi, Kelton T. Halbert,Blake Elmer, Junhong Wang

Source: Journal of the Atmospheric Sciences, https://doi.org/10.1175/JAS-D-17-0172.1
Published Online**:** 18 December 2018.

This investigation explores the relationship among bores, gravity waves, and convection within the nocturnal environment through the utilization of measurements taken during the International H_2O Project (IHOP_2002) over the Southern Great Plains. The most favorable conditions for deep convection were found to occur within the boundary layer during the late afternoon and early evening hours in association with the diurnal cycle of solar insolation. At night, the layers most favorable for deep convection occur at and above the height of the nocturnal southerly low-level jet in association with distinct maxima in both the southerly and westerly components of the wind. Observations taken during the passage of 13 nocturnal wave disturbances over a comprehensive profiling site show the average maximum and net upward displacements with these waves were estimated to be ~900 and ~660 m, respectively. The lifting was not limited to the stable boundary layer, but reached into the conditionally unstable layers aloft. Since the net upward displacements persisted for many hours as the disturbances propagated away from the convection, areas well in excess of 10 000 km^2 are likely impacted by this ascent. This lifting can directly maintain existing convection and aid in the initiation of new convection by reducing the convective inhibition in the vicinity of the active convection. In agreement with past studies, strong ascent in the lowest ~1.5 km was generally consistent with the passage of a bore. However, separate wave responses also occurred well above the bores, and low-frequency gravity waves may explain such disturbances.

Keywords:
North America; Convection; Gravity waves; Mesoscale processes; Density currents; Diurnal effects

---

On the Momentum Budget of the Quasi-Biennial Oscillation in the Whole Atmosphere Community Climate Model

Rolando R. Garcia, Jadwiga H. Richter

Source: Journal of the Atmospheric Sciences, https://doi.org/10.1175/JAS-D-18-0088.1
Published online: 18 December 2018.

This study documents the contribution of equatorial waves and mesoscale gravity waves to the momentum budget of the quasi-biennial oscillation (QBO) in a 110-level version of the Whole Atmosphere Community Climate Model. The model has high vertical resolution, 500 m, above the boundary layer and through the lower and middle stratosphere, decreasing gradually to about 1.5 km near the stratopause. Parameterized mesoscale gravity waves and resolved equatorial waves contribute comparable easterly and westerly accelerations near the equator. Westerly acceleration by resolved waves is due mainly to Kelvin waves of zonal wavenumber in the range k = 1–15 and is broadly distributed about the equator. Easterly acceleration near the equator is due mainly to Rossby–gravity (RG) waves with zonal wavenumbers in the range k = 4–12. These RG waves appear to be generated in situ during both the easterly and westerly phases of the QBO, wherever the meridional curvature of the equatorial westerly jet is large enough to produce reversals of the zonal-mean barotropic vorticity gradient, suggesting that they are excited by the instability of the jet. The RG waves produce a characteristic pattern of Eliassen–Palm flux divergence that includes strong easterly acceleration close to the equator and westerly acceleration farther from the equator, suggesting that the role of the RG waves is to redistribute zonal-mean vorticity such as to neutralize the instability of the westerly jet. Insofar as unstable RG waves might be present in the real atmosphere, mixing due to these waves could have important implications for transport in the tropical stratosphere.

Keywords: Quasibiennial oscillation; Quasibiennial oscillation; General circulation models

---

On the Choice of Momentum Control Variables and Covariance Modeling for Mesoscale Data Assimilation

Qin Xu

Source: Journal of the Atmospheric Sciences, https://doi.org/10.1175/JAS-D-18-0093.1,
Published Online: 26 December 2018.

For mesoscale variational data assimilation with high-resolution observations, there has been an issue concerning the choice of momentum control variables and related covariance modeling. This paper addresses the theoretical aspect of this issue. First, relationships between background error covariance functions for differently chosen momentum control variables are derived, and different choices of momentum control variables are proven to be theoretically equivalent in the sense that they lead to the same optimally analyzed incremental wind field in the limit of infinitely high spatial resolution provided their error covariance functions satisfy the derived relationships. It is then shown that when the velocity potential χ and streamfunction ψ are used as momentum control variables with their background error autocovariance functions modeled by single-Gaussian functions, the derived velocity autocovariance functions contain significant negative sidelobes. These negative sidelobes can represent background wind error structures associated with baroclinic waves on the synoptic scale but become unrepresentative on the mesoscale. To reduce or remove these negative sidelobes for mesoscale variational data assimilation, Gaussian functions are used with two types of modifications to model the velocity covariance functions in consistency with the assumed homogeneity and isotropy in variational data assimilation. In this case, the random (χ, ψ) background error fields have no classically valid homogeneous and isotropic covariance functions, but generalized (χ, ψ) covariance functions can be derived from the modified velocity covariance functions for choosing (χ, ψ) as momentum control variables. Mathematical properties of generalized covariance functions are explored with physical interpretations. Their important implications are discussed for mesoscale data assimilation.

Keywords: Atmosphere; Variational analysis; Data assimilation

---

Inhomogeneous Mixing in Lagrangian Cloud Models: Effects on the Production of Precipitation Embryos

Fabian Hoffmann; Takanobu Yamaguchi; Graham Feingold

Source: Journal of the Atmospheric Sciences, https://doi.org/10.1175/JAS-D-18-0087.1, Published Online: 26 December 2018.

Although small-scale turbulent mixing at cloud edge has substantial effects on the microphysics of clouds, most models do not represent these processes explicitly, or parameterize them rather crudely. This study presents a first use of the linear eddy model (LEM) to represent unresolved turbulent mixing at the subgrid scale (SGS) of large-eddy simulations (LESs) with a coupled Lagrangian cloud model (LCM). The method utilizes Lagrangian particles to provide the trajectory of air masses within LES grid boxes, while

the LEM is used to redistribute these air masses among the Lagrangian particles based on the local features of turbulence, allowing for the appropriate representation of inhomogeneous to homogeneous SGS mixing. The new approach has the salutary effect of mitigating spurious supersaturations. At low turbulence intensities, as found in the early stages of an idealized bubble cloud simulation, cloud-edge SGS mixing tends to be inhomogeneous and the new approach is shown to be essential for the production of raindrop embryos. At higher turbulence intensities, as found in a field of shallow cumulus, SGS mixing tends to be more homogeneous and the new approach does not significantly alter the results, indicating that a grid spacing of 20 m may be sufficient to resolve all relevant scales of inhomogeneous mixing. In both cases, droplet in-cloud residence times are important for the production of precipitation embryos in the absence of small-scale inhomogeneous mixing, either naturally due to strong turbulence or artificially as a result of coarse resolution or by not using the LEM as an SGS model.

Keywords: Mixing; Turbulence; Cumulus clouds; Cloud microphysics; Large eddy simulations; Subgrid-scale processes

---

Impacts of Radiation and Upper-Tropospheric Temperatures on Tropical Cyclone Structure and Intensity

Benjamin C. Trabing

Source: Journal of the Atmospheric Sciences, https://doi.org/10.1175/JAS-D-18-0165.1, published Online: 28 December 2018.

Potential intensity theory predicts that the upper-tropospheric temperature acts as an important constraint on tropical cyclone (TC) intensity. The physical mechanisms through which the upper troposphere impacts TC intensity and structure have not been fully explored, however, due in part to limited observations and the complex interactions between clouds, radiation, and TC dynamics. In this study, idealized Weather Research and Forecasting Model ensembles initialized with a combination of three different tropopause temperatures and with no radiation, longwave radiation only, and full diurnal radiation are used to examine the physical mechanisms in the TC–upper-tropospheric temperature relationship on weather time scales. Simulated TC intensity and structure are strongly sensitive to colder tropopause temperatures using only longwave radiation, but are less sensitive using full radiation and no radiation. Colder tropopause temperatures result in deeper convection and increased ice mass aloft in all cases, but are more intense only when radiation was included. Deeper convection leads to increased local longwave cooling rates but reduced top-of-the-atmosphere outgoing longwave radiation, such that the total

radiative heat sink is reduced from a Carnot engine perspective in stronger storms. We hypothesize that a balanced response in the secondary circulation described by the Eliassen equation arises from upper-troposphere radiative cooling anomalies that lead to stronger tangential winds. The results of this study further suggest that radiation and cloud–radiative feedbacks have important impacts on weather time scales.

Keywords: Tropical cyclones; Upper troposphere; Longwave radiation; Shortwave radiation; Numerical analysis/modeling; Mesoscale models

---

Effect of Upper- and Lower-Level Baroclinicity on the Persistence of the Leading Mode of Midlatitude Jet Variability

Loïc Robert and Gwendal Rivière, Francis Codron

Source: Journal of the Atmospheric Sciences, https://doi.org/10.1175/JAS-D-18-0010.1, published Online: 31 December 2018

The sensitivity of the variability of an eddy-driven jet to the upper- and lower-level baroclinicity of the mean state is analyzed using a three-level quasigeostrophic model on the sphere. The model is forced by a relaxation in temperature to a steady, zonally symmetric profile with varying latitude and intensity of the maximum baroclinicity. The leading EOF of the zonally and vertically averaged zonal wind is characterized by a meridional shift of the eddy-driven jet. While changes in the upper-level baroclinicity have no significant impact on the persistence of this leading EOF, an increase in lower-level baroclinicity leads to a reduced persistence. For small lower-level baroclinicity, the leading EOF follows a classical zonal index regime, for which the meridional excursions of the zonal wind anomalies are maintained by a strong positive eddy feedback. For strong lower-level baroclinicity, the jet enters a poleward-propagation regime, for which the eddy forcing continuously acts to push the jet poleward and prevents its maintenance at a fixed latitude. The enhanced poleward propagation when the lower-level baroclinicity increases is interpreted as resulting from the broader and weaker potential vorticity gradient that enables the waves to propagate equatorward and facilitates the poleward migration of the critical latitude. Finally, the decrease in the persistence of the leading EOF as the lower-level baroclinicity increases is shown not to result from the impact of changes in the mean climatological jet latitude.

Keywords: Atmosphere; Annular mode; Feedback; Jets; Storm tracks.

Upscale Impact of Mesoscale Disturbances of Tropical Convection on 2-Day Waves

Qiu Yang, Andrew J. Majda

Source: Journal of the Atmospheric Sciences, https://doi.org/10.1175/JAS-D-18-0049.1
Published Online: 2 January 2019.

Westward-propagating 2-day waves with embedded mesoscale disturbances contribute a large portion of synoptic variability of tropical convection over the western Pacific. It is of crucial importance to assess the upscale impact on 2-day waves of these mesoscale disturbances that propagate at various tilt angles. Also, it will be informative to consider the upscale impact on both symmetric and asymmetric 2-day waves in terms of convection, morphology of circulation, and tropical cyclogenesis. A simple multiscale asymptotic model is used to simulate the two-scale structure of 2-day waves. The synoptic-scale circulation response is driven by westward-propagating mean heating and eddy transfer of momentum and temperature. The latter is interpreted as the upscale impact of mesoscale fluctuations. The upscale impact of mesoscale disturbances that propagate at a tilt angle between 315° and 45° induces low-level negative potential temperature anomalies and westerly inflow. Shallow congestus convection triggered in a moist environment at the leading edge of the 2-day waves supports the westward propagation. For asymmetric 2-day waves in the Northern Hemisphere, the upscale impact of mesoscale disturbances propagating at a tilt angle between 315° and 0° induces lower-tropospheric cyclonic flows and negative pressure perturbation. This provides a new mechanism to precondition tropical cyclogenesis. A comparison of the upscale impact on symmetric westward-propagating 2-day waves and eastward-propagating convectively coupled Kelvin waves shows that their tilt angle ranges with favorable conditions for convection and enhanced inflow are simply opposite.

Keywords: Convection; Gravity waves; Mesoscale systems; Synoptic-scale processes; Tropical cyclones; Tropical variability.

Inferences from Simple Models of Slow, Convectively Coupled Processes

Kerry Emanuel

Source: Journal of the Atmospheric Sciences, https://doi.org/10.1175/JAS-D-18-0090.1,
published Online: 2 January 2019.

A framework for conceptual understanding of slow, convectively coupled disturbances is developed and applied to several canonical tropical problems, including the water vapor content of an atmosphere in radiative–convective equilibrium, the relationship between convective precipitation and column water vapor, Walker-like circulations, self-aggregation

of convection, and the Madden–Julian oscillation. The framework is a synthesis of previous work that developed four key approximations: boundary layer energy quasi equilibrium, conservation of free-tropospheric moist and dry static energies, and the weak temperature gradient approximation. It is demonstrated that essential features of slow, convectively coupled processes can be understood without reference to complex turbulent and microphysical processes, even though accounting for such complexity is essential to quantitatively accurate modeling. In particular, we demonstrate that the robust relationship between column water vapor and precipitation observed over tropical oceans does not necessarily imply direct sensitivity of convection to free-tropospheric moisture. We also show that to destabilize the radiative–convective equilibrium state, feedbacks between radiation and clouds and water vapor must be sufficiently strong relative to the gross moist stability.

Keywords: Convection; Deep convection; Hadley circulation; Madden-Julian oscillation; Walker circulation.

Tropopause Evolution in a Rapidly Intensifying Tropical Cyclone: A Static Stability Budget Analysis in an Idealized Axisymmetric Framework

Patrick Duran[a], John Molinari

Source: Journal of the Atmospheric Sciences, https://doi.org/10.1175/JAS-D-18-0097.1, published Online: 2 January 2019.

Upper-level static stability (N^2) variations can influence the evolution of the transverse circulation and potential vorticity in intensifying tropical cyclones (TCs). This paper examines these variations during the rapid intensification (RI) of a simulated TC. Over the eye, N^2 near the tropopause decreases and the cold-point tropopause rises by up to 4 km at the storm center. Outside of the eye, N^2 increases considerably just above the cold-point tropopause and the tropopause remains near its initial level. A budget analysis reveals that the advection terms, which include differential advection of potential temperature θ and direct advection of N^2, are important throughout the upper troposphere and lower stratosphere. These terms are particularly pronounced within the eye, where they destabilize the layer near and above the cold-point tropopause. Outside of the eye, a radial–vertical circulation develops during RI, with strong outflow below the tropopause and weak inflow above. Differential advection of θnear the outflow jet provides forcing for stabilization below the outflow maximum and destabilization above. Turbulence induced by vertical wind shear on the flanks of the outflow maximum also modifies the vertical stability profile. Meanwhile, radiative cooling tendencies at the top of the cirrus canopy generally act to destabilize the upper troposphere and stabilize the lower stratosphere. The results suggest that turbulence and radiation, alongside differential advection, play fundamental roles in the upper-level N^2 evolution of TCs. These N^2 tendencies could have

implications for both the TC diurnal cycle and the tropopause-layer potential vorticity evolution in TCs.

Keywords: Hurricanes; Turbulence; Tropical cyclones; Tropopause; Budgets; Cloud radiative effects [a] Current affiliation: Earth System Science Center, University of Alabama in Huntsville, Huntsville, Alabama.

Vertical Profiles of Aerosol Composition over Beijing, China: Analysis of In Situ Aircraft Measurements

Quan Liu, Jiannong Quan, Xingcan Jia, Zhaobin Sun, Xia Li, Yang Gao, Yangang Liu

Source: Journal of the Atmospheric Sciences, https://doi.org/10.1175/JAS-D-18-0157.1, published Online: 2 January 2019.

Aerosol samples were collected over Beijing, China, during several flights in November 2011. Aerosol composition of nonrefractory submicron particles (NR-PM_1) was measured by an Aerodyne compact time-of-flight aerosol mass spectrometer (C-ToF-AMS). This measurement on the aircraft provided vertical distribution of aerosol species over Beijing, including sulfate (SO_4), nitrate (NO_3), ammonium (NH_4), chloride (Chl), and organic aerosols [OA; hydrocarbon-like OA (HOA) and oxygenated OA (OOA)]. The observations showed that aerosol compositions varied drastically with altitude, especially near the top of the planetary boundary layer (PBL). On average, organics (34%) and nitrate (32%) were dominant components in the PBL, followed by ammonium (15%), sulfate (14%), and chloride (4%); in the free troposphere (FT), sulfate (34%) and organics (28%) were dominant components, followed by ammonium (20%), nitrate (19%), and chloride (1%). The dominant OA species was primarily HOA in the PBL but changed to OOA in the FT. For sulfate, nitrate, and ammonium, the sulfate mass fraction increased from the PBL to the FT, nitrate mass fraction decreased, and ammonium remained relatively constant. Analysis of

the sulfate-to-nitrate molar ratio further indicated that this ratio was usually less than one in the FT but larger than one in the PBL. Further analysis revealed that the vertical aerosol composition profiles were influenced by complex processes, including PBL structure, regional transportation, emission variation, and the aging process of aerosols and gaseous precursors during vertical diffusion.

Keywords: Aerosols/particulates; Air pollution; Atmospheric composition; Urban meteorology

---

An Evaluation of Size-Resolved Cloud Microphysics Scheme Numerics for Use with Radar Observations. Part I: Collision–Coalescence

Hyunho Lee, Ann M. Fridlind, Andrew S. Ackerman

Source: Journal of the Atmospheric Sciences, https://doi.org/10.1175/JAS-D-18-0174.1, published Online: 3 January 2019

This study evaluates some available schemes designed to solve the stochastic collection equation (SCE) for collision–coalescence of hydrometeors using a size-resolved (bin) microphysics approach and documents their numerical properties within the framework of a box model. Comparing three widely used SCE schemes, we find that all converge to almost identical solutions at sufficiently fine mass grids. However, one scheme converges far slower than the other two and shows pronounced numerical diffusion at the large-drop tail of the size distribution. One of the remaining two schemes is recommended on the basis that it is well converged on a relatively coarse mass grid, stable for large time steps, strictly mass conservative, and computationally efficient. To examine the effects of SCE scheme choice on simulating clouds and precipitation, two of the three schemes are compared in large-eddy simulations of a drizzling stratocumulus field. A forward simulator that produces Doppler spectra from the large-eddy simulation results is used to compare the model output directly with radar observations. The scheme with pronounced numerical diffusion predicts excessively large mean Doppler velocities and overly broad and negatively skewed spectra compared with observations, consistent with numerical diffusion demonstrated in the box model. Statistics obtained using the recommended scheme are closer to observations, but notable differences remain, indicating that factors other than SCE scheme accuracy are limiting simulation fidelity.

Keywords:
Clouds; Drizzle; Stratiform clouds; Cloud resolving models; Large eddy simulations; Model evaluation/performance

---

Extratropical Influence on 200-hPa Easterly Acceleration over the Western Indian Ocean Preceding Madden–Julian Oscillation Convective Onset

Jennifer Gahtan, Paul Roundy

Source: Journal of the Atmospheric Sciences, https://doi.org/10.1175/JAS-D-18-0069.1, published Online: 3 January 2019.

The onset of Madden–Julian oscillation (MJO) deep convection often occurs over the western Indian Ocean and has upper-tropospheric circulation precursors that consist of eastward-circumnavigating tropical easterlies and subtropical cyclonic Rossby gyres near eastern Africa. Moreover, the evolution of the large-scale circulation and its ability to reduce subsidence may be necessary for the initial development of organized deep convection. To better understand the evolution of the circulation precursors and their interaction with convective onset, this paper analyzes the upper-tropospheric zonal momentum budget using a regional index based on the temporal progression of the meridional structure of intraseasonal outgoing longwave radiation anomalies over eastern Africa and the western Indian Ocean. The circumnavigating intraseasonal easterly acceleration produces upper-level divergence when it reaches the western extent of a region of intraseasonal westerlies and may provide a forcing for the in-phase midtropospheric upward vertical motion. For about three-quarters of the identified cases, the easterly acceleration over the western Indian Ocean is a response to the zonal pressure gradient over the region. In the composite, the negative pressure gradient force may be initially induced by the injection of negative geopotential height anomalies from the extratropics of both hemispheres to the tropics over eastern Africa, though tropically circumnavigating and local signals may also contribute to the easterly acceleration, especially in the days following convective onset.

Keywords: Madden-Julian oscillation

An Improved Double-Gaussian Closure for the Subgrid Vertical Velocity Probability Distribution Function

A. C. Fitch

Source: Journal of the Atmospheric Sciences, https://doi.org/10.1175/JAS-D-18-0149.1 Published Online: 3 January 2019.

The vertical velocity probability distribution function (PDF) is analyzed throughout the depth of the lower atmosphere, including the subcloud and cloud layers, in four large-eddy simulation (LES) cases of shallow cumulus and stratocumulus. Double-Gaussian PDF closures are examined to test their ability to represent a wide range of turbulence statistics, from stratocumulus cloud layers characterized by Gaussian turbulence to shallow cumulus cloud layers displaying strongly non-Gaussian turbulence statistics. While the majority of the model closures are found to perform well in the former case, the latter presents a

considerable challenge. A new model closure is suggested that accounts for high skewness and kurtosis seen in shallow cumulus cloud layers. The well-established parabolic relationship between skewness and kurtosis is examined, with results in agreement with previous studies for the subcloud layer. In cumulus cloud layers, however, a modified relationship is necessary to improve performance. The new closure significantly improves the estimation of the vertical velocity PDF for shallow cumulus cloud layers, in addition to performing well for stratocumulus. In particular, the long updraft tail representing the bulk of cloudy points is much better represented and higher-order moments diagnosed from the PDF are also greatly improved. However, some deficiencies remain owing to fundamental limitations of representing highly non-Gaussian turbulence statistics with a double-Gaussian PDF.

Keywords: Turbulence; Boundary layer; Cloud parameterizations; Clouds; Large eddy simulations.

A General Method for Estimating Bulk 2D Projections of Ice Particle Shape: Theory and Applications

Edwin L. Dunnavan, Zhiyuan Jiang

Source: Journal of the Atmospheric Sciences, https://doi.org/10.1175/JAS-D-18-0177.1, published Online: 4 January 2019.

The orientation of falling ice particles directly influences estimates of microphysical and radiative bulk quantities as well as in situ retrievals of size, shape, and mass. However, retrieval efforts and bulk calculations often incorporate very basic orientations or ignore these effects altogether. To address this deficiency, this study develops a general method for projecting bulk distributions of particle shape for arbitrary orientations. The Amoroso distribution provides the most general bulk aspect ratio distribution for gamma-distributed particle axis lengths. The parameters that govern the behavior of this aspect ratio distribution depend on the assumed relationship between mass, maximum dimension, and aspect ratio. Individual spheroidal geometry allows for eccentricity quantities to linearly map onto ellipse analogs, whereas aspect ratio quantities map nonlinearly. For particles viewed from their side, this analytic distinction leads to substantially larger errors in projected aspect ratio than for projected eccentricity. Distribution transformations using these mapping equations and numerical integration of projection kernels show that both truncation of size distributions and changes in Gaussian dispersion can alter the modality and shape of projection distributions. As a result, the projection process can more than triple the relative entropy between the spheroidal and projection distributions for commonly assumed model and orientation parameters. This shape uncertainty is maximized for distributions of highly eccentric particles and for

particles like aggregates that are thought to fall with large canting-angle deviations. As a result, the methods used to report projected aspect ratios and the corresponding values should be questioned.

Keywords: Cloud microphysics; Ice crystals; Ice particles; Aircraft observations; In situ atmospheric observations; Model comparison

---

On the Nonlinearity of Winter Northern Hemisphere Atmospheric Variability

A. Hannachi, W. Iqbal

Source: Journal of the Atmospheric Sciences, https://doi.org/10.1175/JAS-D-18-0182.1, published Online: 4 January 2019

Nonlinearity in the Northern Hemisphere's wintertime atmospheric flow is investigated from both an intermediate-complexity model of the extratropics and reanalyses. A long simulation is obtained using a three-level quasigeostrophic model on the sphere. Kernel empirical orthogonal functions (EOFs), which help delineate complex structures, are used along with the local flow tendencies. Two fixed points are obtained, which are associated with strong bimodality in two-dimensional kernel principal component (PC) space, consistent with conceptual low-order dynamics. The regimes reflect zonal and blocked flows. The analysis is then extended to ERA-40 and JRA-55 using daily sea level pressure (SLP) and geopotential heights in the stratosphere (20 hPa) and troposphere (500 hPa). In the stratosphere, trimodality is obtained, representing disturbed, displaced, and undisturbed states of the winter polar vortex. In the troposphere, the probability density functions (PDFs), for both fields, within the two-dimensional (2D) kernel EOF space are strongly bimodal. The modes correspond broadly to opposite phases of the Arctic Oscillation with a signature of the negative North Atlantic Oscillation (NAO). Over the North Atlantic–European sector, a trimodal PDF is also obtained with two strong and one weak modes. The strong modes are associated, respectively, with the north (or +NAO) and south (or −NAO) positions of the eddy-driven jet stream. The third weak mode is interpreted as a transition path between the two positions. A climate change signal is also observed in the troposphere of the winter hemisphere, resulting in an increase (a decrease) in the frequency of the polar high (low), consistent with an increase of zonal flow frequency.

Keywords: Nonlinear dynamics.

Trends in erythemal doses at the Polish Polar Station, Hornsund, Svalbard based on the homogenized measurements (1996–2016) and reconstructed data (1983–1995)

Janusz W. Krzyścin and Piotr S. Sobolewski

Source: Atmosphere Chemistry and Physics, Volume 18, issue 1
DOI: 02 Jan 2018

Erythemal daily doses measured at the Polish Polar Station, Hornsund (77°00′N, 15°33′E), for the periods 1996–2001 and 2005–2016 are homogenized using yearly calibration constants derived from the comparison of observed doses for cloudless conditions with the corresponding doses calculated by radiative transfer (RT) simulations. Modeled all-sky doses are calculated by the multiplication of cloudless RT doses by the empirical cloud modification factor dependent on the daily sunshine duration. An all-sky model is built using daily erythemal doses measured in the period 2005–2006–2007. The model is verified by comparisons with the 1996–1997–1998 and 2009–2010–2011 measured data. The daily doses since 1983 (beginning of the proxy data) are reconstructed using the all-sky model with the historical data of the column ozone from satellite measurements (SBUV merged ozone data set), the snow depth (for ground albedo estimation), and the observed daily sunshine duration at the site. Trend analyses of the monthly and yearly time series comprised of the reconstructed and observed doses do not reveal a statistically significant trend in the period 1983–2016. The trends based on the observed data only (1996–2001 and 2005–2016) show declining tendency (about −1% per year) in the monthly mean of daily erythemal doses in May and June, and in the yearly sum of daily erythemal doses. An analysis of sources of the yearly dose variability since 1983 shows that cloud cover changes are a basic driver of the long-term UV changes at the site.

Effects of model resolution and parameterizations on the simulations of clouds, precipitation, and their interactions with aerosols

Seoung Soo Lee1, Zhanqing Li1, Yuwei Zhang1, Hyelim Yoo2, Seungbum Kim3, Byung-Gon Kim4, Yong-Sang Choi5,Jungbin Mok1, Junshik Um6, Kyoung Ock Choi7, and Danhong Dong

Source : Atmosphere Chemistry and Physics, Volume 18, issue 1
DOI: 03 Jan 2018

This study investigates the roles played by model resolution and microphysics parameterizations in the well-known uncertainties or errors in simulations of clouds, precipitation, and their interactions with aerosols by the numerical weather prediction (NWP) models. For this investigation, we used cloud-system-resolving model (CSRM) simulations as benchmark simulations that adopt high-resolution and full-fledged microphysical processes. These simulations were evaluated against observations, and this evaluation demonstrated that the CSRM simulations can function as benchmark simulations. Comparisons between the CSRM simulations and the simulations at the coarse resolutions that are generally adopted by current NWP models indicate that the use of coarse resolutions as in the NWP models can lower not only updrafts and other cloud variables (e.g., cloud mass, condensation, deposition, and evaporation) but also their sensitivity to increasing aerosol concentration. The parameterization of the saturation process plays an important role in the sensitivity of cloud variables to aerosol concentrations. while the parameterization of the sedimentation process has a substantial impact on how cloud variables are distributed vertically. The variation in cloud variables with resolution is much greater than what happens with varying microphysics parameterizations, which suggests that the uncertainties in the NWP simulations are associated with resolution much more than microphysics parameterizations.

Investigation of short-term effective radiative forcing of fire aerosols over North America using nudged hindcast ensembles

Yawen Liu1,2, Kai Zhang2, Yun Qian2, Yuhang Wang3, Yufei Zou3, Yongjia Song3, Hui Wan2, Xiaohong Liu4,and Xiu-Qun Yang1
Source: Atmosphere Chemistry and Physics, , Volume 18, issue 1
DOI: 03 Jan 2018

Aerosols from fire emissions can potentially have large impact on clouds and radiation. However, fire aerosol sources are often intermittent, and their effect on weather and climate is difficult to quantify. Here we investigated the short-term effective radiative forcing of fire aerosols using the global aerosol–climate model Community Atmosphere Model version 5 (CAM5). Different from previous studies, we used nudged hindcast ensembles to quantify the forcing uncertainty due to the chaotic response to small perturbations in the atmosphere state. Daily mean emissions from three fire inventories were used to consider the uncertainty in emission strength and injection heights. The simulated aerosol optical depth (AOD) and mass concentrations were evaluated against in situ measurements and reanalysis data. Overall, the results show the model has reasonably

good predicting skills. Short (10-day) nudged ensemble simulations were then performed with and without fire emissions to estimate the effective radiative forcing. Results show fire aerosols have large effects on both liquid and ice clouds over the two selected regions in April 2009. Ensemble mean results show strong negative shortwave cloud radiative effect (SCRE) over almost the entirety of southern Mexico, with a 10-day regional mean value of −3.0Wm−2. Over the central US, the SCRE is positive in the north but negative in the south, and the regional mean SCRE is small (−0.56Wm−2). For the 10-day average, we found a large ensemble spread of regional mean shortwave cloud radiative effect over southern Mexico (15.6% of the corresponding ensemble mean) and the central US (64.3%), despite the regional mean AOD time series being almost indistinguishable during the 10-day period. Moreover, the ensemble spread is much larger when using daily averages instead of 10-day averages. This demonstrates the importance of using a large ensemble of simulations to estimate the short-term aerosol effective radiative forcing.

Observations of ozone depletion events in a Finnish boreal forest

Xuemeng Chen1, Lauriane L. J. Quéléver1, Pak L. Fung1, Jutta Kesti2, Matti P. Rissanen1, Jaana Bäck1, Petri Keronen1,Heikki Junninen1,3, Tuukka Petäjä1, Veli-Matti Kerminen1, and Markku Kulmala1

Source: Atmosphere Chemistry and Physics, , Volume 18, issue 1
DOI: 03 Jan 2018

We investigated the concentrations and vertical profiles of ozone over a 20-year period (1996–2016) at the SMEAR II station in southern Finland. Our results showed that the typical daily median ozone concentrations were in the range of 20–50ppb with clear diurnal and annual patterns. In general, the profile of ozone concentrations illustrated an increase as a function of heights. The main aim of our study was to address the frequency and strength of ozone depletion events at this boreal forest site. We observed more than a thousand of 10min periods at 4.2m, with ozone concentrations below 10ppb, and a few tens of cases with ozone concentrations below 2ppb. Among these observations, a number of ozone depletion events that lasted for more than 3h were identified, and they occurred mainly in autumn and winter months. The low ozone concentrations were likely related to the formation of a low mixing layer under the conditions of low temperatures, low wind speeds, high relative humidities and limited intensity of solar radiation.

Influence of temperature on the molecular composition of ions and charged clusters during pure biogenic nucleation

Kulmala3, Douglas R. Worsnop3,14,15, Paul M. Winkler5, Josef Dommen1, and Urs Baltensperger1

Source: Atmosphere Chemistry and Physics, Volume 18, issue 1
DOI: 04 Jan 2018

It was recently shown by the CERN CLOUD experiment that biogenic highly oxygenated molecules (HOMs) form particles under atmospheric conditions in the absence of sulfuric acid, where ions enhance the nucleation rate by 1–2 orders of magnitude. The biogenic HOMs were produced from ozonolysis of α-pinene at 5°C. Here we extend this study to compare the molecular composition of positive and negative HOM clusters measured with atmospheric pressure interface time-of-flight mass spectrometers (APi-TOFs), at three different temperatures (25, 5 and −25°C). Most negative HOM clusters include a nitrate (NO_3^-) ion, and the spectra are similar to those seen in the nighttime boreal forest. On the other hand, most positive HOM clusters include an ammonium (NH_4^+) ion, and the spectra are characterized by mass bands that differ in their molecular weight by ∼20 C atoms, corresponding to HOM dimers. At lower temperatures the average oxygen to carbon (O:C) ratio of the HOM clusters decreases for both polarities, reflecting an overall reduction of HOM formation with decreasing temperature. This indicates a decrease in the rate of autoxidation with temperature due to a rather high activation energy as has previously been determined by quantum chemical calculations. Furthermore, at the lowest temperature (−25°C), the presence of C30 clusters shows that HOM monomers start to contribute to the nucleation of positive clusters. These experimental findings are supported by quantum chemical calculations of the binding energies of representative neutral and charged clusters.

Thirteen years of observations on primary sugars and sugar alcohols over remote Chichijima Island in the western North Pacific

Santosh Kumar Verma1,2, Kimitaka Kawamura1,a, Jing Chen1,b, and Pingqing Fu1,c

Source : Atmosphere Chemistry and Physics, Volume 18, issue 1
DOI: 04 Jan 2018

In order to understand the atmospheric transport of bioaerosols, we conducted long-term observations of primary sugars and sugar alcohols over remote Chichijima Island in the western North Pacific from 2001 to 2013. Our results showed that concentrations of total sugar compounds for 13 years ranged from 1.2 to 310ngm−3 (average of 46±49ngm−3). We found that atmospheric circulations significantly affect the seasonal variations of bioaerosol distributions over the western North Pacific. The primary sugars (glucose and fructose) maximized in summer, possibly due to an increased emission of the vegetation products from local vascular plants in Chichijima. We also found higher concentrations of sugar components (arabitol, mannitol, and trehalose) in more recent years during summer and autumn, suggesting an enhanced emission of fungal and microbial species over the island. Sucrose peaked in late winter to early spring, indicating a springtime pollen contribution by long-range atmospheric transport, while elevated concentrations of sucrose in early summer could be explained by long-range transport of soil dust from Southeast Asia to Chichijima. Sucrose and trehalose were found to present increasing trends from 2001 to 2013, while total sugar components did not show any clear trends during the 13-year period. Positive matrix factorization analyses suggested the locally emitted sugar compounds as well as long-range-transported airborne pollen grains, microbes, and fungal spores are the major contributors to total sugar compounds in the Chichijima aerosols. Backward air mass trajectories support the atmospheric transport of continental aerosols from the Asian continent during winter and spring over Chichijima.

Impact of regional climate change and future emission scenarios on surface O3 and PM2.5over India

Matthieu Pommier1, Hilde Fagerli1, Michael Gauss1, David Simpson1,2, Sumit Sharma3, Vinay Sinha4, Sachin D. Ghude5,Oskar Landgren1, Agnes Nyiri1, and Peter Wind1

Source: Atmosphere Chemistry and Physics, Volume 18, issue 1
DOI: 04 Jan 2018

Eleven of the world's 20 most polluted cities are located in India and poor air quality is already a major public health issue. However, anthropogenic emissions are predicted to increase substantially in the short-term (2030) and medium-term (2050) futures in India, especially if no further policy efforts are made. In this study, the EMEP/MSC-W chemical transport model has been used to predict changes in surface ozone (O3) and fine particulate matter (PM2.5) for India in a world of changing emissions and climate. The reference scenario (for present-day) is evaluated against surface-based measurements,

mainly at urban stations. The evaluation has also been extended to other data sets which are publicly available on the web but without quality assurance. The evaluation shows high temporal correlation for O3 (r = 0.9) and high spatial correlation for PM2.5 (r = 0.5 and r = 0.8 depending on the data set) between the model results and observations. While the overall bias in PM2.5 is small (lower than 6%), the model overestimates O3 by 35%. The underestimation in NOx titration is probably the main reason for the O3 overestimation in the model. However, the level of agreement can be considered satisfactory in this case of a regional model being evaluated against mainly urban measurements, and given the inevitable uncertainties in much of the input data.

For the 2050s, the model predicts that climate change will have distinct effects in India in terms of O3 pollution, with a region in the north characterized by a statistically significant increase by up to 4% (2ppb) and one in the south by a decrease up to −3% (−1.4ppb). This variation in O3 is assumed to be partly related to changes in O3 deposition velocity caused by changes in soil moisture and, over a few areas, partly also by changes in biogenic non-methane volatile organic compounds.

Our calculations suggest that PM2.5 will increase by up to 6.5% over the Indo-Gangetic Plain by the 2050s. The increase over India is driven by increases in dust, particulate organic matter (OM) and secondary inorganic aerosols (SIAs), which are mainly affected by the change in precipitation, biogenic emissions and wind speed.

The large increase in anthropogenic emissions has a larger impact than climate change, causing O3 and PM2.5 levels to increase by 13 and 67% on average in the 2050s over the main part of India, respectively. By the 2030s, secondary inorganic aerosol is predicted to become the second largest contributor to PM2.5 in India, and the largest in the 2050s, exceeding OM and dust.

Mercury fluxes over an Australian alpine grassland and observation of nocturnal atmospheric mercury depletion events

Dean Howard and Grant C. Edwards

Source : Atmosphere Chemistry and Physics, Volume 18, issue 1
DOI: 05 Jan 2018

Aerodynamic gradient measurements of the air–surface exchange of gaseous elemental mercury (GEM) were undertaken over a 40ha alpine grassland in Australia's Snowy Mountains region across a 3-week period during the late austral summer. Bi-directional GEM fluxes were observed throughout the study, with overall mean value of

0.2±14.5ngm−2h−1 and mean nocturnal fluxes of −1.5±7.8ngm−2h−1 compared to diurnal fluxes of 1.8±18.6ngm−2h−1. Deposition velocities ranged from −2.2 to 2.9cms−1, whilst ambient GEM concentrations throughout the study were 0.59±0.10ngm−3. Cumulative GEM fluxes correlated well with 24h running mean soil temperatures, and one precipitation event was shown to have a positive impact on diurnal emission fluxes. The underlying vegetation had largely senesced and showed little stomatal control on fluxes. Nocturnal atmospheric mercury depletion events (NAMDEs) were observed concomitant with O3 depletion and dew formation under shallow, stable nocturnal boundary layers. A mass balance box model was able to reproduce ambient GEM concentration patterns during NAMDE and non-NAMDE nights without invoking chemical oxidation of GEM throughout the column, indicating a significant role of surface processes controlling deposition in these events. Surface deposition was enhanced under NAMDE nights, though uptake to dew likely represents less than one-fifth of this enhanced deposition. Instead, enhancement of the surface GEM gradient as a result of oxidation at the surface in the presence of dew is hypothesised to be responsible for a large portion of GEM depletion during these particular events. GEM emission pulses following nights with significant deposition provide evidence for the prompt recycling of 17% of deposited mercury, with the remaining portion retained in surface sinks. The long-term impacts of any sinks are however likely to be minimal, as cumulative GEM flux across the study period was close to zero.

Detectability of the impacts of ozone-depleting substances and greenhouse gases upon stratospheric ozone accounting for nonlinearities in historical forcings

Justin Bandoro1, Susan Solomon1, Benjamin D. Santer2, Douglas E. Kinnison3, and Michael J. Mills3

Source: Atmosphere Chemistry and Physics, Volume 18, issue 1
DOI: 05 Jan 2018

We perform a formal attribution study of upper- and lower-stratospheric ozone changes using observations together with simulations from the Whole Atmosphere Community Climate Model. Historical model simulations were used to estimate the zonal-mean response patterns (fingerprints) to combined forcing by ozone-depleting substances (ODSs) and well-mixed greenhouse gases (GHGs), as well as to the individual forcing by each factor. Trends in the similarity between the searched-for fingerprints and homogenized observations of stratospheric ozone were compared to trends in pattern similarity between the fingerprints and the internally and naturally generated variability inferred from long control runs. This yields estimated signal-to-noise (S/N) ratios for each

of the three fingerprints (ODS, GHG, and ODS+GHG). In both the upper stratosphere (defined in this paper as 1 to 10hPa) and lower stratosphere (40 to 100hPa), the spatial fingerprints of the ODS+GHG and ODS-only patterns were consistently detectable not only during the era of maximum ozone depletion but also throughout the observational record (1984–2016). We also develop a fingerprint attribution method to account for forcings whose time evolutions are markedly nonlinear over the observational record. When the nonlinearity of the time evolution of the ODS and ODS+GHG signals is accounted for, we find that the S/N ratios obtained with the stratospheric ODS and ODS+GHG fingerprints are enhanced relative to standard linear trend analysis. Use of the nonlinear signal detection method also reduces the detection time – the estimate of the date at which ODS and GHG impacts on ozone can be formally identified. Furthermore, by explicitly considering nonlinear signal evolution, the complete observational record can be used in the S/N analysis, without applying piecewise linear regression and introducing arbitrary break points. The GHG-driven fingerprint of ozone changes was not statistically identifiable in either the upper- or lower-stratospheric SWOOSH data, irrespective of the signal detection method used. In the WACCM simulations of future climate change, the GHG signal is statistically identifiable between 2020 and 2030. Our findings demonstrate the importance of continued stratospheric ozone monitoring to improve estimates of the contributions of ODS and GHG forcing to global changes in stratospheric ozone.

Role of ambient ammonia in particulate ammonium formation at a rural site in the North China Plain

Zhaoyang Meng1, Xiaobin Xu1, Weili Lin2,a, Baozhu Ge3, Yulin Xie4,5, Bo Song4, Shihui Jia1,6, Rui Zhang7,8, Wei Peng1,Ying Wang1, Hongbing Cheng1, Wen Yang7, and Huarong Zhao1

Source: Atmosphere Chemistry and Physics, Volume 18, issue 1
DOI: 08 Jan 2018

The real-time measurements of NH3 and trace gases were conducted, in conjunction with semi-continuous measurements of water-soluble ions in PM2.5 at a rural site in the North China Plain (NCP) from May to September 2013 in order to better understand chemical characteristics of ammonia and the impact of secondary ammonium aerosols on formation in the NCP. Extremely high NH3 and NH4+ concentrations were observed after a precipitation event within 7–10 days following urea application. Elevated NH3 levels coincided with elevated NH4+, indicating that NH3 likely influenced particulate ammonium mass. For the sampling period, the average conversion/oxidation ratios for NH4+ (NHR),

SO_4^{2-} (SOR), and NO_3^- (NOR) were estimated to be 0.30, 0.64, and 0.24, respectively. The increased NH_3 concentrations, mainly from agricultural activities and regional transport, coincided with the prevailing meteorological conditions. The high NH_3 level with NHR of about 0.30 indicates that the emission of NH_3 in the NCP is much higher than needed for aerosol acid neutralisation, and NH_3 plays an important role in the formation of secondary aerosols as a key neutraliser. The hourly data obtained were used to investigate gas–aerosol partitioning characteristics using the thermodynamic equilibrium model ISORROPIA-II. Modelled SO_4^{2-}, NO_3^-, and NH_3 values agree well with the measurements, while the modelled NH_4^+ values largely underestimate the measurements. Our observation and modelling results indicate that strong acids in aerosol are completely neutralised. Additional NH_4^+ exists in aerosol, probably a result of the presence of a substantial amount of oxalic and other diacids.

Atmospheric organochlorine pesticides and polychlorinated biphenyls in urban areas of Nepal: spatial variation, sources, temporal trends, and long-range transport potential

Balram Pokhrel1,3,4, Ping Gong1,2, Xiaoping Wang1,2,3, Sanjay Nath Khanal4, Jiao Ren1,3, Chuanfei Wang1,2,Shaopeng Gao1, and Tandong Yao1,2

Source: Atmosphere Chemistry and Physics, Volume 18, issue 2
DOI: 01 Feb 2018

The study of persistent organic pollutants (POPs) in low-latitude tropical and subtropical urban cities is necessary to assess their local and global impacts on ecosystems and human health. Despite studies on levels of POPs in water, soils, and sediments, analysis of the distribution patterns, seasonality, and sources of POPs in urban regions of Nepal remain limited. Polyurethane foam (PUF)-based passive air samplers were deployed in three major cities in Nepal: Kathmandu (the capital city), Pokhara, and Hetauda (agricultural cities). Dichlorodiphenyltrichloroethane (DDT) and hexachlorocyclohexane (HCH) were the dominant organochlorine pesticides in the atmosphere at all sites. The average concentrations of POPs were $\sum$DDTs, 8.7–1.0 × 103pgm−3; $\sum$HCHs, 5.3–3.3 × 103pgm−3; HCB, 5.8–3.4 × 102pgm−3; $\sum$endosulfan, BDL–51pgm−3; and $\sum$6PCBs, 1.4–47pgm−3. Isomer and metabolite ratio analyses suggested that the concentrations present were from both new and historical applications of the POPs. Vegetable production sites and their market places appeared to be the major DDT and HCH source areas. Higher atmospheric concentrations of DDT and HCH occurred during the pre-monsoon and monsoon seasons, and winter, respectively, closely associated with their local application for soil preparation and vegetable spraying. The estimated travel distances of the POPs (HCB, α-HCH, γ-HCH, and p, p′-DDT) under the Nepalese tropical climate were all above 1000km, suggesting that high precipitation levels in the tropical climate were not enough to scavenge the POPs and that Nepal could be an important source region for POPs. Due to their close proximity and cold trapping (driven by low temperatures), the high Himalayas and the Tibetan Plateau

are likely the key receptors of POPs emitted in Nepal. These results add to the information available on POPs from tropical developing countries.

Nine-year spatial and temporal evolution of desert dust aerosols over South and East Asia as revealed by CALIOP

Emmanouil Proestakis1,2, Vassilis Amiridis1, Eleni Marinou1, Aristeidis K. Georgoulias3,4, Stavros Solomos1,Stelios Kazadzis5,6, Julien Chimot7, Huizheng Che8,9, Georgia Alexandri3, Ioannis Binietoglou10,Vasiliki Daskalopoulou1,11, Konstantinos A. Kourtidis3, Gerrit de Leeuw12,13, and Ronald J. van der A14

Source: Atmosphere Chemistry and Physics, Volume 18, issue 2
DOI: 01 Feb 2018

We present a 3-D climatology of the desert dust distribution over South and East Asia derived using CALIPSO (Cloud-Aerosol Lidar and Infrared Pathfinder Satellite Observation) data. To distinguish desert dust from total aerosol load we apply a methodology developed in the framework of EARLINET (European Aerosol Research Lidar Network). The method involves the use of the particle linear depolarization ratio and updated lidar ratio values suitable for Asian dust, applied to multiyear CALIPSO observations (January 2007–December 2015). The resulting dust product provides information on the horizontal and vertical distribution of dust aerosols over South and East Asia along with the seasonal transition of dust transport pathways. Persistent high D_AOD (dust aerosol optical depth) values at 532nm, of the order of 0.6, are present over the arid and semi-arid desert regions. Dust aerosol transport (range, height and intensity) is subject to high seasonality, with the highest values observed during spring for northern China (Taklimakan and Gobi deserts) and during summer over the Indian subcontinent (Thar Desert). Additionally, we decompose the CALIPSO AOD (aerosol optical depth) into dust and non-dust aerosol components to reveal the non-dust AOD over the highly industrialized and densely populated regions of South and East Asia, where the non-dust aerosols yield AOD values of the order of 0.5. Furthermore, the CALIPSO-based short-term AOD and D_AOD time series and trends between January 2007 and December 2015 are calculated over South and East Asia and over selected subregions. Positive trends are observed over northwest and east China and the Indian subcontinent, whereas over southeast China trends are mostly negative. The calculated AOD trends agree well with the trends derived from Aqua MODIS (Moderate Resolution Imaging Spectroradiometer), although significant differences are observed over specific regions.

Soil fluxes of carbonyl sulfide (COS), carbon monoxide, and carbon dioxide in a boreal forest in southern Finland

Wu Sun1, Linda M. J. Kooijmans2, Kadmiel Maseyk3, Huilin Chen2,7, Ivan Mammarella4, Timo Vesala4,5,Janne Levula4,5,6, Helmi Keskinen4,5,6, and Ulli Seibt1

Source: Atmosphere Chemistry and Physics, Volume 18, issue 2
DOI: 01 Feb 2018.

Soil is a major contributor to the biosphere–atmosphere exchange of carbonyl sulfide (COS) and carbon monoxide (CO). COS is a tracer with which to quantify terrestrial photosynthesis based on the coupled leaf uptake of COS and CO2, but such use requires separating soil COS flux, which is unrelated to photosynthesis, from ecosystem COS uptake. For CO, soil is a significant natural sink that influences the troposphere CO budget. In the boreal forest, magnitudes and variabilities of soil COS and CO fluxes remain poorly understood. We measured hourly soil fluxes of COS, CO, and CO2 over the 2015 late growing season (July to November) in a Scots pine forest in Hyytiälä, Finland. The soil acted as a net sink of COS and CO, with average uptake rates around 3pmol m−2 s−1 for COS and 1nmol m−2 s−1 for CO. Soil respiration showed seasonal dynamics controlled by soil temperature, peaking at around 4µmol m−2 s−1 in late August and September and dropping to 1–2µmol m−2 s−1 in October. In contrast, seasonal variations of COS and CO fluxes were weak and mainly driven by soil moisture changes through diffusion limitation. COS and CO fluxes did not appear to respond to temperature variation, although they both correlated well with soil respiration in specific temperature bins. However, COS:CO2 and CO : CO2 flux ratios increased with temperature, suggesting possible shifts in active COS- and CO-consuming microbial groups. Our results show that soil COS and CO fluxes do not have strong variations over the late growing season in this boreal forest and can be represented with the fluxes during the photosynthetically most active period. Well-characterized and relatively invariant soil COS fluxes strengthen the case for using COS as a photosynthetic tracer in boreal forests.

Evidence for a continuous decline in lower stratospheric ozone offsetting ozone layer recovery

William T. Ball1,2, Justin Alsing3,4, Daniel J. Mortlock4,5,6, Johannes Staehelin2,Joanna D. Haigh4,7, Thomas Peter2, Fiona Tummon2, Rene Stübi8, Andrea Stenke2,John Anderson9, Adam Bourassa10, Sean M. Davis11,12, Doug Degenstein10, Stacey Frith13,14,Lucien Froidevaux15, Chris Roth10, Viktoria Sofieva16, Ray Wang17, Jeannette Wild18,19,Pengfei Yu11,12, Jerald R. Ziemke13,20, and Eugene V. Rozanov1,2

Source: Atmosphere Chemistry and Physics, Volume 18, issue 2
DOI: 06 Feb 2018.

Ozone forms in the Earth's atmosphere from the photodissociation of molecular oxygen, primarily in the tropical stratosphere. It is then transported to the extratropics by the Brewer–Dobson circulation (BDC), forming a protective ozone layer around the globe. Human emissions of halogen-containing ozone-depleting substances (hODSs) led to a decline in stratospheric ozone until they were banned by the Montreal Protocol, and since 1998 ozone in the upper stratosphere is rising again, likely the recovery from halogen-induced losses. Total column measurements of ozone between the Earth's surface and the top of the atmosphere indicate that the ozone layer has stopped declining across the globe, but no clear increase has been observed at latitudes between 60°S and 60°N outside the polar regions (60–90°). Here we report evidence from multiple satellite measurements that ozone in the lower stratosphere between 60°S and 60°N has indeed continued to decline since 1998. We find that, even though upper stratospheric ozone is recovering, the continuing downward trend in the lower stratosphere prevails, resulting in a downward trend in stratospheric column ozone between 60°S and 60°N. We find that total column ozone between 60°S and 60°N appears not to have decreased only because of increases in tropospheric column ozone that compensate for the stratospheric decreases. The reasons for the continued reduction of lower stratospheric ozone are not clear; models do not reproduce these trends, and thus the causes now urgently need to be established.

Emission or atmospheric processes? An attempt to attribute the source of large bias of aerosols in eastern China simulated by global climate models

Tianyi Fan1, Xiaohong Liu2,1, Po-Lun Ma3, Qiang Zhang4, Zhanqing Li1,5, Yiquan Jiang6, Fang Zhang1,Chuanfeng Zhao1, Xin Yang1, Fang Wu1, and Yuying Wang1

Source: Atmosphere Chemistry and Physics, Volume 18, issue 2
DOI: 01 Feb 2018

Global climate models often underestimate aerosol loadings in China, and these biases can have significant implications for anthropogenic aerosol radiative forcing and climate effects. The biases may be caused by either the emission inventory or the treatment of aerosol processes in the models, or both, but so far no consensus has been reached. In this study, a relatively new emission inventory based on energy statistics and technology, Multi-resolution Emission Inventory for China (MEIC), is used to drive the Community Atmosphere Model version 5 (CAM5) to evaluate aerosol distribution and radiative effects against observations in China. The model results are compared with the model simulations with the widely used Intergovernmental Panel on Climate Change Fifth Assessment Report (IPCC AR5) emission inventory. We find that the new MEIC emission improves the aerosol optical depth (AOD) simulations in eastern China and explains 22–28% of the AOD low bias simulated with the AR5 emission. However, AOD is still biased low in eastern China.

Seasonal variation of the MEIC emission leads to a better agreement with the observed seasonal variation of primary aerosols than the AR5 emission, but the concentrations are still underestimated. This implies that the atmospheric loadings of primary aerosols are closely related to the emission, which may still be underestimated over eastern China. In contrast, the seasonal variations of secondary aerosols depend more on aerosol processes (e.g., gas- and aqueous-phase production from precursor gases) that are associated with meteorological conditions and to a lesser extent on the emission. It indicates that the emissions of precursor gases for the secondary aerosols alone cannot explain the low bias in the model. Aerosol secondary production processes in CAM5 should also be revisited. The simulation using MEIC estimates the annual-average aerosol direct radiative effects (ADREs) at the top of the atmosphere (TOA), at the surface, and in the atmosphere to be −5.02, −18.47, and 13.45Wm−2, respectively, over eastern China, which are enhanced by −0.91, −3.48, and 2.57Wm−2 compared with the AR5 emission. The differences of ADREs by using MEIC and AR5 emissions are larger than the decadal changes of the modeled ADREs, indicating the uncertainty of the emission inventories. This study highlights the importance of improving both the emission and aerosol secondary production processes in modeling the atmospheric aerosols and their radiative effects. Yet, if the estimations of MEIC emissions in trace gases do not suffer similar biases to those in the AOD, our findings will help affirm a fundamental error in the conversion from precursor gases to secondary aerosols as hinted in other recent studies following different approaches.

The optical properties, physical properties and direct radiative forcing of urban columnar aerosols in the Yangtze River Delta, China

Bingliang Zhuang1, Tijian Wang1, Jane Liu1,2, Huizheng Che3, Yong Han1, Yu Fu4, Shu Li1, Min Xie1, Mengmeng Li1,Pulong Chen1, Huimin Chen1, Xiu-qun Yang1, and Jianning Sun1

Source : Atmosphere Chemistry and Physics, Volume 18, issue 2
DOI: 01 Feb 2018

The optical and physical properties as well as the direct radiative forcings (DRFs) of fractionated aerosols in the urban area of the western Yangtze River Delta (YRD) are investigated with measurements from a Cimel sun photometer combined with a radiation transfer model. Ground-based observations of aerosols have much higher temporal resolutions than satellite retrievals. An initial analysis reveals the characteristics of the optical properties of different types of fractionated aerosols in the western YRD. The total aerosols, mostly composed of scattering components (93.8%), have mean optical depths of 0.65 at 550nm and refractive index of 1.44+0.0084i at 440nm. The fine aerosols are

approximately four times more abundant and have very different compositions from coarse aerosols. The absorbing components account for only ∼4.6% of fine aerosols and 15.5% of coarse aerosols and have smaller sizes than the scattering aerosols within the same mode. Therefore, fine particles have stronger scattering than coarse ones, simultaneously reflecting the different size distributions between the absorbing and scattering aerosols. The relationships among the optical properties quantify the aerosol mixing and imply that approximately 15 and 27.5% of the total occurrences result in dust- and black-carbon-dominating mixing aerosols, respectively, in the western YRD. Unlike the optical properties, the size distributions of aerosols in the western YRD are similar to those found at other sites over eastern China on a climatological scale, peaking at radii of 0.148 and 2.94μm. However, further analysis reveals that the coarse-dominated particles can also lead to severe haze pollution over the YRD. Observation-based estimations indicate that both fine and coarse aerosols in the western YRD exert negative DRFs, and this is especially true for fine aerosols (−11.17Wm−2 at the top of atmosphere, TOA). A higher absorption fraction leads directly to the negative DRF being further offset for coarse aerosols (−0.33Wm−2) at the TOA. Similarly, the coarse-mode DRF contributes to only 13.3% of the total scattering aerosols but >33.7% to the total absorbing aerosols. A sensitivity analysis states that aerosol DRFs are not highly sensitive to their profiles in clear-sky conditions. Most of the aerosol properties and DRFs have substantial seasonality in the western YRD. The results further reveal the contributions of each component of the different size particles to the total aerosol optical depths (AODs) and DRFs. Additionally, these results can be used to improve aerosol modelling performance and the modelling of aerosol effects in the eastern regions of China.

Representation of solar tides in the stratosphere and lower mesosphere in state-of-the-art reanalyses and in satellite observations

Takatoshi Sakazaki1,2,3, Masatomo Fujiwara4, and Masato Shiotani3

Source: Atmosphere Chemistry and Physics, Volume 18, issue 2
DOI: 01 Feb 2018

Atmospheric solar tides in the stratosphere and the lower mesosphere are investigated using temperature data from five state-of-the-art reanalysis data sets (MERRA-2, MERRA, JRA-55, ERA-Interim, and CFSR) as well as TIMED SABER and Aura MLS satellite measurements. The main focus is on the period 2006–2012 during which the satellite observations are available for direct comparison with the reanalyses. Diurnal migrating tides, semidiurnal migrating tides, and nonmigrating tides are diagnosed. Overall the reanalyses agree reasonably well with each other and with the satellite observations for

both migrating and nonmigrating components, including their vertical structure and the seasonality. However, the agreement among reanalyses is more pronounced in the lower stratosphere and relatively weaker in the upper stratosphere and mesosphere. A systematic difference between SABER and the reanalyses is found for diurnal migrating tides in the upper stratosphere and the lower mesosphere; specifically, the amplitude of trapped modes in reanalyses is significantly smaller than that in SABER, although such difference is less clear between MLS and the reanalyses. The interannual variability and the possibility of long-term changes in migrating tides are also examined using the reanalyses during 1980–2012. All the reanalyses agree in exhibiting a clear quasi-biennial oscillation (QBO) in the tides, but the most significant indications of long-term changes in the tides represented in the reanalyses are most plausibly explained by the evolution of the satellite observing systems during this period. The tides are also compared in the full reanalyses produced by the Japan Meteorological Agency (i.e., JRA-55) and in two parallel data sets from this agency: one (JRA-55C) that repeats the reanalysis procedure but without any satellite data assimilated and one (JRA-55AMIP) that is a free-running integration of the model constrained only by observed sea surface temperatures. Many aspects of the tides are closer in JRA-55C and JRA-55AMIP than these are to the full reanalysis JRA-55, demonstrating the importance of the assimilation of satellite data in representing the diurnal variability of the middle atmosphere. In contrast to the assimilated data sets, the free-running model has no QBO in equatorial stratospheric mean circulation and our results show that it displays no quasi-biennial variability in the tides.

Assessing the ability to derive rates of polar middle-atmospheric descent using trace gas measurements from remote sensors

Niall J. Ryan[1], Douglas E. Kinnison[2], Rolando R. Garcia[2], Christoph G. Hoffmann[3], Mathias Palm[1], Uwe Raffalski[4],and Justus Notholt[1]

Source: Atmosphere Chemistry and Physics, Volume 18, issue 3
02 Feb 2018.

We investigate the reliability of using trace gas measurements from remote sensing instruments to infer polar atmospheric descent rates during winter within 46–86km altitude. Using output from the Specified Dynamics Whole Atmosphere Community Climate Model (SD-WACCM) between 2008 and 2014, tendencies of carbon monoxide (CO) volume mixing ratios (VMRs) are used to assess a common assumption of dominant vertical advection of tracers during polar winter. The results show that dynamical processes other than vertical advection are not negligible, meaning that the transport rates derived from trace gas measurements do not represent the mean descent of the atmosphere. The relative importance of vertical advection is lessened, and exceeded by other processes, during

periods directly before and after a sudden stratospheric warming, mainly due to an increase in eddy transport. It was also found that CO chemistry cannot be ignored in the mesosphere due to the night-time layer of OH at approximately 80km altitude. CO VMR profiles from the Kiruna Microwave Radiometer and the Microwave Limb Sounder were compared to SD-WACCM output, and show good agreement on daily and seasonal timescales. SD-WACCM CO profiles are combined with the CO tendencies to estimate errors involved in calculating the mean descent of the atmosphere from remote sensing measurements. The results indicate errors on the same scale as the calculated descent rates, and that the method is prone to a misinterpretation of the direction of air motion. The true rate of atmospheric descent is seen to be masked by processes, other than vertical advection, that affect CO. We suggest an alternative definition of the rate calculated using remote sensing measurements: not as the mean descent of the atmosphere, but as an effective rate of vertical transport for the trace gas under observation.

Relating large-scale subsidence to convection development in Arctic mixed-phase marine stratocumulus

Gillian Young[1,a], Paul J. Connolly[1], Christopher Dearden[1,b], and Thomas W. Choularton[1]

Source: Atmosphere Chemistry and Physics, Volume 18, issue 3
02 Feb 2018.

Large-scale subsidence, associated with high-pressure systems, is often imposed in large-eddy simulation (LES) models to maintain the height of boundary layer (BL) clouds. Previous studies have considered the influence of subsidence on warm liquid clouds in subtropical regions; however, the relationship between subsidence and mixed-phase cloud microphysics has not specifically been studied. For the first time, we investigate how widespread subsidence associated with synoptic-scale meteorological features can affect the microphysics of Arctic mixed-phase marine stratocumulus (Sc) clouds. Modelled with LES, four idealised scenarios – a stable Sc, varied droplet (N_{drop}) or ice (N_{ice}) number concentrations, and a warming surface (representing motion southwards) – were subjected to different levels of subsidence to investigate the cloud microphysical response. We find strong sensitivities to large-scale subsidence, indicating that high-pressure systems in the ocean-exposed Arctic regions have the potential to generate turbulence and changes in cloud microphysics in any resident BL mixed-phase clouds.

Increased cloud convection is modelled with increased subsidence, driven by longwave radiative cooling at cloud top and rain evaporative cooling and latent heating from snow growth below cloud. Subsidence strengthens the BL temperature inversion, thus reducing entrainment and allowing the liquid- and ice-water paths (LWPs, IWPs) to increase. Through increased cloud-top radiative cooling and subsequent convective overturning,

precipitation production is enhanced: rain particle number concentrations (N_{rain}), in-cloud rain mass production rates, and below-cloud evaporation rates increase with increased subsidence.

Ice number concentrations (N_{ice}) play an important role, as greater concentrations suppress the liquid phase; therefore, N_{ice} acts to mediate the strength of turbulent overturning promoted by increased subsidence. With a warming surface, a lack of – or low – subsidence allows for rapid BL turbulent kinetic energy (TKE) coupling, leading to a heterogeneous cloud layer, cloud-top ascent, and cumuli formation below the Sc cloud. In these scenarios, higher levels of subsidence act to stabilise the Sc layer, where the combination of these two forcings counteract one another to produce a stable, yet dynamic, cloud layer.

Aerosol characteristics in the entrainment interface layer in relation to the marine boundary layer and free troposphere

Hossein Dadashazar[1], Rachel A. Braun[1], Ewan Crosbie[2,3], Patrick Y. Chuang[4], Roy K. Woods[5], Haflidi H. Jonsson[5],and Armin Sorooshian[1,6]

Source: Atmosphere Chemistry and Physics, Volume 18, issue 3
02 Feb 2018.

This study uses airborne data from two field campaigns off the California coast to characterize aerosol size distribution characteristics in the entrainment interface layer (EIL), a thin and turbulent layer above marine stratocumulus cloud tops, which separates the stratocumulus-topped boundary layer (STBL) from the free troposphere (FT). The vertical bounds of the EIL are defined in this work based on considerations of buoyancy and turbulence using thermodynamic and dynamic data. Aerosol number concentrations are examined from three different probes with varying particle diameter (D_p) ranges: >3nm, >10nm, and 0.11–3.4μm. Relative to the EIL and FT layers, the sub-cloud (SUB) layer exhibited lower aerosol number concentrations and higher surface area concentrations. High particle number concentrations between 3 and 10nm in the EIL are indicative of enhanced nucleation, assisted by high actinic fluxes, cool and moist air, and much lower surface area concentrations than the STBL. Slopes of number concentration versus altitude in the EIL were correlated with the particle number concentration difference between the SUB and lower FT layers. The EIL aerosol size distribution was influenced by varying degrees from STBL aerosol versus subsiding FT aerosol depending on the case examined. These results emphasize the important role of the EIL in influencing nucleation and aerosol–cloud–climate interactions.

Aerosol optical properties and trace gas emissions by PAX and OP-FTIR for laboratory-simulated western US wildfires during FIREX

Vanessa Selimovic[1], Robert J. Yokelson[1], Carsten Warneke[2], James M. Roberts[2], Joost de Gouw[3], James Reardon[4],and David W. T. Griffith[5]

Source: Atmosphere Chemistry and Physics, Volume 18, issue 4
01 Mar 2018.

Western wildfires have a major impact on air quality in the US. In the fall of 2016, 107 test fires were burned in the large-scale combustion facility at the US Forest Service Missoula Fire Sciences Laboratory as part of the Fire Influence on Regional and Global Environments Experiment (FIREX). Canopy, litter, duff, dead wood, and other fuel components were burned in combinations that represented realistic fuel complexes for several important western US coniferous and chaparral ecosystems including ponderosa pine, Douglas fir, Engelmann spruce, lodgepole pine, subalpine fir, chamise, and manzanita. In addition, dung, Indonesian peat, and individual coniferous ecosystem fuel components were burned alone to investigate the effects of individual components (e.g., duff) and fuel chemistry on emissions. The smoke emissions were characterized by a large suite of state-of-the-art instruments. In this study we report emission factor (EF, grams of compound emitted per kilogram of fuel burned) measurements in fresh smoke of a diverse suite of critically important trace gases measured using open-path Fourier transform infrared spectroscopy (OP-FTIR). We also report aerosol optical properties (absorption EF; single-scattering albedo, SSA; and Ångström absorption exponent, AAE) as well as black carbon (BC) EF measured by photoacoustic extinctiometers (PAXs) at 870 and 401nm. The average trace gas emissions were similar across the coniferous ecosystems tested and most of the variability observed in emissions could be attributed to differences in the consumption of components such as duff and litter, rather than the dominant tree species. Chaparral fuels produced lower EFs than mixed coniferous fuels for most trace gases except for NO_x and acetylene. A careful comparison with available field measurements of wildfires confirms that several methods can be used to extract data representative of real wildfires from the FIREX laboratory fire data. This is especially valuable for species rarely or not yet measured in the field. For instance, the OP-FTIR data alone show that ammonia ($1.62 g kg^{-1}$), acetic acid ($2.41 g kg^{-1}$), nitrous acid (HONO, $0.61 g kg^{-1}$), and other trace gases such as glycolaldehyde ($0.90 g kg^{-1}$) and formic acid ($0.36 g kg^{-1}$) are significant emissions that were poorly characterized or not characterized for US wildfires in previous work. The PAX measurements show that the ratio of brown carbon (BrC) absorption to BC absorption is strongly dependent on modified combustion efficiency (MCE) and that BrC absorption is most dominant for combustion of duff (AAE 7.13) and rotten wood (AAE 4.60): fuels that are consumed in greater amounts during wildfires than prescribed fires. Coupling our laboratory data with field data suggests that fresh wildfire smoke typically has an EF for BC near $0.2 g kg^{-1}$, an SSA of ~ 0.91, and an AAE of ~ 3.50, with the latter implying that about 86% of the aerosol absorption at 401nm is due to BrC.

Water vapor increase in the lower stratosphere of the Northern Hemisphere due to the Asian monsoon anticyclone observed during the TACTS/ESMVal campaigns

Christian Rolf[1], Bärbel Vogel[1], Peter Hoor[2], Armin Afchine[1], Gebhard Günther[1], Martina Krämer[1], Rolf Müller[1],Stefan Müller[2,3], Nicole Spelten[1], and Martin Riese[1]

Source: Atmosphere Chemistry and Physics, Volume 18, issue 4

01 Mar 2018.

The impact of air masses originating in Asia and influenced by the Asian monsoon anticyclone on the Northern Hemisphere stratosphere is investigated based on in situ measurements. A statistically significant increase in water vapor (H_2O) of about 0.5ppmv (11%) and methane (CH_4) of up to 20ppbv (1.2%) in the extratropical stratosphere above a potential temperature of 380K was detected between August and September 2012 during the HALO aircraft missions Transport and Composition in the UT/LMS (TACTS) and Earth System Model Validation (ESMVal). We investigate the origin of the increased water vapor and methane using the three-dimensional Chemical Lagrangian Model of the Stratosphere (CLaMS). We assign the source of the moist air masses in the Asian region (northern and southern India, eastern China, southeast Asia, and the tropical Pacific) based on tracers of air mass origin used in CLaMS. The water vapor increase is correlated with an increase of the simulated Asian monsoon air mass contribution from about 10% in August to about 20% in September, which corresponds to a doubling of the influence from the Asian monsoon region. Additionally, back trajectories starting at the aircraft flight paths are used to differentiate transport from the Asian monsoon anticyclone and other source regions by calculating the Lagrangian cold point (LCP). The geographic location of the LCPs, which indicates the region where the set point of water vapor mixing ratio along these trajectories occurs, can be predominantly attributed to the Asian monsoon region.

The maintenance of elevated active chlorine levels in the Antarctic lower stratosphere through HCl null cycles

Rolf Müller[1], Jens-Uwe Grooß[1], Abdul Mannan Zafar[1,a], Sabine Robrecht[1], and Ralph Lehmann[2]

Source: Atmosphere Chemistry and Physics, Volume 18, issue 4

01 Mar 2018

The Antarctic ozone hole arises from ozone destruction driven by elevated levels of ozone destroying (active) chlorine in Antarctic spring. These elevated levels of active chlorine have to be formed first and then maintained throughout the period of ozone destruction. It

is a matter of debate how this maintenance of active chlorine is brought about in Antarctic spring, when the rate of formation of HCl (considered to be the main chlorine deactivation mechanism in Antarctica) is extremely high. Here we show that in the heart of the ozone hole (16–18km or 85–55hPa, in the core of the vortex), high levels of active chlorine are maintained by effective chemical cycles (referred to as HCl null cycles hereafter). In these cycles, the formation of HCl is balanced by immediate reactivation, i.e. by immediate reformation of active chlorine. Under these conditions, polar stratospheric clouds sequester HNO_3 and thereby cause NO_2concentrations to be low. These HCl null cycles allow active chlorine levels to be maintained in the Antarctic lower stratosphere and thus rapid ozone destruction to occur. For the observed almost complete activation of stratospheric chlorine in the lower stratosphere, the heterogeneous reaction HCl + HOCl is essential; the production of HOCl occurs via $HO_2 + ClO$, with the HO_2 resulting from CH_2O photolysis. These results are important for assessing the impact of changes of the future stratospheric composition on the recovery of the ozone hole. Our simulations indicate that, in the lower stratosphere, future increased methane concentrations will not lead to enhanced chlorine deactivation (through the reaction $CH_4 + Cl \longrightarrow HCl + CH_3$) and that extreme ozone destruction to levels below ≈ 0.1ppm will occur until mid-century.

Extraction of wind and temperature information from hybrid 4D-Var assimilation of stratospheric ozone using NAVGEM

Douglas R. Allen, Karl W. Hoppel, and David D. Kuhl

Source: Atmosphere Chemistry and Physics, Volume 18, issue 4
01 Mar 2018

Extraction of wind and temperature information from stratospheric ozone assimilation is examined within the context of the Navy Global Environmental Model (NAVGEM) hybrid 4-D variational assimilation (4D-Var) data assimilation (DA) system. Ozone can improve the wind and temperature through two different DA mechanisms: (1) through the flow-of-the-day ensemble background error covariance that is blended together with the static background error covariance and (2) via the ozone continuity equation in the tangent linear model and adjoint used for minimizing the cost function. All experiments assimilate actual conventional data in order to maintain a similar realistic troposphere. In the stratosphere, the experiments assimilate simulated ozone and/or radiance observations in various combinations. The simulated observations are constructed for a case study based on a 16-day cycling truth experiment (TE), which is an analysis with no stratospheric observations. The impact of ozone on the analysis is evaluated by comparing the experiments to the TE for the last 6 days, allowing for a 10-day spin-up. Ozone assimilation benefits the wind and temperature when data are of sufficient quality and frequency. For example, assimilation of perfect (no applied error) global hourly ozone data constrains the stratospheric wind and temperature to within $\sim 2 ms^{-1}$ and ~ 1K. This demonstrates that there is dynamical information in the ozone distribution that can potentially be used to

improve the stratosphere. This is particularly important for the tropics, where radiance observations have difficulty constraining wind due to breakdown of geostrophic balance. Global ozone assimilation provides the largest benefit when the hybrid blending coefficient is an intermediate value (0.5 was used in this study), rather than 0.0 (no ensemble background error covariance) or 1.0 (no static background error covariance), which is consistent with other hybrid DA studies. When perfect global ozone is assimilated in addition to radiance observations, wind and temperature error decreases of up to $\sim 3 ms^{-1}$ and $\sim 1K$ occur in the tropical upper stratosphere. Assimilation of noisy global ozone (2% errors applied) results in error reductions of $\sim 1 ms^{-1}$ and $\sim 0.5K$ in the tropics and slightly increased temperature errors in the Northern Hemisphere polar region. Reduction of the ozone sampling frequency also reduces the benefit of ozone throughout the stratosphere, with noisy polar-orbiting data having only minor impacts on wind and temperature when assimilated with radiances. An examination of ensemble cross-correlations between ozone and other variables shows that a single ozone observation behaves like a potential vorticity (PV) charge, or a monopole of PV, with rotation about a vertical axis and vertically oriented temperature dipole. Further understanding of this relationship may help in designing observation systems that would optimize the impact of ozone on the dynamics.

Technical Note: Atmospheric CO_2 inversions on the mesoscale using data-driven prior uncertainties: methodology and system evaluation

Panagiotis Kountouris[1], Christoph Gerbig[1], Christian Rödenbeck[1], Ute Karstens[1,a], Thomas Frank Koch[2],and Martin Heimann[1]

Source: Atmosphere Chemistry and Physics, Volume 18, issue 4
02 Mar 2018.

Atmospheric inversions are widely used in the optimization of surface carbon fluxes on a regional scale using information from atmospheric CO_2 dry mole fractions. In many studies the prior flux uncertainty applied to the inversion schemes does not directly reflect the true flux uncertainties but is used to regularize the inverse problem. Here, we aim to implement an inversion scheme using the Jena inversion system and applying a prior flux error structure derived from a model–data residual analysis using high spatial and temporal resolution over a full year period in the European domain. We analyzed the performance of the inversion system with a synthetic experiment, in which the flux constraint is derived following the same residual analysis but applied to the model–model mismatch. The synthetic study showed a quite good agreement between posterior and true fluxes on European, country, annual and monthly scales. Posterior monthly and country-aggregated fluxes improved their correlation coefficient with the known truth by 7% compared to the prior estimates when compared to the reference, with a mean correlation of 0.92. The ratio of the SD between the posterior and reference and between the prior and reference was

also reduced by 33% with a mean value of 1.15. We identified temporal and spatial scales on which the inversion system maximizes the derived information; monthly temporal scales at around 200km spatial resolution seem to maximize the information gain.

Atmospheric CO_2 inversions on the mesoscale using data-driven prior uncertainties: quantification of the European terrestrial CO_2 fluxes

Panagiotis Kountouris[1], Christoph Gerbig[1], Christian Rödenbeck[1], Ute Karstens[1,a], Thomas F. Koch[2],and Martin Heimann[1]

Source : Atmosphere Chemistry and Physics, Volume 18, issue 4
02 Mar 2018

Optimized biogenic carbon fluxes for Europe were estimated from high-resolution regional-scale inversions, utilizing atmospheric CO_2 measurements at 16 stations for the year 2007. Additional sensitivity tests with different data-driven error structures were performed. As the atmospheric network is rather sparse and consequently contains large spatial gaps, we use a priori biospheric fluxes to further constrain the inversions. The biospheric fluxes were simulated by the Vegetation Photosynthesis and Respiration Model (VPRM) at a resolution of 0.1° and optimized against eddy covariance data. Overall we estimate an a priori uncertainty of $0.54GtCyr^{-1}$ related to the poor spatial representation between the biospheric model and the ecosystem sites. The sink estimated from the atmospheric inversions for the area of Europe (as represented in the model domain) ranges between 0.23 and $0.38GtCyr^{-1}$ (0.39 and $0.71GtCyr^{-1}$ up-scaled to geographical Europe). This is within the range of posterior flux uncertainty estimates of previous studies using ground-based observations.

Contrasting the co-variability of daytime cloud and precipitation over tropical land and ocean

Daeho Jin[1,2], Lazaros Oreopoulos[2], Dongmin Lee[2,3], Nayeong Cho[1,2], and Jackson Tan[1,2]

Source: Atmosphere Chemistry and Physics, Volume 18, issue 4
02 Mar 2018.

The co-variability of cloud and precipitation in the extended tropics (35°N–35°S) is investigated using contemporaneous data sets for a 13-year period. The goal is to quantify potential relationships between cloud type fractions and precipitation events of particular strength. Particular attention is paid to whether the relationships exhibit different characteristics over tropical land and ocean. A primary analysis metric is the correlation

coefficient between fractions of individual cloud types and frequencies within precipitation histogram bins that have been matched in time and space. The cloud type fractions are derived from Moderate Resolution Imaging Spectroradiometer (MODIS) joint histograms of cloud top pressure and cloud optical thickness in 1° grid cells, and the precipitation frequencies come from the Tropical Rainfall Measuring Mission (TRMM) Multi-satellite Precipitation Analysis (TMPA) data set aggregated to the same grid.

It is found that the strongest coupling (positive correlation) between clouds and precipitation occurs over ocean for cumulonimbus clouds and the heaviest rainfall. While the same cloud type and rainfall bin are also best correlated over land compared to other combinations, the correlation magnitude is weaker than over ocean. The difference is attributed to the greater size of convective systems over ocean. It is also found that both over ocean and land the anti-correlation of strong precipitation with weak (i.e., thin and/or low) cloud types is of greater absolute strength than positive correlations between weak cloud types and weak precipitation. Cloud type co-occurrence relationships explain some of the cloud–precipitation anti-correlations. Weak correlations between weaker rainfall and clouds indicate poor predictability for precipitation when cloud types are known, and this is even more true over land than over ocean.

Nighttime wind and scalar variability within and above an Amazonian canopy

Pablo E. S. Oliveira[1], Otávio C. Acevedo[1], Matthias Sörgel[2], Anywhere Tsokankunku[2], Stefan Wolff[2],Alessandro C. Araújo[3], Rodrigo A. F. Souza[4], Marta O. Sá[5], Antônio O. Manzi[5], and Meinrat O. Andreae[2]

Source: Atmosphere Chemistry and Physics, Volume 18, issue 5
05 Mar 2018.

Nocturnal turbulent kinetic energy (TKE) and fluxes of energy, CO_2 and O_3 between the Amazon forest and the atmosphere are evaluated for a 20-day campaign at the Amazon Tall Tower Observatory (ATTO) site. The distinction of these quantities between fully turbulent (weakly stable) and intermittent (very stable) nights is discussed. Spectral analysis indicates that low-frequency, nonturbulent fluctuations are responsible for a large portion of the variability observed on intermittent nights. In these conditions, the low-frequency exchange may dominate over the turbulent transfer. In particular, we show that within the canopy most of the exchange of CO_2 and H_2O happens on temporal scales longer than 100s. At 80m, on the other hand, the turbulent fluxes are almost absent in such very stable conditions, suggesting a boundary layer shallower than 80m. The relationship between

TKE and mean winds shows that the stable boundary layer switches from the very stable to the weakly stable regime during intermittent bursts of turbulence. In general, fluxes estimated with long temporal windows that account for low-frequency effects are more dependent on the stability over a deeper layer above the forest than they are on the stability between the top of the canopy and its interior, suggesting that low-frequency processes are controlled over a deeper layer above the forest.

Lower tropospheric ozone over India and its linkage to the South Asian monsoon

Xiao Lu[1,2], Lin Zhang[1], Xiong Liu[3], Meng Gao[2], Yuanhong Zhao[1], and Jingyuan Shao[1]

Source: Atmosphere Chemistry and Physics, Volume 18, issue 5
05 Mar 2018

Lower tropospheric (surface to 600hPa) ozone over India poses serious risks to both human health and crops, and potentially affects global ozone distribution through frequent deep convection in tropical regions. Our current understanding of the processes controlling seasonal and long-term variations in lower tropospheric ozone over this region is rather limited due to spatially and temporally sparse observations. Here we present an integrated process analysis of the seasonal cycle, interannual variability, and long-term trends of lower tropospheric ozone over India and its linkage to the South Asian monsoon using the Ozone Monitoring Instrument (OMI) satellite observations for years 2006–2014 interpreted with a global chemical transport model (GEOS-Chem) simulation for 1990–2010. OMI observed lower tropospheric ozone over India averaged for 2006–2010, showing the highest concentrations (54.1ppbv) in the pre-summer monsoon season (May) and the lowest concentrations (40.5ppbv) in the summer monsoon season (August). Process analyses in GEOS-Chem show that hot and dry meteorological conditions and active biomass burning together contribute to 5.8Tg more ozone being produced in the lower troposphere in India in May than January. The onset of the summer monsoon brings ozone-unfavorable meteorological conditions and strong upward transport, which all lead to large decreases in the lower tropospheric ozone burden. Interannually, we find that both OMI and GEOS-Chem indicate strong positive correlations ($r = 0.55–0.58$) between ozone and surface temperature in pre-summer monsoon seasons, with larger correlations found in high NO_x emission regions reflecting NO_x-limited production conditions. Summer monsoon seasonal mean ozone levels are strongly controlled by monsoon strengths. Lower ozone concentrations are found in stronger monsoon seasons mainly due to less ozone net chemical production. Furthermore, model simulations over 1990–2010 estimate a mean annual trend of 0.19±0.07 (p value < 0.01)ppbvyr^{-1} in Indian lower tropospheric ozone over this period, which are mainly driven by increases in anthropogenic emissions with a small contribution (about 7%) from global methane concentration increases.

Aerosol–cloud interactions in mixed-phase convective clouds – Part 1: Aerosol perturbations

Annette K. Miltenberger[1], Paul R. Field[1,2], Adrian A. Hill[2], Phil Rosenberg[1], Ben J. Shipway[2], Jonathan M. Wilkinson[2],Robert Scovell[2], and Alan M. Blyth[3]

Source: Atmosphere Chemistry and Physics, Volume 18, issue 5

05 Mar 2018

Changes induced by perturbed aerosol conditions in moderately deep mixed-phase convective clouds (cloud top height ~ 5km) developing along sea-breeze convergence lines are investigated with high-resolution numerical model simulations. The simulations utilise the newly developed Cloud–AeroSol Interacting Microphysics (CASIM) module for the Unified Model (UM), which allows for the representation of the two-way interaction between cloud and aerosol fields. Simulations are evaluated against observations collected during the COnvective Precipitation Experiment (COPE) field campaign over the southwestern peninsula of the UK in 2013. The simulations compare favourably with observed thermodynamic profiles, cloud base cloud droplet number concentrations (CDNC), cloud depth, and radar reflectivity statistics. Including the modification of aerosol fields by cloud microphysical processes improves the correspondence with observed CDNC values and spatial variability, but reduces the agreement with observations for average cloud size and cloud top height.

Accumulated precipitation is suppressed for higher-aerosol conditions before clouds become organised along the sea-breeze convergence lines. Changes in precipitation are smaller in simulations with aerosol processing. The precipitation suppression is due to less efficient precipitation production by warm-phase microphysics, consistent with parcel model predictions.

In contrast, after convective cells organise along the sea-breeze convergence zone, accumulated precipitation increases with aerosol concentrations. Condensate production increases with the aerosol concentrations due to higher vertical velocities in the convective cores and higher cloud top heights. However, for the highest-aerosol scenarios, no further increase in the condensate production occurs, as clouds grow into an upper-level stable layer. In these cases, the reduced precipitation efficiency (PE) dominates the precipitation response and no further precipitation enhancement occurs. Previous studies of deep convective clouds have related larger vertical velocities under high-aerosol conditions to enhanced latent heating from freezing. In the presented simulations changes in latent heating above the 0°C are negligible, but latent heating from condensation increases with aerosol concentrations. It is hypothesised that this increase is related to changes in the cloud field structure reducing the mixing of environmental air into the convective core.

The precipitation response of the deeper mixed-phase clouds along well-established convergence lines can be the opposite of predictions from parcel models. This occurs when clouds interact with a pre-existing thermodynamic environment and cloud field structural changes occur that are not captured by simple parcel model approaches.

Effects of convective ice evaporation on interannual variability of tropical tropopause layer water vapor

Hao Ye, Andrew E. Dessler, and Wandi Yu

Source: Atmosphere Chemistry and Physics, Volume 18, issue 7
03 Apr 2018.

Water vapor interannual variability in the tropical tropopause layer (TTL) is investigated using satellite observations and model simulations. We break down the influences of the Brewer–Dobson circulation (BDC), the quasi-biennial oscillation (QBO), and the tropospheric temperature (ΔT) on TTL water vapor as a function of latitude and longitude using a two-dimensional multivariate linear regression. This allows us to examine the spatial distribution of the impact of each process on TTL water vapor. In agreement with expectations, we find that the impacts from the BDC and QBO act on TTL water vapor by changing TTL temperature. For ΔT, we find that TTL temperatures alone cannot explain the influence. We hypothesize a moistening role for the evaporation of convective ice from increased deep convection as the troposphere warms. Tests using a chemistry–climate model, the Goddard Earth Observing System Chemistry Climate Model (GEOSCCM), support this hypothesis.

Comparing airborne and satellite retrievals of cloud optical thickness and particle effective radius using a spectral radiance ratio technique: two case studies for cirrus and deep convective clouds

Trismono C. Krisna[1], Manfred Wendisch[1], André Ehrlich[1], Evelyn Jäkel[1], Frank Werner[1,a], Ralf Weigel[3,4],Stephan Borrmann[3,4], Christoph Mahnke[3], Ulrich Pöschl[4], Meinrat O. Andreae[4,6], Christiane Voigt[2,3],and Luiz A. T. Machado[5]

Source : Atmosphere Chemistry and Physics, Volume 18, issue 7
03 Apr 2018

Solar radiation reflected by cirrus and deep convective clouds (DCCs) was measured by the Spectral Modular Airborne Radiation Measurement System (SMART) installed on the

German High Altitude and Long Range Research Aircraft (HALO) during the Mid-Latitude Cirrus (ML-CIRRUS) and the Aerosol, Cloud, Precipitation, and Radiation Interaction and Dynamic of Convective Clouds System – Cloud Processes of the Main Precipitation Systems in Brazil: A Contribution to Cloud Resolving Modelling and to the Global Precipitation Measurement (ACRIDICON-CHUVA) campaigns. On particular flights, HALO performed measurements closely collocated with overpasses of the Moderate Resolution Imaging Spectroradiometer (MODIS) aboard the Aqua satellite. A cirrus cloud located above liquid water clouds and a DCC topped by an anvil cirrus are analyzed in this paper. Based on the nadir spectral upward radiance measured above the two clouds, the optical thickness τ and particle effective radius r_{eff} of the cirrus and DCC are retrieved using a radiance ratio technique, which considers the cloud thermodynamic phase, the vertical profile of cloud microphysical properties, the presence of multilayer clouds, and the heterogeneity of the surface albedo. For the cirrus case, the comparison of τ and r_{eff} retrieved on the basis of SMART and MODIS measurements yields a normalized mean absolute deviation of up to 1.2% for τ and 2.1% for r_{eff}. For the DCC case, deviations of up to 3.6% for τ and 6.2% for r_{eff} are obtained. The larger deviations in the DCC case are mainly attributed to the fast cloud evolution and three-dimensional (3-D) radiative effects. Measurements of spectral upward radiance at near-infrared wavelengths are employed to investigate the vertical profile of r_{eff} in the cirrus. The retrieved values of r_{eff} are compared with corresponding in situ measurements using a vertical weighting method. Compared to the MODIS observations, measurements of SMART provide more information on the vertical distribution of particle sizes, which allow reconstructing the profile of r_{eff} close to the cloud top. The comparison between retrieved and in situ r_{eff} yields a normalized mean absolute deviation, which ranges between 1.5 and 10.3%, and a robust correlation coefficient of 0.82.

Water vapour and methane coupling in the stratosphere observed using SCIAMACHY solar occultation measurements

Stefan Noël, Katja Weigel, Klaus Bramstedt, Alexei Rozanov, Mark Weber, Heinrich Bovensmann, and John P. Burrows

Source : Atmosphere Chemistry and Physics, Volume 18, issue 7

03 Apr 2018.

An improved stratospheric water vapour data set has been retrieved from SCIAMACHY/ENVISAT solar occultation measurements. It is similar to that successfully applied to methane and carbon dioxide. There is now a consistent set of data products for the three constituents covering the altitudes 17–45km, the latitude range between about 50 and 70°N, and the period August 2002 to April 2012.

The new water vapour concentration profiles agree with collocated results from ACE-FTS and MLS/Aura to within $\sim$5%. A significant positive linear change in water vapour for the

time 2003–2011 is observed at lower stratospheric altitudes with a value of about 0.015 ± 0.008 ppmv year^{-1} around 17km. Between 30 and 37km the changes become significantly negative (about -0.01 ± 0.008 ppmv year^{-1}); all errors are 2σ values.

The combined analysis of the SCIAMACHY methane and water vapour time series shows the expected anti-correlation between stratospheric methane and water vapour and a clear temporal variation related to the Quasi-Biennial Oscillation (QBO). Above about 20km most of the additional water vapour is attributed to the oxidation of methane. In addition short-term fluctuations and longer-term variations on a timescale of 5–6 years are observed. The SCIAMACHY data confirm that at lower altitudes the amount of water vapour and methane are transported from the tropics to higher latitudes via the shallow branch of the Brewer–Dobson circulation.

Measurements of aerosol and CCN properties in the Mackenzie River delta (Canadian Arctic) during spring–summer transition in May 2014

Paul Herenz[1], Heike Wex[1], Silvia Henning[1], Thomas Bjerring Kristensen[1,a], Florian Rubach[2],Anja Roth[2], Stephan Borrmann[2], Heiko Bozem[3], Hannes Schulz[4], and Frank Stratmann[1]

Source: Atmosphere Chemistry and Physics, Volume 18, issue 7

04 Apr 2018.

Within the framework of the RACEPAC (Radiation–Aerosol–Cloud Experiment in the Arctic Circle) project, the Arctic aerosol, arriving at a ground-based station in Tuktoyaktuk (Mackenzie River delta area, Canada), was characterized during a period of 3 weeks in May 2014. Basic meteorological parameters and particle number size distributions (PNSDs) were observed and two distinct types of air masses were found. One type were typical Arctic haze air masses, termed accumulation-type air masses, characterized by a monomodal PNSD with a pronounced accumulation mode at sizes above 100nm. These air masses were observed during a period when back trajectories indicate an air mass origin in the north-east of Canada. The other air mass type is characterized by a bimodal PNSD with a clear minimum around 90 nm and with an Aitken mode consisting of freshly formed aerosol particles. Back trajectories indicate that these air masses, termed Aitken-type air masses, originated from the North Pacific. In addition, the application of the PSCF receptor model shows that air masses with their origin in active fire areas in central Canada and Siberia, in areas of industrial anthropogenic pollution (Norilsk and Prudhoe Bay Oil Field) and the north-west Pacific have enhanced total particle number concentrations (N_{CN}). Generally, N_{CN}ranged from 20 to 500cm^{-3}, while cloud condensation nuclei (CCN) number concentrations were found to cover a range from less than 10 up to 250cm^{-3} for a supersaturation (SS) between 0.1 and 0.7%. The hygroscopicity parameter κ of the CCN was determined to be 0.23 on average and variations in κ were largely attributed to measurement uncertainties.

Furthermore, simultaneous PNSD measurements at the ground station and on the Polar 6 research aircraft were performed. We found a good agreement of ground-based PNSDs with those measured between 200 and 1200m. During two of the four overflights, particle number concentrations at 3000m were found to be up to 20 times higher than those measured below 2000m; for one of these two flights, PNSDs measured above 2000m showed a different shape than those measured at lower altitudes. This is indicative of long-range transport from lower latitudes into the Arctic that can advect aerosol from different regions in different heights.

Modelling carbonaceous aerosol from residential solid fuel burning with different assumptions for emissions

Riinu Ots[1,2,a], Mathew R. Heal[1], Dominique E. Young[3,b], Leah R. Williams[4], James D. Allan[3,5], Eiko Nemitz[2],Chiara Di Marco[2], Anais Detournay[2], Lu Xu[6,c], Nga L. Ng[6,7], Hugh Coe[3], Scott C. Herndon[4], Ian A. Mackenzie[8],David C. Green[9], Jeroen J. P. Kuenen[10], Stefan Reis[2,11], and Massimo Vieno[2]

Source: Atmosphere Chemistry and Physics, Volume 18, issue 7

04 Apr 2018.

Evidence is accumulating that emissions of primary particulate matter (PM) from residential wood and coal combustion in the UK may be underestimated and/or spatially misclassified. In this study, different assumptions for the spatial distribution and total emission of PM from solid fuel (wood and coal) burning in the UK were tested using an atmospheric chemical transport model. Modelled concentrations of the PM components were compared with measurements from aerosol mass spectrometers at four sites in central and Greater London (ClearfLo campaign, 2012), as well as with measurements from the UK black carbon network.

The two main alternative emission scenarios modelled were *Base4x* and *combRedist*. For *Base4x*, officially reported $PM_{2.5}$ from the residential and other non-industrial combustion source sector were increased by a factor of four. For the *combRedist* experiment, half of the baseline emissions from this same source were redistributed by residential population density to simulate the effect of allocating some emissions to the smoke control areas (that are assumed in the national inventory to have no emissions from this source). The *Base4x*scenario yielded better daily and hourly correlations with measurements than the *combRedist* scenario for year-long comparisons of the solid fuel organic aerosol (SFOA) component at the two London sites. However, the latter scenario better captured mean measured concentrations across all four sites. A third experiment, *Redist* – all emissions redistributed linearly to population density, is also presented as an indicator of the maximum concentrations an assumption like this could yield.

The modelled elemental carbon (EC) concentrations derived from the *combRedist* experiments also compared well with seasonal average concentrations of black carbon observed across the network of UK sites. Together, the two model scenario simulations of SFOA and EC suggest both that residential solid fuel emissions may be higher than inventory estimates and that the spatial distribution of residential solid fuel burning emissions, particularly in smoke control areas, needs re-evaluation. The model results also suggest the assumed temporal profiles for residential emissions may require review to place greater emphasis on evening (including discretionary) solid fuel burning.

Nucleation of nitric acid hydrates in polar stratospheric clouds by meteoric material

Alexander D. James[1], James S. A. Brooke[1], Thomas P. Mangan[1], Thomas F. Whale[2],John M. C. Plane[1], and Benjamin J. Murray[2]

Source : Atmosphere Chemistry and Physics, Volume 18, issue 7
04 Apr 2018.

Heterogeneous nucleation of crystalline nitric acid hydrates in polar stratospheric clouds (PSCs) enhances ozone depletion. However, the identity and mode of action of the particles responsible for nucleation remains unknown. It has been suggested that meteoric material may trigger nucleation of nitric acid trihydrate (NAT, or other nitric acid phases), but this has never been quantitatively demonstrated in the laboratory. Meteoric material is present in two forms in the stratosphere: smoke that results from the ablation and re-condensation of vapours, and fragments that result from the break-up of meteoroids entering the atmosphere. Here we show that analogues of both materials have a capacity to nucleate nitric acid hydrates. In combination with estimates from a global model of the amount of meteoric smoke and fragments in the polar stratosphere we show that meteoric material probably accounts for NAT observations in early season polar stratospheric clouds in the absence of water ice.

Wintertime hygroscopicity and volatility of ambient urban aerosol particles

Joonas Enroth[1], Jyri Mikkilä[1], Zoltán Németh[2], Markku Kulmala[1], and Imre Salma[2]

Source : Atmosphere Chemistry and Physics, Volume 18, issue 7
04 Apr 2018.

Hygroscopic and volatile properties of atmospheric aerosol particles with dry diameters of (20), 50, 75, 110 and 145nm were determined in situ by using a volatility–hygroscopicity tandem differential mobility analyser (VH-TDMA) system with a relative humidity of 90% and denuding temperature of 270°C in central Budapest during 2 months in winter 2014–2015. The probability density function of the hygroscopic growth factor (HGF) showed a distinct bimodal distribution. One of the modes was characterised by an overall mean HGF of approximately 1.07 (this corresponds to a hygroscopicity parameter κ of 0.033) independently of the particle size and was assigned to nearly hydrophobic (NH) particles. Its mean particle number fraction was large, and it decreased monotonically from 69 to 41% with particle diameter. The other mode showed a mean HGF increasing slightly from 1.31 to 1.38 (κ values from 0.186 to 0.196) with particle diameter, and it was attributed to less hygroscopic (LH) particles. The mode with more hygroscopic particles was not identified. The probability density function of the volatility GF (VGF) also exhibited a distinct bimodal distribution with an overall mean VGF of approximately 0.96 independently of the particle size, and with another mean VGF increasing from 0.49 to 0.55 with particle diameter. The two modes were associated with less volatile (LV) and volatile (V) particles. The mean particle number fraction for the LV mode decreased from 34 to 21% with particle diameter. The bimodal distributions indicated that the urban atmospheric aerosol contained an external mixture of particles with a diverse chemical composition. Particles corresponding to the NH and LV modes were assigned mainly to freshly emitted combustion particles, more specifically to vehicle emissions consisting of large mass fractions of soot likely coated with or containing some water-insoluble organic compounds such as non-hygroscopic hydrocarbon-like organics. The hygroscopic particles were ordinarily volatile. They could be composed of moderately transformed aged combustion particles consisting of partly oxygenated organics, inorganic salts and soot. The larger particles contained internally mixed non-volatile chemical species as a refractory residual in 20–25% of the aerosol material (by volume).

Which processes drive observed variations of HCHO columns over India?

Luke Surl[1,2], Paul I. Palmer[1,2], and Gonzalo González Abad[3]

Source: Atmosphere Chemistry and Physics, Volume 18, issue 7

05 Apr 2018.

We interpret HCHO column variations observed by the Ozone Monitoring Instrument (OMI), aboard the NASA Aura satellite, over India during 2014 using the GEOS-Chem atmospheric chemistry and transport model. We use a nested version of the model with a horizontal resolution of approximately 25km. HCHO columns are related to local emissions of volatile organic compounds (VOCs) with a spatial smearing that increases with the VOC lifetime. Over India, HCHO has biogenic, pyrogenic, and anthropogenic VOC sources. Using a 0-D photochemistry model, we find that isoprene has the largest molar yield of HCHO which is typically realized within a few hours. We also find that forested regions that neighbour major urban conurbations are exposed to high levels of nitrogen oxides. This results in depleted hydroxyl radical concentrations and a delay in the production of HCHO

from isoprene oxidation. We find that propene is the only anthropogenic VOC emitted in major Indian cities that produces HCHO at a comparable (but slower) rate to isoprene. The GEOS-Chem model reproduces the broad-scale annual mean HCHO column distribution observed by OMI ($r = 0.6$), which is dominated by a distinctive meridional gradient in the northern half of the country, and by localized regions of high columns that coincide with forests. Major discrepancies are noted over the Indo-Gangetic Plain (IGP) and Delhi. We find that the model has more skill at reproducing observations during winter (JF) and pre-monsoon (MAM) months with Pearson correlations $r > 0.5$ but with a positive model bias of $\simeq 1\times10^{15}$moleccm^{-2}. During the monsoon season (JJAS) we reproduce only a diffuse version of the observed meridional gradient ($r = 0.4$). We find that on a continental scale most of the HCHO column seasonal cycle is explained by monthly variations in surface temperature ($r = 0.9$), suggesting a role for biogenic VOCs, in agreement with the 0-D and GEOS-Chem model calculations. We also find that the seasonal cycle during 2014 is not significantly different from the 2008 to 2015 mean seasonal variation. There are two main loci for biomass burning (the states of Punjab and Haryana, and northeastern India), which we find makes a significant contribution (up to 1×10^{15}moleccm^{-2}) to observed HCHO columns only during March and April over northeastern India. The slow production of HCHO from propene oxidation results in a smeared hotspot over Delhi that we resolve only on an annual mean timescale by using a temporal oversampling method. Using a linear regression model to relate GEOS-Chem isoprene emissions to HCHO columns we infer seasonal isoprene emissions over two key forest regions from the OMI HCHO column data. We find that the a posteriori emissions are typically lower than the a priori emissions, with a much stronger reduction of emissions during the monsoon season. We find that this reduction in emissions during monsoon months coincides with a large drop in satellite observations of leaf phenology that recovers in post monsoon months. This may signal a forest-scale response to monsoon conditions.

Monitoring of volatile organic compounds (VOCs) from an oil and gas station in northwest China for 1 year

Huang Zheng[1,2], Shaofei Kong[1], Xinli Xing[2,3], Yao Mao[3], Tianpeng Hu[2], Yang Ding[2], Gang Li[4],Dantong Liu[5], Shuanglin Li[1], and Shihua Qi[1,3]

Source: Atmosphere Chemistry and Physics, Volume 18, issue 7

05 Apr 2018.

Oil and natural gas are important for energy supply around the world. The exploring, drilling, transportation and processing in oil and gas regions can release a lot of volatile organic compounds (VOCs). To understand the VOC levels, compositions and sources in such regions, an oil and gas station in northwest China was chosen as the research site and 57 VOCs designated as the photochemical precursors were continuously measured for an entire year (September 2014–August 2015) using an online monitoring system. The average concentration of total VOCs was 297±372ppbv and the main contributor was

alkanes, accounting for 87.5% of the total VOCs. According to the propylene-equivalent concentration and maximum incremental reactivity methods, alkanes were identified as the most important VOC groups for the ozone formation potential. Positive matrix factorization (PMF) analysis showed that the annual average contributions from natural gas, fuel evaporation, combustion sources, oil refining processes and asphalt (anthropogenic and natural sources) to the total VOCs were 62.6±3.04, 21.5±.99, 10.9±1.57, 3.8±0.50 and 1.3±0.69%, respectively. The five identified VOC sources exhibited various diurnal patterns due to their different emission patterns and the impact of meteorological parameters. Potential source contribution function (PSCF) and concentration-weighted trajectory (CWT) models based on backward trajectory analysis indicated that the five identified sources had similar geographic origins. Raster analysis based on CWT analysis indicated that the local emissions contributed 48.4–74.6% to the total VOCs. Based on the high-resolution observation data, this study clearly described and analyzed the temporal variation in VOC emission characteristics at a typical oil and gas field, which exhibited different VOC levels, compositions and origins compared with those in urban and industrial areas.

Nonlinear response of tropical lower-stratospheric temperature and water vapor to ENSO

Chaim I. Garfinkel[1], Amit Gordon[1], Luke D. Oman[2], Feng Li[3], Sean Davis[4], and Steven Pawson[2.]

Source: Atmosphere Chemistry and Physics, Volume 18, issue 7

05 Apr 2018.

A series of simulations using the NASA Goddard Earth Observing System Chemistry–Climate Model are analyzed in order to aid in the interpretation of observed interannual and sub-decadal variability in the tropical lower stratosphere over the past 35 years. The impact of El Niño–Southern Oscillation on temperature and water vapor in this region is nonlinear in boreal spring. While moderate El Niño events lead to cooling in this region, strong El Niño events lead to warming, even as the response of the large-scale Brewer–Dobson circulation appears to scale nearly linearly with El Niño. This nonlinearity is shown to arise from the response in the Indo-West Pacific to El Niño: strong El Niño events lead to tropospheric warming extending into the tropical tropopause layer and up to the cold point in this region, where it allows for more water vapor to enter the stratosphere. The net effect is that both strong La Niña and strong El Niño events lead to enhanced entry water vapor and stratospheric moistening in boreal spring and early summer. These results lead to the following interpretation of the contribution of sea surface temperatures to the decline in water vapor in the early 2000s: the very strong El Niño event in 1997/1998, followed by more than 2 consecutive years of La Niña, led to enhanced lower-stratospheric water vapor. As this period ended in early 2001, entry water vapor concentrations declined. This effect accounts for approximately one-quarter of the observed drop.

The importance of vertical resolution in the free troposphere for modeling intercontinental plumes

Jiawei Zhuang[1], Daniel J. Jacob[1], and Sebastian D. Eastham[2]

Source: Atmosphere Chemistry and Physics, Volume 18, issue 8
02 May 2018.

Chemical plumes in the free troposphere can preserve their identity for more than a week as they are transported on intercontinental scales. Current global models cannot reproduce this transport. The plumes dilute far too rapidly due to numerical diffusion in sheared flow. We show how model accuracy can be limited by either horizontal resolution (Δx) or vertical resolution (Δz). Balancing horizontal and vertical numerical diffusion, and weighing computational cost, implies an optimal grid resolution ratio $(\Delta x/\Delta z)_{opt} \sim 1000$ for simulating the plumes. This is considerably higher than current global models ($\Delta x/\Delta z \sim 20$) and explains the rapid plume dilution in the models as caused by insufficient vertical resolution. Plume simulations with the Geophysical Fluid Dynamics Laboratory Finite-Volume Cubed-Sphere Dynamical Core (GFDL-FV3) over a range of horizontal and vertical grid resolutions confirm this limiting behavior. Our highest-resolution simulation ($\Delta x \approx 25$km, $\Delta z \approx 80$m) preserves the maximum mixing ratio in the plume to within 35% after 8 days in strongly sheared flow, a drastic improvement over current models. Adding free tropospheric vertical levels in global models is computationally inexpensive and would also improve the simulation of water vapor.

Mixing and ageing in the polar lower stratosphere in winter 2015–2016

Jens Krause[1], Peter Hoor[1], Andreas Engel[2], Felix Plöger[3], Jens-Uwe Grooß[3],Harald Bönisch[2,4], Timo Keber[2], Björn-Martin Sinnhuber[4], Wolfgang Woiwode[4],and Hermann Oelhaf[4]

Source: Atmosphere Chemistry and Physics, Volume 18, issue 8
02 May 2018.

We present data from winter 2015–2016, which were measured during the POLSTRACC (The Polar Stratosphere in a Changing Climate) aircraft campaign between December 2015 and March 2016 in the Arctic upper troposphere and lower stratosphere (UTLS). The focus of this work is on the role of transport and mixing between aged and potentially chemically processed air masses from the stratosphere which have midlatitude and low-latitude air mass fractions with small transit times originating at the tropical lower stratosphere. By

combining measurements of CO, N_2O and SF_6 we estimate the evolution of the relative contributions of transport and mixing to the UTLS composition over the course of the winter.

We find an increasing influence of aged stratospheric air partly from the vortex as indicated by decreasing N_2O and SF_6 values over the course of the winter in the extratropical lower and lowermost stratosphere between $\Theta = 360K$ and $\Theta = 410K$ over the North Atlantic and the European Arctic. Surprisingly we also found a mean increase in CO of $(3.00 \pm 1.64)ppb_V$ from January to March relative to N_2O in the lower stratosphere. We show that this increase in CO is consistent with an increased mixing of tropospheric air as part of the fast transport mechanism in the lower stratosphere surf zone. The analysed air masses were partly affected by air masses which originated at the tropical tropopause and were quasi-horizontally mixed into higher latitudes.

This increase in the tropospheric air fraction partly compensates for ageing of the UTLS due to the diabatic descent of air masses from the vortex by horizontally mixed, tropospheric-influenced air masses. This is consistent with simulated age spectra from the Chemical Lagrangian Model of the Stratosphere (CLaMS), which show a respective fractional increase in tropospheric air with transit times under 6 months and a simultaneous increase in aged air from upper stratospheric and vortex regions with transit times longer than 2 years.

We thus conclude that the lowermost stratosphere in winter 2015–2016 was affected by aged air from the upper stratosphere and vortex region. These air masses were significantly affected by increased mixing from the lower latitudes, which led to a simultaneous increase in the fraction of young air in the lowermost Arctic stratosphere by 6% from January to March 2016.

Decadal evolution of ship emissions in China from 2004 to 2013 by using an integrated AIS-based approach and projection to 2040

Cheng Li[1], Jens Borken-Kleefeld[2], Junyu Zheng[1,3], Zibing Yuan[3], Jiamin Ou[4], Yue Li[5], Yanlong Wang[3],and Yuanqian Xu[3]

Source : Atmosphere Chemistry and Physics, Volume 18, issue 8

02 May 2018.

Ship emissions contribute significantly to air pollution and pose health risks to residents of coastal areas in China, but the current research remains incomplete and coarse due to data availability and inaccuracy in estimation methods. In this study, an integrated approach based on the Automatic Identification System (AIS) was developed to address this problem. This approach utilized detailed information from AIS and cargo turnover and the vessel calling number information and is thereby capable of quantifying sectoral contributions by

fuel types and emissions from ports, rivers, coastal traffic and over-the-horizon ship traffic. Based upon the established methodology, ship emissions in China from 2004 to 2013 were estimated, and those to 2040 at 5-year intervals under different control scenarios were projected. Results showed that for the area within 200 nautical miles (Nm) of the Chinese coast, SO_2, NO_x, CO, PM_{10}, $PM_{2.5}$, hydrocarbon (HC), black carbon (BC) and organic carbon (OC) emissions in 2013 were 1010, 1443, 118, 107, 87, 67, 29 and 21ktyr^{-1}, respectively, which doubled over these 10 years. Ship sources contributed $\sim$10% to the total SO_2 and NO_x emissions in the coastal provinces of China. Emissions from the proposed Domestic Emission Control Areas (DECAs) within 12Nm constituted approximately 40% of the all ship emissions along the Chinese coast, and this percentage would double when the DECA boundary is extended to 100Nm. Ship emissions in ports accounted for about one-quarter of the total emissions within 200Nm, within which nearly 80% of the emissions were concentrated in the top 10 busiest ports of China. SO_2 emissions could be reduced by 80% in 2020 under a 0.5% global sulfur cap policy. In comparison, a similar reduction of NO_x emissions would require significant technological change and would likely take several decades. This study provides solid scientific support for ship emissions control policy making in China. It is suggested to investigate and monitor the emissions from the shipping sector in more detail in the future.

The atmospheric impacts of monoterpene ozonolysis on global stabilised Criegee intermediate budgets and SO_2 oxidation: experiment, theory and modelling

Mike J. Newland[1,3], Andrew R. Rickard[2,3], Tomás Sherwen[3], Mathew J. Evans[2,3],Luc Vereecken[4,5], Amalia Muñoz[6], Milagros Ródenas[6], and William J. Bloss[1]

Source : Atmosphere Chemistry and Physics, Volume 18, issue 8
02 May 2018

The gas-phase reaction of alkenes with ozone is known to produce stabilised Criegee intermediates (SCIs). These biradical/zwitterionic species have the potential to act as atmospheric oxidants for trace pollutants such as SO_2, enhancing the formation of sulfate aerosol with impacts on air quality and health, radiative transfer and climate. However, the importance of this chemistry is uncertain as a consequence of limited understanding of the abundance and atmospheric fate of SCIs. In this work we apply experimental, theoretical and numerical modelling methods to quantify the atmospheric impacts, abundance and fate of the structurally diverse SCIs derived from the ozonolysis of monoterpenes, the second most abundant group of unsaturated hydrocarbons in the atmosphere. We have investigated the removal of SO_2 by SCIs formed from the ozonolysis of three atmospherically important monoterpenes (α-pinene, β-pinene and limonene) in the presence of varying amounts of water vapour in large-scale simulation chamber experiments that are representative of boundary layer conditions. The SO_2 removal displays a clear dependence on water vapour concentration, but this dependence is not

linear across the range of $[H_2O]$ explored. At low $[H_2O]$ a strong dependence of SO_2 removal on $[H_2O]$ is observed, while at higher $[H_2O]$ this dependence becomes much weaker. This is interpreted as being caused by the production of a variety of structurally (and hence chemically) different SCIs in each of the systems studied, which displayed different rates of reaction with water and of unimolecular rearrangement or decomposition. The determined rate constants, $k(SCI+H_2O)$, for those SCIs that react primarily with H_2O range from 4 to $310 \times 10^{-15} cm^3 s^{-1}$. For those SCIs that predominantly react unimolecularly, determined rates range from 130 to $240 s^{-1}$. These values are in line with previous results for the (analogous) stereo-specific SCI system of *syn*-/*anti*-CH_3CHOO. The experimental results are interpreted through theoretical studies of the SCI unimolecular reactions and bimolecular reactions with H_2O, characterised for α-pinene and β-pinene at the M06-2X/aug-cc-pVTZ level of theory. The theoretically derived rates agree with the experimental results within the uncertainties. A global modelling study, applying the experimental results within the GEOS-Chem chemical transport model, suggests that >97% of the total monoterpene-derived global SCI burden is comprised of SCIs with a structure that determines that they react slowly with water and that their atmospheric fate is dominated by unimolecular reactions. Seasonally averaged boundary layer concentrations of monoterpene-derived SCIs reach up to $1.4 \times 10^4 cm^{-3}$ in regions of elevated monoterpene emissions in the tropics. Reactions of monoterpene-derived SCIs with SO_2 account for <1% globally but may account for up to 60% of the gas-phase SO_2 removal over areas of tropical forests, with significant localised impacts on the formation of sulfate aerosol and hence the lifetime and distribution of SO_2.

Key drivers of ozone change and its radiative forcing over the 21st century

Fernando Iglesias-Suarez[1,2,a], Douglas E. Kinnison[3], Alexandru Rap[4], Amanda C. Maycock[4],Oliver Wild[1,2], and Paul J. Young[1,2,5]

Source : Atmosphere Chemistry and Physics, Volume 18, issue 9

03 May 2018

Over the 21st century changes in both tropospheric and stratospheric ozone are likely to have important consequences for the Earth's radiative balance. In this study, we investigate the radiative forcing from future ozone changes using the Community Earth System Model (CESM1), with the Whole Atmosphere Community Climate Model (WACCM), and including fully coupled radiation and chemistry schemes. Using year 2100 conditions from the Representative Concentration Pathway 8.5 (RCP8.5) scenario, we quantify the individual contributions to ozone radiative forcing of (1) climate change, (2) reduced concentrations of ozone depleting substances (ODSs), and (3) methane increases. We calculate future ozone radiative forcings and their standard error (SE; associated with inter-annual variability of ozone) relative to year 2000 of (1) $33 \pm 104 mWm^{-2}$, (2) $163 \pm 109 mWm^{-2}$, and (3) $238 \pm 113 mWm^{-2}$ due to climate change, ODSs, and methane, respectively. Our best estimate of net ozone forcing in this set of simulations is $430 \pm 130 mWm^{-2}$ relative to year

2000 and 760±230mWm^{-2} relative to year 1750, with the 95% confidence interval given by ±30%. We find that the overall long-term tropospheric ozone forcing from methane chemistry–climate feedbacks related to OH and methane lifetime is relatively small (46mWm^{-2}). Ozone radiative forcing associated with climate change and stratospheric ozone recovery are robust with regard to background climate conditions, even though the ozone response is sensitive to both changes in atmospheric composition and climate. Changes in stratospheric-produced ozone account for ~50% of the overall radiative forcing for the 2000–2100 period in this set of simulations, highlighting the key role of the stratosphere in determining future ozone radiative forcing.

Impacts of air pollutants from fire and non-fire emissions on the regional air quality in Southeast Asia

Hsiang-He Lee[1], Oussama Iraqui[2], Yefu Gu[3], Steve Hung-Lam Yim[3], Apisada Chulakadabba[4],Adam Yiu-Ming Tonks[5], Zhengyu Yang[6], and Chien Wang[1,7]

Source : Atmosphere Chemistry and Physics, Volume 18, issue 9
03 May 2018.

Severe haze events in Southeast Asia caused by particulate pollution have become more intense and frequent in recent years. Widespread biomass burning occurrences and particulate pollutants from human activities other than biomass burning play important roles in degrading air quality in Southeast Asia. In this study, numerical simulations have been conducted using the Weather Research and Forecasting (WRF) model coupled with a chemistry component (WRF-Chem) to quantitatively examine the contributions of aerosols emitted from fire (i.e., biomass burning) versus non-fire (including fossil fuel combustion, and road dust, etc.) sources to the degradation of air quality and visibility over Southeast Asia. These simulations cover a time period from 2002 to 2008 and are driven by emissions from (a) fossil fuel burning only, (b) biomass burning only, and (c) both fossil fuel and biomass burning. The model results reveal that 39% of observed low-visibility days (LVDs) can be explained by either fossil fuel burning or biomass burning emissions alone, a further 20% by fossil fuel burning alone, a further 8% by biomass burning alone, and a further 5% by a combination of fossil fuel burning and biomass burning. Analysis of an 24h $PM_{2.5}$ air quality index (AQI) indicates that the case with coexisting fire and non-fire $PM_{2.5}$ can substantially increase the chance of AQI being in the moderate or unhealthy pollution level from 23 to 34%. The premature mortality in major Southeast Asian cities due to degradation of air quality by particulate pollutants is estimated to increase from ~4110 per year in 2002 to ~6540 per year in 2008. In addition, we demonstrate the importance of certain missing non-fire anthropogenic aerosol sources including anthropogenic fugitive and industrial dusts in causing urban air quality degradation. An experiment of using machine learning algorithms to forecast the occurrence of haze events in Singapore is also explored in this study. All of these results suggest that besides minimizing biomass burning

activities, an effective air pollution mitigation policy for Southeast Asia needs to consider controlling emissions from non-fire anthropogenic sources.

An automated cirrus classification

Edward Gryspeerdt[1,2], Johannes Quaas[2], Tom Goren[2], Daniel Klocke[3], and Matthias Brueck[4]

Source : Atmosphere Chemistry and Physics, Volume 18, issue 9
03 May 2018

Cirrus clouds play an important role in determining the radiation budget of the earth, but many of their properties remain uncertain, particularly their response to aerosol variations and to warming. Part of the reason for this uncertainty is the dependence of cirrus cloud properties on the cloud formation mechanism, which itself is strongly dependent on the local meteorological conditions.

In this work, a classification system (Identification and Classification of Cirrus or IC-CIR) is introduced to identify cirrus clouds by the cloud formation mechanism. Using reanalysis and satellite data, cirrus clouds are separated into four main types: orographic, frontal, convective and synoptic. Through a comparison to convection-permitting model simulations and back-trajectory-based analysis, it is shown that these observation-based regimes can provide extra information on the cloud-scale updraughts and the frequency of occurrence of liquid-origin ice, with the convective regime having higher updraughts and a greater occurrence of liquid-origin ice compared to the synoptic regimes. Despite having different cloud formation mechanisms, the radiative properties of the regimes are not distinct, indicating that retrieved cloud properties alone are insufficient to completely describe them.

This classification is designed to be easily implemented in GCMs, helping improve future model–observation comparisons and leading to improved parametrisations of cirrus cloud processes.

Secondary organic aerosol production from pinanediol, a semi-volatile surrogate for first-generation oxidation products of monoterpenes

Penglin Ye[1,a,b], Yunliang Zhao[1], Wayne K. Chuang[1], Allen L. Robinson[1], and Neil M. Donahue[1]

Source: Atmosphere Chemistry and Physics, Volume 18, issue 9
03 May 2018.

We have investigated the production of secondary organic aerosol (SOA) from pinanediol (PD), a precursor chosen as a semi-volatile surrogate for first-generation oxidation products of monoterpenes. Observations at the CLOUD facility at CERN have shown that oxidation of organic compounds such as PD can be an important contributor to new-particle formation. Here we focus on SOA mass yields and chemical composition from PD photo-oxidation in the CMU smog chamber. To determine the SOA mass yields from this semi-volatile precursor, we had to address partitioning of both the PD and its oxidation products to the chamber walls. After correcting for these losses, we found OA loading dependent SOA mass yields from PD oxidation that ranged between 0.1 and 0.9 for SOA concentrations between 0.02 and 20μgm^{-3}, these mass yields are 2–3 times larger than typical of much more volatile monoterpenes. The average carbon oxidation state measured with an aerosol mass spectrometer was around −0.7. We modeled the chamber data using a dynamical two-dimensional volatility basis set and found that a significant fraction of the SOA comprises low-volatility organic compounds that could drive new-particle formation and growth, which is consistent with the CLOUD observations.

Advanced source apportionment of carbonaceous aerosols by coupling offline AMS and radiocarbon size-segregated measurements over a nearly 2-year period

Athanasia Vlachou[1], Kaspar R. Daellenbach[1], Carlo Bozzetti[1], Benjamin Chazeau[2],Gary A. Salazar[3], Soenke Szidat[3], Jean-Luc Jaffrezo[4], Christoph Hueglin[5], Urs Baltensperger[1],Imad El Haddad[1], and André S. H. Prévôt[1]

Source: Atmosphere Chemistry and Physics, Volume 18, issue 9

03 May 2018

Carbonaceous aerosols are related to adverse human health effects. Therefore, identification of their sources and analysis of their chemical composition is important. The offline AMS (aerosol mass spectrometer) technique offers quantitative separation of organic aerosol (OA) factors which can be related to major OA sources, either primary or secondary. While primary OA can be more clearly separated into sources, secondary (SOA) source apportionment is more challenging because different sources – anthropogenic or natural, fossil or non-fossil – can yield similar highly oxygenated mass spectra. Radiocarbon measurements provide unequivocal separation between fossil and non-fossil sources of carbon. Here we coupled these two offline methods and analysed the OA and organic carbon (OC) of different size fractions (particulate matter below 10 and 2.5μm – PM_{10} and $PM_{2.5}$, respectively) from the Alpine valley of Magadino (Switzerland) during the years 2013 and 2014 (219 samples). The combination of the techniques gave further insight into the characteristics of secondary OC (SOC) which was rather based on the type of SOC precursor and not on the volatility or the oxidation state of OC, as typically considered. Out of the primary sources separated in this study, biomass burning OC was

the dominant one in winter, with average concentrations of 5.36±2.64μgm^{-3} for PM_{10} and 3.83±1.81μgm^{-3} for $PM_{2.5}$, indicating that wood combustion particles were predominantly generated in the fine mode. The additional information from the size-segregated measurements revealed a primary sulfur-containing factor, mainly fossil, detected in the coarse size fraction and related to non-exhaust traffic emissions with a yearly average PM_{10}($PM_{2.5}$) concentration of 0.20±0.24μgm^{-3} (0.05±0.04μgm^{-3}). A primary biological OC (PBOC) was also detected in the coarse mode peaking in spring and summer with a yearly average PM_{10} ($PM_{2.5}$) concentration of 0.79±0.31μgm^{-3} (0.24±0.20μgm^{-3}). The secondary OC was separated into two oxygenated, non-fossil OC factors which were identified based on their seasonal variability (i.e. summer and winter oxygenated organic carbon, OOC) and a third anthropogenic OOC factor which correlated with fossil OC mainly peaking in winter and spring, contributing on average 13%±7% (10%±9%) to the total OC in PM_{10} ($PM_{2.5}$). The winter OOC was also connected to anthropogenic sources, contributing on average 13%±13% (6%±6%) to the total OC in PM_{10} ($PM_{2.5}$). The summer OOC (SOOC), stemming from oxidation of biogenic emissions, was more pronounced in the fine mode, contributing on average 43%±12% (75%±44%) to the total OC in PM_{10} ($PM_{2.5}$). In total the non-fossil OC significantly dominated the fossil OC throughout all seasons, by contributing on average 75%±24% to the total OC. The results also suggested that during the cold period the prevailing source was residential biomass burning while during the warm period primary biological sources and secondary organic aerosol from the oxidation of biogenic emissions became important. However, SOC was also formed by aged fossil fuel combustion emissions not only in summer but also during the rest of the year.

Sources of reactive nitrogen in marine aerosol over the Northwest Pacific Ocean in spring

Li Luo[1,3], Shuh-Ji Kao[2], Hongyan Bao[2], Huayun Xiao[1,3], Hongwei Xiao[1,3], Xiaohong Yao[4],Huiwang Gao[4], Jiawei Li[5], and Yangyang Lu[2]

Source : Atmosphere Chemistry and Physics, Volume 18, issue 9
03 May 2018.

Atmospheric deposition of long-range transport of anthropogenic reactive nitrogen (N_r, mainly comprised of NH_x, NO_y and water-soluble organic nitrogen, WSON) from continents may have profound impact on marine biogeochemistry. In addition, surface ocean dissolved organic nitrogen (DON) may also contribute to aerosol WSON in the overlying atmosphere. Despite the importance of off-continent dispersion and N_r interactions at the atmosphere–ocean boundary, our knowledge of the sources of various nitrogen species in the atmosphere over the open ocean remains limited due to insufficient observations. We conducted two cruises in the spring of 2014 and 2015 from the coast of China through the East China seas (ECSs, i.e. the Yellow Sea and East China Sea) to the open ocean (i.e. the Northwest Pacific Ocean, NWPO). Concentrations of water-soluble total nitrogen (WSTN), NO_3^- and NH_4^+, as well as the $\delta^{15}N$ of WSTN and NO_3^- in marine aerosol, were measured

during both cruises. In the spring of 2015, we also analysed the concentrations and $\delta^{15}N$ of $NO_3^-$and the DON of surface seawater (SSW; at a depth of 5m) along the cruise track. Aerosol NO_3^-, NH_4^+ and WSON decreased logarithmically (1–2 orders of magnitude) with distance from the shore, reflecting strong anthropogenic emission sources of NO_3^-, NH_4^+ and WSON in China. Average aerosol NO_3^- and NH_4^+ concentrations were significantly higher in 2014 (even in the remote NWOP) than in 2015 due to the stronger wind field in 2014, underscoring the role of the Asian winter monsoon in the seaward transport of anthropogenic NO_3^- and NH_4^+. However, the background aerosol WSON over the NWPO in 2015 (13.3±8.5nmolm^{-3}) was similar to that in 2014 (12.2±6.3nmolm^{-3}), suggesting an additional non-anthropogenic WSON source in the open ocean. Obviously, marine DON emissions should be considered in model and field assessments of net atmospheric WSON deposition in the open ocean. This study contributes information on parallel isotopic marine DON composition and aerosol N_r datasets, but more research is required to explore complex N_r sources and deposition processes in order to advance our understanding of anthropogenic influences on the marine nitrogen cycle and nitrogen exchange at land–ocean and atmosphere–ocean interfaces.

On ozone trend detection: using coupled chemistry–climate simulations to investigate early signs of total column ozone recovery

James Keeble[1], Hannah Brown[1], N. Luke Abraham[1,2], Neil R. P. Harris[3], and John A. Pyle[1,2]

Source: Atmosphere Chemistry and Physics, Volume 18, issue 10
01 Jun 2018

Total column ozone values from an ensemble of UM-UKCA model simulations are examined to investigate different definitions of progress on the road to ozone recovery. The impacts of modelled internal atmospheric variability are accounted for by applying a multiple linear regression model to modelled total column ozone values, and ozone trend analysis is performed on the resulting ozone residuals. Three definitions of recovery are investigated: (i) a slowed rate of decline and the date of minimum column ozone, (ii) the identification of significant positive trends and (iii) a return to historic values. A return to past thresholds is the last state to be achieved. Minimum column ozone values, averaged from 60°S to 60°N, occur between 1990 and 1995 for each ensemble member, driven in part by the solar minimum conditions during the 1990s. When natural cycles are accounted for, identification of the year of minimum ozone in the resulting ozone residuals is uncertain, with minimum values for each ensemble member occurring at different times between 1992 and 2000. As a result of this large variability, identification of the date of minimum ozone constitutes a poor measure of ozone recovery. Trends for the 2000–2017 period are positive at most latitudes and are statistically significant in the mid-latitudes in both hemispheres when natural cycles are accounted for. This significance results largely from

the large sample size of the multi-member ensemble. Significant trends cannot be identified by 2017 at the highest latitudes, due to the large interannual variability in the data, nor in the tropics, due to the small trend magnitude, although it is projected that significant trends may be identified in these regions soon thereafter. While significant positive trends in total column ozone could be identified at all latitudes by ~2030, column ozone values which are lower than the 1980 annual mean can occur in the mid-latitudes until ~2050, and in the tropics and high latitudes deep into the second half of the 21st century.

Impact of high-resolution a priori profiles on satellite-based formaldehyde retrievals

Si-Wan Kim[1,2,3], Vijay Natraj[4], Seoyoung Lee[3], Hyeong-Ahn Kwon[5], Rokjin Park[5],Joost de Gouw[1,2], Gregory Frost[1], Jhoon Kim[3], Jochen Stutz[6], Michael Trainer[1], Catalina Tsai[6],and Carsten Warneke[1,2]

Source: Atmosphere Chemistry and Physics, Volume 18, issue 10
01 Jun 2018

Formaldehyde (HCHO) is either directly emitted from sources or produced during the oxidation of volatile organic compounds (VOCs) in the troposphere. It is possible to infer atmospheric HCHO concentrations using space-based observations, which may be useful for studying emissions and tropospheric chemistry at urban to global scales depending on the quality of the retrievals. In the near future, an unprecedented volume of satellite-based HCHO measurement data will be available from both geostationary and polar-orbiting platforms. Therefore, it is essential to develop retrieval methods appropriate for the next-generation satellites that measure at higher spatial and temporal resolution than the current ones. In this study, we examine the importance of fine spatial and temporal resolution a priori profile information on the retrieval by conducting approximately 45000 radiative transfer (RT) model calculations in the Los Angeles Basin (LA Basin) megacity. Our analyses suggest that an air mass factor (AMF, a factor converting observed slant columns to vertical columns) based on fine spatial and temporal resolution a priori profiles can better capture the spatial distributions of the enhanced HCHO plumes in an urban area than the nearly constant AMFs used for current operational products by increasing the columns by ~50% in the domain average and up to 100% at a finer scale. For this urban area, the AMF values are inversely proportional to the magnitude of the HCHO mixing ratios in the boundary layer. Using our optimized model HCHO results in the Los Angeles Basin that mimic the HCHO retrievals from future geostationary satellites, we illustrate the

effectiveness of HCHO data from geostationary measurements for understanding and predicting tropospheric ozone and its precursors.

Assessing the impact of the Kuroshio Current on vertical cloud structure using CloudSat data

Akira Yamauchi[1], Kazuaki Kawamoto[1], Atsuyoshi Manda[1,2], and Jiming Li[3]

Source : Atmosphere Chemistry and Physics, Volume 18, issue 10
01 Jun 2018.

This study analyzed CloudSat satellite data to determine how the warm ocean Kuroshio Current affects the vertical structure of clouds. Rainfall intensity around the middle troposphere (6km in height) over the Kuroshio was greater than that over surrounding areas. The drizzle clouds over the Kuroshio have a higher frequency of occurrence of geometrically thin (0.5–3km) clouds and thicker (7–10km) clouds compared to those around the Kuroshio. Moreover, the frequency of occurrence of precipitating clouds with a geometric thickness of 7 to 10km increased over the Kuroshio. Stronger updrafts over the Kuroshio maintain large droplets higher in the upper part of the cloud layer, and the maximum radar reflectivity within a cloud layer in non-precipitating and drizzle clouds over the Kuroshio is higher than that around the Kuroshio.

Strong impacts on aerosol indirect effects from historical oxidant changes

Inger Helene Hafsahl Karset[1], Terje Koren Berntsen[1,2], Trude Storelvmo[1], Kari Alterskjær[2],Alf Grini[3], Dirk Olivié[3], Alf Kirkevåg[3], Øyvind Seland[3], Trond Iversen[3], and Michael Schulz[3]

Source: Atmosphere Chemistry and Physics, Volume 18, issue 10
01 Jun 2018.

Uncertainties in effective radiative forcings through aerosol–cloud interactions (ERF_{aci}, also called aerosol indirect effects) contribute strongly to the uncertainty in the total preindustrial-to-present-day anthropogenic forcing. Some forcing estimates of the total aerosol indirect effect are so negative that they even offset the greenhouse gas forcing. This

study highlights the role of oxidants in modeling of preindustrial-to-present-day aerosol indirect effects. We argue that the aerosol precursor gases should be exposed to oxidants of its era to get a more correct representation of secondary aerosol formation. Our model simulations show that the total aerosol indirect effect changes from −1.32 to $-1.07 Wm^{-2}$ when the precursor gases in the preindustrial simulation are exposed to preindustrial instead of present-day oxidants. This happens because of a brightening of the clouds in the preindustrial simulation, mainly due to large changes in the nitrate radical (NO_3). The weaker oxidative power of the preindustrial atmosphere extends the lifetime of the precursor gases, enabling them to be transported higher up in the atmosphere and towards more remote areas where the susceptibility of the cloud albedo to aerosol changes is high. The oxidation changes also shift the importance of different chemical reactions and produce more condensate, thus increasing the size of the aerosols and making it easier for them to activate as cloud condensation nuclei.

Particle and VOC emission factor measurements for anthropogenic sources in West Africa

Sekou Keita[1], Cathy Liousse[2], Véronique Yoboué[1], Pamela Dominutti[3], Benjamin Guinot[2],Eric-Michel Assamoi[1], Agnès Borbon[3], Sophie L. Haslett[4], Laetitia Bouvier[3], Aurélie Colomb[3],Hugh Coe[4], Aristide Akpo[5], Jacques Adon[2], Julien Bahino[1], Madina Doumbia[1], Julien Djossou[5],Corinne Galy-Lacaux[2], Eric Gardrat[2], Sylvain Gnamien[1], Jean F. Léon[2], Money Ossohou[1],E. Touré N'Datchoh[1], and Laurent Roblou[2]

Source: Atmosphere Chemistry and Physics, Volume 18, issue 10
01 Jun 2018.

A number of campaigns have been carried out to establish the emission factors of pollutants from fuel combustion in West Africa, as part of work package 2 (Air Pollution and Health) of the DACCIWA (Dynamics-Aerosol-Chemistry-Cloud Interactions in West Africa) FP7 program. Emission sources considered here include wood (hevea and iroko) and charcoal burning, charcoal making, open trash burning, and vehicle emissions, including trucks, cars, buses and two-wheeled vehicles. Emission factors of total particulate matter (TPM), elemental carbon (EC), primary organic carbon (OC) and volatile organic compounds (VOCs) have been established. In addition, emission factor measurements were performed in combustion chambers in order to reproduce field burning conditions for a tropical hardwood (hevea), and obtain particulate emission factors by size ($PM_{0.25}$, PM_1, $PM_{2.5}$ and PM_{10}). Particle samples were collected on quartz fiber filters and analyzed using gravimetric method for TPM and thermal methods for EC and OC. The emission factors of 58 VOC species were determined using offline sampling on a sorbent tube. Emission factor

results for two species of tropical hardwood burning of EC, OC and TPM are 0.98±0.46gkg^{-1} of fuel burned (gkg^{-1}), 11.05±4.55 and 41.12±24.62gkg^{-1}, respectively. For traffic sources, the highest emission factors among particulate species are found for the two-wheeled vehicles with two-stroke engines (2.74gkg^{-1} fuel for EC, 65.11gkg^{-1} fuel for OC and 496gkg^{-1} fuel for TPM). The largest VOC emissions are observed for two-stroke two-wheeled vehicles, which are up to 3 times higher than emissions from light-duty and heavy-duty vehicles. Isoprene and monoterpenes, which are usually associated with biogenic emissions, are present in almost all anthropogenic sources investigated during this work and could be as significant as aromatic emissions in wood burning (1gkg^{-1} fuel). EC is primarily emitted in the ultrafine fraction, with 77% of the total mass being emitted as particles smaller than 0.25µm. The particles and VOC emission factors obtained in this study are generally higher than those in the literature whose values are discussed in this paper. This study underlines the important role of in situ measurements in deriving realistic and representative emission factors.

How much of the global aerosol optical depth is found in the boundary layer and free troposphere?

Quentin Bourgeois[1,a], Annica M. L. Ekman[1], Jean-Baptiste Renard[2], Radovan Krejci[3],Abhay Devasthale[4], Frida A.-M. Bender[1], Ilona Riipinen[3], Gwenaël Berthet[2], and Jason L. Tackett[5]

Source: Atmosphere Chemistry and Physics, Volume 18, issue 10
01 Jun 2018.

The global aerosol extinction from the CALIOP space lidar was used to compute aerosol optical depth (AOD) over a 9-year period (2007–2015) and partitioned between the boundary layer (BL) and the free troposphere (FT) using BL heights obtained from the ERA-Interim archive. The results show that the vertical distribution of AOD does not follow the diurnal cycle of the BL but remains similar between day and night highlighting the presence of a residual layer during night. The BL and FT contribute 69 and 31%, respectively, to the global tropospheric AOD during daytime in line with observations obtained in Aire sur l'Adour (France) using the Light Optical Aerosol Counter (LOAC) instrument. The FT AOD contribution is larger in the tropics than at mid-latitudes which indicates that convective transport largely controls the vertical profile of aerosols. Over oceans, the FT AOD contribution is mainly governed by long-range transport of aerosols from emission sources located within neighboring continents. According to the CALIOP aerosol classification, dust and smoke particles are the main aerosol types transported into the FT. Overall, the study shows that the fraction of AOD in the FT – and thus potentially located above low-level clouds – is substantial and deserves more attention when

evaluating the radiative effect of aerosols in climate models. More generally, the results have implications for processes determining the overall budgets, sources, sinks and transport of aerosol particles and their description in atmospheric models.

Future changes in the stratosphere-to-troposphere ozone mass flux and the contribution from climate change and ozone recovery

Stefanie Meul[1], Ulrike Langematz[1], Philipp Kröger[1], Sophie Oberländer-Hayn[1], and Patrick Jöckel[2]

Source: Atmosphere Chemistry and Physics, Volume 18, issue 10
01 Jun 2018.

Using a state-of-the-art chemistry–climate model we investigate the future change in stratosphere–troposphere exchange (STE) of ozone, the drivers of this change, as well as the future distribution of stratospheric ozone in the troposphere. Supplementary to previous work, our focus is on changes on the monthly scale. The global mean annual influx of stratospheric ozone into the troposphere is projected to increase by 53% between the years 2000 and 2100 under the RCP8.5 greenhouse gas scenario. The change in ozone mass flux (OMF) into the troposphere is positive throughout the year with maximal increase in the summer months of the respective hemispheres. In the Northern Hemisphere (NH) this summer maximum STE increase is a result of increasing greenhouse gas (GHG) concentrations, whilst in the Southern Hemisphere(SH) it is due to equal contributions from decreasing levels of ozone depleting substances (ODS) and increasing GHG concentrations. In the SH the GHG effect is dominating in the winter months. A large ODS-related ozone increase in the SH stratosphere leads to a change in the seasonal breathing term which results in a future decrease of the OMF into the troposphere in the SH in September and October. The resulting distributions of stratospheric ozone in the troposphere differ for the GHG and ODS changes due to the following: (a) ozone input occurs at different regions for GHG- (midlatitudes) and ODS-changes (high latitudes); and (b) stratospheric ozone is more efficiently mixed towards lower tropospheric levels in the case of ODS changes, whereas tropospheric ozone loss rates grow when GHG concentrations rise. The comparison between the moderate RCP6.0 and the extreme RCP8.5 emission scenarios reveals that the annual global OMF trend is smaller in the moderate scenario, but the resulting change in the contribution of ozone with stratospheric origin (O3s) to ozone in the troposphere is of comparable magnitude in both scenarios. This is due to the larger tropospheric ozone precursor emissions and hence ozone production in the RCP8.5 scenario.

Comparison of the optical depth of total ozone and atmospheric aerosols in Poprad-Gánovce, Slovakia

Peter Hrabčák

Source: Atmosphere Chemistry and Physics, Volume 18, issue 10
01 Jun 2018.

The amount of ultraviolet solar radiation reaching the Earth's surface is significantly affected by atmospheric ozone along with aerosols. The present paper is focused on a comparison of the total ozone and atmospheric aerosol optical depth in the area of Poprad-Gánovce, which is situated at the altitude of 706m a. s. l. in the vicinity of the highest mountain in the Carpathian mountains. The direct solar ultraviolet radiation has been measured here continuously since August 1993 using a Brewer MKIV ozone spectrophotometer. These measurements have been used to calculate the total amount of atmospheric ozone and, subsequently, its optical depth. They have also been used to determine the atmospheric aerosol optical depth (AOD) using the Langley plot method. Results obtained by this method were verified by means of comparison with a method that is part of the Brewer operating software, as well as with measurements made by a Cimel sun photometer. Diffuse radiation, the stray-light effect and polarization corrections were applied to calculate the AOD using the Langley plot method. In this paper, two factors that substantially attenuate the flow of direct ultraviolet solar radiation to the Earth's surface are compared. The paper presents results for 23 years of measurements, namely from 1994 to 2016. Values of optical depth were determined for the wavelengths of 306.3, 310, 313.5, 316.8 and 320nm. A statistically significant decrease in the total optical depth of the atmosphere was observed with all examined wavelengths. Its root cause is the statistically significant decline in the optical depth of aerosols.

Stable sulfur isotope measurements to trace the fate of SO_2 in the Athabasca oil sands region

Neda Amiri[1], Roghayeh Ghahremaninezhad[2], Ofelia Rempillo[3], Travis W. Tokarek[4],Charles A. Odame-Ankrah[4,a], Hans D. Osthoff[4], and Ann-Lise Norman[1]

Source : Atmosphere Chemistry and Physics, Volume 18, issue 11
04 Jun 2018

Concentrations and $\delta^{34}S$ values for SO_2 and size-segregated sulfate aerosols were determined for air monitoring station 13 (AMS 13) at Fort MacKay in the Athabasca oil sands region, northeastern Alberta, Canada as part of the Joint Canada-Alberta Implementation Plan for Oil Sands Monitoring (JOSM) campaign from 13 August to 5 September 2013. Sulfate aerosols and SO_2 were collected on filters using a high-volume sampler, with 12 or 24h time intervals.

Sulfur dioxide (SO_2) enriched in ^{34}S was exhausted by a chemical ionization mass spectrometer (CIMS) operated at the measurement site and affected isotope samples for a portion of the sampling period. It was realized that this could be a useful tracer and samples collected were divided into two sets. The first set includes periods when the CIMS was not running (CIMS-OFF) and no $^{34}SO_2$ was emitted. The second set is for periods when the CIMS was running (CIMS-ON) and $^{34}SO_2$ was expected to affect SO_2 and sulfate high-volume filter samples.

$\delta^{34}S$ values for sulfate aerosols with diameter $D > 0.49$μm during CIMS-OFF periods (no tracer $^{34}SO_2$ present) indicate the sulfur isotope characteristics of secondary sulfate in the region. Such aerosols had $\delta^{34}S$ values that were isotopically lighter (down to −5.3‰) than what was expected according to potential sulfur sources in the Athabasca oil sands region (+3.9 to +11.5‰). Lighter $\delta^{34}S$ values for larger aerosol size fractions are contrary to expectations for primary unrefined sulfur from untreated oil sands (+6.4‰) mixed with secondary sulfate from SO_2 oxidation and accompanied by isotope fractionation in gas phase reactions with OH or the aqueous phase by H_2O_2 or O_3. Furthermore, analysis of ^{34}S enhancements of sulfate and SO_2 during CIMS-ON periods indicated rapid oxidation of SO_2 from this local source at ground level on the surface of aerosols before reaching the high-volume sampler or on the collected aerosols on the filters in the high-volume sampler. Anti-correlations between $\delta^{34}S$ values of dominantly secondary sulfate aerosols with $D < 0.49$μm and the concentrations of Fe and Mn ($r = -0.80$ and $r = -0.76$, respectively) were observed, suggesting that SO_2 was oxidized by a transition metal ion (TMI) catalyzed pathway involving O_2 and Fe^{3+} and/or Mn^{2+}, an oxidation pathway known to favor lighter sulfur isotopes.

Correlations between SO_2 to sulfate conversion ratio ($F(s)$) and the concentrations of α-pinene ($r = 0.85$), β-pinene ($r = 0.87$), and limonene ($r = 0.82$) during daytime suggests that SO_2 oxidation by Criegee biradicals may be a potential oxidation pathway in the study region.

Secondary aerosol formation promotes water uptake by organic-rich wildfire haze particles in equatorial Asia

Jing Chen[1], Sri Hapsari Budisulistiorini[1], Takuma Miyakawa[2], Yuichi Komazaki[2],and Mikinori Kuwata[1,3,4]

Source : Atmosphere Chemistry and Physics, Volume 18, issue 11
04 Jun 2018

The diameter growth factor (GF) of 100nm haze particles at 85% relative humidity (RH) and their chemical characteristics were simultaneously monitored at Singapore in October 2015 during a pervasive wildfire haze episode that was caused by peatland burning in Indonesia. Non-refractory submicron particles (NR-PM_1) were dominated by organics (OA; approximating 77.1% in total mass), whereas sulfate was the most abundant inorganic constituent (11.7% on average). A statistical analysis of the organic mass spectra showed that most organics (36.0% of NR-PM_1 mass) were highly oxygenated. Diurnal variations of GF, number fractions of more hygroscopic mode particles, mass fractions of sulfate, and mass fractions of oxygenated organics (OOA) synchronized well, peaking during the day. The mean hygroscopicity parameter (κ) of the haze particles was 0.189±0.087, and the mean κ values of organics were 0.157±0.108 (κ_{org}, bulk organics) and 0.266±0.184 (κ_{OOA}, OOA), demonstrating the important roles of both sulfate and highly oxygenated organics in the hygroscopic growth of organics-dominated wildfire haze particles. κ_{org} correlated with the water-soluble organic fraction insignificantly, but it positively correlated with f_{44} (fraction of the ion fragment at m/z44 in total organics) (R = 0.70), implying the oxygenation degree of organics could be more critical for the water uptake of organic compounds. These results further suggest the importance of sulfate and secondary organic aerosol formation in promoting the hygroscopic growth of wildfire haze particles. Further detailed size-resolved as well as molecular-level chemical information about organics is necessary for the profound exploration of water uptake by wildfire haze particles in equatorial Asia.

Direct radiative effects during intense Mediterranean desert dust outbreaks

Antonis Gkikas[1,2], Vincenzo Obiso[2], Carlos Pérez García-Pando[2], Oriol Jorba[2],Nikos Hatzianastassiou[3], Lluis Vendrell[2], Sara Basart[2], Stavros Solomos[1], Santiago Gassó[4],and José Maria Baldasano[2,4]

Source: Atmosphere Chemistry and Physics, Volume 18, issue 12
21 Jun 2018.

The direct radiative effect (DRE) during 20 intense and widespread dust outbreaks, which affected the broader Mediterranean basin over the period March 2000–February 2013, has been calculated with the NMMB-MONARCH model at regional (Sahara and European continent) and short-term temporal (84h) scales. According to model simulations, the maximum dust aerosol optical depths (AODs) range from ~ 2.5 to ~ 5.5 among the identified cases. At midday, dust outbreaks locally induce a NET (shortwave plus longwave) strong atmospheric warming (DRE_{ATM} values up to $285 Wm^{-2}$; Niger–Chad; dust AODs up to ~ 5.5) and a strong surface cooling ($DRE_{NETSURF}$values down to $-337 Wm^{-2}$), whereas they strongly reduce the downward radiation at the ground level (DRE_{SURF} values down to $-589 Wm^{-2}$ over the Eastern Mediterranean, for extremely high dust AODs, 4.5–5). During night-time, reverse effects of smaller magnitude are found. At the top of the atmosphere (TOA), positive (planetary warming) DREs up to $85 Wm^{-2}$ are found over highly reflective surfaces (Niger–Chad; dust AODs up to ~ 5.5) while negative (planetary cooling) DREs down to $-184 Wm^{-2}$ (Eastern Mediterranean; dust AODs 4.5–5) are computed over dark surfaces at noon. Dust outbreaks significantly affect the mean regional radiation budget, with NET DREs ranging from −8.5 to $0.5 Wm^{-2}$, from −31.6 to $2.1 Wm^{-2}$, from −22.2 to $2.2 Wm^{-2}$ and from −1.7 to $20.4 Wm^{-2}$ for TOA, SURF, NETSURF and ATM, respectively. Although the shortwave DREs are larger than the longwave ones, the latter are comparable or even larger at TOA, particularly over the Sahara at midday. As a response to the strong surface day-time cooling, dust outbreaks cause a reduction in the regional sensible and latent heat fluxes by up to 45 and $4 Wm^{-2}$, respectively, averaged over land areas of the simulation domain. Dust outbreaks reduce the temperature at 2m by up to 4K during day-time, whereas a reverse tendency of similar magnitude is found during night-time. Depending on the vertical distribution of dust loads and time, mineral particles heat (cool) the atmosphere by up to 0.9K (0.8K) during day-time (night-time) within atmospheric dust layers. Beneath and above the dust clouds, mineral particles cool (warm) the atmosphere by up to 1.3K (1.2K) at noon (night-time). On a regional mean basis, negative feedbacks on the total emitted dust (reduced by 19.5%) and dust AOD (reduced by 6.9%) are found

when dust interacts with the radiation. Through the consideration of dust radiative effects in numerical simulations, the model positive and negative biases for the downward surface SW or LW radiation, respectively, with respect to Baseline Surface Radiation Network (BSRN) measurements, are reduced. In addition, they also reduce the model near-surface (at 2m) nocturnal cold biases by up to 0.5K (regional averages), as well as the model warm biases at 950 and 700hPa, where the dust concentration is maximized, by up to 0.4K. However, improvements are relatively small and do not happen in all episodes because other model first-order errors may dominate over the expected improvements, and the misrepresentation of the dust plumes' spatiotemporal features and optical properties may even produce a double penalty effect. The enhancement of dust forecasts via data assimilation techniques may significantly improve the results.

A statistical examination of the effects of stratospheric sulfate geoengineering on tropical storm genesis

Qin Wang[1], John C. Moore[1,2,3], and Duoying Ji[1]

Source: Atmosphere Chemistry and Physics, Volume 18, issue 13
02 Jul 2018.

The thermodynamics of the ocean and atmosphere partly determine variability in tropical cyclone (TC) number and intensity and are readily accessible from climate model output, but an accurate description of TC variability requires much higher spatial and temporal resolution than the models used in the GeoMIP (Geoengineering Model Intercomparison Project) experiments provide. The genesis potential index (GPI) and ventilation index (VI) are combinations of dynamic and thermodynamic variables that provide proxies for TC activity under different climate states. Here we use five CMIP5 models that have run the RCP4.5 experiment and the GeoMIP stratospheric aerosol injection (SAI) G4 experiment to calculate the two TC indices over the 2020 to 2069 period across the six ocean basins that generate TCs. GPI is consistently and significantly lower under G4 than RCP4.5 in five out of six ocean basins, but it increases under G4 in the South Pacific. The models project potential intensity and relative humidity to be the dominant variables affecting GPI. Changes in vertical wind shear are significant, but it is correlated with relative humidity, though with different relations across both models and ocean basins. We find that tropopause temperature is not a useful addition to sea surface temperature (SST) in projecting TC genesis, perhaps because the earth system models (ESMs) vary in their simulation of the various upper-tropospheric changes induced by the aerosol injection.

Harmonisation and trends of 20-year tropical tropospheric ozone data

Elpida Leventidou[1], Mark Weber[1], Kai-Uwe Eichmann[1], John P. Burrows[1], Klaus-Peter Heue[2],Anne M. Thompson[3], and Bryan J. Johnson[4]

Source: Atmosphere Chemistry and Physics, Volume 18, issue 13
03 Jul 2018.

Using a convective-cloud differential (CCD) method, developed in-house and applied to retrievals of total ozone and cloud data from three European satellite instruments (viz. GOME/ERS-2, 1995–2003; SCIAMACHY/Envisat, 2002–2012 and GOME-2/MetOp-A, 2007–2015), monthly mean tropical tropospheric columns of ozone (TTCO) have been retrieved, which are in good agreement with ozonesondes (biases less than 6DU). As small differences in TTCO between the individual instruments were evident, it was necessary to develop a scheme to harmonise the three datasets into one consistent time series starting from 1996 until 2015. Correction offsets (biases) between the instruments using SCIAMACHY as intermediate reference have been calculated and six different harmonisation or merging scenarios have been evaluated. Depending on the merging approach, the magnitude, pattern and uncertainty in the trends strongly vary. The harmonisation or merging represents an additional source of uncertainty in the trends (2DUdecade^{-1} on average, in most of the cases exceeding the uncertainty from the regression). For studying further details on tropospheric ozone trends on various spatial scales in the tropics, we stick with one preferred merged dataset that shows best agreement with ozonesondes. In this merged dataset, no correction was applied for GOME, and mean biases with respect to SCIAMACHY in the overlapping period (2007–2012) were calculated and applied for GOME-2 in each grid box (2.5° × 5°). In contrast with other studies we found that the tropospheric trend averaged over the tropics (−15°S to 15°N) is not statistically significant. The mean tropospheric ozone trend equals −0.2±0.6DUdecade^{-1} (2σ). Regionally, tropospheric ozone has a statistically significant increase of ∼3DUdecade^{-1} over southern Africa (∼1.5%yr^{-1}), the southern tropical Atlantic (∼1.5%yr^{-1}), southeastern tropical Pacific Ocean (∼1%yr^{-1}), and central Oceania (∼2%yr^{-1}) and by ∼2DUdecade^{-1} over central Africa (2–2.5%yr^{-1}) and south India (∼1.5%yr^{-1}). On the other hand, tropospheric O_3 decreases by ∼3DUdecade^{-1} over the Caribbean Sea and parts of the North Pacific Ocean (∼2%yr^{-1}), and by less than 2DUdecade^{-1} over some regions of the southern Pacific and Indian oceans (∼0.5–1%yr^{-1}).

Morphological features and mixing states of soot-containing particles in the marine boundary layer over the Indian and Southern oceans

Sayako Ueda[1], Kazuo Osada[1], Keiichiro Hara[2], Masanori Yabuki[3], Fuminori Hashihama[4],and Jota Kanda[4]

Source : Atmosphere Chemistry and Physics, Volume 18, issue 13
03 Jul 2018

Mixing states of soot-containing aerosol particles constitute important information for the simulation of climatic effects of black carbon in the atmosphere. To elucidate the mixing states and morphological features of soot-containing particles over remote oceans, we conducted on-board observations over the southern Indian Ocean and the Southern Ocean during the TR/V *Umitaka-maru UM-08-09*cruise, which started from Benoa, Indonesia, on 1 December 2008 via Cape Town, South Africa, and which terminated in Fremantle, Australia, on 6 February 2009. The light absorption coefficients of size-segregated particles (< 0.5 and < 1.0μm diameter) and aerosol number concentrations (0.1–0.5μm diameter) were measured to assist direct aerosol sampling. Size-segregated aerosol particles were collected for chemical analysis using ion chromatography. For transmission electron microscopy (TEM) analyses using water-dialysis methods, dried submicrometer aerosol particles were collected using a cascade impactor. We analyzed 13 TEM samples. Results of water-dialysis analysis demonstrate that most particles were water-soluble. However, for all TEM samples, particles were rarely found (2.1% of particles on a TEM sample at a maximum) containing insoluble residuals with the characteristic soot shape. For samples collected over the Indian and Southern oceans at latitudes less than 62°S, some (20–35%) soot-containing particles were found as bare soot. For samples collected near the Antarctic coast (65–68°S, 38–68°E), all soot-containing particles were mixed with water-soluble materials. Furthermore, 56% of soot-containing particles had a satellite structure formed by the impact of droplets such as sulfuric acid. Chemical analysis of submicrometer particles near the Antarctic coast revealed high concentrations of non-sea-salt (nss) SO_4^{2-} and $CH_3SO_3^-$, suggesting that aged soot-containing particles were transformed by soluble materials derived from dimethyl sulfide (DMS) oxidation. The obtained information of soot at various remote ocean areas is expected to be useful to understand long-range transport processes and to improve simulations of global soot concentration.

Multi-species inversion and IAGOS airborne data for a better constraint of continental-scale fluxes

Fabio Boschetti[1], Valerie Thouret[2], Greet Janssens Maenhout[3], Kai Uwe Totsche[4],Julia Marshall[1], and Christoph Gerbig[1]

Source: Atmosphere Chemistry and Physics, Volume 18, issue 13
03 Jul 2018.

Airborne measurements of CO_2, CO, and CH_4 proposed in the context of IAGOS (In-service Aircraft for a Global Observing System) will provide profiles from take-off and landing of airliners in the vicinity of major metropolitan areas useful for constraining sources and sinks. A proposed improvement of the top-down method to constrain sources and sinks is the use of a multispecies inversion. Different species such as CO_2 and CO have partially overlapping emission patterns for given fuel-combustion-related sectors, and thus share part of the uncertainties related both to the a priori knowledge of emissions and to model–data mismatch error. We use a regional modelling framework consisting of the Lagrangian particle dispersion model STILT (Stochastic Time-Inverted Lagrangian Transport) combined with the high-resolution (10km× 10km) EDGARv4.3 (Emission Database for Global Atmospheric Research) emission inventory, differentiated by emission sector and fuel type for CO_2, CO, and CH_4, and combined with the VPRM (Vegetation Photosynthesis and Respiration Model) for biospheric fluxes of CO_2. Applying the modelling framework to synthetic IAGOS profile observations, we evaluate the benefits of using correlations between different species' uncertainties on the performance of the atmospheric inversion. The available IAGOS CO observations are used to validate the modelling framework. Prior uncertainty values are conservatively assumed to be 20%, for CO_2 and 50% for CO and CH_4, while those for GEE (gross ecosystem exchange) and respiration are derived from existing literature. Uncertainty reduction for different species is evaluated in a domain encircling 50% of the profile observations' surface influence over Europe. We found that our modelling framework reproduces the CO observations with an average correlation of 0.56, but simulates lower mixing ratios by a factor of 2.8, reflecting a low bias in the emission inventory. Mean uncertainty reduction achieved for CO_2 fossil fuel emissions is roughly 38%; for photosynthesis and respiration flux it is 41 and 44% respectively. For CO and CH_4 the uncertainty reduction is roughly 63 and 67% respectively. Considering correlation between different species, posterior uncertainty can be reduced by up to 23%; such a reduction depends on the assumed error structure of the prior and on the considered time frame. The study suggests a significant uncertainty constraint on regional emissions using multi-species inversions of IAGOS in situ observations.

High occurrence of new particle formation events at the Maïdo high-altitude observatory (2150 m), Réunion (Indian Ocean)

Brice Foucart[1,2], Karine Sellegri[2], Pierre Tulet[1], Clémence Rose[2], Jean-Marc Metzger[3],and David Picard[2]

Source: Atmosphere Chemistry and Physics, Volume 18, issue 13
03 Jul 2018.

This study aims to report and characterise the frequent new particle formation (NPF) events observed at the Maïdo observatory, Réunion, a Southern Hemisphere site located at 2150m (a.s.l.) and surrounded by the Indian Ocean. From May 2014 to December 2015, continuous aerosol measurements were made using both a differential mobility particle sizer (DMPS) and an air ion spectrometer (AIS) to characterise the NPF events down to the lowest particle-size scale. Carbon monoxide (CO) and black carbon (BC) concentrations were monitored, as well as meteorological parameters, in order to identify the conditions that were favourable to the occurrence of nucleation in this specific environment. We point out that the annual NPF frequency average (65%) is one of the highest reported so far. Monthly averages show a bimodal variation in the NPF frequency, with a maximum observed during transition periods (autumn and spring). A high yearly median particle growth rate (GR) of 15.16nmh^{-1} is also measured showing a bimodal seasonal variation with maxima observed in July and November. Yearly medians of 2 and 12nm particle formation rates (J_2 and J_{12}) are 0.858 and 0.508cm^{-3}s^{-1}, respectively, with a seasonal variation showing a maximum during winter, that correspond to low temperature and RH typical of the dry season, but also to high BC concentrations. We show that the condensation sink exceeds a threshold value (1.04×10^{-3}s^{-1}) with a similar seasonal variation than the one of the NPF event frequency, suggesting that the occurrence of the NPF process might be determined by the availability of condensable vapours, which are likely to be transported together with pre-existing particles from lower altitudes.

High- and low-temperature pyrolysis profiles describe volatile organic compound emissions from western US wildfire fuels

Kanako Sekimoto[1,2,3,*], Abigail R. Koss[1,2,4,a,*], Jessica B. Gilman[1], Vanessa Selimovic[5],Matthew M. Coggon[1,2], Kyle J. Zarzana[1,2], Bin Yuan[1,2,6], Brian M. Lerner[1,2,b],Steven S. Brown[1,4], Carsten Warneke[1,2], Robert J. Yokelson[5], James M. Roberts[1],and Joost de Gouw[1,2,4]

Source : Atmosphere Chemistry and Physics, Volume 18, issue 13
03 Jul 2018

Biomass burning is a large source of volatile organic compounds (VOCs) and many other trace species to the atmosphere, which can act as precursors to secondary pollutants such as ozone and fine particles. Measurements performed with a proton-transfer-reaction time-of-flight mass spectrometer during the FIREX 2016 laboratory intensive were analyzed with positive matrix factorization (PMF), in order to understand the instantaneous variability in VOC emissions from biomass burning, and to simplify the description of these types of emissions. Despite the complexity and variability of emissions, we found that a solution including just two emission profiles, which are mass spectral representations of the relative abundances of emitted VOCs, explained on average 85% of the VOC emissions across various fuels representative of the western US (including various coniferous and chaparral fuels). In addition, the profiles were remarkably similar across almost all of the fuel types tested. For example, the correlation coefficient r^2 of each profile between ponderosa pine (coniferous tree) and manzanita (chaparral) is higher than 0.84. The compositional differences between the two VOC profiles appear to be related to differences in pyrolysis processes of fuel biopolymers at high and low temperatures. These pyrolysis processes are thought to be the main source of VOC emissions. High-temperature and low-temperature pyrolysis processes do not correspond exactly to the commonly used flaming and smoldering categories as described by modified combustion efficiency (MCE). The average atmospheric properties (e.g., OH reactivity, volatility, etc) of the high- and low-temperature profiles are significantly different. We also found that the two VOC profiles can describe previously reported VOC data for laboratory and field burns.

In situ observation of atmospheric oxygen and carbon dioxide in the North Pacific using a cargo ship

Yu Hoshina, Yasunori Tohjima, Keiichi Katsumata, Toshinobu Machida, and Shin-ichiro Nakaoka

Source: Atmosphere Chemistry and Physics, Volume 18, issue 13
03 Jul 2018.

Atmospheric oxygen (O_2) and carbon dioxide (CO_2) variations in the North Pacific were measured aboard a cargo ship, the *New Century 2* (NC2), while it cruised between Japan and the United States between December 2015 and November 2016. A fuel cell analyzer and a nondispersive infrared analyzer were used for the measurement of O_2 and CO_2, respectively. To achieve parts-per-million precision for the O_2 measurements, we precisely controlled the flow rates of the sample and reference air introduced into the analyzers and the outlet pressure. A relatively low airflow rate ($10 cm^3 min^{-1}$) was adopted to reduce the

consumption rate of the reference gases. In the laboratory, the system achieved measurement precisions of 3.8 per meg for $\delta(O_2/N_2)$, which is commonly used to express atmospheric O_2 variation, and 0.1ppm for the CO_2 mole fraction. After the in situ observation started aboard NC2, we found that the ship's motion caused false wavy variations in the O_2 signal with an amplitude of more than several tens of ppm and a period of about 20s. Although we have not resolved the problem at this stage, hourly averaging considerably suppressed the variation associated with ship motion. Comparison between the in situ observation and flask sampling of air samples aboard NC2 showed that the averaged differences (in situ–flask) and the standard deviations ($\pm 1\sigma$) are −2.8±9.4 per meg for $\delta(O_2/N_2)$ and −0.02±0.33ppm for the CO_2 mole fraction. We compared 1 year of in situ data for atmospheric potential oxygen (APO; $O_2 + 1.1 \times CO_2$) obtained from the broad middle-latitude region (140°E–130°W, 29°N–45°N) with previous flask sampling data from the North Pacific. This comparison showed that longitudinal differences in the seasonal amplitude of APO, ranging from 51 to 73 per meg, were smaller than the latitudinal differences.

Estimation of rate coefficients and branching ratios for gas-phase reactions of OH with aliphatic organic compounds for use in automated mechanism construction

Michael E. Jenkin[1,2], Richard Valorso[3], Bernard Aumont[3], Andrew R. Rickard[4,5],and Timothy J. Wallington[6]

Source: Atmosphere Chemistry and Physics, Volume 18, issue 13
03 Jul 2018.

Reaction with the hydroxyl (OH) radical is the dominant removal process for volatile organic compounds (VOCs) in the atmosphere. Rate coefficients for reactions of OH with VOCs are therefore essential parameters for chemical mechanisms used in chemistry transport models, and are required more generally for impact assessments involving the estimation of atmospheric lifetimes or oxidation rates for VOCs. Updated and extended structure–activity relationship (SAR) methods are presented for the reactions of OH with aliphatic organic compounds, with the reactions of aromatic organic compounds considered in a companion paper. The methods are optimized using a preferred set of data including reactions of OH with 489 aliphatic hydrocarbons and oxygenated organic compounds. In each case, the rate coefficient is defined in terms of a summation of partial rate coefficients for H abstraction or OH addition at each relevant site in the given organic compound, so that the attack distribution is defined. The information can therefore guide the representation of the OH reactions in the next generation of explicit detailed chemical

mechanisms. Rules governing the representation of the subsequent reactions of the product radicals under tropospheric conditions are also summarized, specifically their reactions with O_2 and competing processes.

Estimation of rate coefficients and branching ratios for gas-phase reactions of OH with aromatic organic compounds for use in automated mechanism construction

Michael E. Jenkin[1,2], Richard Valorso[3], Bernard Aumont[3], Andrew R. Rickard[4,5],and Timothy J. Wallington[6]

Source: Atmosphere Chemistry and Physics, Volume 18, issue 13
04 Jul 2018.

Reaction with the hydroxyl (OH) radical is the dominant removal process for volatile organic compounds (VOCs) in the atmosphere. Rate coefficients for the reactions of OH with VOCs are therefore essential parameters for chemical mechanisms used in chemistry transport models, and are required more generally for impact assessments involving estimation of atmospheric lifetimes or oxidation rates for VOCs. A structure–activity relationship (SAR) method is presented for the reactions of OH with aromatic organic compounds, with the reactions of aliphatic organic compounds considered in the preceding companion paper. The SAR is optimized using a preferred set of data including reactions of OH with 67 monocyclic aromatic hydrocarbons and oxygenated organic compounds. In each case, the rate coefficient is defined in terms of a summation of partial rate coefficients for H abstraction or OH addition at each relevant site in the given organic compound, so that the attack distribution is defined. The SAR can therefore guide the representation of the OH reactions in the next generation of explicit detailed chemical mechanisms. Rules governing the representation of the reactions of the product radicals under tropospheric conditions are also summarized, specifically the rapid reaction sequences initiated by their reactions with O_2.

Future changes in surface ozone over the Mediterranean Basin in the framework of the Chemistry-Aerosol Mediterranean Experiment (ChArMEx)

Nizar Jaidan[1], Laaziz El Amraoui[1], Jean-Luc Attié[2], Philippe Ricaud[1], and François Dulac[3]

Source: Atmosphere Chemistry and Physics, Volume 18, issue 13
04 Jul 2018.

In the framework of the Chemistry-Aerosol Mediterranean Experiment (ChArMEx; http://charmex.lsce.ipsl.fr, last access: 22 June 2018) project, we study the evolution of surface ozone over the Mediterranean Basin (MB) with a focus on summertime over the time period 2000–2100, using the Atmospheric Chemistry and Climate Model Intercomparison Project (ACCMIP) outputs from 13 models. We consider three different periods (2000, 2030 and 2100) and the four Representative Concentration Pathways (RCP2.6, RCP4.5, RCP6.0 and RCP8.5) to study the changes in the future ozone and its budget. We use a statistical approach to compare and discuss the results of the models. We discuss the behavior of the models that simulate the surface ozone over the MB. The shape of the annual cycle of surface ozone simulated by ACCMIP models is similar to the annual cycle of the ozone observations, but the model values are biased high. For the summer, we found that most of the models overestimate surface ozone compared to observations over the most recent period (1990–2010). Compared to the reference period (2000), we found a net decrease in the ensemble mean surface ozone over the MB in 2030 (2100) for three RCPs: −14% (−38%) for RCP2.6, −9% (−24%) for RCP4.5 and −10% (−29%) for RCP6.0. The surface ozone decrease over the MB for these scenarios is much more pronounced than the relative changes of the global tropospheric ozone burden. This is mainly due to the reduction in ozone precursors and to the nitrogen oxide ($NO_x = NO + NO_2$)-limited regime over the MB. For RCP8.5, the ensemble mean surface ozone is almost constant over the MB from 2000 to 2100. We show how the future climate change and in particular the increase in methane concentrations can offset the benefits from the reduction in emissions of ozone precursors over the MB.

Non-polar organic compounds in autumn and winter aerosols in a typical city of eastern China: size distribution and impact of gas–particle partitioning on $PM_{2.5}$ source apportionment

Deming Han[1], Qingyan Fu[2], Song Gao[2], Li Li[3], Yingge Ma[3], Liping Qiao[3], Hao Xu[1], Shan Liang[1],Pengfei Cheng[4], Xiaojia Chen[1], Yong Zhou[1], Jian Zhen Yu[5], and Jinping Cheng[1]

Source : Atmosphere Chemistry and Physics, Volume 18, issue 13
04 Jul 2018

Aerosol-associated non-polar organic compounds (NPOCs), including 15 polycyclic aromatic hydrocarbons (PAHs), 30 *n*-alkanes, 2 *iso*-alkanes, 5 hopanes and 5 steranes, were identified and quantified in $PM_{2.5}$ samples using the thermal desorption–gas chromatography–mass spectrometry (TD–GC–MS) method. The samples were mainly collected in autumn and winter in a typical city of eastern China. The total concentrations

of NPOCs were 31.7–388.7ngm^{-3}, and *n*-alkanes were the most abundant species (67.2%). The heavy-molecular-weight PAHs (four- and five-ring) contributed 67.9% of the total PAHs, and the middle-chain-length *n*-alkanes (C_{25}–C_{34}) were the most abundant (72.3%) in *n*-alkanes. PAHs and *n*-alkanes were mainly distributed in the 0.56–1.00μm fraction, while ∑(hopanes+steranes) were associated with the 0.32–1.00μm fraction, suggesting condensation of combustion products was their important origin. The ratio–ratio plots indicated that NPOCs in the local area were affected by photochemical degradation. To reduce the uncertainty caused by only particle NPOC data for source apportionment, the particle and predicted gaseous-phase NPOCs, incorporated with other $PM_{2.5}$ compound were used as input data for the positive matrix factorization (PMF) model. Eight factors were extracted for both cases: secondary aerosol formation, vehicle exhaust, industrial emission, coal combustion, biomass burning, ship emission, and dust and light NPOCs. These findings highlight the emissions from different aerosol-associated NPOC origins, which caused different size-specific distributions, photodegradation and gas–particle partitioning, which further affect $PM_{2.5}$ source apportionment. Considering these effects on organic tracers will help us accurately identify the potential sources of aerosols and then asses the contributions from each source.

Light absorption by polar and non-polar aerosol compounds from laboratory biomass combustion

Deep Sengupta[1], Vera Samburova[1], Chiranjivi Bhattarai[1], Elena Kirillova[2], Lynn Mazzoleni[2],Michealene Iaukea-Lum[1], Adam Watts[1], Hans Moosmüller[1], and Andrey Khlystov[1]

Source: Atmosphere Chemistry and Physics, Volume 18, issue 15
03 Aug 2018

Fresh and atmospherically aged biomass-burning (BB) aerosol mass is mostly comprised of strongly light-absorbing black carbon (BC) and of organic carbon (OC) with its light-absorbing fraction – brown carbon (BrC). There is a lack of data on the physical and chemical properties of atmospheric BB aerosols, leading to high uncertainties in estimates of the BB impact on air quality and climate, especially for BrC. The polarity of chemical compounds influences their fate in the atmosphere including wet/dry deposition and chemical and physical processing. So far, most of the attention has been given to the water-soluble (polar) fraction of BrC, while the non-polar BrC fraction has been largely ignored. In the present study, the light absorption properties of polar and non-polar fractions of fresh

and aged BB emissions were examined to estimate the contribution of different-polarity organic compounds to the light absorption properties of BB aerosols.

In our experiments, four globally and regionally important fuels were burned under flaming and smoldering conditions in the Desert Research Institute (DRI) combustion chamber. To mimic atmospheric oxidation processes (5–7 days), BB emissions were aged using an oxidation flow reactor (OFR). Fresh and OFR-aged BB aerosols were collected on filters and extracted with water and hexane to study absorption properties of polar and non-polar organic species. Results of spectrophotometric measurements (absorption weighted by the solar spectrum and normalized to mass of fuel consumed) over the 190 to 900nm wavelength range showed that the non-polar (hexane-soluble) fraction is 2–3 times more absorbing than the polar (water-soluble) fraction. However, for emissions from fuels that undergo flaming combustion, an increased absorbance was observed for the water extracts of oxidized/aged emissions while the absorption of the hexane extracts was lower for the aged emissions for the same type of fuels. Absorption Ångström exponent (AAE) values, computed based on absorbance values from spectrophotometer measurements, were changed with aging and the nature of this change was fuel dependent. The light absorption by humic-like substances (HULIS) was found to be higher in fuels characteristic of the southwestern USA. The absorption of the HULIS fraction was lower for OFR-aged BB emissions. Comparison of the light absorption properties of different-polarity extracts (water, hexane, HULIS) provides insight into the chemical nature of BB BrC and its transformation during oxidation processes.

Does afforestation deteriorate haze pollution in Beijing–Tianjin–Hebei (BTH), China?

Xin Long[1,3], Naifang Bei[2], Jiarui Wu[1], Xia Li[1], Tian Feng[1], Li Xing[1], Shuyu Zhao[1], Junji Cao[1],Xuexi Tie[1,4], Zhisheng An[1], and Guohui Li[1]

Source: Atmosphere Chemistry and Physics, Volume 18, issue 15
03 Aug 2018.

Although aggressive emission control strategies have been implemented recently in the Beijing–Tianjin–Hebei area (BTH), China, pervasive and persistent haze still frequently engulfs the region during wintertime. Afforestation in BTH, primarily concentrated in the Taihang and Yan Mountains, has constituted one of the controversial factors exacerbating the haze pollution due to its slowdown of the surface wind speed. We report here an increasing trend of forest cover in BTH during 2001–2013 based on long-term satellite

measurements and the impact of the afforestation on the fine-particle ($PM_{2.5}$) level. Simulations using the Weather Research and Forecast model with chemistry reveal that afforestation in BTH since 2001 has generally been deteriorating the haze pollution in BTH to some degree, enhancing $PM_{2.5}$ concentrations by up to 6% on average. Complete afforestation or deforestation in the Taihang and Yan Mountains would increase or decrease the $PM_{2.5}$ level within 15% in BTH. Our model results also suggest that implementing a large ventilation corridor system would not be effective or beneficial to mitigate the haze pollution in Beijing.

Polar stratospheric cloud climatology based on CALIPSO spaceborne lidar measurements from 2006 to 2017

Michael C. Pitts[1], Lamont R. Poole[2], and Ryan Gonzalez[3,a]

Source: Atmosphere Chemistry and Physics, Volume 18, issue 15
03 Aug 2018.

The Cloud-Aerosol Lidar with Orthogonal Polarization (CALIOP) on the CALIPSO (Cloud-Aerosol Lidar and Infrared Pathfinder Satellite Observations) satellite has been observing polar stratospheric clouds (PSCs) from mid-June 2006 until the present. The spaceborne lidar profiles PSCs with unprecedented spatial (5 km horizontal × 180m vertical) resolution and its dual-polarization capability enables classification of PSCs according to composition. Nearly coincident Aura Microwave Limb Sounder (MLS) measurements of the primary PSC condensables (HNO_3 and H_2O) provide additional constraints on particle composition. A new CALIOP version 2 (v2) PSC detection and composition classification algorithm has been implemented that corrects known deficiencies in previous algorithms and includes additional refinements to improve composition discrimination. Major v2 enhancements include dynamic adjustment of composition boundaries to account for effects of denitrification and dehydration, explicit use of measurement uncertainties, addition of composition confidence indices, and retrieval of particulate backscatter, which enables simplified estimates of particulate surface area density (SAD) and volume density (VD). The over 11 years of CALIOP PSC observations in each v2 composition class conform to their expected thermodynamic existence regimes, which is consistent with previous analyses of data from 2006 to 2011 and underscores the robustness of the v2 composition discrimination approach.

The v2 algorithm has been applied to the CALIOP dataset to produce a PSC reference data record spanning the 2006–2017 time period, which is the foundation for a new

comprehensive, high-resolution climatology of PSC occurrence and composition for both the Antarctic and Arctic. Time series of daily-averaged, vortex-wide PSC areal coverage versus altitude illustrate that Antarctic PSC seasons are similar from year to year, with about 25% relative standard deviation in Antarctic PSC spatial volume at the peak of the season in July and August. Multi-year average, monthly zonal mean cross sections depict the climatological patterns of Antarctic PSC occurrence in latitude–altitude and also equivalent-latitude–potential-temperature coordinate systems, with the latter system better capturing the microphysical processes controlling PSC existence. Polar maps of the multi-year mean geographical patterns in PSC occurrence frequency show a climatological maximum between longitudes 90°W and 0°, which is the preferential region for forcing by orography and upper tropospheric anticyclones. The climatological mean distributions of particulate SAD and VD also show maxima in this region due to the large enhancements from the frequent ice clouds.

Stronger wave activity in the Northern Hemisphere leads to a more disturbed Arctic polar vortex, whose evolution and lifetime vary significantly from year to year. Accordingly, Arctic PSC areal coverage is distinct from year to year with no typical year, and the relative standard deviation in Arctic PSC spatial volume is $> 100\%$ throughout most of the season. When PSCs are present in the Arctic, they most likely occur between longitudes 60°W and 90°E, which is consistent with the preferential location of the Arctic vortex.

Comparisons of CALIOP v2 and Michelson Interferometer for Passive Atmospheric Sounding (MIPAS) Antarctic PSC observations show excellent correspondence in the overall spatial and temporal evolution, as well as for different PSC composition classes. Climatological patterns of CALIOP v2 PSC occurrence frequency in the vicinity of McMurdo Station, Antarctica, and Ny-Ålesund, Spitsbergen, are similar in nature to those derived from local ground-based lidar measurements. To investigate the possibility of longer-term trends, appropriately subsampled and averaged CALIOP v2 PSC observations from 2006 to 2017 were compared with PSC data during the 1978–1989 period obtained by the spaceborne solar occultation instrument SAM II (Stratospheric Aerosol Measurement II). There was good consistency between the two instruments in column Antarctic PSC occurrence frequency, suggesting that there has been no long-term trend. There was less overall consistency between the Arctic records, but it is very likely due to the high degree of interannual variability in PSCs rather than a long-term trend.

Influence of the vapor wall loss on the degradation rate constants in chamber experiments of levoglucosan and other biomass burning markers

Amelie Bertrand[1,2,a], Giulia Stefenelli[3], Simone M. Pieber[3], Emily A. Bruns[3],Brice Temime-Roussel[1], Jay G. Slowik[3], Henri Wortham[1], André S. H. Prévôt[3], Imad El Haddad[3],and Nicolas Marchand[1]

Source: Atmosphere Chemistry and Physics, Volume 18, issue 15
03 Aug 2018.

Vapor wall loss has only recently been shown a potentially significant bias in atmospheric chamber studies. Yet, previous works aiming at the determination of the degradation rate of semi-volatile organic compounds (SVOCs) often did not account for this process. Here, we evaluate the influence of vapor wall loss on the determination of the gas-phase reaction rate k_{OH} of several biomass burning markers (levoglucosan, mannosan, coniferyl aldehyde, 3-guaiacyl propanol, and acetosyringone) with hydroxyl radicals (OH). Emissions from the combustion of beech wood were injected into a 5.5m^3 Teflon atmospheric chamber, and aged for 4h (equivalent to 5–8h in the atmosphere). The particle-phase compound concentrations were monitored using a thermal desorption aerosol gas chromatograph coupled to a high-resolution time-of-flight aerosol mass spectrometer (TAG-AMS). The observed depletion of the concentration was later modeled using two different approaches: the previously published approach which does not take into consideration partitioning and vapor wall loss, and an approach with a more complex theoretical framework which integrates all the processes likely influencing the particle-phase concentration. We find that with the first approach one fails to predict the measured markers' concentration time evolution. With the second approach, we determine that partitioning and vapor wall loss play a predominant role in the particle-phase concentration depletion of all the compounds, while the reactivity with OH has a non-significative effect. Furthermore, we show that k_{OH} cannot be determined precisely without a strong constraint of the whole set of physical parameters necessary to formally describe the various processes involved. It was found that the knowledge of the saturation mass concentration C^* is especially crucial. Therefore, previously published rate constants of levoglucosan and more generally SVOCs with hydroxyl radicals inferred from atmospheric chamber experiments must be, at least, considered with caution.

Spatial–temporal patterns of inorganic nitrogen air concentrations and deposition in eastern China

Wen Xu[1,2], Lei Liu[3], Miaomiao Cheng[4], Yuanhong Zhao[5], Lin Zhang[5], Yuepeng Pan[6],Xiuming Zhang[7], Baojing Gu[8], Yi Li[9], Xiuying Zhang[3], Jianlin Shen[10], Li Lu[11], Xiaosheng Luo[12],Yu Zhao[13], Zhaozhong Feng[2], Jeffrey L. Collett Jr.[14], Fusuo Zhang[1], and Xuejun Liu[1]

Source: Atmosphere Chemistry and Physics, Volume 18, issue 15
06 Aug 2018.

Five-year (2011–2015) measurements of gaseous NH_3, NO_2, and HNO_3 and particulate NH_4^+ and NO_3^- in air and/or precipitation were conducted at 27 sites in the Nationwide Nitrogen Deposition Monitoring Network (NNDMN) to better understand spatial and temporal (seasonal and annual) characteristics of reactive nitrogen (N_r) concentrations and deposition in eastern China. Our observations reveal annual average concentrations (16.4–32.6μgNm^{-3}), dry deposition fluxes (15.8–31.7kgNha^{-1}yr^{-1}), and wet/bulk deposition fluxes (18.4–28.0kgNha^{-1}yr^{-1}) based on land use, ranked as urban>rural>background sites. Annual concentrations and dry deposition fluxes of each N_r species in air were comparable at urban and background sites in northern and southern regions, but were significantly higher at northern rural sites. These results, together with good agreement between spatial distributions of NH_3 and NO_2concentrations determined from ground measurements and satellite observations, demonstrate that atmospheric N_r pollution is heavier in the northern region than in the southern region. No significant inter-annual trends were found in the annual N_r dry and wet/bulk N deposition at almost all of the selected sites. A lack of significant changes in annual averages between the 2013–2015 and 2011–2012 periods for all land use types suggests that any effects of current emission controls are not yet apparent in N_r pollution and deposition in the region. Ambient concentrations of total N_r exhibited non-significant seasonal variation at all land use types, although significant seasonal variations were found for individual N_r species (e.g. NH_3, NO_2, and pNO_3^-) in most cases. In contrast, dry deposition of total $N_r$exhibited a consistent and significant seasonal variation at all land use types, with the highest fluxes in summer and the lowest in winter. Based on sensitivity tests by the GEOS-Chem model, we found that NH_3 emissions from fertilizer use (including chemical and organic fertilizers) were the largest contributor (36%) to total inorganic N_r deposition over eastern China. Our results not only improve the understanding of spatial–temporal variations of N_r concentrations and deposition in this pollution hotspot, but also provide useful information for policy-makers that mitigation of NH_3 emissions should be a priority to tackle serious N deposition in eastern China.

Forecasting carbon monoxide on a global scale for the ATom-1 aircraft mission: insights from airborne and satellite observations and modeling

Sarah A. Strode[1,2], Junhua Liu[1,2], Leslie Lait[2,3], Róisín Commane[4,a], Bruce Daube[4],Steven Wofsy[4], Austin Conaty[2,5], Paul Newman[2], and Michael Prather[6]

Source: Atmosphere Chemistry and Physics, Volume 18, issue 15
06 Aug 2018.

The first phase of the Atmospheric Tomography Mission (ATom-1) took place in July–August 2016 and included flights above the remote Pacific and Atlantic oceans. Sampling of atmospheric constituents during these flights is designed to provide new insights into the chemical reactivity and processes of the remote atmosphere and how these processes are affected by anthropogenic emissions. Model simulations provide a valuable tool for interpreting these measurements and understanding the origin of the observed trace gases and aerosols, so it is important to quantify model performance. Goddard Earth Observing System Model version 5 (GEOS-5) forecasts and analyses show considerable skill in predicting and simulating the CO distribution and the timing of CO enhancements observed during the ATom-1 aircraft mission. We use GEOS-5's tagged tracers for CO to assess the contribution of different emission sources to the regions sampled by ATom-1 to elucidate the dominant anthropogenic influences on different parts of the remote atmosphere. We find a dominant contribution from non-biomass-burning sources along the ATom transects except over the tropical Atlantic, where African biomass burning makes a large contribution to the CO concentration. One of the goals of ATom is to provide a chemical climatology over the oceans, so it is important to consider whether August 2016 was representative of typical boreal summer conditions. Using satellite observations of 700hPa and column CO from the Measurement of Pollution in the Troposphere (MOPITT) instrument, 215hPaCO from the Microwave Limb Sounder (MLS), and aerosol optical thickness from the Moderate Resolution Imaging Spectroradiometer (MODIS), we find that CO concentrations and aerosol optical thickness in August 2016 were within the observed range of the satellite observations but below the decadal median for many of the regions sampled. This suggests that the ATom-1 measurements may represent relatively clean but not exceptional conditions for lower-tropospheric CO.

Synthesis and characterisation of peroxypinic acids as proxies for highly oxygenated molecules (HOMs) in secondary organic aerosol

Sarah S. Steimer[1], Aurélie Delvaux[1], Steven J. Campbell[1], Peter J. Gallimore[1], Peter Grice[1],Duncan J. Howe[1], Dominik Pitton[2], Magda Claeys[3], Thorsten Hoffmann[2], and Markus Kalberer[1]

Source : Atmosphere Chemistry and Physics, Volume 18, issue 15
06 Aug 2018.

Peroxy acids were recently found to be involved in new particle formation in the atmosphere and could also substantially contribute towards particle toxicity. However, a lack of suitable analytical methods for the detection and characterisation of peroxy acids in the particle phase is currently hindering the quantitative investigation of their contribution to these important atmospheric processes. Further development of appropriate techniques and relevant standards is therefore urgently needed. In this study, we synthesised three peroxypinic acids, developed a liquid chromatography separation method and characterised them with tandem mass spectrometry. The observed fragmentation patterns clearly distinguish the different peroxypinic acids from both the acid and each other, showing several neutral losses previously already observed for other peroxy acids. Both monoperoxypinic acids were found to be present in secondary organic aerosol generated from ozonolysis of α-pinene in laboratory experiments. The yield of monoperoxypinic acid formation was not influenced by humidity. Monoperoxypinic acid quickly degrades on the filter, with about 60% lost within the first 5h. This fast degradation shows that time delays in traditional off-line analysis will likely lead to severe underestimates of peroxy compound concentrations in ambient particles.

Establishing the impact of model surfactants on cloud condensation nuclei activity of sea spray aerosol mimics

Sara D. Forestieri[1,a], Sean M. Staudt[2], Thomas M. Kuborn[2], Katharine Faber[3], Christopher R. Ruehl[4],Timothy H. Bertram[2], and Christopher D. Cappa[1]

Source: Atmosphere Chemistry and Physics, Volume 18, issue 15
07 Aug 2018.

Surface-active compounds present in aerosols can increase their cloud condensation nuclei (CCN) activation efficiency by reducing the surface tension (σ) in the growing droplets. However, the importance of this effect is poorly constrained by measurements.

Here we present estimates of droplet surface tension near the point of activation derived from direct measurement of droplet diameters using a continuous flow streamwise thermal gradient chamber (CFSTGC). The experiments used sea spray aerosol (SSA) mimics composed of NaCl coated by varying amounts of (i) oleic acid, palmitic acid or myristic acid, (ii) mixtures of palmitic acid and oleic acid, and (iii) oxidized oleic acid. Significant reductions in σ relative to that for pure water were observed for these mimics at relative humidity (RH) near activation (~99.9%) when the coating was sufficiently thick. The calculated surface pressure ($\pi = \sigma_{H2}O - \sigma_{observed}$) values for a given organic compound or mixture collapse onto one curve when plotted as a function of molecular area for different NaCl seed sizes and measured RH. The observed critical molecular area (A_0) for oleic acid determined from droplet growth was similar to that from experiments conducted using macroscopic solutions in a Langmuir trough. However, the observations presented here suggest that oleic acid in microscopic droplets may exhibit larger π values during monolayer compression. For myristic acid, the observed A_0 compared well to macroscopic experiments on a fresh subphase, for which dissolution has an important impact. A significant kinetic limitation to water uptake was observed for NaCl particles coated with pure palmitic acid, likely as a result of palmitic acid (with coating thicknesses ranging from 67 to 132nm) being able to form a solid film. However, for binary palmitic-acid–oleic-acid mixtures there was no evidence of a kinetic limitation to water uptake. Oxidation of oleic acid had a minor impact on the magnitude of the surface tension reductions observed, potentially leading to a slight reduction in the effect compared to pure oleic acid. A CCN counter was also used to assess the impact on critical supersaturations of the substantial σ reductions observed at very high RH. For the fatty-acid-coated NaCl particles, when the organic fraction (ε_{org}) was >0.90 small depressions in critical supersaturation were observed. However, when ε_{org} <0.90 the impact on critical supersaturation was negligible. Thus, for the fatty acids considered here, the substantial σ reductions observed at high RH values just below activation have limited impact on the ultimate critical supersaturation. A surface film model is used to establish the properties that surface-active organic molecules must have if they are to ultimately have a substantial impact on the activation efficiency of SSA. To influence activation, the average properties of surface-active marine-derived organic molecules must differ substantially from the long-chain fatty acids examined, having either smaller molecular volumes or larger molecular areas. The model results also indicate that organic-compound-driven surface tension depression can serve to buffer the critical supersaturation against changes to the organic-to-salt ratio in particles in which the organic fraction is sufficiently large.

Revolatilisation of soil-accumulated pollutants triggered by the summer monsoon in India

Gerhard Lammel[1,2], Céline Degrendele[2], Sachin S. Gunthe[3], Qing Mu[1], Akila Muthalagu[3],Ondřej Audy[2], Chelackal V. Biju[4], Petr Kukučka[2], Marie D. Mulder[2], Mega Octaviani[1],Petra Příbylová[2], Pourya Shahpoury[1], Irene Stemmler[5], and Aswathy E. Valsan[3]

Source: Atmosphere Chemistry and Physics, Volume 18, issue 15
07 Aug 2018.

Persistent organic pollutants that have accumulated in soils can be remobilised by volatilisation in response to chemical equilibrium with the atmosphere. Clean air masses from the Indian Ocean, advected with the onset of the summer monsoon, are found to reduce concentrations of hexachlorocyclohexane (HCH), dichlorodiphenyltrichloroethane (DDT) and its derivatives, endosulfan and polychlorinated biphenyls (PCBs) in air at a mountain site (all in the range 5–20 pg m^{-3}) by 77 %, 70 %, 82 % and 45 %, respectively. The analysis of fugacities in soil and air suggest that the arrival of summer monsoon triggers net volatilisation or enhances ongoing revolatilisation of the now-banned chemicals HCH and PCBs from background soils in southern India. The response of the air–soil exchange was modelled using a regional air pollution model, WRF-Chem PAH/POP. The results suggest that the air is increasingly polluted during transport by the south-westerly monsoon winds across the subcontinent. Using a multidecadal multimedia mass balance model, it is found that air–surface exchange of HCH and DDT have declined since the ban of these substances from agriculture, but remobilisation of higher chlorinated PCBs may have reached a historical high, 40 years after peak emission.

A model intercomparison of CCN-limited tenuous clouds in the high Arctic

Robin G. Stevens[1,a], Katharina Loewe[2], Christopher Dearden[3,b], Antonios Dimitrelos[4],Anna Possner[5,6], Gesa K. Eirund[5], Tomi Raatikainen[7], Adrian A. Hill[8], Benjamin J. Shipway[8],Jonathan Wilkinson[8], Sami Romakkaniemi[9], Juha Tonttila[9], Ari Laaksonen[7],Hannele Korhonen[7], Paul Connolly[3], Ulrike Lohmann[5], Corinna Hoose[2],Annica M. L. Ekman[4], Ken S. Carslaw[1], and Paul R. Field[1,8]

Source: Atmosphere Chemistry and Physics, Volume 18, issue 15
08 Aug 2018.

We perform a model intercomparison of summertime high Arctic (> 80° N) clouds observed during the 2008 Arctic Summer Cloud Ocean Study (ASCOS) campaign, when observed cloud condensation nuclei (CCN) concentrations fell below 1 cm^{-3}. Previous analyses have

suggested that at these low CCN concentrations the liquid water content (LWC) and radiative properties of the clouds are determined primarily by the CCN concentrations, conditions that have previously been referred to as the tenuous cloud regime. The intercomparison includes results from three large eddy simulation models (UCLALES-SALSA, COSMO-LES, and MIMICA) and three numerical weather prediction models (COSMO-NWP, WRF, and UM-CASIM). We test the sensitivities of the model results to different treatments of cloud droplet activation, including prescribed cloud droplet number concentrations (CDNCs) and diagnostic CCN activation based on either fixed aerosol concentrations or prognostic aerosol with in-cloud processing.

There remains considerable diversity even in experiments with prescribed CDNCs and prescribed ice crystal number concentrations (ICNC). The sensitivity of mixed-phase Arctic cloud properties to changes in CDNC depends on the representation of the cloud droplet size distribution within each model, which impacts autoconversion rates. Our results therefore suggest that properly estimating aerosol–cloud interactions requires an appropriate treatment of the cloud droplet size distribution within models, as well as in situ observations of hydrometeor size distributions to constrain them.

The results strongly support the hypothesis that the liquid water content of these clouds is CCN limited. For the observed meteorological conditions, the cloud generally did not collapse when the CCN concentration was held constant at the relatively high CCN concentrations measured during the cloudy period, but the cloud thins or collapses as the CCN concentration is reduced. The CCN concentration at which collapse occurs varies substantially between models. Only one model predicts complete dissipation of the cloud due to glaciation, and this occurs only for the largest prescribed ICNC tested in this study. Global and regional models with either prescribed CDNCs or prescribed aerosol concentrations would not reproduce these dissipation events. Additionally, future increases in Arctic aerosol concentrations would be expected to decrease the frequency of occurrence of such cloud dissipation events, with implications for the radiative balance at the surface. Our results also show that cooling of the sea-ice surface following cloud dissipation increases atmospheric stability near the surface, further suppressing cloud formation. Therefore, this suggests that linkages between aerosol and clouds, as well as linkages between clouds, surface temperatures, and atmospheric stability need to be considered for weather and climate predictions in this region.

Technical note: Use of an atmospheric simulation chamber to investigate the effect of different engine conditions on unregulated VOC-IVOC diesel exhaust emissions

Kelly L. Pereira[1], Rachel Dunmore[1], James Whitehead[2], M. Rami Alfarra[2,3],James D. Allan[2,3], Mohammed S. Alam[4], Roy M. Harrison[4,5], Gordon McFiggans[2],and Jacqueline F. Hamilton[1]

Source: Atmosphere Chemistry and Physics, Volume 18, issue 15
09 Aug 2018.

Diesel exhaust emissions were introduced into an atmospheric simulation chamber and measured using thermal desorption (TD) comprehensive two-dimensional gas chromatography coupled to a flame ionisation detector (GC × GC-FID). An extensive set of measurements were performed to investigate the effect of different engine conditions (i.e. load, speed, "driving scenarios") and emission control devices (with or without diesel oxidative catalyst, DOC) on the composition and abundance of unregulated exhaust gas emissions from a light-duty diesel engine, fuelled with ultra-low sulfur diesel (ULSD). A range of exhaust dilution ratios were investigated (range = 1 : 60 to 1 : 1158), simulating the chemical and physical transformations of the exhaust gas from near to downwind of an emission source. In total, 16 individual and 8 groups of compounds (aliphatics and single-ring aromatics) were measured in the exhaust gas ranging from volatile to intermediate volatility (VOC-IVOC), providing both detailed chemical speciation and groupings of compounds based on their structure and functionality. Measured VOC-IVOC emission rates displayed excellent reproducibility from replicate experiments using similar exhaust dilution ratios. However, at the extremes of the investigated exhaust dilution ratios (comparison of 1 : 60 and 1 : 1158), measured VOC-IVOC emission rates displayed some disagreement owing to poor reproducibility and highlighted the importance of replicate sample measurements. The investigated DOC was found to remove 43±10 % (arithmetic mean ± experimental uncertainty) of the total speciated VOC-IVOC (∑SpVOC-IVOC) emissions. The compound class-dependant removal efficiencies for the investigated DOC were 39±12 % and 83±3 % for the aliphatics and single-ring aromatics, respectively. The DOC aliphatic removal efficiency generally decreased with increasing carbon chain length. The ∑SpVOC-IVOC emission rates varied significantly with different engine conditions, ranging from 70 to 9268 mg kg^{-1} (milligrams of mass emitted per kilogram of fuel burnt). ∑SpVOC-IVOC emission rates generally decreased with increasing engine load and temperature, and to a lesser degree, engine speed. The exhaust gas composition changed considerably as a result of two influencing factors: engine combustion and DOC

hydrocarbon (HC) removal efficiency. Increased engine combustion efficiency resulted in a greater percentage contribution of the C_7 to C_{12} *n*-alkanes to the ∑SpVOC-IVOC emission rate. Conversely, increased DOC HC removal efficiency resulted in a greater percentage contribution of the C_7 to C_{12} branched aliphatics to the ∑SpVOC-IVOC emission rate. At low engine temperatures (<150 °C, below the working temperature of the DOC), the contribution of *n*-alkanes in the exhaust gas increased with increasing combustion efficiency and may be important in urban environments, as *n*-alkanes are more efficient at producing secondary organic aerosol (SOA) than their branched counterparts. At very high engine temperatures (maximum applied engine speed and load, engine temperature = 700 °C), the *n*-alkane contribution increased by a factor of 1.6 times greater than that observed in the cold-start experiment (most similar to unburnt fuel) and may suggest liquid-fuel-based estimates of SOA yields may be inconsistent with exhaust SOA yields, particularly at high engine speeds and loads (i.e. high engine temperatures). Emission rates were found to be 65 times greater from a cold-start experiment than at maximum applied engine speed and load. To our knowledge, this is the first study which uses an atmospheric simulation chamber to separate the effects of the DOC and combustion efficiency on the exhaust gas composition.

Exploring non-linear associations between atmospheric new-particle formation and ambient variables: a mutual information approach

Martha A. Zaidan[1,2,3], Ville Haapasilta[3], Rishi Relan[4], Pauli Paasonen[1], Veli-Matti Kerminen[1],Heikki Junninen[1,5], Markku Kulmala[1,6], and Adam S. Foster[3,7,8]

Source: Atmosphere Chemistry and Physics, Volume 18, issue 17
03 Sep 2018.

Atmospheric new-particle formation (NPF) is a very non-linear process that includes atmospheric chemistry of precursors and clustering physics as well as subsequent growth before NPF can be observed. Thanks to ongoing efforts, now there exists a tremendous amount of atmospheric data, obtained through continuous measurements directly from the atmosphere. This fact makes the analysis by human brains difficult but, on the other hand, enables the usage of modern data science techniques. Here, we calculate and explore the mutual information (MI) between observed NPF events (measured at Hyytiälä, Finland) and a wide variety of simultaneously monitored ambient variables: trace gas and aerosol particle concentrations, meteorology, radiation and a few derived quantities. The purpose of the investigations is to identify key factors contributing to the NPF. The applied mutual

information method finds that the formation events are strongly linked to sulfuric acid concentration and water content, ultraviolet radiation, condensation sink (CS) and temperature. Previously, these quantities have been well-established to be important players in the phenomenon via dedicated field, laboratory and theoretical research. The novelty of this work is to demonstrate that the same results are now obtained by a data analysis method which operates without supervision and without the need of understanding the physics deeply. This suggests that the method is suitable to be implemented widely in the atmospheric field to discover other interesting phenomena and their relevant variables.

Biomass burning emission disturbances of isoprene oxidation in a tropical forest

Fernando Santos[1], Karla Longo[2], Alex Guenther[3], Saewung Kim[3], Dasa Gu[3], Dave Oram[4],Grant Forster[4], James Lee[5], James Hopkins[5], Joel Brito[6,a], and Saulo Freitas[2]

Source: Atmosphere Chemistry and Physics, Volume 18, issue 17
04 Sep 2018.

We present a characterization of the chemical composition of the atmosphere of the Brazilian Amazon rainforest based on trace gas measurements carried out during the South AMerican Biomass Burning Analysis (SAMBBA) airborne experiment in September 2012. We analyzed the observations of primary biomass burning emission tracers, i.e., carbon monoxide (CO), nitrogen oxides (NO_x), ozone (O_3), isoprene, and its main oxidation products, methyl vinyl ketone (MVK), methacrolein (MACR), and isoprene hydroxy hydroperoxide (ISOPOOH). The focus of SAMBBA was primarily on biomass burning emissions, but there were also several flights in areas of the Amazon forest not directly affected by biomass burning, revealing a background with a signature of biomass burning in the chemical composition due to long-range transport of biomass burning tracers from both Africa and the eastern part of Amazonia. We used the [MVK+MACR+ISOPOOH]/[isoprene] ratio and the hydroxyl radical (OH) indirect calculation to assess the oxidative capacity of the Amazon forest atmosphere. We compared the background regions (CO<150ppbv), fresh and aged smoke plumes classified according to their photochemical age ([O_3]/[CO]), to evaluate the impact of biomass burning emissions on the oxidative capacity of the Amazon forest atmosphere. We observed that biomass burning emissions disturb the isoprene oxidation reactions, especially for fresh plumes ([MVK+MACR+ISOPOOH]/[isoprene] = 7) downwind. The oxidation of isoprene is higher in

fresh smoke plumes at lower altitudes (~500m) than in aged smoke plumes, anticipating near the surface a complex chain of oxidation reactions which may be related to secondary organic aerosol (SOA) formation. We proposed a refinement of the OH calculation based on the sequential reaction model, which considers vertical and horizontal transport for both biomass burning regimes and background environment. Our approach for the [OH] estimation resulted in values on the same order of magnitude of a recent observation in the Amazon rainforest [OH]≅10^6 (moleculescm^{-3}). During the fresh plume regime, the vertical profile of [OH] and the [MVK+MACR+ISOPOOH]/[isoprene] ratio showed evidence of an increase in the oxidizing power in the transition from planetary boundary layer to cloud layer (1000–1500m). These high values of [OH] (1.5×10^6moleculescm^{-3}) and [MVK+MACR+ISOPOOH]/[isoprene] (7.5) indicate a significant change above and inside the cloud decks due to cloud edge effects on photolysis rates, which have a major impact on OH production rates.

On the spectral depolarisation and lidar ratio of mineral dust provided in the AERONET version 3 inversion products.

Sung-Kyun Shin[1], Matthias Tesche[1], Kwanchul Kim[2], Maria Kezoudi[1], Boyan Tatarov[1],Detlef Müller[1], and Youngmin Noh[3]

Source: Atmosphere Chemistry and Physics, Volume 18, issue 17
04 Sep 2018.

Knowledge of the particle lidar ratio (S_λ) and the particle linear depolarisation ratio (δ_λ) for different aerosol types allows for aerosol typing and aerosol-type separation in lidar measurements. Reference values generally originate from dedicated lidar observations but might also be obtained from the inversion of AErosol RObotic NETwork (AERONET) sun/sky radiometer measurements. This study investigates the consistency of spectral S_λ and δ_λ provided in the recently released AERONET version 3 inversion product for observations of undiluted mineral dust in the vicinity of the following major deserts: Gobi, Sahara, Arabian, Great Basin, and Great Victoria. Pure dust conditions are identified by an Ångström exponent < 0.4 and a fine-mode fraction < 0.1.

The values of spectral S_λ are found to vary for the different source regions but generally show an increase with decreasing wavelength. The feature correlates to AERONET, retrieving an increase in the imaginary part of the refractive index with decreasing wavelength. The smallest values of $S_\lambda = 35–45$sr are found for mineral dust from the Great Basin desert, while the highest values of 50–70sr have been inferred from AERONET

observations of Saharan dust. Values of S_λ at 675, 870, and 1020nm seem to be in reasonable agreement with available lidar observations, while those at 440nm are up to 10sr higher than the lidar reference. The spectrum of δ_λ shows a maximum of 0.26–0.31 at 1020nm and decreasing values as wavelength decreases. AERONET-derived δ_λ values at 870 and 1020nm are in line with the lidar reference, while values of 0.19–0.24 at 440nm are smaller than the independent lidar observations by a difference of 0.03 to 0.08. This general behaviour is consistent with earlier studies based on AERONET version 2 products.

Exploring the first aerosol indirect effect over Southeast Asia using a 10-year collocated MODIS, CALIOP, and model dataset

Alexa D. Ross[1], Robert E. Holz[1], Gregory Quinn[1], Jeffrey S. Reid[2], Peng Xian[2], F. Joseph Turk[3],and Derek J. Posselt[3]

Source: Atmosphere Chemistry and Physics, Volume 18, issue 17
04 Sep 2018

Satellite observations and model simulations cannot, by themselves, give full insight into the complex relationships between aerosols and clouds. This is especially true over Southeast Asia, an area that is particularly sensitive to changes in precipitation yet poses some of the world's largest observability and predictability challenges. We present a new collocated dataset, the Curtain Cloud-Aerosol Regional A-Train dataset, or CCARA. CCARA includes collocated satellite observations from Aqua's Moderate-resolution Imaging Spectroradiometer (MODIS) and the Cloud-Aerosol Lidar with Orthogonal Polarization (CALIOP) with the Navy Aerosol Analysis and Prediction System (NAAPS). The CCARA dataset is designed with the capability to investigate aerosol–cloud relationships in regions with limited aerosol retrievals due to high cloud amounts by leveraging the NAAPS model reanalysis of aerosol concentration in these regions. This combined aerosol and cloud dataset provides coincident and vertically resolved cloud and aerosol observations for 2006–2016. Using the model reanalysis aerosol fields from the NAAPS and coincident cloud liquid effective radius retrievals from MODIS (cirrus contamination using CALIOP), we investigate the first aerosol indirect effect in Southeast Asia. We find that, as expected, aerosol loading anti-correlates with cloud effective radius, with maximum sensitivity in cumulous mediocris clouds with heights in the 3–4.5km level. The highest susceptibilities in droplet effective radius to modeled perturbations in particle concentrations were found in the more remote and pristine regions of the western Pacific Ocean and Indian Ocean. Conversely, there was much less variability in cloud droplet size near emission sources

over both land and water. We hypothesize this is suggestive of a high aerosol background already saturated with cloud condensation nuclei even during the relatively clean periods, in contrast to the remote ocean regions, which have periods where the aerosol concentrations are low enough to allow for larger droplet growth.

Understanding nitrate formation in a world with less sulfate

Petros Vasilakos[1], Armistead Russell[2], Rodney Weber[3], and Athanasios Nenes[1,3,4,5,a]

Source: Atmosphere Chemistry and Physics, Volume 18, issue 17
05 Sep 2018.

SO_2 emission controls, combined with modestly increasing ammonia, have been thought to generate aerosol with significantly reduced acidity for cases in which sulfate is partially substituted by nitrate. However, neither expectation agrees with decadal observations in the southeastern USA, suggesting that a fundamentally different response of aerosol pH to emissions changes is occurring. We postulate that this nitrate substitution paradox arises from a positive bias in aerosol pH in model simulations. This bias can elevate pH to a level at which nitrate partitioning is readily promoted, leading to behavior consistent with nitrate substitution. CMAQ simulations are used to investigate this hypothesis; modeled $PM_{2.5}$ pH using 2001 emissions compare favorably with pH inferred from observed species concentrations. Using 2011 emissions, however, leads to simulated pH increases of one unit, which is inconsistent with observations from that year. Nonvolatile cations (K^+, Na^+, Ca^{+2}, and Mg^{+2}) in the fine mode are found to be responsible for the erroneous predicted increase in aerosol pH of about 1 unit on average over the USA. Such an increase can induce a nitrate bias of 1–2μgm^{-3}, which may further increase in future projections, reaffirming an otherwise incorrect expectation of a significant nitrate substitution. Evaluation of predicted aerosol pH against thermodynamic analysis of observations is therefore a critically important, but overlooked, aspect of model evaluation for a robust emissions policy.

An 800-year high-resolution black carbon ice core record from Lomonosovfonna, Svalbard

Dimitri Osmont[1,2,3], Isabel A. Wendl[1,2,3], Loïc Schmidely[2,4], Michael Sigl[1,2], Carmen P. Vega[5,a],Elisabeth Isaksson[6], and Margit Schwikowski[1,2,3]

Source: Atmosphere Chemistry and Physics, Volume 18, issue 17
06 Sep 2018

Produced by the incomplete combustion of fossil fuel and biomass, black carbon (BC) contributes to Arctic warming by reducing snow albedo and thus triggering a snow-albedo feedback leading to increased snowmelt. Therefore, it is of high importance to assess past BC emissions to better understand and constrain their role. However, only a few long-term BC records are available from the Arctic, mainly originating from Greenland ice cores. Here, we present the first long-term and high-resolution refractory black carbon (rBC) record from Svalbard, derived from the analysis of two ice cores drilled at the Lomonosovfonna ice field in 2009 (LF-09) and 2011 (LF-11) and covering 800 years of atmospheric emissions. Our results show that rBC concentrations strongly increased from 1860 on due to anthropogenic emissions and reached two maxima, at the end of the 19th century and in the middle of the 20th century. No increase in rBC concentrations during the last decades was observed, which is corroborated by atmospheric measurements elsewhere in the Arctic but contradicts a previous study from another ice core from Svalbard. While melting may affect BC concentrations during periods of high temperatures, rBC concentrations remain well preserved prior to the 20th century due to lower temperatures inducing little melt. Therefore, the preindustrial rBC record (before 1800), along with ammonium (NH_4^+), formate ($HCOO^-$) and specific organic markers (vanillic acid, VA, and *p*-hydroxybenzoic acid, *p*-HBA), was used as a proxy for biomass burning. Despite numerous single events, no long-term trend was observed over the time period 1222–1800 for rBC and NH_4^+. In contrast, formate, VA, and *p*-HBA experience multi-decadal peaks reflecting periods of enhanced biomass burning. Most of the background variations and single peak events are corroborated by other ice core records from Greenland and Siberia. We suggest that the paleofire record from the LF ice core primarily reflects biomass burning episodes from northern Eurasia, induced by decadal-scale climatic variations.

The climate impact of aerosols on the lightning flash rate: is it detectable from long-term measurements?

Qianqian Wang[1], Zhanqing Li[1,2], Jianping Guo[3], Chuanfeng Zhao[1], and Maureen Cribb[2]

Source: Atmosphere Chemistry and Physics, Volume 18, issue 17
06 Sep 2018.

The effect of aerosols on lightning has been noted in many case studies, but much less is known about the long-term impact, relative importance of dynamics–thermodynamics versus aerosol, and any difference by different types of aerosols. Attempts are made to tackle all these factors, whose distinct roles are discovered by analyzing 11-year datasets of lightning, aerosol loading and composition, and dynamic–thermodynamic data from satellite and model reanalysis. Variations in the lightning rate are analyzed with respect to changes in dynamic–thermodynamic variables and indices such as the convective available potential energy (CAPE) and vertical wind shear. In general, lightning has strong diurnal and seasonal variations, peaking in the afternoon and during the summer. The lightning flash rate is much higher in moist central Africa than in dry northern Africa presumably because of the combined influences of surface heating, CAPE, relative humidity (RH), and aerosol type. In both regions, the lightning flash rate changes with aerosol optical depth (AOD) in a boomerang shape: first increasing with AOD, tailing off around AOD = 0.3, and then behaving differently, i.e., decreasing for dust and flattening for smoke aerosols. The deviation is arguably caused by the tangled influences of different thermodynamics (in particular humidity and CAPE) and aerosol type between the two regions. In northern Africa, the two branches of the opposite trends seem to echo the different dominant influences of the aerosol microphysical effect and the aerosol radiative effect that are more pronounced under low and high aerosol loading conditions, respectively. Under low-AOD conditions, the aerosol microphysical effect more likely invigorates deep convection. This may gradually yield to the suppression effect as AOD increases, leading to more and smaller cloud droplets that are highly susceptible to evaporation under the dry conditions of northern Africa. For smoke aerosols in moist central Africa, the aerosol invigoration effect can be sustained across the entire range of AOD by the high humidity and CAPE. This, plus a potential heating effect of the smoke layer, jointly offsets the suppression of convection due to the radiative cooling at the surface by smoke aerosols. Various analyses were done that tend to support this hypothesis.

Black and brown carbon over central Amazonia: long-term aerosol measurements at the ATTO site

Jorge Saturno[1,a], Bruna A. Holanda[1], Christopher Pöhlker[1], Florian Ditas[1], Qiaoqiao Wang[1,2],Daniel Moran-Zuloaga[1], Joel Brito[3,4], Samara Carbone[3,5], Yafang Cheng[1], Xuguang Chi[6],Jeannine Ditas[1,2], Thorsten Hoffmann[7], Isabella Hrabe de Angelis[1], Tobias Könemann[1],Jošt V. Lavrič[8], Nan Ma[1,2], Jing Ming[1], Hauke Paulsen[9], Mira L. Pöhlker[1], Luciana V. Rizzo[10],Patrick Schlag[3], Hang Su[1], David Walter[1], Stefan Wolff[1], Yuxuan Zhang[1], Paulo Artaxo[3],Ulrich Pöschl[1], and Meinrat O. Andreae[1,11]

Source: Atmosphere Chemistry and Physics, Volume 18, issue 17

06 Sep 2018.

The Amazon rainforest is a sensitive ecosystem experiencing the combined pressures of progressing deforestation and climate change. Its atmospheric conditions oscillate between biogenic and biomass burning (BB) dominated states. The Amazon further represents one of the few remaining continental places where the atmosphere approaches pristine conditions during occasional wet season episodes. The Amazon Tall Tower Observatory (ATTO) has been established in central Amazonia to investigate the complex interactions between the rainforest ecosystem and the atmosphere. Physical and chemical aerosol properties have been analyzed continuously since 2012. This paper provides an in-depth analysis of the aerosol's optical properties at ATTO based on data from 2012 to 2017. The following key results have been obtained.

- The aerosol scattering and absorption coefficients at 637nm, $\sigma_{sp,637}$ and $\sigma_{ap,637}$, show a pronounced seasonality with lowest values in the clean wet season (mean±SD: $\sigma_{sp,637} = 7.5\pm9.3 Mm^{-1}$; $\sigma_{ap,637} = 0.68\pm0.91 Mm^{-1}$) and highest values in the BB-polluted dry season ($\sigma_{sp,637} = 33\pm25 Mm^{-1}$; $\sigma_{ap,637} = 4.0\pm2.2 Mm^{-1}$). The single scattering albedo at 637nm, ω_0, is lowest during the dry season ($\omega_0 = 0.87\pm0.03$) and highest during the wet season ($\omega_0 = 0.93\pm0.04$).

- The retrieved BC mass absorption cross sections, α_{abs}, are substantially higher than values widely used in the literature (i.e., $6.6 m^2 g^{-1}$ at 637nm wavelength), likely related to thick organic or inorganic coatings on the BC cores. Wet season values of $\alpha_{abs} = 11.4\pm1.2 m^2 g^{-1}$ (637nm) and dry season values of $\alpha_{abs} = 12.3\pm1.3 m^2 g^{-1}$ (637nm) were obtained.

- The BB aerosol during the dry season is a mixture of rather fresh smoke from local fires, somewhat aged smoke from regional fires, and strongly aged smoke from African fires. The

African influence appears to be substantial, with its maximum from August to October. The interplay of African vs. South American BB emissions determines the aerosol optical properties (e.g., the fractions of black vs. brown carbon, BC vs. BrC).

- By analyzing the diel cycles, it was found that particles from elevated aerosol-rich layers are mixed down to the canopy level in the early morning and particle number concentrations decrease towards the end of the day. Brown carbon absorption at 370nm, $\sigma_{ap,BrC,370}$, was found to decrease earlier in the day, likely due to photo-oxidative processes.

- BC-to-CO enhancement ratios, ER_{BC}, reflect the variability of burnt fuels, combustion phases, and atmospheric removal processes. A wide range of ER_{BC} between 4 and 15ngm^{-3}ppb^{-1} was observed with higher values during the dry season, corresponding to the lowest ω_0 levels (0.86–0.93).

- The influence of the 2009/2010 and 2015/2016 El Niño periods and the associated increased fire activity on aerosol optical properties was analyzed by means of 9-year σ_{sp} and σ_{ap} time series (combination of ATTO and ZF2 data). Significant El Niño-related enhancements were observed: in the dry season, $\sigma_{sp,637}$ increased from 24±18 to 48±33Mm^{-1} and $\sigma_{ap,\,637}$ from 3.8±2.8 to 5.3±2.5Mm^{-1}.

- The absorption Ångström exponent, $å_{abs}$, representing the aerosol absorption wavelength dependence, was mostly <1.0 with episodic increases upon smoke advection. A parameterization of $å_{abs}$ as a function of the BC-to-OA mass ratio for Amazonian aerosol ambient measurements is presented. The brown carbon (BrC) contribution to σ_{ap} at 370nm was obtained by calculating the theoretical BC $å_{abs}$, resulting in BrC contributions of 17%–29% (25th and 75th percentiles) to $\sigma_{ap\,370}$ for the entire measurement period. The BrC contribution increased to 27%–47% during fire events under El Niño-related drought conditions from September to November 2015.

  The results presented here may serve as a basis to understand Amazonian atmospheric aerosols in terms of their interactions with solar radiation and the physical and chemical-aging processes that they undergo during transport. Additionally, the analyzed aerosol properties during the last two El Niño periods in 2009/2010 and 2015/2016 offer insights that could help to assess the climate change-related potential for forest-dieback feedbacks under warmer and drier conditions.

Stratospheric aerosol radiative forcing simulated by the chemistry climate model EMAC using Aerosol CCI satellite data

Christoph Brühl[1], Jennifer Schallock[1], Klaus Klingmüller[1], Charles Robert[2], Christine Bingen[2],Lieven Clarisse[3], Andreas Heckel[4], Peter North[4], and Landon Rieger[5]

Source : Atmosphere Chemistry and Physics, Volume 18, issue 17
06 Sep 2018

This paper presents decadal simulations of stratospheric and tropospheric aerosol and its radiative effects by the chemistry general circulation model EMAC constrained with satellite observations in the framework of the ESA Aerosol CCI project such as GOMOS (Global Ozone Monitoring by Occultation of Stars) and (A)ATSR ((Advanced) Along Track Scanning Radiometer) on the ENVISAT (European Environmental Satellite), IASI (Infrared Atmospheric Sounding Interferometer) on MetOp (Meteorological Operational Satellite), and, additionally, OSIRIS (Optical Spectrograph and InfraRed Imaging System). In contrast to most other studies, the extinctions and optical depths from the model are compared to the observations at the original wavelengths of the satellite instruments covering the range from the UV (ultraviolet) to terrestrial IR (infrared). This avoids conversion artifacts and provides additional constraints for model aerosol and interpretation of the observations.

MIPAS (Michelson Interferometer for Passive Atmospheric Sounding) SO_2 limb measurements are used to identify plumes of more than 200 volcanic eruptions. These three-dimensional SO_2 plumes are added to the model SO_2 at the eruption times. The interannual variability in aerosol extinction in the lower stratosphere, and of stratospheric aerosol radiative forcing at the tropopause, is dominated by the volcanoes. To explain the seasonal cycle of the GOMOS and OSIRIS observations, desert dust simulated by a new approach and transported to the lowermost stratosphere by the Asian summer monsoon and tropical convection turns out to be essential. This also applies to the radiative heating by aerosol in the lowermost stratosphere. The existence of wet dust aerosol in the lowermost stratosphere is indicated by the patterns of the wavelength dependence of extinction in observations and simulations. Additional comparison with (A)ATSR total aerosol optical depth at different wavelengths and IASI dust optical depth demonstrates that the model is able to represent stratospheric as well as tropospheric aerosol consistently.

Concentration, temporal variation, and sources of black carbon in the Mt. Everest region retrieved by real-time observation and simulation

Xintong Chen[1,4], Shichang Kang[1,2,4], Zhiyuan Cong[2,3], Junhua Yang[1], and Yaoming Ma[2,3]

Source: Atmosphere Chemistry and Physics, Volume 18, issue 17
06 Sep 2018.

Based on the high-resolution measurement of black carbon (BC) at the Qomolangma (Mt. Everest) Station (QOMS, 28.36°N, 86.95°E, 4276ma.s.l.) from 15 May 2015 to 31 May 2017, we investigated the seasonal and diurnal variations in BC and its potential source regions. Both monthly and daily mean BC concentrations reached the highest values in the pre-monsoon season and the lowest values in the monsoon season. The highest monthly and daily mean BC concentrations were at least 1 order of magnitude higher than the lowest concentrations. For the diurnal variation, the BC concentrations remained significantly high from late at night to morning in the pre-monsoon season. Meanwhile, the westerly winds prevailed during this period, implying the potential for pollutants to be transported across the Himalayas from long-distance sources to QOMS along the valley. In the monsoon season, the BC concentrations remained low but peaked in the morning and at noon, which might be caused by local emissions from cooking. By analyzing the simulation results from the backward trajectories of air masses and the fire spot distribution from the MODIS data, we found that the seasonal cycle of BC was significantly influenced by the atmospheric circulation and combustion intensity in the Mt. Everest region. The transport mechanisms of BC were further revealed using a WRF-Chem simulation during severe pollution episodes. For the pollution event in the monsoon season, BC aerosols in southern Asia were uplifted and transported to the Mt. Everest region by the southerly winds in the upper atmosphere. However, for the events in the pre-monsoon season, BC from northern India was transported and concentrated on the southern slope of the Himalayas by the northwesterly winds in the lower atmosphere and then transported across the Himalayas by the mountain-valley wind. A relatively smaller amount of BC from northwestern India and central Asia was transported to the Mt. Everest region by the westerly winds in the upper atmosphere.

Are atmospheric PBDE levels declining in central Europe? Examination of the seasonal and semi-long-term variations, gas–particle partitioning and implications for long-range atmospheric transport

Céline Degrendele[1], Jake Wilson[2], Petr Kukučka[1], Jana Klánová[1], and Gerhard Lammel[1,2]

Source: Atmosphere Chemistry and Physics, Volume 18, issue 17

06 Sep 2018.

This study presents multi-year monitoring data on atmospheric polybrominated diphenyl ethers (PBDEs) in central Europe. Air was sampled on a weekly basis at a background site in the central Czech Republic from 2011 to 2014 ($N = 114$). Σ_8PBDEs (without BDE209) total (gas and particulate) concentrations ranged from 0.084 to 6.08pgm^{-3}, while BDE209 was at 0.05–5.01pgm^{-3}. BDE47, BDE99 and BDE183 were the major contributors to Σ_8PBDEs.

Overall, the atmospheric concentrations of individual PBDEs were controlled by deposition processes, meteorological parameters and long-range atmospheric transport. Regarding gas–particle partitioning, with the exception of BDE28 (gaseous) and BDE209 (particulate), all congeners were consistently detected in both phases. Clear seasonal variations with significantly higher measured particulate fraction ($\theta_{measured}$) in winter compared to summer was found for all PBDEs except BDE209. For example, while the average $\theta_{measured}$ of BDE47 was 0.53±0.19 in winter, this was only 0.01±0.02 in summer. Similarly, for BDE99, $\theta_{measured}$ was 0.89±0.13 in winter, while it was only 0.12±0.08 in summer. The observed gas–particle partitioning coefficient (K_p, in m^{3}µg^{-1}) was compared with three model predictions, assuming equilibrium or a steady state. None of the models could provide a satisfactory prediction of the partitioning, suggesting the need for a universally applicable model.

Statistically significant decreases of the atmospheric concentrations during 2011–2014 were found for BDE99, 100, 153 and 209. Estimated apparent atmospheric halving times for these congeners ranged from 2.8 (BDE209) to 4.8 (BDE153) years. The results suggest that photolytic debromination to lower brominated congeners may significantly influence PBDE concentration levels and patterns in the atmosphere.

Modeling the formation and composition of secondary organic aerosol from diesel exhaust using parameterized and semi-explicit chemistry and thermodynamic models

Sailaja Eluri[1], Christopher D. Cappa[2], Beth Friedman[3], Delphine K. Farmer[3],and Shantanu H. Jathar[1]

Source: Atmosphere Chemistry and Physics, Volume 18, issue 19
01 Oct 2018.

Laboratory-based studies have shown that combustion sources emit volatile organic compounds that can be photooxidized in the atmosphere to form secondary organic aerosol (SOA). In some cases, this SOA can exceed direct emissions of primary organic aerosol (POA). Jathar et al. (2017a) recently reported on experiments that used an oxidation flow reactor (OFR) to measure the photochemical production of SOA from a diesel engine operated at two different engine loads (idle, load), two fuel types (diesel, biodiesel), and two aftertreatment configurations (with and without an oxidation catalyst and particle filter). In this work, we used two different SOA models, the Volatility Basis Set (VBS) model and the Statistical Oxidation Model (SOM), to simulate the formation and composition of SOA for those experiments. Leveraging recent laboratory-based parameterizations, both frameworks accounted for a semi-volatile and reactive POA; SOA production from semi-volatile, intermediate-volatility, and volatile organic compounds (SVOC, IVOC and VOC); NO_x-dependent parameterizations; multigenerational gas-phase chemistry; and kinetic gas–particle partitioning. Both frameworks demonstrated that for model predictions of SOA mass to agree with measurements across all engine load–fuel–aftertreatment combinations, it was necessary to model the kinetically limited gas–particle partitioning in OFRs and account for SOA formation from IVOCs, which were on average found to account for 70% of the model-predicted SOA. Accounting for IVOCs, however, resulted in an average underprediction of 28% for OA atomic O:C ratios. Model predictions of the gas-phase organic compounds (resolved in carbon and oxygen space) from the SOM compared favorably to gas-phase measurements from a chemical ionization mass spectrometer (CIMS), substantiating the semi-explicit chemistry captured by the SOM. Model–measurement comparisons were improved on using SOA parameterizations corrected for vapor wall loss. As OFRs are increasingly used to study SOA formation and evolution in laboratory and field environments, models such as those developed in this work can be used to interpret the OFR data.

Long-term measurements of volatile organic compounds highlight the importance of sesquiterpenes for the atmospheric chemistry of a boreal forest

Heidi Hellén[1], Arnaud P. Praplan[1], Toni Tykkä[1], Ilona Ylivinkka[2], Ville Vakkari[1], Jaana Bäck[3],Tuukka Petäjä[2], Markku Kulmala[2], and Hannele Hakola[1]

Source: Atmosphere Chemistry and Physics, Volume 18, issue 19
01 Oct 2018.

The concentrations of terpenoids (isoprene; monoterpenes, MTs; and sesquiterpenes, SQTs) and oxygenated volatile organic compounds (OVOCs; i.e. aldehydes, alcohols, acetates and volatile organic acids, VOAs) were investigated during 2 years at a boreal forest site in Hyytiälä, Finland, using in situ gas chromatograph mass spectrometers (GC-MSs). Seasonal and diurnal variations of terpenoid and OVOC concentrations as well as their relationship with meteorological factors were studied.

Of the VOCs examined, C_2–C_7 unbranched VOAs showed the highest concentrations, mainly due to their low reactivity. Of the terpenoids, MTs showed the highest concentrations at the site, but seven different highly reactive SQTs were also detected. The monthly and daily mean concentrations of most terpenoids, aldehydes and VOAs were highly dependent on the temperature. The highest exponential correlation with temperature was found for a SQT (β-caryophyllene) in summer. The diurnal variations in the concentrations could be explained by sources, sinks and vertical mixing. The diurnal variations in MT concentrations were strongly affected by vertical mixing. Based on the temperature correlations and mixing layer height (MLH), simple proxies were developed for estimating the MT and SQT concentrations.

To estimate the importance of different compound groups and compounds in local atmospheric chemistry, reactivity with main oxidants (hydroxyl radical, OH; nitrate radical, NO_3; and ozone, O_3) and production rates of oxidation products (OxPRs) were calculated. The MTs dominated OH and NO_3 radical chemistry, but the SQTs greatly impacted O_3 chemistry, even though the concentrations of SQT were 30 times lower than the MT concentrations. SQTs were also the most important for the production of oxidation products. Since the SQTs show high secondary organic aerosol (SOA) yields, the results clearly indicate the importance of SQTs for local SOA production.

Enhancements of airborne particulate arsenic over the subtropical free troposphere: impact of southern Asian biomass burning

Yu-Chi Lin[1,2,3,4], Shih-Chieh Hsu[4], Chuan-Yao Lin[4], Shuen-Hsin Lin[4], Yi-Tang Huang[4],Yunhua Chang[1,2,3], and Yan-Lin Zhang[1,2,3]

Source: Atmosphere Chemistry and Physics, Volume 18, issue 19
01 Oct 2018.

Arsenic (As) has long been recognized as a toxic element of mainly anthropogenic origins, having adverse effects on human health. However, there is insufficient understanding regarding As released into atmosphere from biomass burning (BB). To this end, daily airborne As concentrations in total particulate matter (TSP) were determined at Mount Hehuan (24.16°N, 121.29°E, 3001ma.s.l.), Taiwan from September 2011 to September 2012. During the sampling period, As concentrations varied from 0.02 to 5.9ngm^{-3}, with a mean value of 0.5±1.0ngm^{-3}. Significantly seasonal variations of As were found over the subtropical free troposphere, and higher As concentrations were observed in the southern (S) and southeastern (SE) Asian BB seasons (from January to May). Principal component analysis (PCA) results showed that BB activities seemed to be a major source of As during the S and SE Asian BB periods, which were very distinct from the major source of coal-fired power plant during the periods between July and December. Based on backward trajectory analyses and WRF-Chem model simulations, we found that the high As concentrations during the BB periods were attributed to the biomass burning activities over S Asia where groundwater, soil and crops are severely contaminated by arsenic. A strong correlation (r = 0.73 p < 0.05) between As and potassium ion (K^+, a chemical tracer of BB activities) in S Asian BB events also supported this hypothesis. During the S Asian BB events, the high As⁄Pb ratios (> 0.2) were also observed, indicating that burning crops contaminated by lead arsenate might be a crucial candidate for high As concentrations at Mount Hehuan. Nevertheless, the net influence of S Asian BB activities on airborne As concentrations has been estimated by comparing the differences of As concentrations on BB and non-BB days. On average, the difference in As concentrations was 1.0ngm^{-3}, which accounted for 63% of the average As concentration on BB days. Moreover, a ratio of ΔAs⁄ΔCO (~ 0.00001) in the S Asian BB events was obtained. Using this value, arsenic emissions from S Asian BB activities were estimated to be 0.17tonsyr^{-1}, resulting in high airborne As concentrations over the subtropical free troposphere and impacting As cycles on a regional scale in the S and SE Asian BB seasons.

Atmospheric CO and CH_4 time series and seasonal variations on Reunion Island from ground-based in situ and FTIR (NDACC and TCCON) measurements

Minqiang Zhou[1], Bavo Langerock[1], Corinne Vigouroux[1], Mahesh Kumar Sha[1], Michel Ramonet[2],Marc Delmotte[2], Emmanuel Mahieu[3], Whitney Bader[3], Christian Hermans[1], Nicolas Kumps[1],Jean-Marc Metzger[4], Valentin Duflot[5,4], Zhiting Wang[6,7], Mathias Palm[6], and Martine De Mazière[1]

Source: Atmosphere Chemistry and Physics, Volume 18, issue 19
01 Oct 2018.

Atmospheric carbon monoxide (CO) and methane (CH_4) mole fractions are measured by ground-based in situ cavity ring-down spectroscopy (CRDS) analyzers and Fourier transform infrared (FTIR) spectrometers at two sites (St Denis and Maïdo) on Reunion Island (21°S, 55°E) in the Indian Ocean. Currently, the FTIR Bruker IFS 125HR at St Denis records the direct solar spectra in the near-infrared range, contributing to the Total Carbon Column Observing Network (TCCON). The FTIR Bruker IFS 125HR at Maïdo records the direct solar spectra in the mid-infrared (MIR) range, contributing to the Network for the Detection of Atmospheric Composition Change (NDACC). In order to understand the atmospheric CO and CH_4 variability on Reunion Island, the time series and seasonal cycles of CO and CH_4 from in situ and FTIR (NDACC and TCCON) measurements are analyzed. Meanwhile, the difference between the in situ and FTIR measurements are discussed.

The CO seasonal cycles observed from the in situ measurements at Maïdo and FTIR retrievals at both St Denis and Maïdo are in good agreement with a peak in September–November, primarily driven by the emissions from biomass burning in Africa and South America. The dry-air column averaged mole fraction of CO (X_{CO}) derived from the FTIR MIR spectra (NDACC) is about 15.7ppb larger than the CO mole fraction near the surface at Maïdo, because the air in the lower troposphere mainly comes from the Indian Ocean while the air in the middle and upper troposphere mainly comes from Africa and South America. The trend for CO on Reunion Island is unclear during the 2011–2017 period, and more data need to be collected to get a robust result.

A very good agreement is observed in the tropospheric and stratospheric CH_4 seasonal cycles between FTIR (NDACC and TCCON) measurements, and in situ and the Michelson Interferometer for Passive Atmospheric Sounding (MIPAS) satellite measurements, respectively. In the troposphere, the CH_4 mole fraction is high in August–September and

low in December–January, which is due to the OH seasonal variation. In the stratosphere, the CH_4 mole fraction has its maximum in March–April and its minimum in August–October, which is dominated by vertical transport. In addition, the different CH_4 mole fractions between the in situ, NDACC and TCCON CH_4 measurements in the troposphere are discussed, and all measurements are in good agreement with the GEOS-Chem model simulation. The trend of $X_{CH4}$is 7.6±0.4ppbyr^{-1} from the TCCON measurements over the 2011 to 2017 time period, which is consistent with the CH_4 trend of 7.4±0.5ppbyr^{-1} from the in situ measurements for the same time period at St Denis.

Coal fly ash: linking immersion freezing behavior and physicochemical particle properties

Sarah Grawe[1], Stefanie Augustin-Bauditz[1,a], Hans-Christian Clemen[2], Martin Ebert[3],Stine Eriksen Hammer[3], Jasmin Lubitz[1], Naama Reicher[4], Yinon Rudich[4], Johannes Schneider[2],Robert Staacke[5], Frank Stratmann[1], André Welti[1,b], and Heike Wex[1]

Source: Atmosphere Chemistry and Physics, Volume 18, issue 19
02 Oct 2018.

To date, only a few studies have investigated the potential of coal fly ash particles to trigger heterogeneous ice nucleation in cloud droplets. The presented measurements aim at expanding the sparse dataset and improving process understanding of how physicochemical particle properties can influence the freezing behavior of coal fly ash particles immersed in water.

Firstly, immersion freezing measurements were performed with two single particle techniques, i.e., the Leipzig Aerosol Cloud Interaction Simulator (LACIS) and the SPectrometer for Ice Nuclei (SPIN). The effect of suspension time on the efficiency of the coal fly ash particles when immersed in a cloud droplet is analyzed based on the different residence times of the two instruments and employing both dry and wet particle generation. Secondly, two cold-stage setups, one using microliter sized droplets (Leipzig Ice Nucleation Array) and one using nanoliter sized droplets (WeIzmann Supercooled Droplets Observation on Microarray setup) were applied.

We found that coal fly ash particles are comparable to mineral dust in their immersion freezing behavior when being dry generated. However, a significant decrease in immersion freezing efficiency was observed during experiments with wet-generated particles in LACIS

and SPIN. The efficiency of wet-generated particles is in agreement with the cold-stage measurements. In order to understand the reason behind the deactivation, a series of chemical composition, morphology, and crystallography analyses (single particle mass spectrometry, scanning electron microscopy coupled with energy dispersive X-ray microanalysis, X-ray diffraction analysis) were performed with dry- and wet-generated particles. From these investigations, we conclude that anhydrous $CaSO_4$ and CaO – which, if investigated in pure form, show the same qualitative immersion freezing behavior as observed for dry-generated coal fly ash particles – contribute to triggering heterogeneous ice nucleation at the particle–water interface. The observed deactivation in contact with water is related to changes in the particle surface properties which are potentially caused by hydration of $CaSO_4$ and CaO. The contribution of coal fly ash to the ambient population of ice-nucleating particles therefore depends on whether and for how long particles are immersed in cloud droplets.

Seasonal ozone vertical profiles over North America using the AQMEII3 group of air quality models: model inter-comparison and stratospheric intrusions

Marina Astitha[1], Ioannis Kioutsioukis[2], Ghezae Araya Fisseha[1], Roberto Bianconi[3],Johannes Bieser[4,5], Jesper H. Christensen[6], Owen R. Cooper[7,8], Stefano Galmarini[9],Christian Hogrefe[10], Ulas Im[6], Bryan Johnson[7], Peng Liu[11], Uarporn Nopmongcol[12],Irina Petropavlovskikh[7], Efisio Solazzo[9], David W. Tarasick[13], and Greg Yarwood[12]

Source: Atmosphere Chemistry and Physics, Volume 18, issue 19
02 Oct 2018.

This study evaluates simulated vertical ozone profiles produced in the framework of the third phase of the Air Quality Model Evaluation International Initiative (AQMEII3) against ozonesonde observations in North America for the year 2010. Four research groups from the United States (US) and Europe have provided modeled ozone vertical profiles to conduct this analysis. Because some of the modeling systems differ in their meteorological drivers, wind speed and temperature are also included in the analysis. In addition to the seasonal ozone profile evaluation for 2010, we also analyze chemically inert tracers designed to track the influence of lateral boundary conditions on simulated ozone profiles within the modeling domain. Finally, cases of stratospheric ozone intrusions during May–June 2010 are investigated by analyzing ozonesonde measurements and the corresponding model simulations at Intercontinental Chemical Transport Experiment Ozonesonde

Network Study (IONS) experiment sites in the western United States. The evaluation of the seasonal ozone profiles reveals that, at a majority of the stations, ozone mixing ratios are underestimated in the 1–6km range. The seasonal change noted in the errors follows the one seen in the variance of ozone mixing ratios, with the majority of the models exhibiting less variability than the observations. The analysis of chemically inert tracers highlights the importance of lateral boundary conditions up to 250hPa for the lower-tropospheric ozone mixing ratios (0–2km). Finally, for the stratospheric intrusions, the models are generally able to reproduce the location and timing of most intrusions but underestimate the magnitude of the maximum mixing ratios in the 2–6km range and overestimate ozone up to the first kilometer possibly due to marine air influences that are not accurately described by the models. The choice of meteorological driver appears to be a greater predictor of model skill in this altitude range than the choice of air quality model.

Characterization of biogenic primary and secondary organic aerosols in the marine atmosphere over the East China Sea

Mingjie Kang[1,2,3], Pingqing Fu[1,2,4], Kimitaka Kawamura[5], Fan Yang[2], Hongliang Zhang[6],Zhengchen Zang[7], Hong Ren[2,8], Lujie Ren[1], Ye Zhao[3], Yele Sun[2,8], and Zifa Wang[2,8]

Source: Atmosphere Chemistry and Physics, Volume 18, issue 19
02 Oct 2018.

Molecular composition and abundance of sugars and secondary organic aerosols (SOA) from biogenic sources over the East China Sea were investigated based on gas chromatography–mass spectrometry. Biogenic SOA tracers and sugars exhibit higher levels in the samples affected by continental air masses, demonstrating the terrestrial outflows of organic matter to the East China Sea. Glucose was the dominant sugar species (0.31–209, 18.8ngm^{-3}), followed by mannitol – a fungal spore tracer. All sugar compounds show generally higher average concentrations in the nighttime than in the daytime. 3-Methyl-1,2,3-butanetricarboxylic acid, one higher generation photooxidation tracer of monoterpene SOA, was found to be the most abundant species among measured biogenic SOA markers, suggesting the input of aged organic aerosols through long-range transport. Fungal-spore-derived organic carbon (OC) was the biggest contributor to total OC (0.03%–19.8%, 3.1%), followed by sesquiterpene-derived secondary OC (SOC), biomass-burning-derived OC, and monoterpene- and isoprene-derived SOC. Larger carbon percentages of biogenic primary OCs and SOCs in total OC presented in the terrestrially influenced aerosols indicate significant contributions of continental aerosols through long-range

transport. Positive matrix factorization results illustrate that the secondary nitrate and biogenic SOA, biomass burning, and fungal spores were the main sources of OC in marine aerosols over the East China Sea, again highlighting the importance of the Asian continent as a natural emitter of biogenic organic aerosols together with anthropogenic aerosols over the coastal marine atmosphere.

Daytime HONO, NO_2 and aerosol distributions from MAX-DOAS observations in Melbourne

Robert G. Ryan[1,2], Steve Rhodes[3], Matthew Tully[3], Stephen Wilson[4], Nicholas Jones[4],Udo Frieß[5], and Robyn Schofield[1,2]

Source: Atmosphere Chemistry and Physics, Volume 18, issue 19
02 Oct 2018

Toxic nitrogen oxides produced by high temperature combustion are prevalent in urban environments, contributing to a significant health burden. Nitrogen oxides such as NO_2 and HONO in pollution are important for hydroxyl radical (OH) production and overall oxidative capacity in urban environments; however, current mechanisms cannot explain high daytime levels of HONO observed in many urban and rural locations around the world. Here we present HONO, NO_2 and aerosol extinction vertical distributions retrieved from multi-axis differential optical absorption spectroscopy (MAX-DOAS) measurements in suburban Melbourne, which are the first MAX-DOAS results from the Australian continent. Using the optimal estimation algorithm HEIPRO we show that vertical profiles for NO_2 and HONO can be calculated with a low dependence on the retrieval forward model and a priori parameters, despite a lack of independent co-located aerosol or trace gas measurements. Between December 2016 and April 2017 average peak NO_2 values of 8±2ppb indicated moderate traffic pollution levels, and high daytime peak values of HONO were frequently detected, averaging 220±30ppt in the middle of the day. HONO levels measured in Melbourne were typically lower than those recorded in the morning in other places around the world, indicating minimal overnight accumulation, but peaked in the middle of the day to be commensurate with midday concentrations in locations with much higher NO_2 pollution. Regular midday peaks in the diurnal cycle of HONO surface concentrations have only previously been reported in rural locations. The HONO measured implies a daytime source term $1ppbh^{-1}$ above the predicted photostationary state (PSS) concentration and represents an OH radical source up to 4 times stronger than from ozone photolysis alone in the lowest 500m of the troposphere. The dependence of the high

midday HONO levels on soil moisture, combined with the observed diurnal and vertical profiles, provides evidence for a strong photoactivated and ground-based daytime HONO source.

Composition of ice particle residuals in mixed-phase clouds at Jungfraujoch (Switzerland): enrichment and depletion of particle groups relative to total aerosol

Stine Eriksen Hammer[1], Stephan Mertes[2], Johannes Schneider[3], Martin Ebert[1], Konrad Kandler[1],and Stephan Weinbruch[1]

Source: Atmosphere Chemistry and Physics, Volume 18, issue 19
02 Oct 2018.

Ice particle residuals (IRs) and the total aerosol particle population were sampled in parallel during mixed-phase cloud events at the high-altitude research station Jungfraujoch in January–February 2017. Particles were sampled behind an ice-selective counterflow impactor (Ice-CVI) for IRs and a heated total inlet for the total aerosol particles. A dilution set-up was used to collect total particles with the same sampling duration as for IRs to prevent overloading of the substrates. About 4000 particles from 10 Ice-CVI samples (from 7 days of cloud events at temperatures at the site between −10 and −18°C) were analysed and classified with operator-controlled scanning electron microscopy. Contamination particles (identified by their chemical composition), most likely originating from abrasion in the Ice-CVI and collection of secondary ice, were excluded from further analysis. Approximately 3000 total aerosol particles (IRs and interstitial particles) from 5 days in clouds were also analysed. Enrichment and depletion of the different particle groups (within the IR fraction relative to the total aerosol reservoir) are presented as an odds ratio relative to alumosilicate (particles only consisting of Al, Si, and O), which was chosen as reference due to the large enrichment of this group relative to total aerosol and the relatively high number concentration of this group in both total aerosol and the IR samples. Complex secondary particles and soot are the major particle groups in the total aerosol samples but are not found in the IR fraction and are hence strongly depleted. C-rich particles (most likely organic particles) showed a smaller enrichment compared to aluminosilicates by a factor of ~ 20. The particle groups with enrichment similar to aluminosilicate are silica, Fe aluminosilicates, Ca-rich particles, Ca sulfates, sea-salt-containing particles, and metal/metal oxide. Other aluminosilicates – consisting of variable amounts of Na, K, Ca, Si, Al, O, Ti, and Fe – are somewhat more enriched (factor ~ 2) and

Pb-rich particles are more (factor ~ 8) enriched than aluminosilicates. None of the sampled IR groups showed a temperature or size dependence in respect to ice activity, which might be due to the limited sampling temperature interval and the similar size of the particles. Footprint plots and wind roses could explain the different total aerosol composition in one sample (carbonaceous particle emission from the urban/industrial area of Po Valley), but this did not affect the IR composition. Taking into account the relative abundance of the particle groups in total aerosol and the ice nucleation ability, we found that silica, aluminosilicates, and other aluminosilicates were the most important ice particle residuals at Jungfraujoch during the mixed-phase cloud events in winter 2017.

Reactive quenching of electronically excited NO_2^* and NO_3^* by H_2O as potential sources of atmospheric HO_x radicals

Terry J. Dillon[1,a] and John N. Crowley[1]

Source: Atmosphere Chemistry and Physics, Volume 18, issue 19
02 Oct 2018.

Pulsed laser excitation of NO_2 (532–647nm) or NO_3 (623–662nm) in the presence of H_2O was used to initiate the gas-phase reaction $NO_2^* + H_2O \rightarrow$ products (Reaction R5) and $NO_3^* + H_2O \rightarrow$ products (Reaction R12). No evidence for OH production in Reactions (R5) or (R12) was observed and upper limits for OH production of $k_{5b}/k_5 < 1\times10^{-5}$ and $k_{12b}/k_{12} < 0.03$ were assigned. The upper limit for k_{5b}/k_5renders this reaction insignificant as a source of OH in the atmosphere and extends the studies (Crowley and Carl, 1997; Carr et al., 2009; Amedro et al., 2011) which demonstrate that the previously reported large OH yield by Li et al. (2008) was erroneous. The upper limit obtained for k_{12b}/k_{12} indicates that non-reactive energy transfer is the dominant mechanism for Reaction (R12), though generation of small but significant amounts of atmospheric HO_x and HONO cannot be ruled out. In the course of this work, rate coefficients for overall removal of NO_3^* by N_2 (Reaction R10) and by H_2O (Reaction R12) were determined: $k_{10} = (2.1\pm0.1) \times 10^{-11}cm^3molecule^{-1}s^{-1}$ and $k_{12} = (1.6\pm0.3) \times 10^{-10}cm^3molecule^{-1}s^{-1}$. Our value of k_{12} is more than a factor of 4 smaller than the single previously reported value.

Trends in air pollutants and health impacts in three Swedish cities over the past three decades

Henrik Olstrup[1], Bertil Forsberg[3], Hans Orru[3,4], Mårten Spanne[5], Hung Nguyen[6], Peter Molnár[7],and Christer Johansson[1,2]

Source: Atmosphere Chemistry and Physics, Volume 18, issue 21
01 Nov 2018.

Air pollution concentrations have been decreasing in many cities in the developed countries. We have estimated time trends and health effects associated with exposure to NO_x, NO_2, O_3, and PM_{10} (particulate matter) in the Swedish cities Stockholm, Gothenburg, and Malmö from the 1990s to 2015. Trend analyses of concentrations have been performed by using the Mann–Kendall test and the Theil–Sen method. Measured concentrations are from central monitoring stations representing urban background levels, and they are assumed to indicate changes in long-term exposure to the population. However, corrections for population exposure have been performed for NO_x, O_3, and PM_{10} in Stockholm, and for NO_x in Gothenburg. For NO_x and PM_{10}, the concentrations at the central monitoring stations are shown to overestimate exposure when compared to dispersion model calculations of spatially resolved, population-weighted exposure concentrations, while the reverse applies to O_3. The trends are very different for the pollutants that are studied; NO_x and NO_2 have been decreasing in all cities, O_3 exhibits an increasing trend in all cities, and for PM_{10}, there is a slowly decreasing trend in Stockholm, a slowly increasing trend in Gothenburg, and no significant trend in Malmö. Trends associated with $NO_x$and NO_2 are mainly attributed to local emission reductions from traffic. Long-range transport and local emissions from road traffic (non-exhaust PM emissions) and residential wood combustion are the main sources of PM_{10}. For O_3, the trends are affected by long-range transport, and there is a net removal of O_3in the cities. The increasing trends are attributed to decreased net removal, as NO_x emissions have been reduced.

Health effects in terms of changes in life expectancy are calculated based on the trends in exposure to NO_x, NO_2, O_3, and PM_{10} and the relative risks associated with exposure to these pollutants. The decreased levels of NO_x are estimated to increase the life expectancy by up to 11 months for Stockholm and 12 months for Gothenburg. This corresponds to up to one-fifth of the total increase in life expectancy (54–70 months) in the cities during the period of 1990–2015. Since the increased concentrations in O_3 have a relatively small impact on the changes in life expectancy, the overall net effect is increased life expectancies in the cities that have been studied.

Forcing mechanisms of the terdiurnal tide

Friederike Lilienthal, Christoph Jacobi, and Christoph Geißler

Source: Atmosphere Chemistry and Physics, Volume 18, issue 21
02 Nov 2018

Using a nonlinear mechanistic global circulation model we analyze the migrating terdiurnal tide in the middle atmosphere with respect to its possible forcing mechanisms, i.e., the absorption of solar radiation in the water vapor and ozone band, nonlinear tidal interactions, and gravity wave–tide interactions. In comparison to the forcing mechanisms of diurnal and semidiurnal tides, these terdiurnal forcings are less well understood and there are contradictory opinions about their respective relevance. In our simulations we remove the wave number 3 pattern for each forcing individually and analyze the remaining tidal wind and temperature fields. We find that the direct solar forcing is dominant and explains most of the migrating terdiurnal tide's amplitude. Nonlinear interactions due to other tides or gravity waves are most important during local winter. Further analyses show that the nonlinear forcings are locally counteracting the solar forcing due to destructive interferences. Therefore, tidal amplitudes can become even larger for simulations with removed nonlinear forcings.

Simulating secondary organic aerosol from anthropogenic and biogenic precursors: comparison to outdoor chamber experiments, effect of oligomerization on SOA formation and reactive uptake of aldehydes

Florian Couvidat[1], Marta G. Vivanco[2], and Bertrand Bessagnet[1,a]

Source: Atmosphere Chemistry and Physics, Volume 18, issue 21
02 Nov 2018.

New parameterizations for the formation of organic aerosols were developed. These parameterizations cover secondary organic aerosol (SOA) formation from biogenic and anthropogenic precursors, NO_x dependency, oligomerization and the reactive uptake of pinonaldehyde. These parameterizations were implemented in a box model in which the condensation and/or evaporation of semi-volatile organic compounds was simulated by the Secondary Organic Aerosol Processor (SOAP) model to take the dynamic evolution of concentrations into account.

The parameterizations were tested against several experiments carried out in previous studies in the EUPHORE outdoor chamber. Two datasets of experiments were used: the anthropogenic experiments (in which SOA is formed mainly from a mixture of toluene,

1,3,5-trimethylbenzene and o-xylene) and the biogenic experiments (in which SOA is formed mainly from α-pinene and limonene).

When assuming no wall deposition of organic vapors, satisfactory results (bias lower than 20%) were obtained for the biogenic experiments and for most of the anthropogenic experiments. However, a decrease of SOA concentrations (up to 30%) was found when taking wall deposition of organic vapors into account (with the parameters of Zhang et al., 2014). The anthropogenic experiments seem to indicate a complex NO_x dependency that could not be reproduced by the model. Oligomerization was found to have a strong effect on SOA composition (oligomers were estimated to account for up to 78% of the SOA mass) and could therefore have a strong effect on the formation of SOA. The uptake of pinonaldehyde (which is a high-volatility semi-volatile organic compound, SVOC) onto acidic aerosol was found to be too slow to be significant under atmospheric conditions (no significant amount of SOA formed after 3 days of evolution), indicating that the parameterization of Pun and Seigneur (2007) used in some air quality models may lead to an overestimation of SOA concentrations. The uptake of aldehydes could nevertheless be an important SOA formation pathway for less volatile or more reactive aldehydes than pinonaldehyde.

Regarding viscosity, a low effect of viscosity on SOA concentrations was estimated by the model, although a decrease of SVOC evaporation was found when taking it into account, as well as a lower sensitivity of concentrations to changes of temperature during the experiments.

Additional global climate cooling by clouds due to ice crystal complexity

Emma Järvinen[1,a], Olivier Jourdan[2], David Neubauer[3], Bin Yao[4], Chao Liu[4],Meinrat O. Andreae[5,6], Ulrike Lohmann[3], Manfred Wendisch[7], Greg M. McFarquhar[8,9],Thomas Leisner[1], and Martin Schnaiter[1]

Source: Atmosphere Chemistry and Physics, Volume 18, issue 21
02 Nov 2018

Ice crystal submicron structures have a large impact on the optical properties of cirrus clouds and consequently on their radiative effect. Although there is growing evidence that atmospheric ice crystals are rarely pristine, direct in situ observations of the degree of ice crystal complexity are largely missing. Here we show a comprehensive in situ data set of ice crystal complexity coupled with measurements of the cloud angular scattering functions collected during a number of observational airborne campaigns at diverse geographical

locations. Our results demonstrate that an overwhelming fraction (between 61 % and 81 %) of atmospheric ice crystals sampled in the different regions contain mesoscopic deformations and, as a consequence, a similar flat and featureless angular scattering function is observed. A comparison between the measurements and a database of optical particle properties showed that severely roughened hexagonal aggregates optimally represent the measurements in the observed angular range. Based on this optical model, a new parameterization of the cloud bulk asymmetry factor was introduced and its effects were tested in a global climate model. The modelling results suggest that, due to ice crystal complexity, ice-containing clouds can induce an additional short-wave cooling effect of $-1.12\ \mathrm{W\,m^2}$ on the top-of-the-atmosphere radiative budget that has not yet been considered.

Effective radiative forcing in the aerosol–climate model CAM5.3-MARC-ARG

Benjamin S. Grandey[1], Daniel Rothenberg[2], Alexander Avramov[2,3], Qinjian Jin[2],Hsiang-He Lee[1], Xiaohong Liu[4], Zheng Lu[4], Samuel Albani[5,6], and Chien Wang[2,1]

Source: Atmosphere Chemistry and Physics, Volume 18, issue 21
02 Nov 2018.

We quantify the effective radiative forcing (ERF) of anthropogenic aerosols modelled by the aerosol–climate model CAM5.3-MARC-ARG. CAM5.3-MARC-ARG is a new configuration of the Community Atmosphere Model version 5.3 (CAM5.3) in which the default aerosol module has been replaced by the two-Moment, Multi-Modal, Mixing-state-resolving Aerosol model for Research of Climate (MARC). CAM5.3-MARC-ARG uses the ARG aerosol-activation scheme, consistent with the default configuration of CAM5.3. We compute differences between simulations using year-1850 aerosol emissions and simulations using year-2000 aerosol emissions in order to assess the radiative effects of anthropogenic aerosols. We compare the aerosol lifetimes, aerosol column burdens, cloud properties, and radiative effects produced by CAM5.3-MARC-ARG with those produced by the default configuration of CAM5.3, which uses the modal aerosol module with three log-normal modes (MAM3), and a configuration using the modal aerosol module with seven log-normal modes (MAM7). Compared with MAM3 and MAM7, we find that MARC produces stronger cooling via the direct radiative effect, the shortwave cloud radiative effect, and the surface albedo radiative effect; similarly, MARC produces stronger warming via the longwave cloud radiative effect. Overall, MARC produces a global mean net ERF of $-1.79\pm0.03\ \mathrm{W\,m^{-2}}$, which is stronger than the global mean net ERF of $-1.57\pm0.04\ \mathrm{W\,m^{-2}}$ produced by MAM3 and $-1.53\pm0.04\ \mathrm{W\,m^{-2}}$ produced by MAM7. The regional distribution of ERF also differs between MARC and MAM3, largely due to differences in the regional distribution of the shortwave cloud radiative effect. We conclude that the specific representation of aerosols in global climate models, including aerosol mixing state, has important implications for climate modelling.

Impacts of shipping emissions on $PM_{2.5}$ pollution in China

Zhaofeng Lv[1,2], Huan Liu[1,2], Qi Ying[3], Mingliang Fu[4,5], Zhihang Meng[1,2], Yue Wang[1,2], Wei Wei[6],Huiming Gong[7], and Kebin He[1,2]

Source: Atmosphere Chemistry and Physics, Volume 18, issue 21
02 Nov 2018.

With the fast development of seaborne trade and relatively more efforts on reducing emissions from other sources in China, shipping emissions contribute more and more significantly to air pollution. In this study, based on a shipping emission inventory with high spatial and temporal resolution within 200 nautical miles (Nm) to the Chinese coastline, the Community Multiscale Air Quality (CMAQ) model was applied to quantify the impacts of the shipping sector on the annual and seasonal concentrations of $PM_{2.5}$ for the base year 2015 in China. Emissions within 12 Nm accounted for 51.2 %–56.5 % of the total shipping emissions, and the distinct seasonal variations in spatial distribution were observed. The modeling results showed that shipping emissions increased the annual averaged $PM_{2.5}$ concentrations in eastern China up to 5.2 $\mu g\, m^{-3}$, and the impacts in YRD (Yangtze River Delta) and PRD (Pearl River Delta) were much greater than those in BTH (Beijing–Tianjin–Hebei). Shipping emissions influenced the air quality in not only coastal areas but also the inland areas hundreds of kilometers (up to 960 km) away from the sea. The impacts on the $PM_{2.5}$ showed obvious seasonal variations, and patterns in the north and south of the Yangtze River were also quite different. In addition, since the onshore wind can carry ship pollutants to inland areas, the daily contributions of shipping emissions in onshore flow days were about 1.8–2.7 times higher than those in the rest of the days. A source-oriented CMAQ was used to estimate the contributions of shipping emissions from maritime areas within 0–12, 12–50, 50–100 and 100–200 Nm to $PM_{2.5}$ concentrations. The results indicated that shipping emissions within 12 Nm were the dominant contributor, with contributions 30 %–90 % of the total impacts induced by emissions within 200 Nm, while a relatively high contribution (40 %–60 %) of shipping emissions within 20–100 Nm was observed in the north of the YRD region and south of Lianyungang, due to the major water traffic lanes far from land. The results presented in this work implied that shipping emissions had significant influence on air quality in China, and to reduce its pollution, the current Domestic Emission Control Area (DECA) should be expanded to at least 100 Nm from the coastline.

Understanding mercury oxidation and air–snow exchange on the East Antarctic Plateau: a modeling study

Shaojie Song[1,a], Hélène Angot[2], Noelle E. Selin[1,2], Hubert Gallée[3], Francesca Sprovieri[4],Nicola Pirrone[5], Detlev Helmig[6], Joël Savarino[3], Olivier Magand[3], and Aurélien Dommergue[3]

Source: Atmosphere Chemistry and Physics, Volume 18, issue 21
05 Nov 2018.

Distinct diurnal and seasonal variations of mercury (Hg) have been observed in near-surface air at Concordia Station on the East Antarctic Plateau, but the processes controlling these characteristics are not well understood. Here, we use a box model to interpret the Hg^0(gaseous elemental mercury) measurements in thes year 2013. The model includes atmospheric Hg^0 oxidation (by OH, O_3, or bromine), surface snow Hg^{II} (oxidized mercury) reduction, and air–snow exchange, and is driven by meteorological fields from a regional climate model. The simulations suggest that a photochemically driven mercury diurnal cycle occurs at the air–snow interface in austral summer. The fast oxidation of Hg^0 in summer may be provided by a two-step bromine-initiated scheme, which is favored by low temperature and high nitrogen oxides at Concordia. The summertime diurnal variations of Hg^0 (peaking during daytime) may be confined within several tens of meters above the snow surface and affected by changing mixed layer depths. Snow re-emission of Hg^0 is mainly driven by photoreduction of snow Hg^{II} in summer. Intermittent warming events and a hypothesized reduction of Hg^{II} occurring in snow in the dark may be important processes controlling the mercury variations in the non-summer period, although their relative importance is uncertain. The Br-initiated oxidation of Hg^0 is expected to be slower at Summit Station in Greenland than at Concordia (due to their difference in temperature and levels of nitrogen oxides and ozone), which may contribute to the observed differences in the summertime diurnal variations of Hg^0 between these two polar inland stations.

Physical state of 2-methylbutane-1,2,3,4-tetraol in pure and internally mixed aerosols

Jörn Lessmeier[1,*], Hans Peter Dette[1,*], Adelheid Godt[1], and Thomas Koop[1]

Source : Atmosphere Chemistry and Physics, Volume 18, issue 21
05 Nov 2018.

2-Methylbutane-1,2,3,4-tetraol (hereafter named tetraol) is an important oxidation product of isoprene and can be considered as a marker compound for isoprene-derived secondary organic aerosols (SOAs). Little is known about this compound's physical phase state, although some field observations indicate that isoprene-derived secondary organic aerosols in the tropics tend to be in a liquid rather than a solid state. To gain more knowledge about the possible phase states of tetraol and of tetraol-containing SOA

particles, we synthesized tetraol as racemates as well as enantiomerically enriched materials. Subsequently the obtained highly viscous dry liquids were investigated calorimetrically by differential scanning calorimetry revealing subambient glass transition temperatures T_g. We also show that only the diastereomeric isomers differ in their T_g values, albeit only by a few kelvin. We derive the phase diagram of water–tetraol mixtures over the whole tropospheric temperature and humidity range from determining glass transition temperatures and ice melting temperatures of aqueous tetraol mixtures. We also investigated how water diffuses into a sample of dry tetraol. We show that upon water uptake two homogeneous liquid domains form that are separated by a sharp, locally constrained concentration gradient. Finally, we measured the glass transition temperatures of mixtures of tetraol and an important oxidation product of α-pinene-derived SOA: 3-methylbutane-1,2,3-tricarboxylic acid (3-MBTCA). Overall, our results imply a liquid-like state of isoprene-derived SOA particles in the lower troposphere at moderate to high relative humidity (RH), but presumably a semisolid or even glassy state at upper tropospheric conditions, particularly at low relative humidity, thus providing experimental support for recent modeling calculations.

Long-range transport of volcanic aerosol from the 2010 Merapi tropical eruption to Antarctica

Xue Wu[1,2], Sabine Griessbach[1], and Lars Hoffmann[1]

Source: Atmosphere Chemistry and Physics, Volume 18, issue 21
06 Nov 2018.

Volcanic sulfate aerosol is an important source of sulfur for Antarctica, where other local sources of sulfur are rare. Midlatitude and high-latitude volcanic eruptions can directly influence the aerosol budget of the polar stratosphere. However, tropical eruptions can also enhance polar aerosol load following long-range transport. In the present work, we analyze the volcanic plume of a tropical eruption, Mount Merapi in 2010, and investigate the transport pathway of the volcanic aerosol from the tropical tropopause layer (TTL) to the lower stratosphere over Antarctica. We use the Lagrangian particle dispersion model Massive-Parallel Trajectory Calculations (MPTRAC) and Atmospheric Infrared Sounder (AIRS) SO_2 measurements to reconstruct the altitude-resolved SO_2 injection time series during the explosive eruption period and simulate the transport of the volcanic plume using the MPTRAC model. AIRS SO_2 and aerosol measurements, the aerosol cloud index values provided by Michelson Interferometer for Passive Atmospheric Sounding (MIPAS), are used to verify and complement the simulations. The Lagrangian transport simulation of the volcanic plume is compared with MIPAS aerosol measurements and shows good agreement. Both the simulations and the observations presented in this study suggest that volcanic plumes from the Merapi eruption were transported to the south of 60° S 1 month after the eruption and even further to Antarctica in the following months. This relatively fast meridional transport of volcanic aerosol was mainly driven by quasi-horizontal mixing

from the TTL to the extratropical lower stratosphere, and most of the quasi-horizontal mixing occurred between the isentropic surfaces of 360 to 430 K. When the plume went to Southern Hemisphere high latitudes, the polar vortex was displaced from the South Pole, so that the volcanic plume was carried to the South Pole without penetrating the polar vortex. Although only 4 % of the sulfur injected by the Merapi eruption was transported into the lower stratosphere south of 60° S, the Merapi eruption contributed up to 8800 t of sulfur to the Antarctic lower stratosphere. This indicates that the long-range transport under favorable meteorological conditions enables a moderate tropical volcanic eruption to be an important remote source of sulfur for the Antarctic stratosphere.

An automatic observation-based aerosol typing method for EARLINET

Nikolaos Papagiannopoulos[1,2], Lucia Mona[1], Aldo Amodeo[1], Giuseppe D'Amico[1],Pilar Gumà Claramunt[1], Gelsomina Pappalardo[1], Lucas Alados-Arboledas[3,4],Juan Luís Guerrero-Rascado[3,4], Vassilis Amiridis[5], Panagiotis Kokkalis[5,6], Arnoud Apituley[7],Holger Baars[8], Anja Schwarz[8], Ulla Wandinger[8], Ioannis Binietoglou[9], Doina Nicolae[9],Daniele Bortoli[10], Adolfo Comerón[2], Alejandro Rodríguez-Gómez[2], Michaël Sicard[2,11],Alex Papayannis[6], and Matthias Wiegner[12]

Source: Atmosphere Chemistry and Physics, Volume 18, issue 21
06 Nov 2018.

We present an automatic aerosol classification method based solely on the European Aerosol Research Lidar Network (EARLINET) intensive optical parameters with the aim of building a network-wide classification tool that could provide near-real-time aerosol typing information. The presented method depends on a supervised learning technique and makes use of the Mahalanobis distance function that relates each unclassified measurement to a predefined aerosol type. As a first step (training phase), a reference dataset is set up consisting of already classified EARLINET data. Using this dataset, we defined 8 aerosol classes: clean continental, polluted continental, dust, mixed dust, polluted dust, mixed marine, smoke, and volcanic ash. The effect of the number of aerosol classes has been explored, as well as the optimal set of intensive parameters to separate different aerosol types. Furthermore, the algorithm is trained with literature particle linear depolarization ratio values. As a second step (testing phase), we apply the method to an already classified EARLINET dataset and analyze the results of the comparison to this classified dataset. The predictive accuracy of the automatic classification varies between 59 % (minimum) and 90 % (maximum) from 8 to 4 aerosol classes, respectively, when evaluated against pre-classified EARLINET lidar. This indicates the potential use of the automatic classification to all network lidar data. Furthermore, the training of the algorithm with particle linear depolarization values found in the literature further improves the accuracy with values for all the aerosol classes around 80 %. Additionally, the algorithm has proven to be highly versatile as it adapts to changes in the size of the training

dataset and the number of aerosol classes and classifying parameters. Finally, the low computational time and demand for resources make the algorithm extremely suitable for the implementation within the single calculus chain (SCC), the EARLINET centralized processing suite.

Application of a hygroscopicity tandem differential mobility analyzer for characterizing PM emissions in exhaust plumes from an aircraft engine burning conventional and alternative fuels

Max B. Trueblood[1], Prem Lobo[1,a], Donald E. Hagen[1], Steven C. Achterberg[1], Wenyan Liu[2],and Philip D. Whitefield[1]

Source: Atmosphere Chemistry and Physics, Volume 18, issue 23
03 Dec 2018.

In the last several decades, significant efforts have been directed toward better understanding the gaseous and particulate matter (PM) emissions from aircraft gas turbine engines. However, limited information is available on the hygroscopic properties of aircraft engine PM emissions which play an important role in the water absorption, airborne lifetime, obscuring effect, and detrimental health effects of these particles. This paper reports the description and detailed lab-based performance evaluation of a robust hygroscopicity tandem differential mobility analyzer (HTDMA) in terms of hygroscopic properties such as growth factor (GF) and the hygroscopicity parameter (κ). The HTDMA system was subsequently deployed during the Alternative Aviation Fuel EXperiment (AAFEX) II field campaign to measure the hygroscopic properties of aircraft engine PM emissions in the exhaust plumes from a CFM56-2C1 engine burning several types of fuels. The fuels used were conventional JP-8, tallow-based hydroprocessed esters and fatty acids (HEFA), Fischer–Tropsch, a blend of HEFA and JP-8, and Fischer–Tropsch doped with tetrahydrothiophene (an organosulfur compound). It was observed that GF and κ increased with fuel sulfur content and engine thrust condition, and decreased with increasing dry particle diameter. The highest GF and κ values were found in the smallest particles, typically those with diameters of 10 nm.

The relative impact of cloud condensation nuclei and ice nucleating particle concentrations on phase partitioning in Arctic mixed-phase stratocumulus clouds

Amy Solomon[1,2], Gijs de Boer[1,2], Jessie M. Creamean[1,2,a], Allison McComiskey[2],Matthew D. Shupe[1,2], Maximilian Maahn[1,2], and Christopher Cox[1,2]

Source: Atmosphere Chemistry and Physics, Volume 18, issue 23, 03 Dec 2018.

This study investigates the interactions between cloud dynamics and aerosols in idealized large-eddy simulations (LES) of Arctic mixed-phase stratocumulus clouds (AMPS) observed at Oliktok Point, Alaska, in April 2015. This case was chosen because it allows the cloud to form in response to radiative cooling starting from a cloud-free state, rather than requiring the cloud ice and liquid to adjust to an initial cloudy state. Sensitivity studies are used to identify whether there are buffering feedbacks that limit the impact of aerosol perturbations. The results of this study indicate that perturbations in ice nucleating particles (INPs) dominate over cloud condensation nuclei (CCN) perturbations; i.e., an equivalent fractional decrease in CCN and INPs results in an increase in the cloud-top longwave cooling rate, even though the droplet effective radius increases and the cloud emissivity decreases. The dominant effect of ice in the simulated mixed-phase cloud is a thinning rather than a glaciation, causing the mixed-phase clouds to radiate as a grey body and the radiative properties of the cloud to be more sensitive to aerosol perturbations. It is demonstrated that allowing prognostic CCN and INPs causes a layering of the aerosols, with increased concentrations of CCN above cloud top and increased concentrations of INPs at the base of the cloud-driven mixed layer. This layering contributes to the maintenance of the cloud liquid, which drives the dynamics of the cloud system.

On the effect of upwind emission controls on ozone in Sequoia National Park

Claire E. Buysse[1], Jessica A. Munyan[2], Clara A. Bailey[2], Alexander Kotsakis[3,a,b], Jessica A. Sagona[4],Annie Esperanza[5], and Sally E. Pusede[2]

Source: Atmosphere Chemistry and Physics, Volume 18, issue 23
04 Dec 2018.

Ozone (O_3) air pollution in Sequoia National Park (SNP) is among the worst of any national park in the US. SNP is located on the western slope of the Sierra Nevada Mountains downwind of the San Joaquin Valley (SJV), which is home to numerous cities ranked in the top 10 most O_3-polluted in the US. Here, we investigate the influence of emission controls in the SJV on O_3 concentrations in SNP over a 12-year time period (2001–2012). We show that the export of nitrogen oxides (NO_x) from the SJV has played a larger role in driving

high O_3 in SNP than transport of O_3. As a result, O_3 in SNP has been more responsive to NO_x emission reductions than in the upwind SJV city of Visalia, and O_3 concentrations have declined faster at a higher-elevation monitoring station in SNP than at a low-elevation site nearer to the SJV. We report O_3 trends by various concentration metrics but do so separately for when environmental conditions are conducive to plant O_3uptake and for when high O_3 is most common, which are time periods that occur at different times of day and year. We find that precursor emission controls have been less effective at reducing O_3 concentrations in SNP in springtime, which is when plant O_3 uptake in Sierra Nevada forests has been previously measured to be greatest. We discuss the implications of regulatory focus on high O_3 days in SJV cities for O_3 concentration trends and ecosystem impacts in SNP.

Molecular dynamics simulation of the surface tension of aqueous sodium chloride: from dilute to highly supersaturated solutions and molten salt

Xiaoxiang Wang[1], Chuchu Chen[1], Kurt Binder[2], Uwe Kuhn[1], Ulrich Pöschl[1], Hang Su[3,1],and Yafang Cheng[1,3]

Source: Atmosphere Chemistry and Physics, Volume 18, issue 23
04 Dec 2018.

Sodium chloride (NaCl) is one of the key components of atmospheric aerosols. The surface tension of aqueous NaCl solution ($\sigma_{NaCl,sol}$) and its concentration dependence are essential to determine the equilibrium water vapor pressure of aqueous NaCl droplets. Supersaturated NaCl solution droplets are observed in laboratory experiments and under atmospheric conditions, but the experimental data for $\sigma_{NaCl,sol}$ are mostly limited up to subsaturated solutions. In this study, the surface tension of aqueous NaCl is investigated by molecular dynamics (MD) simulations and the pressure tensor method from dilute to highly supersaturated solutions. We show that the linear approximation of concentration dependence of $\sigma_{NaCl,sol}$ at molality scale can be extended to the supersaturated NaCl solution until a molality of ~10.7 mol kg^{-1} (i.e., solute mass fraction (x_{NaCl}) of ~0.39). Energetic analyses show that this monotonic increase in surface tension is driven by the increase in excess surface enthalpy (ΔH) as the solution becomes concentrated. After that, the simulated $\sigma_{NaCl,sol}$ remains almost unchanged until x_{NaCl} of ~0.47 (near the concentration upon efflorescence). The existence of the "inflection point" at x_{NaCl} of ~0.39 and the stable surface tension of x_{NaCl} between ~0.39 and ~0.47 can be attributed to the nearly unchanged excess surface entropy term ($T{\cdot}\Delta S$) and the excess surface enthalpy term (ΔH). After a "second inflection point" at x_{NaCl} of ~0.47, the simulated $\sigma_{NaCl,sol}$ gradually regains the growing momentum with a tendency to approach the surface tension of molten NaCl (~175.58 mN m^{-1} at 298.15 K, MD simulation-based extrapolation). This fast increase in $\sigma_{NaCl,sol}$ at x_{NaCl}>0.47 is a process driven by excess surface enthalpy and excess surface entropy. Our results reveal different regimes of concentration dependence of the surface

tension of aqueous NaCl at 298.15 K: a water-dominated regime (x_{NaCl} from 0 to ~0.39), a transition regime (x_{NaCl} from ~0.39 to ~0.47) and a molten NaCl-dominated regime (x_{NaCl} from ~0.47 to 1).

Quantifying the large-scale electrification equilibrium effects in dust storms using field observations at Qingtu Lake Observatory

Huan Zhang[1] and Xiaojing Zheng[1,2]

Source: Atmosphere Chemistry and Physics, Volume 18, issue 23
04 Dec 2018.

Dust and sand electrification, which is a ubiquitous phenomenon in dust events, has a potentially dramatic effect on dust and sand lifting and transport processes. However, the effect of such electrification is still largely unclear, mainly due to its complexity and sparse observations. Here, we conducted an extensive observational analysis involving mild and severe dust storms with minimum visibility, ranging from ~0.09 to 0.93 km, to assess the electrical properties of airborne dust particles in dust storms. The space charge density has been estimated indirectly based on Gauss's law. Using the wavelet coherence analysis that is a method for evaluating the correlations between two non-stationary time series in the time–frequency domain, we found that the space charge density and dust concentration were significantly correlated over the 10 min timescales (on the order of the typical integral timescale of atmospheric turbulence). We further presented a simple linear regression (SLR) model to quantify such large timescale correlations and found that there was a significant linear relationship between space charge density and dust concentration at given ambient temperature and relative humidity (RH), suggesting that the estimated mean charge-to-mass ratio of dust particles was expected to remain constant (termed as the equilibrium value μ^*). In addition, the influences of ambient temperature and RH on μ^* were evaluated by a multiple linear regression (MLR) model, showing that the μ^* is nonlinearly related to environmental factors. The present study provides observational evidence for the environmental-dependent electrification equilibrium effects in dust storms. This finding may reduce challenges in future quantifications of dust electrification, as it is possible to exclude effects, such as the particles' collisional dynamics, on dust electrification.

Quantifying the variability of the annular modes: reanalysis uncertainty vs. sampling uncertainty

Edwin P. Gerber[1] and Patrick Martineau[2]

Source: Atmosphere Chemistry and Physics, Volume 18, issue 23
04 Dec 2018.

The annular modes characterize the dominant variability of the extratropical circulation in each hemisphere, quantifying vacillations in the position of the tropospheric jet streams and the strength of the stratospheric polar vortices. Their representation in all available reanalysis products is assessed. *Reanalysis uncertainty* associated with limitations in the ability to constrain the circulation with available observations, i.e., the inter-reanalysis spread, is contrasted with *sampling uncertainty* associated with the finite length of the reanalysis records.

It is shown that the annular modes are extremely consistent across all modern reanalyses during the satellite era (ca. 1979 onward). Consequently, uncertainty in annular mode variability, e.g., the coupling between the stratosphere and troposphere and the variation in the amplitude and timescale of jet variations throughout the annual cycle, is dominated by sampling uncertainty. Comparison of reanalyses based on conventional (i.e., nonsatellite) or surface observations alone with those using all available observations indicates that there is limited ability to characterize the Southern Annular Mode (SAM) in the presatellite era. Notably, prior to 1979, surface-input reanalyses better capture the SAM at near-surface levels than full-input reanalyses. For the Northern Annular Mode, however, there is evidence that conventional observations are sufficient, at least from 1958 onward. The addition of 2 additional decades of records substantially reduces sampling uncertainty in several key measures of annular mode variability, demonstrating the value of more historic reanalyses. Implications for the assessment of atmospheric models and the strength of coupling between the surface and upper atmosphere are discussed.

On the thermodynamic and kinetic aspects of immersion ice nucleation

Donifan Barahona

Source: Atmosphere Chemistry and Physics, Volume 18, issue 23
04 Dec 2018.

Heterogeneous ice nucleation initiated by particles immersed within droplets is likely the main pathway of ice formation in the atmosphere. Theoretical models commonly used to describe this process assume that it mimics ice formation from the vapor, neglecting interactions unique to the liquid phase. This work introduces a new approach that accounts for such interactions by linking the ability of particles to promote ice formation to the modification of the properties of water near the particle–liquid interface. It is shown that the same mechanism that lowers the thermodynamic barrier for ice nucleation also tends to decrease the mobility of water molecules, hence the ice–liquid interfacial flux. Heterogeneous ice nucleation in the liquid phase is thus determined by the competition between thermodynamic and kinetic constraints to the formation and propagation of ice. At the limit, ice nucleation may be mediated by kinetic factors instead of the nucleation work. This new ice nucleation regime is termed spinodal ice nucleation. The comparison of predicted nucleation rates against published data suggests that some materials of atmospheric relevance may nucleate ice in this regime.

The influence of particle composition upon the evolution of urban ultrafine diesel particles on the neighbourhood scale

Irina Nikolova[1], Xiaoming Cai[1], Mohammed Salim Alam[1], Soheil Zeraati-Rezaei[2], Jian Zhong[1],A. Rob MacKenzie[1,3], and Roy M. Harrison[1,a]

Source: Atmosphere Chemistry and Physics, Volume 18, issue 23
05 Dec 2018.

A recent study demonstrated that diesel particles in urban air undergo evaporative shrinkage when advected to a cleaner atmosphere (Harrison et al., 2016). We explore, in a structured and systematic way, the sensitivity of nucleation-mode diesel particles (diameter < 30 nm) to changes in particle composition, saturation vapour pressure, and the mass accommodation coefficient. We use a multicomponent aerosol microphysics model based on surrogate molecule (C_{16}–C_{32} *n*-alkane) volatilities. For standard atmospheric conditions (298 K, 1013.25 hPa), and over timescales (ca. 100 s) relevant for dispersion on the neighbourhood scale (up to 1 km), the choice of a particular vapour pressure dataset changes the range of compounds that are appreciably volatile by two to six carbon numbers. The nucleation-mode peak diameter, after 100 s of model runtime, is sensitive to the vapour pressure parameterisations for particles with compositions centred on surrogate molecules between $C_{22}H_{46}$ and $C_{24}H_{50}$. The vapour pressure range, derived from published data, is between 9.23×10^{-3} and 8.94×10^{-6} Pa for $C_{22}H_{46}$ and between 2.26×10^{-3} and 2.46×10^{-7} Pa for $C_{24}H_{50}$. Therefore, the vapour pressures of components in this range are critical for the modelling of nucleation-mode aerosol dynamics on the neighbourhood scale and need to be better constrained. Laboratory studies have shown this carbon number fraction to derive predominantly from engine lubricating oil. The accuracy of vapour pressure data for other (more and less volatile) components from laboratory experiments is less critical. The influence of a core of non-volatile material is also considered; non-volatile core fractions of more than 5 % are inconsistent with the field measurements that we test the model against. We consider mass accommodation coefficient values less than unity and find that model runs with more volatile vapour pressure parameterisations and lower accommodation coefficients are similar to runs with less volatile vapour pressure parameterisations and higher accommodation coefficients. The new findings of this study may also be used to identify semi-volatile organic compound (SVOC) compositions that play dominating roles in the evaporative shrinkage of the nucleation mode observed in field measurements (Dall'Osto et al., 2011).

Attributing differences in the fate of lateral boundary ozone in AQMEII3 models to physical process representations

Peng Liu[1], Christian Hogrefe[2], Ulas Im[3], Jesper H. Christensen[3], Johannes Bieser[4],Uarporn Nopmongcol[5], Greg Yarwood[5], Rohit Mathur[2], Shawn Roselle[2], and Tanya Spero[2]

Source: Atmosphere Chemistry and Physics, Volume 18, issue 23
05 Dec 2018.

Increasing emphasis has been placed on characterizing the contributions and the uncertainties of ozone imported from outside the US. In chemical transport models (CTMs), the ozone transported through lateral boundaries (referred to as LB ozone hereafter) undergoes a series of physical and chemical processes in CTMs, which are important sources of the uncertainty in estimating the impact of LB ozone on ozone levels at the surface. By implementing inert tracers for LB ozone, the study seeks to better understand how differing representations of physical processes in regional CTMs may lead to differences in the simulated LB ozone that eventually reaches the surface across the US. For all the simulations in this study (including WRF/CMAQ, WRF/CAMx, COSMO-CLM/CMAQ, and WRF/DEHM), three chemically inert tracers that generally represent the altitude ranges of the planetary boundary layer (BC1), free troposphere (BC2), and upper troposphere–lower stratosphere (BC3) are tracked to assess the simulated impact of LB specification.

Comparing WRF/CAMx with WRF/CMAQ, their differences in vertical grid structure explain 10 %–60 % of their seasonally averaged differences in inert tracers at the surface. Vertical turbulent mixing is the primary contributor to the remaining differences in inert tracers across the US in all seasons. Stronger vertical mixing in WRF/CAMx brings more BC2 downward, leading to higher BCT (BCT=BC1+BC2+BC3) and BC2/BCT at the surface in WRF/CAMx. Meanwhile, the differences in inert tracers due to vertical mixing are partially counteracted by their difference in sub-grid cloud mixing over the southeastern US and the Gulf Coast region during summer. The process of dry deposition adds extra gradients to the spatial distribution of the differences in DM8A BCT by 5–10 ppb during winter and summer.

COSMO-CLM/CMAQ and WRF/CMAQ show similar performance in inert tracers both at the surface and aloft through most seasons, which suggests similarity between the two models at process level. The largest difference is found in summer. Sub-grid cloud mixing plays a primary role in their differences in inert tracers over the southeastern US and the oceans in summer. Our analysis of the vertical profiles of inert tracers also suggests that the model differences in dry deposition over certain regions are offset by the model differences in vertical turbulent mixing, leading to small differences in inert tracers at the surface in these regions.

Two years of online measurement of fine particulate nitrate in the western Yangtze River Delta: influences of thermodynamics and N_2O_5 hydrolysis

Peng Sun[1], Wei Nie[1,2], Xuguang Chi[1,2], Yuning Xie[1], Xin Huang[1,2], Zheng Xu[1,2], Ximeng Qi[1,2],Zhengning Xu[1], Lei Wang[1], Tianyi Wang[1], Qi Zhang[3], and Aijun Ding[1,2]

Source: Atmosphere Chemistry and Physics, Volume 18, issue 23
05 Dec 2018.

Particulate nitrate contributes a large fraction of secondary aerosols. Despite understanding of its important role in regional air quality and global climate, long-term continuous measurements are rather limited in China. In this study, we conducted online measurement of $PM_{2.5}$(particulate matter with diameters less than 2.5 μm) nitrate for 2 years from March 2014 to February 2016 using the Monitor for AeRosols and Gases in ambient Air (MARGA) in the western Yangtze River Delta (YRD), eastern China, and investigate the main factors that influenced its temporal variations and formation pathways. Compared to other sites in China, an overall high concentration of particulate nitrate was observed, with a mean value of 15.8 $\mu g\, m^{-3}$ (0.5 to 92.6 $\mu g\, m^{-3}$). Nitrate on average accounted for 32 % of the total mass of water-soluble ions and the proportion increased with PM loading, indicating that nitrate is a major driver of haze pollution episodes in this region. Sufficient ammonia drove most nitrate into the particle phase in the form of ammonium nitrate. A typical seasonal cycle of nitrate was observed, with the concentrations in winter on average 2 times higher than those in summer mainly due to different meteorological conditions. In summer, the diurnal variation of particulate nitrate was determined by thermodynamic equilibrium, resulting in a much lower concentration during daytime despite a considerable photochemical production. Air masses from the polluted YRD and biomass burning region contributed to the high nitrate concentration during summer. In winter, particulate nitrate did not reveal an evident diurnal variation. Regional transport from northern China played an important role in enhancing nitrate concentration. A total of 18 nitrate episodes were selected to understand the processes that drive the formation of high concentration of nitrate. Rapid nitrate formation was observed during the pre-episode (the day before nitrate episode day) nights, and dominated the increase of total water-soluble ions. Calculated nitrate from N_2O_5 hydrolysis was highly correlated to and accounted for 80 % of the observed nitrate, suggesting that N_2O_5hydrolysis was a major contributor to the nitrate episodes. Our results suggested that rapid formation of nitrate could be a main cause for extreme aerosol pollution events in the YRD during winter, and illustrated the urgent need to control NO_x emission.

In situ measurements of cloud microphysical and aerosol properties during the break-up of stratocumulus cloud layers in cold air outbreaks over the North Atlantic

Gary Lloyd[1,2], Thomas W. Choularton[2], Keith N. Bower[2], Martin W. Gallagher[2],Jonathan Crosier[1,2], Sebastian O'Shea[1], Steven J. Abel[3], Stuart Fox[3], Richard Cotton[3],and Ian A. Boutle[3]

Source: Atmosphere Chemistry and Physics, Volume 18, issue 23
05 Dec 2018.

A key challenge for numerical weather prediction models is representing boundary layer clouds in cold air outbreaks (CAOs). One important aspect is the evolution of microphysical properties as stratocumulus transitions to open cellular convection. Abel et al. (2017) have shown, for the first time from in situ field observations, that the break-up in CAOs over the eastern Atlantic may be controlled by the development of precipitation in the cloud system while the boundary layer becomes decoupled. This paper describes that case and examines in situ measurements from three more CAOs. Flights were conducted using the UK Facility for Airborne Atmospheric Measurements (FAAM) British Aerospace-146 (BAe-146) aircraft in the North Atlantic region around the UK, making detailed microphysical measurements in the stratiform boundary layer. As the cloudy boundary layer evolves prior to break-up, increasing liquid water paths (LWPs) and drop sizes and the formation of liquid precipitation are observed. Small numbers of ice particles, typically a few per litre, are also observed. Eventually LWPs reduce significantly due to loss of water from the stratocumulus cloud (SC) layer. In three of the cases, aerosols are removed from the boundary layer across the transition. This process appears to be similar to those observed in warm clouds and pockets of open cells (POCs) in the subtropics. After break-up, deeper convective clouds form with bases warm enough for secondary ice production (SIP), leading to rapid glaciation. It is concluded that the precipitation is strongly associated with the break-up, with both weakening of the capping inversion and boundary layer decoupling also observed.

जहाँ है हरियाली ।
वहाँ है खुशहाली ।।

Indian Institute of Tropical Meteorology
Dr. Homi Bhabha Road, Pashan, Pune - 411 008, India
Telephone: +91-20-2590-4200
E-mail: iitm-env@nic.in
Website: www.iitmenvis.nic.in